DESIGN AND DEVELOPMENT OF A PULSATILE AXIAL FLOW BLOOD PUMP AS A LEFT VENTRICULAR ASSIST DEVICE

A Thesis Submitted for the Degree of Doctor of Philosophy

By

KARNAL PATEL

Brunel Institute for Bioengineering
Brunel University

December 2011

Declaration of Authenticity

I hereby declare that I am the sole author of this thesis.

KARNAL PATEL

ॐ असतो मा सद्गमय । तमसो मा ज्योतिर्गमय । मृत्योर्मामृतं गमय ।।

Om
asato ma sad gamaya,
tamaso ma jyotir gamaya ,
mrutyor ma amritam gamaya.

Meaning of Prayer
All mighty God, please Lead me from the unreal to the real.
Lead me from darkness to light. Lead me from materialism to spirituality.
May there be peace everywhere.

— Brhadaranyaka Upanisad, Section 1,3,28.

This Thesis is Dedicated

To My Father, Mother and GuruHari

Narendra Patel , Devyani Patel and PramukhSwami Maharaj

For Their Unconditional Love , Support and Blessings

Throughout My Life

ACKNOWLEDGMENT

This thesis would not have been possible without the help of several people, whose names require particular, mention here and to whom I would be indebted throughout my life. First, I would like to take this opportunity to express my sincerest gratitude to my supervisor Dr Ashraf Khir for his father like help, guidance and encouragement throughout the PhD experience.

I am grateful to Prof Colin Clark and Dr. Quan long for their incommensurable advices and Roger Paton for the help with the electrical equipments.

I would like to thank Jenny and Caroline for their kindness and everyone at Brunel Institute for Bioengineering for contributing to my personal and professional development in a multicultural and multinational working environment. I would like to express my gratitude towards BRUNEL UNIVERSITY, WEST LONDON for allowing me to work as a research student, opening doors of opportunity that changed my life.

I like to thank all fantastic staff and colleagues who had given their help and support throughout my tenure. Special thanks to Francesco, Ahsan, Hao , Marcel, Jakub, Alessandra, Gianpaolo, Lukasz, Masoud, Samantha, Yi, and Luigi for being colleagues and great friends in the same time.

I could not have survived my PhD without the support of special people that have characterized the overall experience in London. Starting from my wife Dr. Nayna for her big support while I wrote this thesis. Francesco, Ahsan and Hao for sharing since the beginning of this big adventure, Bhumika, Maulik and Deveshi for being always part of the crew.

Last but not least, to my parents Mr. Narendra and Mrs. Devyani Patel and my uncle Mr. Manharbhai and other family members ,whose patience support enabled me to complete my thesis.

May the Blessings Be

Abbreviations

ACC - American College of Cardiology

AHA - American Heart Association

BIVAD - Biventricular Assist Device

BPM – Beats Per Minute.

BTD – Bridge To Decision

BTR – Bridge To Recovery

BTT – Bridge To Transplant

CAD - Computer Aided Design

CCD - Central Composite Design

CFD - Computational Fluid Dynamics.

CHF – Congestive Heart Failure

CPB – Cardiopulmonary Bypass

CT - Cardiac Transplantation

DOE - Design of Experiment

DSP – Design Support Process.

DT – Destination Therapy

GDO - Goal Driven Optimisation

GUI - Graphic User Interface

HR – Heart Rate

LVAD – Left Ventricular Assist Device

MCS – Mechanical Circulatory Support

MI - Myocardial Infarction

MOGA – Multi Objective Genetic Algorithm

MOSF - Multiple System Organ Failure

NSGA - Non-dominated Sorted Genetic Algorithm

NYSHA - The New York State Heart Association

RPM – Revolution Per Minute.

RVAD – Right Ventricular Assist Device

TAH - Total Artificial Heart

VAD – Ventricular Assist Device

VIF - Variation Inflation Factor

Abstract

Each year all over the world, Millions of patients from infants to adults are diagnosed with heart failure. A limited number of donor hearts available for these patients results in a tremendous demand of mechanical circulatory support (MCS) system, either in the form of total artificial heart (TAH) or a ventricular assist device (VAD). Physiologically MCS are expected to provide heart; a time to rest and potential recovery by unloading the ventricle, while maintaining the adequate peripheral as well as coronary circulation.

Existing ventricular assist devices (VAD) have employed either displacement type pulsatile flow pumping systems or continuous flow type centrifugal/rotodynamic pumps systems. Displacement type devices produce a pulsatile outflow, which has significant benefits on vital organ function and end organ recovery. Continuous flow devices are small and can be placed within body using minimal invasive procedures, in addition they reduces infection as well as mechanical failure related complications. Despite availability of success stories for both types of pumping systems, the selection of the either of them is an ongoing debate.

This thesis aims to merge the advantages of displacement pumps (pulsatile flow) and axial-flow pumps (continuous flow) into a novel left vertical assist device (LVAD), by designing a novel minimal invasive, miniature axial-flow pump producing pulsating outflow for the patients having early heart failure and myocardial infarction as a *Bridge-To-Recovery (BTR)* or *Bridge-To-Decision (BTD)* device. The design of VAD, the experimental setup and dedicated control system were developed for the in vitro evaluation of pulsatile flow. Computational fluid dynamics (CFD) had been employed for the detail investigation of pulsatile flow. In addition, CFD was also applied to optimize the pulse generation for low haemolysis levels.

Outcome of the study produces comprehensive understanding for the generation of pulsatile flow using an axial flow pump. Further, it provides the means of generating a controlled pulse that can regulate flow rate for varying heart rate within low haemolysis levels.

INDEX

List of Figures

LIST OF TABLE

Chapter 1 Background

1.1 Abstract

This chapter highlights the prevalence as well as the clinical scenario of various heart diseases with its classification system. Brief overview of pharmacological and surgical treatments is given along with need and expectations from the Mechanical Circulatory Support (MCS). Further, detail classification of MCS is discussed at the end of this chapter.

1.2 Introduction

Heart disease continues to be the leading cause of death across the globe (Mathers and Loncar, 2006). Heart disease is a disorder in the normal functioning of the heart. Although heart disease may be present from birth, often the ageing process leads to higher-pressure levels and reduction in the overall elasticity of the vessels, making the heart unable to generate adequate cardiac output for peripheral and cardiac circulation. Each year heart disease causes over 4.3 millions deaths in Europe, approximately 48% of all deaths(Allender et al., 2008). In recent years only in the United Kingdom (UK), around 2.6 million people are diagnosed with Coronary Artery Disease (CAD)(Allender et al., 2008). Along with CAD, occurrence of other circulatory disease appears to be rising, dominantly for men in older age group (2009a). Despite significant progress made over the last 30 years in the medical field and a decrease in death rate from all cardiovascular disease up to 45% in Unite States of America (USA), each year over 5 million people suffer from chronic heart disease and around 1.5 million people suffer from myocardial infarction (MI) that is commonly referred to as a heart attack (2009b). According to the National Heart, Lung, and Blood Institute (2009b) , an estimated 4.8 million Americans suffer from Congestive Heart Failure (CHF), a condition in which the heart cannot pump enough blood to meet the need of various body organs.

1.2.1 Myocardial Infarction

Myocardial infarction, MI is a form of necrosis of the heart muscle caused by an acute insufficiency of blood flow through the coronary arteries nourishing the heart tissues. For most of the cases, MI is a consequence of atherosclerosis of the coronary arteries, which causes acute interruption in coronary flow due to stenosis of coronary vessels. Stenosis is an occlusion of the lumen due to gradual deposition of atherosclerosis plaque or thrombus. Hypertension, diabetes, high cholesterol, cigarette smoking, coronary artery diseases, close family members with cardiac disease history and obesity are all factors that increase the risk of myocardial infarction.

Infection is one of the causes of dilated cardiomyopathy, a disease of heart muscle, in which the heart cavity is dilated. Infection may also affect the endocardium, heart valves, or electric conduction system of cardiac tissues and muscles. The most common viral infections leading to myocarditis are coxsackievirus-B, hepatitis viruses, adenovirus, arbovirus, cytomegalovirus, echovirus, influenza virus, and HIV.
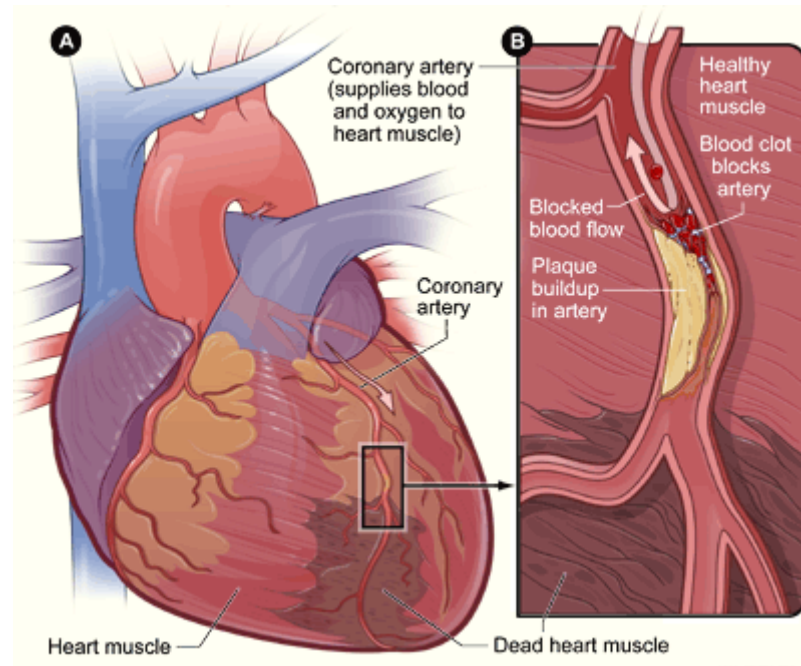
Figure 1-1 [A] an overview of a heart and coronary artery showing damage (dead heart muscle) caused by a myocardial infarction. [B] Is a cross-section of the coronary artery with plaque build up and a blood clot (National Heart Lung and Blood Institute, 2011).

The most severe consequence of myocardial infarction is a cardiogenic shock (CS). It can be best described as an inability of heart to generate sufficient blood pressure & flow. During cardiogenic shock, blood pressure falls sharply (below 90/60 mm Hg) and cold sweats appear with weakness in body. On a mechanical level, a noticeable decline in contractility reduces the ejection fraction and cardiac output. Subsequently it leads to increased ventricular filling pressures, dilatation of cardiac chamber, and ultimately uni-ventricular or bi-ventricular failure that result in lower blood pressure and/or pulmonary edema in which lung alveoli are filled with fluid.

1.2.2 Congestive Heart Failure

Congestive heart failure (CHF) is a complex clinical syndrome with various factors compromising the heart's ability to pump blood through body. The syndrome of CHF arises because of an abnormality in cardiac structure, function, rhythm, or conduction (Figueroa and Peters, 2006). CHF is characterized by ventricular malfunction leading to a decrease in cardiac output, neurohumoral activation, and a decrease in exercise capacity as well as the endurance. There is also a "vicious cycle" of blood flow maldistribution with hypoperfusion of vital organs. The most common reasons are ischemic heart disease and hypertension, resulting in ischemic dysfunction of the myocardium. Other important causes of CHF include valvular heart disease, primary myocardial disease (idiopathic, infiltrative, or inflammatory) and congenital cardiac malformations (Hunt and Frazier, 1998).

The New York State Heart Association (NYSHA) has established a classification system for CHF (The Criteria Committee of the New York Heart Association, 1994). A classification system is based upon the severity of the symptoms associated with CHF. In each class, the patient has already been diagnosed with CHF. The NYSHA classes, or "stages", are as follows,

Class I − No limitation of physical activity. Ordinary physical activity does not cause excess fatigue, shortness of breath, or palpitations.

Class II − There is slight limitation of physical activity. Patients are comfortable at rest but ordinary physical activity results in fatigue, shortness of breath, palpitations, or angina.

Class III − There is marked limitation of physical activity. Although patients are comfortable at rest, even less than ordinary activity will result in symptoms.

Class IV − There is inability of the patient to carry out any physical activity without significant discomfort. Symptoms of congestive heart failure are present even when patient is at rest. With any physical activity, the patient experiences increased discomfort.

Each class identifies the cardiac status associated with probable course and outcome of a disease. *Class-1* is a person with uncompromised cardiac status having a good

prognosis. The prognosis is worse with each subsequent class, where *Class IV* group of patients rely on heart transplantation for their survival.

A more recent classification system for CHF was released by the American College of Cardiology Foundation (ACCF) and American Heart Association (AHA) in November of 2001 (Rooke et al., 2012). The new system of classification is not limited to patients already diagnosed with CHF. As such, it is intended to be used in combination with the NYSHA classification system, rather than as a replacement. The ACCF/AHA classes are as follows,

Class A − The patient is at risk for developing CHF, but has no structural disorder of the heart. These would include patients at high risk for CHF due to the presence of hypertension, coronary artery disease, diabetes mellitus, a history of drug or alcohol abuse, a history of rheumatic fever, a history of cardiomyopathy, etc.

Class B − The patient has a structural disorder of the heart but has never developed CHF. This would include patients with structural heart disease such as left heart enlargement, heart fibrosis, valve disease, or a previous heart attack.

Class C − The patient has current or past CHF symptoms and underlying structural heart disease.

Class D − The patient has end-stage disease and is frequently hospitalized for CHF, or requires special treatments such as a left ventricular assist device (LVAD), artificial heart, inotropic infusion, heart transplant, or hospital care.

1.3 Treatment for Heart Disease

Pharmacological treatments are usually implemented with certain level of change in life style for patients diagnosed with heart disease. Surgical treatments are essential for the patients with structural abnormalities of heart, associated cardio vascular system or heart valves(Tahy, 1998). Heart transplantation is the last option to consider for the severely affected cardiac patients *(NYSHA Class IV and ACC/AHA Class D).*

Dietary changes to maintain appropriate weight and reduce salt intake may be required. Reducing salt intake helps to decrease swelling in the legs, feet, and abdomen. Appropriate exercise also recommended, but it is important that heart failure patients only begin an exercise program according to the guidance of their doctors. Walking, bicycling, swimming, or low-impact aerobic exercises may be recommended. Other lifestyle changes that may decrease the symptoms of heart failure include, stopping smoking as well as other tobacco uses, eradicating or reducing alcohol consumption, and not using harmful drugs(Tahy, 1998).

1.3.1 Pharmacological Therapy

The objective of the pharmacological therapy is to reduce mortality and morbidity, and to improve quality of life (Uretsky et al., 1993). One or more of the following types of medicines can be prescribed for heart failure is as follows,

- Diuretics
- Digitalis
- Vasodilators
- Beta blockers
- Angiotensin Converting Enzyme inhibitors (ACE inhibitors)
- Angiotensin Receptor Blockers (ARBS)
- Calcium channel blockers

Diuretics help to get rid of excess salt and water from the kidneys by increasing the urine output. This helps to reduce the swelling caused by accumulated fluid in the tissues. **Digitalis** helps the heart muscle to have stronger pumping action (Packer et

al., 1993) . *Amyl Nitrate*, *Mercurial Diuretics* and *Digitalis Glycosides* becoming available in the early part of the twentieth century (1997).

Vasodilators for heart failure were introduced by the acute use of *Nitroprusside* in 1974, followed by *Hydralazine* in 1977, demonstrating improved survival with the *Hydralazine-Isosorbide Dinitrate* combination (Richardson et al., 1987, Parker et al., 1996). With the release of *Captopril* in 1980 and *Enalapril* in 1984, multiple large, randomized, placebo-controlled trials established the Angiotensin Converting Enzyme (ACE) inhibitors as the cornerstone of therapy, with extensive unforeseen benefits for this drug class occurring beyond that expected only from vasodilatation (Swedberg and Kjekshus, 1988, Pfeffer et al., 1992, Cohn et al., 1991, 1992). **Vasodilators, ACE inhibitors, ARBs,** and **Calcium Channel Blockers** lower blood pressure and expand the blood vessels so blood can move more easily through them. This action makes it easier for the heart to pump blood through the vessels.

ACE inhibitors reduce both mortality and morbidity in patients with depressed LV systolic function (1991). Inhibition of the chronic sympathetic stimulation with *β-blockers* is safe (Waagstein et al., 1993). The combined use of *ACE inhibitors and β-blockers* has improved functional status of the patients, improved LV function and reduced mortality and morbidity, more than applying each strategy alone (Hjalmarson et al., 2000). Cholesterol-lowering drugs called **Statins** can help prevent death from heart failure. *Spironolactone* which is a potassium sporting diuretic has in addition to standard therapy (Pitt et al., 1999), reduced mortality, and morbidity in patients with CHF.

Metabolic intervention can be helpful for decreasing the duration and extent of myocardial stunning (Vinten-Johansen and Nakanishi, 1993, Svedjeholm et al., 1995b, Lazar et al., 1980), It has been reported that metabolic intervention prior to administration of *Inotropic* agents can be helpful for myocardial recovery (Svedjeholm et al., 1995a, Lazar et al., 1981). The administration of supraphysiological doses of *insulin*, 1 U/kg/hour, overcomes the stress induced insulin resistance in the myocardium, leading to a shift towards carbohydrate oxidation, which provides the heart with a better oxygen economy (Svensson et al., 1990). High doses of *insulin* also encourage a dilatation of the arterial vascular bed

(Svensson et al., 1989). These effects are favourable for the failing left ventricle. Administration of amino acids, i.e. *Glutamate* and *Aspartate,* alone or in combination with Glucose-Insulin-Potassium (GIK) treatment can be used during the post ischemic phase (Vanhanen et al., 1998) or when signs of myocardial ischemia exist.

1.3.2 Surgical Therapy

Surgical therapies are considered as an option, when pharmacological treatments are not sufficient to cure heart disease. Surgical procedures are carried out based on the severity of myocardial dysfunction aiming to improve the quality of life. Surgical therapy for cardiac failure (mainly for left ventricular failure) includes coronary revascularization, ventricular remodelling, valvular heart surgery, and the use of Mechanical circulatory support. One of the listed surgical procedures, which can be applied for patients suffering from severe heart disease.

- Thyroidectomy
- Pericardiectomy
- Valvular heart surgery
- Coronary revascularization
    - Coronary artery bypass grafting(CABG)
    - Stenting
- Cardiac remodelling
- Aneurysmorrhaphy/aneurysmectomy
- Infarct reduction
- Ventricular reduction surgery
- Cardiac transplantation
    - Orthotopic
    - Heterotopic
- Mechanical circulatory support
    - Post-Cardiotomy
    - Bridge to Recovery from Cardiomyopathy
    - Bridge to Transplant
    - Destination Therapy

Surgical procedures for heart failure as *thyroidectomy, pericardiectomy,* and valve replacement are available from early days. **Thyroidectomy** is an operation that involves the surgical removal of all or part of the thyroid gland. Thyroidectomy helps by decreasing the demands of the heart by decreasing the basal metabolic rate. **Pericardiectomy** is a surgical removal of part or most of the pericardium. This operation is most commonly done to relieve constrictive pericarditis, or to remove a pericardium that is calcified and fibrous. Valvular heart surgical procedures like *Valvuloplasty* and *Rose Procedures* are performed to repair or replace heart valves.

Use of counter pulsating intra-aortic balloon pump for Cardiogenic Shock was proposed in 1967 (Moulopoulos et al., 1962), and LV *aneurysmectomy* which refers to removal of aneurysm, introduced for chronic HF in 1962 (Masters, 1999). *Cardiac Remodelling* refers to the changes in size, shape, and function of the heart after injury to the ventricles. Various cardiac remodelling procedures like *neurysmorrhaphy/aneurysmectomy*, infarct reduction, application of cardiac restraining and ventricular splinting devices have recently been introduced and reported in small numbers.

Cardiac Transplantation **(CT)** is a surgical transplant procedure performed on patients with end-stage heart failure *(NYSHA Class IV and ACC/AHA Class D)* or severe coronary artery disease. Cardiac transplantation was introduced as a therapy for end-stage heart disease in 1967 (Barnard, 1967). The most common procedure is to take a working heart from an organ donor (cadaveric allograft) and implant it into the patient. The patient's own heart may either be removed (*Orthotopic Procedure*) or, less commonly, left in to support the donor heart (*Heterotopic Procedure*). Post-operative CT complications include infection, sepsis, organ rejection, as well as the side effects of the immunosuppressive drugs. Since the transplanted heart originates from another organism, the recipient's immune system may attempt to reject it. Immunosuppressive drugs reduce the risk of rejection, but it might create unwanted side effects, such as increased risk of infections or nephrotoxic effects.

1.4 Need of Mechanical Circulatory Support (MCS) as a Therapy

A limiting factor for cardiac transplantation is a significant shortage of donor hearts. Around 50,000 patients requiring heart transplantation with availability of around 2500 donor hearts every year. An average waiting period prior to heart transplant is approximately three to six months (2009a, 2009b, Allender et al., 2008, Mathers and Loncar, 2006) . Many patients died or become ineligible for cardiac transplant due to irreversible failure of vital organs during their waiting period.

The lack of available donor hearts, emphasise the need for an alternative option of treatment. Mechanical circulatory support (MCS) can provide the circulatory support for patients waiting for heart transplant. Along with circulatory support, MCS restores the optimum level of health for patient suffering cardiac dysfunction. The severe shortage of donor heart has supported the idea for the development of permanent artificial pumping devices (artificial heart) as a solution to the existing problem. Artificial hearts are also known as total artificial heart (TAH).

Another reason for the requirement of MCSs & TAHs is financial, which relates the cost of care for patients suffering cardiovascular disease. Heart disease is one of the top causes of hospitalisation that require longer period of stay at hospitals, as well as it consumes the major portion of the overall spending on health by government. MCSs can be helpful in reducing the number of days for hospitalisation, decreasing the amount of resources consumed along with the improvement in quality of life for the patients with end stage heart failure.

1.4.1 Physiological expectation from MCS

Physiologically MCS are expected to provide heart a time to rest and potential to recover by unloading the ventricle, while maintaining the adequate peripheral as well as coronary circulation. Insufficient cellular perfusion results in anaerobic metabolism and triggers the release of mediators causing further damage to cells. If this cycle of injury continues, can lead to multiple system organ failure (MOSF).The mortality for single organ dysfunction is 30%, which increases as more organ systems fails. With four organ failure mortality rate is 100% (Ayres et al., 1988).MCS should restore the adequate circulation and break the deadly cycle of MOSF.

The primary objective is to sustain systemic/peripheral circulation as in case of NYSHA Class IV patients. When patients are waiting for donor's heart to survive, MCS are expected to support patients with circulatory assistance as a **Bridge-To-Transplant** (BTT) device.

In case of patients with cardiogenic shock, myocardial infection and myocardial infarction MCS are expected to provide support as a **Bridge-To-Recovery** (BTR) device to save the patient's heart by reducing the workload of left ventricle and increasing in coronary perfusion. The group of patients having severe heart failure in an extremely critical condition, MCS are expected to provide support as a **Bridge-To-Decision** (BTD) device, where patients have end stage organ failure or uncertain neurological status.

In some cases, despite having NYSHA Class IV symptoms patients cannot be treated with transplant due to Immunodeficiency virus disease, degenerative, neuromuscular disease, liver cirrhosis, severe renal failure, severe chronic obstructive pulmonary disease, malignancy or Patients with a fixed high pulmonary vascular resistance or patients with diabetic end-organ dysfunction. In such cases MCS are likely to provide circulatory support as an **Alternative-To-Transplant** (ATT) or **Destination-Therapy** (DT) device.

MCS are used to support either left ventricle (most cases) only or in some cases the right ventricle. Due to this fact, MCS are generally referred as Ventricular Assist Devices (VADs). Survival rate of patients with severe myocardial dysfunction treated with VADs after CPB has been reported to be in the range of 30 to 60% (Wiebalck et al., 1993, Mehta et al., 1996, Hedenmark et al., 1989, Creswell et al., 1992). The overall survival rate of patients treated with VAD for long-term use as a BTT is reported to be around 70 to 80% (Sun et al., 1999, McCarthy et al., 1998) .

1.5 Classification of MCS

To satisfy the patient specific therapeutic objective, numerous different types of designs and pumping technology have been used to construct MCSs. It is difficult to judge any specific design as right or wrong due to lack of awareness of constraints and parameters influencing the results. This is the reason for an existing variety of different designs and pumping technologies. Different identifiable therapeutic needs also motivate the use of different designs for the construction of MCSs.

In general, MCSs consist of three different components
1) Pump and Cannulas,
2) Energy source
3) Control and Monitoring console.

All the MCSs can be divided between extracorporeal verses implantable devices based on the location of the placement of device. For example, the roller pump is an extracorporeal device placed outside of body with cannulas entering the body. While the Jarvik 2000 heart pump is an example of an implantable device, where pump and cannulas are placed within body. A key benefit of an Implantable device is a reduced risk of infection.

MCSs can be broadly classified in two major groups,
1. Total Artificial Heart (TAH)
2. Ventricular Assist Devices (VAD)

1.5.1 Total Artificial Heart (TAH)

Total artificial heart (TAH) is a mechanical circulatory support (MCS) system that replaces the native heart. The TAH consists of two blood pumps that are implanted in the place of the patient's native heart within the pericardium **(Orthotopic Procedure).** TAH is also different from a cardiopulmonary bypass machine (CPB), which is an external device used to provide the functions of both the heart and lungs. Cardio-pulmonary bypass (CPB) is only used for a few hours at a time, most commonly during heart surgery.
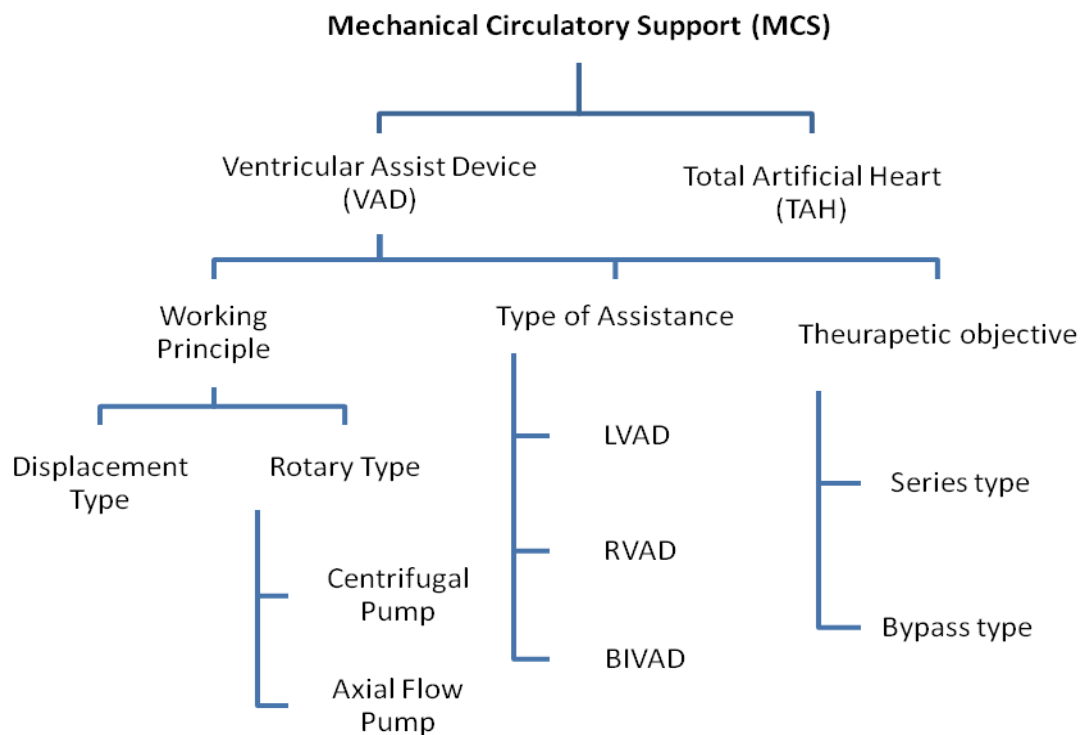
Figure 1-2 Classification of Mechanical circulatory support with sub classification of VAD

1.5.2 Ventricular Assist Device (VAD)

A Ventricular assist device, or VAD, is a type of MCS that is used to partially or completely replace the function of a failing ventricle. The VADs can support or replace the function of the failing left ventricle, right ventricle, or both ventricles. The VADs do not require removal of the native heart and therefore can be used as a bridge-to-transplantation (BTT) as well as a temporary bridge-to-recovery (BTR) in patients with expected myocardial recovery. VADs can be further classified into groups based on

1. Working Principle/Pumping Technology
2. Type of Assistance
3. Therapeutic Method
4. Output flow Characteristics
5. Application Time
6. Power Supply
7. Generations
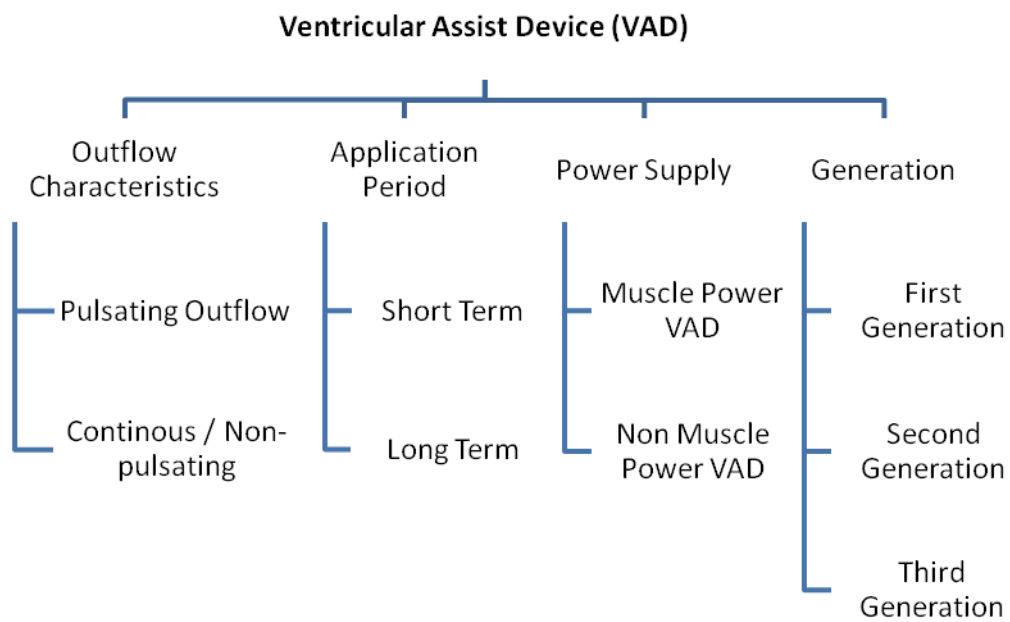
Figure 1-3 continued sub classification of ventricular assist device.

1.5.3 Working principle/pumping technology

Based on the working principle Ventricular assist devices can be classified into two main categories; Displacement Type VAD and Rotary Type VAD.

1.5.3.1 Displacement Type VAD

In displacement type pump, the fluid is pumped using the periodic change of working space. That produces a pulsating inflow and a pulsating outflow. Displacement pumps can be easily controlled because output is directly related to the stroke volume and the pumping frequency. This makes it very easy to maintain a precise and accurate outflow even under varying inflow and outflow conditions. Displacement pump ejects and fills during two separate phases of the pumping cycle. These pumps are usually large in sized to satisfy for clinical requirements. Examples of these types of pumps are:

- Push-plate pumps
- Membrane (blood sac, or diaphragm) pumps
- Balloon pumps
- Roller Pump

1.5.3.2 Rotary Type VAD.

In case of rotary pump, the energy transfer to fluid is established by the velocity change within the impeller. These devices create the pressure difference at its inlet and outlet. Fluid enters axially through an inlet on a rotating impeller blades, or concentric cones. These devices impose a rotating motion on the fluid, accelerates it through the pump, producing a non-pulsating inflow and outflow.

Rotary flow pumps can provide high flow rates at low pressures. These pumps are incapable of maintaining a precise output under changing inflow and outflow conditions. This device gives maximum efficiency at a design speed. For example:

- Centrifugal pump
- Axial flow pump

Generally, for a large volume and low-pressure requirement, a rotary pump could be the preferred choice for the application. While for low volume and high-pressure demand, the displacement type pumps are more suitable. Displacement pump requires open-heart surgery for installation. Hence, they are prone to infection. Compared to displacement pump, axial flow rotary pump are very small and non-invasive.

1.5.4 Type of Assistance

VAD are used to assist either left (LVAD) or right ventricle (RVAD) and in some cases they are use to assist both ventricles (BIVAD). The VAD use to support both ventricles is known as biventricular assist device.

1.5.4.1 Left ventricular assist devices (LVAD)

In case of LVAD, Blood is withdrawn from left atrium or the apex of the LV and returned to the ascending aorta (figure 1-4). Atrial cannulation is easier to perform and it is less traumatic for the heart in comparison to the apical cannulation. Therefore, the left atrial cannulation is preferred for a temporary LV support. However, a LV cannulation via the apex provides better LV unloading and better VAD performance. For that reason, the apical cannulation is preferred for LV assist as a bridge to transplantation.
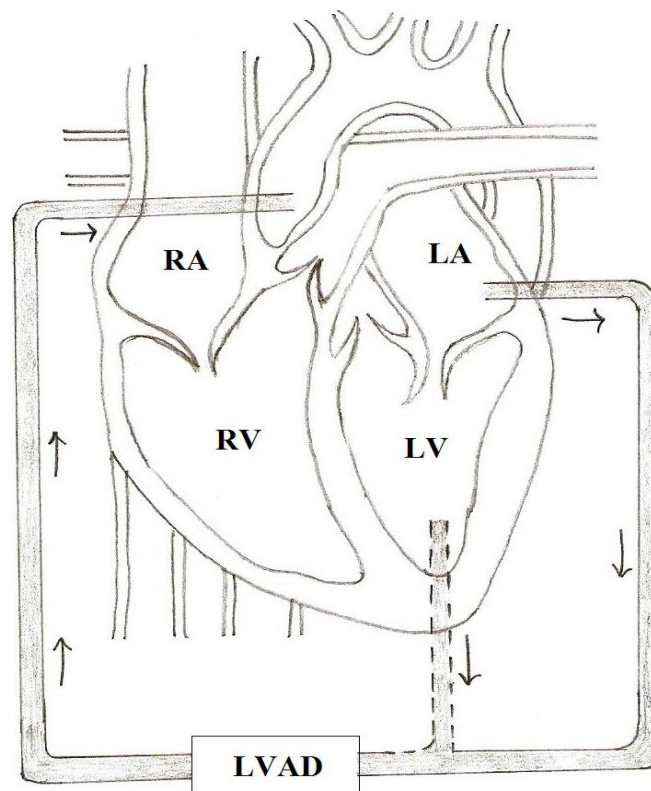
Figure 1-4: Schematic overview of cannulation approach for LVAD. Arrows shows that blood is delivered directly to ascending aorta from either left atrium or apex of left ventricle or pulmonary veins by use of LVAD. [Sketch by Author]

1.5.4.2 Right Ventricular Assist Devices (RVAD)

In case of RVADs, blood is withdrawn from the right atrium and returned to the main pulmonary artery. Figure 1-5 depicts the schematic overview of cannulation approach for RVAD.
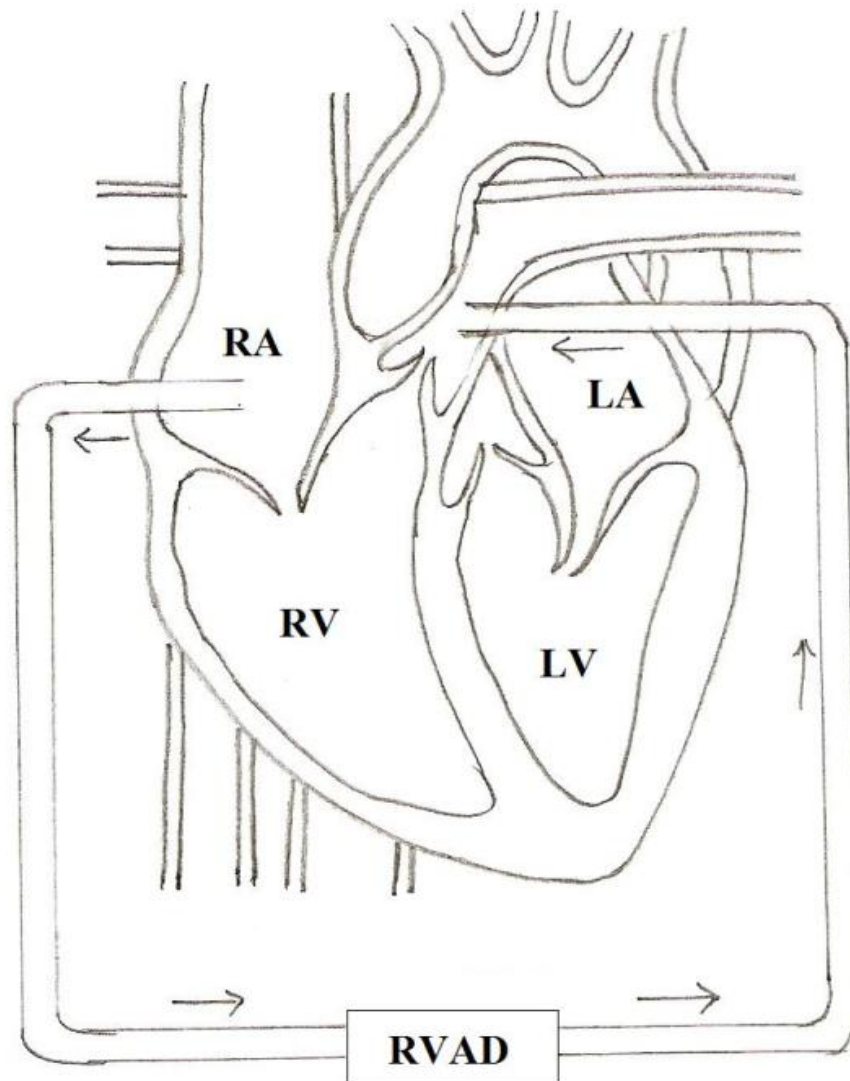
Figure 1-5: Schematic overview of cannulation approach for RVAD. Arrow indicates the direction of blood flow from right atrium to main pulmonary artery by RVAD. [Sketch by Author]

1.5.4.3 Biventricular Devices (BiVAD)

The BiVADs are actually a combination between LVAD and RVAD, and can be seen as a functional heart. Figure 1-6 depicts the schematic overview of cannulation approach for BiVAD.
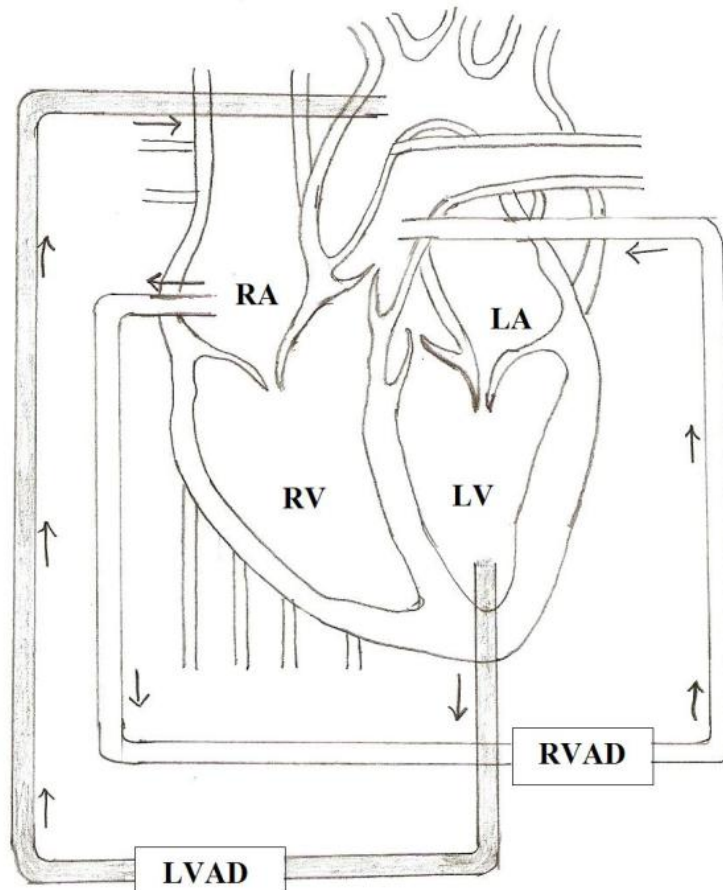
Figure 1-6: Schematic overview of cannulation approach for BiVAD. Arrows in LVAD indicates blood is withdrawn from apex of left ventricle and delivered directly in ascending aorta and in case of RVAD, blood is withdrawn from right atrium and delivered to the pulmonary artery. [Sketch by Author]

1.5.5 Therapeutic Objective

Different techniques can be used to reduce the after load and/or myocardial oxygen consumption. Two different ways to assist the heart are the series type VAD and bypass type VAD.

1.5.5.1 Series Type Ventricular Assist Device

A series-type ventricular assist device is a device pumping from the ascending aorta to the descending aorta. In this case, the VAD is working in series with a natural heart and operates synchronously. It should achieve lower LV output pressure during diastole, to reduce the workload. In this type of VAD, blood is filled during the systolic phase of the natural heart, allowing the heart to eject blood into the ascending aorta at a lower ventricular resistance. Consequently the VAD ejects blood during the diastolic phase of the natural heart, when the intra myocardial pressure is low, directing flow into the coronary arteries.
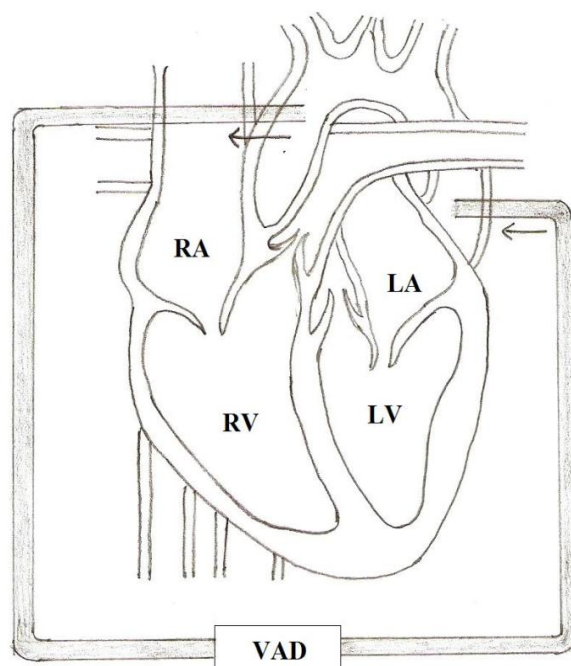
Figure 1-7: General principle of Series-type ventricular assist device. Arrows indicate the direction of blood flow directly from ascending aorta to descending aorta. [Sketch by Author]

Series-type ventricular assist method is advantageous because of no in- and outflow valves requirement. The blood is pumped from the ascending aorta to the

descending aorta, both having the same haemodynamic pressure. Hence, no pressure gradients are able to create back flow through the pump. VAD without valves is a very useful concept.

1.5.5.2 Bypass-Type Ventricular Assist Device

In this method of assistance, the blood is pumped directly from the atrium to the aorta or from the ventricular apex to the aorta bypassing the mitral valve.
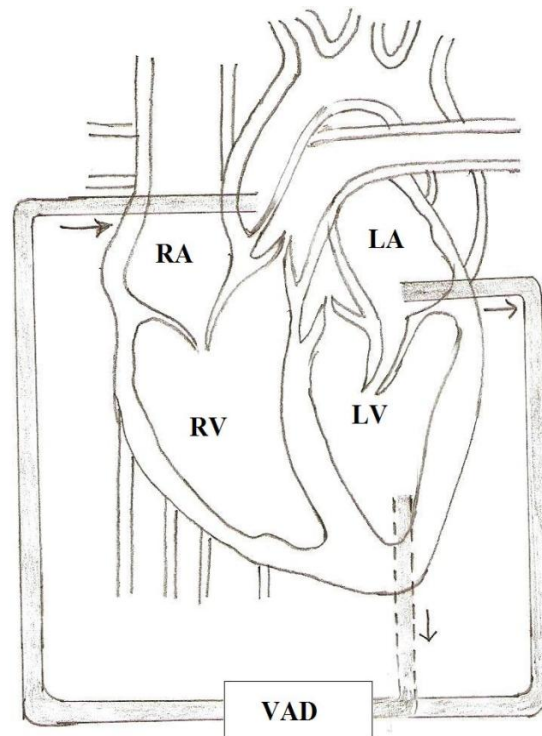
Figure 1-8: General principle of Bypass-type ventricular assist device. Arrow depicts that blood is pumped directly from the left atrium to ascending aorta or from the left ventricle to ascending aorta, thereby bypassing the mitral valve. [Sketch by Author]

In this case, the VAD works parallel to the natural heart and almost whole volume of the blood is pumped by the VAD. Here VAD is allowed to fill directly either from left atrium or left ventricle during the systolic phase of the natural heart, which than eject blood into the ascending aorta at a lower ventricular resistance. Rotary pumps can be used as a bypass-type ventricular assist device. One example is the Jarvik 2000 FlowMaker marketed by Jarvik Heart, Inc.

1.5.6 Output flow characteristics

VAD designs can also be divided into groups by considering their outflow characteristics, i.e. pulsating outflow or non- pulsating outflow. Generally, the displacement pumps generate a pulsating outflow, while the radial-flow pumps generate a non- pulsating outflow.

1.5.6.1 Pulsating outflow

Pulsatile type pump were the first to be used as VAD. The pulsatile pump mimics the natural heart in terms of generating the body pulse, with pulsating inflow as well as outflow. For that reason, pulsating outflow pumps rest on decades of clinical experience. In addition, the REMATCH trial (Rose et al., 2001) was also based on the use of the Heart Mate VAD system, which is a pulsating outflow pump.

1.5.6.2 Continuous / Non-pulsating outflow

Continuous pumps are smaller than the pulsatile pump for the similar output capacity. Lower volume (small size) makes them ideal for the total implantation. These devices are widely used for the short-term cardiac assistance. These types of pumps are also advantageous during cardiopulmonary bypass, while operating on the heart. The effects of non-pulsatile outflow pumps on the human body are still unknown.

1.5.7 Application period

VAD used as a bridge to transplant have short-term application. Therefore they are designed for specific period. Based on their application period they can be categorised as short-term assist device or a long-term assist device.

1.5.8 Power supply

Majority of VAD use electrical power to pump the blood. Some VAD use the chest muscle to pump the blood. Based on their power supply we can categorise the VAD in two groups as Muscle power VAD and non-muscle power VAD (Birks, 2010) . Non-muscle power VADs can be further divided into pneumatically driven or electrically driven VADs .

1.5.9 Generations

Based on overall technological development VADs can be classified into three generations.

1.5.9.1 First generation

First-generation blood pumps are positive-displacement or pulsatile pumps. In the 1980s, in vivo studies gave evidence that animals could survive for a long period of time in an entirely non pulsatile state, proving that pulsatile blood flow does not represent a necessarily physiological condition. Until today, the debate continues among investigators on whether pulsatile mechanical support provides any substantial benefit to the patient by reproducing the natural heartbeat and blood flow.

1.5.9.2 Second generation

Second-generation blood pumps are non-pulsatile pumps. They are characterised by the use of a spinning impeller providing a continuous blood flow. Typically, second-generation VADs use contact bearings and/or seals, where the bearings are immersed in the blood stream or separated from the stream by seals.

1.5.9.3 Third generation

The transition from second- to third-generation rotary blood pumps is characterised by magnetic bearings allowing the impeller to be magnetically supported in housing. The work by Wood (Wood et al., 2005) and the references there in argue that the third-generation systems are at present the leading technology in the development of mechanical circulatory support.

Chapter 2 Review of Mechanical Circulatory Support

2.1 Abstract

This chapter overviews the historical development of MCS along with the worldwide inventory of famous blood pumps, including FDA approved and under trial devices. It is based on an extensive literature review and hopefully fairly complete. This chapter discusses details of the existing device technology and the rationale behind the development of a pulsatile axial flow blood pump as a Left Ventricle Assist Device (LVAD). Furthermore, this chapter shows the pathway by setting up the aims and objectives of the research work.

2.2 Historical Development of MCS

Providing temporary MCS in severely ill cardiac patients can mean the difference between life and death. Mechanical cardiac support with ventricular assist devices (VAD) and total artificial heart (TAH) is an established therapy for a variety of clinical scenarios, including postcardiotomy shock, BTT and DT. Recent REMATCH Study has demonstrated conclusively the benefits of a MCS over pharmacological treatment (Frazier and Delgado, 2003) for patients with irreversible heart failure. The following is a historical summary of VAD and TAH, based on the previous published papers by Magovern (Magovern and Pierce, 1990) , G. A. Maccioli (Maccioli, 1997), Reul & Akdis (Reul and Akdis, 2000), Wheeldon (Wheeldon, 2003), Wood (Wood et al., 2005) and Rose (Rose et al., 2001) .

It has been observed by Spencer (Spencer et al., 1965),Dennis (Trauma, 1966), DeBakey(DeBakey et al., 1964) that some patient who cannot be weaned off from cardiopulmonary bypass (CPB) after surgery, can be easily detached from heart-lung machine if they are allowed to have rest and recover for longer period of time. These observations have stimulated the development of MCS as a BTR of heart.

Physiological and hematologic trauma caused by the oxygenator was the main obstacle for long-term use of the heart-lung machine for cardiac recovery. If MCS could be used to maintain circulation for more prolonged periods using patients own lungs for oxygenation then the probability of improvement in cardiac recovery increases.

The work of Drs Michael DeBakey, Domingo Liotta, and William Hall, led to the first use of an implantable left ventricular assist device (LVAD) in 1963 (Hall et al., 1964) at Baylor College of Medicine, in Houston, Texax. A similar VAD device was successfully implanted in 1966 in a young woman for 10 days. She was the first long-term Survivor of the use of VAD technology.

In a classic article published in 1971, Dr. DeBakey reviewed his experience in the 1960s with LVAD technology and summarises its limitations. In summary, the drawbacks of VAD (Hall et al., 1964, DeBakey, 1971) at that time were lack of electronic controllers, efficient portable power sources, lack of biocompatible materials, and need of extensive implant surgery, along with the high price of VAD.

In the late 1960s and early 1970s, the failure of cardiac transplantation (Frazier and Delgado, 2003) to fulfil its initial promise encouraged the development of implantable MCS for DT, as an option to cardiac transplantation. This was the original goal outlined in a 1976 request for proposal (RFP) issued by the National Heart, Lung, and Blood Institute, for a pump that could provide assistance for up to 2 years without external venting.

Current devices such as the Novacor Left Ventricular Assist System (World Heart, Inc), the HeartMate implantable LVAD (Thoratec Corporation), and the Thoratec Ventricular Assist Device System (Thoratec Corporation) evolved from this program. Among the first patients to undergo successful BTR were 3 patients at Texas Heart Institute, two of whom received a TAH in 1969 and 1981. LVAD implanted in 1978 in one of those three patient (Cooley, 1988) .Despite having satisfactory TAH & LVAD performance, all this three patients died due to infection complication related to immune suppression.

Since early of 1980s introduction of the immunosuppressive drug cyclosporine has allowed several newer technologies to be successfully apply for BTR. The Novacor (1984), the Jarvik-7 TAH (Jarvik Heart, Inc) (1985), and the HeartMate (1986). Since the mid-1980s, the use of MCS for this purpose has gradually increased. In 2001, approximately 20.1% of all heart transplant recipients in the United States underwent MCS before transplantation (Sun et al., 1999). Despite the fact that the US Food and Drug Administration (FDA) had approved these pumps only for 30-day implants, the initial goal of 2-year assistance using MCS has been achieved by both the implantable Novacor and the Heart Mate.

Till January 2003, the HeartMate LVAD had been used to support 217 patients for more than 1 year, 33 patients for more than 2 years, and 3 patients for more than 3years, all on an outpatient basis. These patients initially received the HeartMate as a BTR and remained on the transplant waiting list. The Novacor

implantable pump has a similar record (Wheeldon et al., 2002), 1 patient having been supported by it for more than 4.5 years. In Europe, the Berlin Heart group have reported the use of MCS for 38 patients (Drews et al., 2003). This group of patients were living their normal life without hospitalisation for an average of 454 days in the range 20 to 769 days.

In 2001, the control study (REMATCH) has been carried out with the objective of examining the use of VAD as destination therapy (DT). This study has reported the successful use of HeartMate LVAD (Rose et al., 2001). Valuable experience has been gained with the extensive use and success of MCS for BTR. In fact, the more than 2-year durability and reliability of the HeartMate pump was demonstrated because of the prolonged waiting times endured by BTT patients, and these waiting times will likely continue to increase.

In 2000, the average waiting time for O–blood-type patients was 869 days in those lucky enough to receive a transplant (Transplantation et al., 1993). The first patient to be discharged from the hospital with an electrically powered LVAD occurred in 1991 and was reported by Texas Heart Institute researchers in 1994 (Frazier, 1994). Other patients were soon able to return to productive work while awaiting transplants as outpatients. In 1995, one patient had worked productively for 6 months before receiving a transplant. In these cases, MCS offered long-term effectiveness and the potential to return patients to full, active lives. Currently, most patients who need MCS for more than 90 days are discharged from the hospital.

A number of patients have had their devices removed, generally because of device malfunction, and were able to survive with conventional pharmacological therapy and without transplantation or additional device support (Khan et al., 2003, Hetzer et al., 2001). To date, the number of patients treated in this manner has been limited, but numerous studies from a wide range of transplantation centres have reported improvement histologically, biochemically, neurohormonally, and ultrastructurally in the BTT patient population. Adjunctive therapy may further enhance the chance of ventricular recovery. For example, cell transplantation at the time of LVAD implantation may enhance myocardial functional recovery, and Yacoub in Great Britain (Yacoub, 2001) has reported the use of the β-antagonist clenbuterol with promising results. Controlled clinical studies around a wider range of patients will further define the role of ventricular recovery with MCS.

2.3 Existing Ventricular Assist Devices (VADs)

The numbers of VAD systems that are commercially available with the FDA and CE approval or in their final stage of development. Table 2-1 provides the tabular overview of the general advantages and disadvantages of existing and future VAD technology.

Note: Appendix-1 provides the images of the VAD systems mentioned in table 2-1.

NAME OF EXISTING VAD	PLACEMENT	WORKING PRINICIPLE	OUTPUT	TYPE OF ASSITANCE	APPLICATION PERIOD	PUMP ACTUATION	AMBULATION	FDA STATUS	CE STATUS
AbioMed BVS 5000 system	Extra corporeal	Displace-ment	5 L/min (100ml stroke)	LVAD/RVAD/ BIVAD	Short	Pneumatic	No	BTR	BTR
AbioMed AB 5000 system	Extra corporeal	Displace-ment	6 L/min (100ml stroke)	LVAD/RVAD/ BIVAD	Intermediate	Pneumatic	Fair-short transportation	BTR	BTR
Arrow Int.Intra aortic ballon pump	Internal	Displace-ment	N/A increase coronary perfusion	----------	Short	Pneumatic	No	BTR	BTR
Datascope CS100/Syatem 98XT	Internal	Displace-ment	N/A increase coronary perfusion	----------	Short	Pneumatic	No	BTR	BTR
Medtronic Biopump(80 ml &48ml)	Extra corporeal	Radial flow	10 L/min (80 ml version)	LVAD/RVAD/ BIVAD	Short for <5 days	Electrical	No	BTR/BTT	BTR/BTT
Thoratec VAD	Extra corporeal	Displace-ment	1.3-7.2 L/min (65ml stroke)	LVAD/RVAD/ BIVAD	Intermediate-months	Pneumatic	Fair with TLC-II portable VAD driver	BTR/BTT	BTR/BTT

NAME OF EXISTING VAD	PLACEMENT	WORKING PRINICIPLE	OUTPUT	TYPE OF ASSITANCE	APPLICATION PERIOD	PUMP ACTUATION	AMBULATION	FDA STATUS	CE STATUS
Thoratec Heartmate XVE LVAS	Internal	Displace-ment	11 L/min (85ml stroke)	LVAD	Long-years	Electrical	Good, discharge possible	BTT/DT	BTT/DT
World Heart Novacor	Internal	Displace-ment	10 L/min (85 ml stroke)	LVAD	Long-years	Electrical	Good, discharge possible	BTT	BTR/BTT/DT
AbioMed Abiocor	Internal	Displace-ment	12 L/min	TAH	Long-years	Electrical	Good, discharge possible	Not approve (in trial)	Not approve (in trial)
Arrow Int.CorAide	Internal	Centrifugal (radial flow)	4.1 ± 0.8 L/min	LVAD	Long-years	Electrical	Good, discharge possible	Not approve (in trial)	Not approve (in trial)
Berlin Heart Incor	Internal	Centrifugal (axial flow)	7 L/min	LVAD	Long-years	Electrical	Good	Not approve (in trial)	BTR/BTT
Impella Recover LP2,5 & LP 5,0	Internal	Radial flow	2.5 and 5 L/min	LVAD	Short for 5-7 days	Electrical	Fair-short transportation	Not approve (in trial)	BTR

NAME OF EXISTING VAD	PLACEMENT	WORKING PRINICIPLE	OUTPUT	TYPE OF ASSITANCE	APPLICATION PERIOD	PUMP ACTUATION	AMBULATION	FDA STATUS	CE STATUS
Jarvik Heart Jarvik 2000 Flow Maker	Internal	Axial flow	7 L/min	LVAD	Long-years	Electrical	Good	In trial	BTT/DT
Micromed DeBakey	Internal	Axial flow	10 L/min	LVAD	Long-years	Electrical	Good	Not approve (in trial)	BTT
Terumo DuraHeart	Internal	Centrifugal	No informa-tion	LVAD	Long-upto 5 years	Electrical	Good	Not approve (in trial)	Not approve (in trial)
Thoratec Heartmate III	Internal	Axial flow	12 L/min	LVAD	Long	Electrical	Good	Pre clinical	Pre clinical
Ventracor VentrAssist	Internal	Centrifugal (radial flow)	12 L/min	LVAD	Long-years	Electrical	Good	Approve for pilot study	In trial
World Heart HeartQuest VAD	Internal	Centrifugal (radial flow)	No informa-tion	LVAD	Long-years	Electrical	Good	Pre clinical	Pre clinical

Table 2-1: list of the existing VAD

2.4 Evaluation of Existing VAD Technology

Most of the FDA approved VAD/TAH are positive displacement type systems. Due to their large size, they are not suitable for implantation in many of the paediatric and female patients. The external displacement pumps allow for support of smaller sized patients.

Displacement pumps like the HeartMate IP / VE, Thoratec and Novacor are able to deliver flow rates up to 10 L / min with maximum heart rate of 120 BPM and have a well-established clinical history of up to 20 years. Developments that are more recent include the Novacor II and HeartSaver.

Most of this positive displacement pumps consist of one or more chambers with a pusher plate mechanism to create the pulsatile flow. In case of the IABP, pulsatile flow is generated by inflation and deflation of a balloon placed in the descending aorta, which is inserted through the femoral arteries.

Apart from this extra chamber, all existing external as well as internal VAD systems requires either transcutaneous cannulas/catheters, or transcutaneous pneumatic or electric lead. This constitutes a serious issue of infection in all existing VAD systems. Pennington (Pennington et al., 1994) and Murakami (Murakami et al., 1994) have observed that 20% to 55% of the patients receiving displacement type VAD also receive transcutaneous driveline related infections. The use of many moving parts, mechanical failure of membranes and valves, resulting in blood damage and spallation (Hetzer et al., 2001) make displacement type VAD suitable only for short-term application.

In case of pulsatile pump, sometimes blood looses contact with the moving surfaces of the blood sac resulting in the formation of thrombus. Farrar and colleagues (Farrar et al., 1988) have observed the need of consistent washing of all blood contacting surfaces to avoid the risk of thrombus formation. Anticoagulation agents like Heparin and Warfarin help in avoiding the risk of lethal thromboemboli. HeartMate and DuraHeart VAD systems have claimed their devices are free from thrombus and hemolysis.

Most of the FDA and CE approved VAD requires the highly invasive procedures to insert and removal of device. Patient with external VAD support for bridge-to-recovery (BTR) also require cannulas and consequently a sternotomy(opening made in sternum) for insertion. .

In case of failure, bulky implantable devices increases surgical stress on the patient's body.

Most of the VAD systems under development need to address the shortcoming of the FDA approved systems. These systems focused on miniaturising, less invasive, and fully implantable solutions. Many of the developing system use the centrifugal or axial flow pumping system over the displacement type of devices. DeBakey , Jarvik 2000, HeartMate III and Berlin Heart Incor are comparable to the size of a battery.

Miniaturization has been a key in the most of the ongoing VAD's development projects. These VAD can also be implanted in paediatric patients. The Impella pump was a modern incarnation of the Hemopump, and a very good example of catheter mounted miniature pumping system that require only a small cut on femoral artery to be implanted within body with minimal surgical trauma. These types of systems are also very easy to remove in case of device failure. Miniaturization has also benefited the management of patients as they can be managed outpatient bases or requires shorter duration of hospitalisation.

The existing VAD developments also focus on achieving completely implantable system. That involves combining the various components with implantable power sources and controllers that can be recharged and reprogrammed without removing them from the body.

As with all new technology, axial-flow and centrifugal VADs have also introduced a different set of management issues, as well as certain complications, that were previously absent or unimportant with pulsatile VADs (Stevenson et al., 2001). Many of the centrifugal devices use blood immersed bearings for the lubrication and cooling purpose. That increases the risk of in-situ thrombus and thromboemboli. Due to rotating impeller, a certain degree of hemolysis is common and the long-term effects of hemolysis on body are unknown. Concerns include, increased incidence of gastrointestinal bleeding and ventricular arrhythmias, as well as the effects of partial unloading on pulmonary hemodynamic. Chronic anticoagulation is necessary. In addition, Feedback systems for controlling pump speed are complex and most of them are clinically unproven or under development.

2.5 Study Rationale

The rationale behind this study is to take an advantage of the pulsatile flow by producing it using an axial flow-pumping device. Due to tubular configuration and small size of axial flow pump requires less time to implant without major surgical procedure. It is easy to implant an axial flow pump compared to other centrifugal device that has different location of inlet and outlet ports. That reduces cost of surgery as well as surgical stress on the body. Due to their small size the blood-contacting surfaces are less than those of other devices. That helps in reducing the risk of infection as well as blood trauma. It also reduces the residence time for blood within rotating impeller region. Axial flow pump has an absence of secondary flow that minimise the risk of flow stagnation. By performing optimisation of design, low stress tip clearance region can be achieved to have minimum traumatic effects on blood components.

Both existing pulsatile and non-pulsatile VAD technologies have their advantages and disadvantages. Both types of VAD systems have complications of bleeding, thrombosis, hemolysis, infection, Right ventricle (RV) dysfunction/failure, device malfunction and in case of continuous flow pump ventricle might collapse in the absence of preload. Displacement type devices produce a pulsatile output, which has significant benefits on vital organ function and end organ recovery after acute or chronic mechanical circulatory support (Undar, 2004). While centrifugal and axial flow pumps produces continuous non-pulsatile flow. However, the implications of long-term continuous flow conditions remain unclear. Pro, non-pulsatile flow investigators have claimed that, there is no difference between pulsatile and non-pulsatile systems in terms of end organ recovery (Undar, 2004). In-depth research has been carried out to determine the effects of providing circulatory support by means of continuous or pulsatile flow. Despite that, choice between pulsatile and non-pulsatile assistance is an ongoing debate, although hundreds of CHF patients have had continuous flow support exceeding thousands of hours (Allen et al., 1997). Pulsatile Devices are noisy and more susceptible to mechanical failure than the continuous flow pumps due to failing membranes and valves (Goldstein and Oz, 2000). While continuous flow pumps are quiet and cannot be heard outside of patient's body.

2.6 Aims and Objectives

This thesis aims to design a novel minimal invasive, miniature axial-flow pump with pulsating outflow to work as a left ventricle assist device (LVAD) for patients with heart conditions including myocardial infarction, myocardial infection, and cardiogenic shock as a *Bridge-To-Recovery (BTR)* or *Bridge-To-Decision (BTD)* device.

This thesis focuses on the design of an axial flow pump that can generate a pulsatile flow by achieving the listed objective.

2.6.1 Objectives

> ➢ Design an axial flow pump that can satisfy the hydraulic and clinical requirement of LVAD.

> ➢ CFD based statistical design of experiment (DOE), investigation of the design parameters to determine the response of the pressure rise, flow rate, and shear stress for the range of the rotating speed of LVAD impeller.

> ➢ Optimisation of the design parameters using Multi Objective Genetic Algorithm, to derive the operating speed of rotation for the low hemolysis level in LVAD.

> ➢ CFD based evaluation of the performance of LVAD as a continuous axial flow pump.

> ➢ In vitro experimental evaluation of LVAD, as a continuous flow pump to validate the CFD model.

> ➢ CFD based evaluation of LVAD as pulsatile axial flow pump, using the validated CFD model and time varying rotating speed of impeller.

> ➢ In vitro experimental evaluation of LVAD as Pulsatile flow axial flow pump.

The main objective of the thesis is to develop a pulsatile flow using an axial flow pump. Conventional design theories presented by Stepanoff, Csanady GT, and Balje OE, for the axial flow pumps focus mainly to generate constant head and flow rate at a constant rotating speed. In absence of the design theory for the pulsatile flow generation using an axial flow pump; it is a difficult task for any designer to derive

the specification for the pulsatile axial flow pump. The basic specifications of conventional axial flow pump are the pressure rise and the mass flow rate, for which the rotating speed of impeller is derived. In case of pulsatile flow pump the pulse are generated based on the heart rate. Hence, heart rate is an added specification along with the pressure rise and flow rate. For the generation of pulse, the LVAD's impeller is accelerated up to the limit speed of rotation and decelerated back to zero, within systolic period of heartbeat according to heart rate. Thus, to find out the limit speed of rotation, which is able to satisfy the hydraulic and clinical requirement of LVAD is a key design objective of the thesis. To investigate the effects of heart rate on the pressure rise and flow rate, the initial design specifications are generated using the traditional design theory. In addition, it provides the base to initiate the study as well as for the evaluation of pulsatile flow.

Chapter 3 Methodology

3.1 Abstract

Designing an implantable medical device requires the broad understanding of the effects of device on the body and effects of body on the device. This chapter illustrates the methods used for the design and development of a pulsatile axial flow blood pump as LVAD that addresses the hydraulic and clinical requirements. The conventional design equations produced a geometrical estimation to initialize pump design. CFD was used to carry out a parametric study using statistical design of experiment and Goal driven optimization of the design parameters. Mesh generation and boundary condition are discussed in detail as they are essential to generate an appropriate mathematical (CFD) model for a reliable design.

3.2 Introduction

Designing an axial flow pump for the generation of pulsatile flow within safe limit of hemolysis is a novel feature and the main objective of this thesis. The important primary step for the design of VAD is to identify the specifications or requirement of VAD for treatment of patients. This thesis demonstrates the method to design axial flow LVAD that can generate pulsatile flow and satisfy the clinical requirement. As shown in figure 3-1, the specifications for LVAD can be divided into two parts that are the hydraulic and clinical requirement.
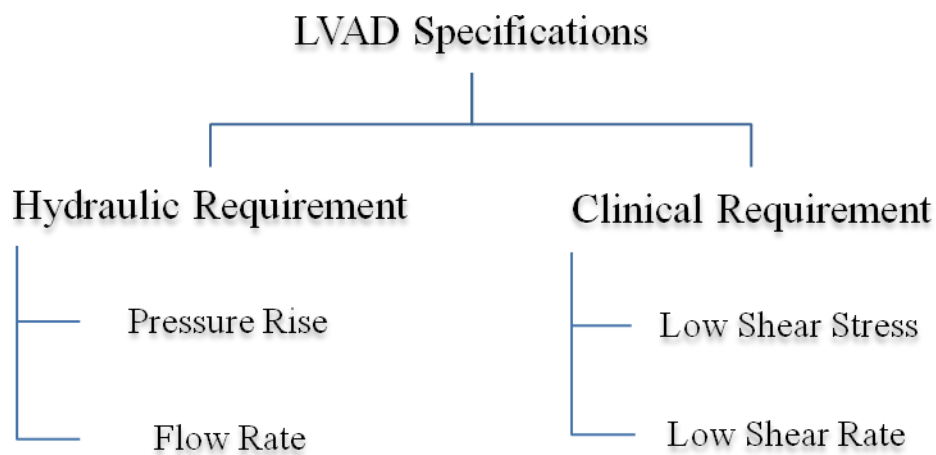
Figure 3-1: specification for VAD

Hydraulic requirements from the LVADs are mainly the pressure rise and flow rate. The patient specific requirements vary according to their heart condition. In general, VAD should be able to generate 60 to 120mmHg pressure rise, with the flow rate of 2 to 12 lit/min (Wood et al., 2005). These pressure and flow rate requirement help in determining the size of pump.

The clinical requirements from the LVADs are mainly low hemolysis and good washout of rotating and non-rotating components. The hemolysis and platelet activation are the consequence of high shear stress acting on the blood components mainly near the tip region of the impeller. Blood is a viscoelastic fluid and its rheological properties mainly viscosity and elasticity are depend on the rate of flow or shear rate. Shear rate that is a product of shear stress and angular velocity is also an important parameter for the designing of VAD. Sallam and Hwang et al. (Sallam and Hwang, 1984) measured approximately a threshold stress level of 400Pa for 100

milliseconds during a turbulent jet experiment where Reynolds stresses dominated the flow field.

In case of implantable axial flow LVAD, the size of pump has clinical constraints based on the surgical procedures as well as the place of installation. Geometry of blade also plays a critical role in generation of pressure head and the flow rate which is also dependent on the rotational speed. Clinical demand emphasis that LVAD should deliver the flow rate according to the physical activities of patient, that means the difference between left ventricular pressure and aortic pressure should be maintained irrespective of the flow rate along with the low hemolysis. According to the theory of axial flow pump, the size of pump and rotating speed of impeller are the important parameters that can deliver the required flow rate and the pressure rise.

In case of pulsatile axial flow LVAD; for the generation of pulse, impeller is accelerated up to the limit speed of rotation and then decelerated back to zero, within systolic period of heartbeat. The rotating speed of impeller never remains constant apart from the halt during diastolic phase of heartbeat. Hence, the heart rate becomes a critical design parameter that can also influence the flow rate, pressure rise and the shear stress.

Design method adopted for the purpose of this thesis is a combination of both classical design and computational fluid dynamics (CFD).

1. Design of axial flow pump is derived to satisfying the hydraulic and clinical requirement of LVAD that is 6L/min of flow rate at 100mmHg pressure head with shear stress below 400Pa.

2. Design of Experiment has been carried out to investigate the response of design parameters for the range of rotating speed up to 30000 RPM.

3. Goal Driven Optimisation using Multi Objective Genetic Algorithm is used to investigate the range of rotating speed that can generate the flow rate and pressure rise with the low level of hemolysis.

4. The axial flow pump performance as a continuous flow LVAD carried out for the optimized range of speed of rotation.

5. The experimental evaluation is carried out for LVAD as continuous flow pump to validate the CFD model and design of experimental study.

6. Using the validated CFD model and time varying the rotating speed, LVAD performance is predicted for the pulsatile flow.

7. Experimental investigation is carried out for the LVAD as a pulsatile axial flow pump to characterise the pressure rise and mass flow rate based on the heart rate.

3.3 Clinical design Criteria of an Implantable LVAD

Design of any implantable device requires comprehensive understanding of the effects of the device on the body and the effects of body on the device. Conventional design theories are helpful for the initial estimation of the size and shape of various rotating and static components of pump. Along with conventional theories, designing a VAD requires consideration of blood compatibility, implantability, durability, portability, control feasibility, and reliability during design phase (Wood et al., 2005).

In order to design a completely implantable pump, the overall size of the device becomes the most important engineering constraint during the initial design phase. Designing a pump with high efficiency and low power consumption helps in minimizing the size of the motor, thereby reducing the overall size of the axial flow pump. If one wished to make the pump as small as possible (small D), this would dictate not only a higher rotational speed, ω, but also higher impellers tip speed $\omega D / 2$. Consequently, the increase in tip speed, suggested above could lead to a cavitation problem (Brennen, 2011). The cavitation number is inversely proportional to the square of the tip speed or $\dfrac{\omega D^2}{4}$. Often therefore, one designs the smallest pump that will still operate without cavitation; this implies a particular size and speed for the device. Generally, industrial pumps are designed to operate at specific design point; at which the pump works with maximum efficiency. While blood pumps are required quite frequently to perform well at off-design conditions (Wu et al., 2004b, Wu et al., 2003, Wu et al., 2004a). Most of adult cardiac failure patients require 6 L/min at 100mmHg pressure rise. VADs must be able to produce flows from 2 to 12 L/min (Wood et al., 2005) for the pressures rise of 60 to 120mmHg (physiological). Depending on the diversity of patients and the level of

their physical exertion (from sleeping to walking to climbing stairs), the VAD must be able to operate over a wide range of flow conditions.

Pump's operational speed is inversely proportional to the pump's size; thus, a smaller pump corresponds to a higher rotational speed of the impeller. A higher rotor speed implies a higher value of fluid stresses, which could have a traumatic effect on blood components. With respect to allowable rotational speed, important limitations are cavitation threshold and maximum allowable shear stress. With respect to blood, this limitation results in the tip speed of 10 m/s for any pump rotor (Reul and Akdis, 2000) . Cavitation is most critical for axial flow pump; likely to occur at the low-pressure inlet section. Longer lasting cavitation can damage the pump as well as blood.

In addition to meeting hydraulic requirements, red blood destruction and platelets activation is one of the most important issues in the design of rotary pump. Rotary pump has the gap between the tip of moving blade and static casing. As shown in figure 3-2. This is responsible for the tip leakage flow as well as the back flow at the inlet, due to pressure difference from inlet to outlet. The back flow and tip leakage flow are associated with turbulent mixing, superimposed by high shear flow in the same region causes the blood damage. Shearing or lysing of red blood cell may compromise the delivery of oxygen and nutrition to muscle or tissues. Formation of thromboemboli can occlude major arteries. This occlusion can result in oxygen deprivation and likely death to surrounding tissue as well as muscle.
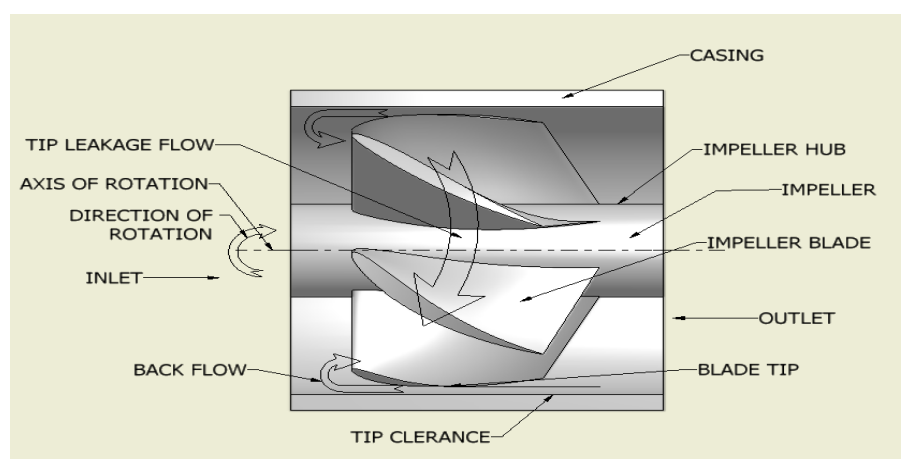
Figure 3-2 : Lateral View Of Impeller Inlet Flow Showing Tip Leakage Flow Leading To Backflow.

Sealing problem between the rotating shaft and static housing is associated with the heat generation and thrombus formation. If this heat generation occurs in low washout areas of the pump, this may lead to local thrombus formation(Reul and Akdis, 2000). Many advanced pump uses blood immersed seals or magnetic bearings as an alternative to mechanical seals.

3.3.1 Hemolysis

Haemolysis is the damage or destruction of red blood cells, which causes the contained protein haemoglobin to be released into blood plasma (Leverett et al., 1972, Skalak and Chien, 1987). The main source of haemolysis in blood pumps is the sub lethal damage of the RBCs due to leaking of haemoglobin (Leverett et al., 1972)rather than catastrophic damage due to rupturing at shear rates above $42,000s^{-1}$.

These released haemoglobin contents within plasma may activate platelets and subsequent clot formation. Continuous lysing or damage of red cells reduces the blood's ability to effectively transport oxygen. Premature haemoglobin release shortens the RBC's normal life span, which is 120 days(Skalak and Chien, 1987) for a healthy person. It also increases risk of morbidity to patients with blood pumps.

The available commercial blood pumps have a range 20-100 N/m^2 of Newtonian shear stress with the exposure time of 1s per passage. For small axial pump stress is considerably higher and can reach the peak value of 400 N/m^2, while exposure time or transition time are in order of 100ms. (Reul and Akdis, 2000) According to *Giersiepen* haemolysis and platelet activation are the function of both shear stress level and transition time or exposure time (Giersiepen et al., 1990). *Heuser* and *Giersiepen* used a two-dimensional regression analysis on their data to establish their empirical formula for the calculation of a haemolysis index (HI) (Heuser and Opitz, 1980, Giersiepen et al., 1990) in percentage.

$$HI = C * \tau^{\alpha} * t^{\beta}$$
(3.1)

Where t is the exposure time (s) and τ (N/m^2) indicates the overall single scalar stress tensor. C, α and β are constants. *Heuser* defined these constants (Heuser and Opitz, 1980) [80] as $C = 1.8*10^{-6}$, $\alpha = 1.991$, and $\beta = 0.765$.

Giersiepen (Giersiepen et al., 1990) defined them as $C = 3.62*10^{-5}$, $\alpha = 2.416$, and $\beta = 0.785$. Data obtained by numerous researchers based on the above formulation corroborate that both models gives values similar to hemolysis in blood pumps (Wu et al., 2010) .

The above correlation is valid for steady shear only, while the flow in the axial flow VAD is three-dimensional and unsteady. Therefore, *Bludszuweit* proposed to calculate τ, representing an instantaneous one-dimensional stress parameter in the above equation (Bludszuweit, 1995b, Bludszuweit, 1995a), by summing the components of the viscous and Reynolds stress tensor:

$$\tau = \left[\frac{1}{6}\sum(\tau_{ii} - \tau_{jj})^2 + \sum\tau_{ij}^2\right]^{1/2}$$

(3.2)

More recently, *Arora* (Arora et al., 2004) have proposed a tensor based blood damage model (optional to the above stress-based model) for CFD analysis. Where Time- and space dependent strain is estimated for individual blood cells, and correlated to data from steady shear flow experiments.

The American Society for Testing and Materials (ASTM) recommends the standard normalized index of haemolysis (NIH) (Thom et al., 2006). The NIH is related to the proportion of *ΔHb* and the total amount of haemoglobin *Hb* as:

$$NIH(g \; per \; 100 \; l \; of \; blood) = 100 \times \frac{\Delta Hb}{Hb} \times (1 - H_{ct}) \times k$$

(3.3)

Where H_{ct} denotes the haematocrit (%), i.e. the proportion of blood volume occupied by RBCs (45% for a healthy person and 37% for normal bovine blood), and κ is the haemoglobin content of the blood (150 g L^{-1} for a healthy person).

3.3.2 Thrombosis

Thrombosis is a formation of a clot or a thrombus, which is one of the protecting mechanisms of the body to prevent the blood loss. Under normal, healthy circumstances, this coagulation system constructively promotes clot growth and repairs the damaged vessels (Wood et al., 2005). Thrombosis is dependent upon three main factors: contact surface properties, the state of the blood cells and the flow environment (Virchow Triad). Nevertheless, irregular flow patterns and inflammatory conditions within the vessels due to genetic, hemodynamic, and dietary factors could produce unnecessary and undesired thrombus formation(Gartner et al., 2000). Therefore, inside VADs, regions of high shear stress, recirculation or stagnation or blood contacting surfaces with low haemocompatibility must be avoided. Hence, for manufacturing of implant, surfaces that are exposed to blood should have excellent biocompatibility (Song et al., 2003c, Song et al., 2003b, Song et al., 2003a).

When the thrombus formation mechanism has been triggered by such non-physiological causes, it can lead to a pathologically high degree of clotting (Behbahani et al., 2009). If a thrombus forms on a surface of the VAD, it may compromise its function, and if it circulates as a free thrombus in the blood stream, it can occlude blood vessels in vital organs(Behbahani et al., 2009) . These thromboembolic incidents count among the primary causes of death for patients with ventricular assist support. With respect to VAD design, the listed situations can give rise to hemolysis and thrombosis (Wood et al., 2005) as well as platelet activation/deposition.

1. Recirculation regions
2. cavitation
3. high shear stress areas
4. extremely low shear stress areas
5. flow separation regions
6. surfaces with sharp edges
7. surfaces with high roughness
8. narrow passages within the pump
9. Flow stagnation leading to blood pooling

In summary, the conditions that might lead to hemolysis, thrombosis, and platelet activation in blood pump must be eliminated or minimised during the design phase. With careful design and iterative optimisation of design, these traumatic conditions can be avoided.

3.4 Theory of Axial Flow Pump Design

The physics of axial flow pump presented here is given as a means for determining the outline dimensions of an axial flow pump. Assuming a "free vortex" means there is no head change radially as well as constant axial velocity through the annulus. The input to this classical pump design procedure is the performance specification for design, based on VAD design criteria.

Pump transfer its energy to flowing fluid via impeller. Hence, the impeller is the most important region of VAD which defines its operating range. Impeller receives its energy from an electric motor. Basic design expression of an impeller is a form of Newton's law of motion applied to fluid flowing through the impeller, which states that the torque on the impeller is equal to the rate of change of angular momentum of the fluid (Balje, 1981, Csanády, 1964, Stepanoff, 1957).

$$\mathbf{T} = m(V_{u1}r_1 - V_{u2}r_2) \tag{1}$$

$$V = W + U \tag{2}$$

Equation-1 defines the torque "$\mathbf{T}$" as a function of the mass flow rate "m", the radii (r_1 and r_2) and the tangential absolute velocities (V_{u1} and V_{u2})(Stepanoff, 1957). Derived from Euler's velocity triangles. Equation-2 expresses the absolute fluid velocity "V" as a sum of the relative velocity of fluid "W" with respect to the moving blade and the blade velocity "U", related velocity triangles are shown in figure 3-3.

Pump's power "P" can be derived from torque "T" with rotational speed "Ω" in radians per second, power "P" can be written as

$$P = m(Vu_1 U_1 - Vu_2 U_2) = \Omega T \tag{3}$$

Where the blade speed, U_n, is equivalent to Ωr_n (n representing 1 or 2 to signify inlet or outlet Location, respectively).

By dividing Equation-3 by the mass flow rate "m" and gravity "g", we can derive head equation as

$$H_{th} = \frac{1}{g}(U_2 V_2 - U_1 V_1) = \frac{U_2 V_2}{g} \tag{4}$$

Equation-4 represents the well-known Euler's head equation, where H_{th} corresponds to a theoretical head or pressure as idealized flow has been assumed and hydraulic losses have been ignored.
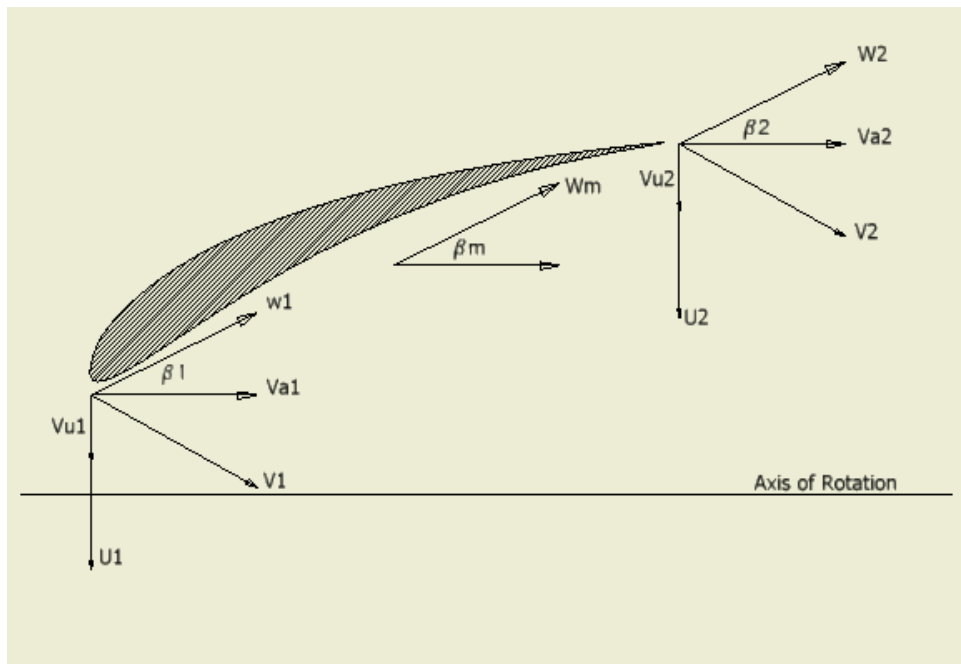
Figure 3-3: Velocity at Inlet and Outlet

Equation 1, 2, 3 & 4 are applied for much larger capacity pumps those used in industrial application where inertial forces dominates the viscous forces which are important in case of VAD.

Dimensionless parameters that are a consequence of dimensional analysis are used to have initial design estimation of an impeller. This parameters relate performance characteristics with the density of the fluid, ρ, the typical rotational speed, N, and the typical diameter, D, of the pump. Thus the volume flow rate through the pump, Q, total head rise across the pump, H, torque, T, and the power absorbed by the pump, P, will scale according to equations mentioned below,

Flow co-efficient "Φ"

$$\phi = \frac{Q}{ND^3} \tag{5}$$

Head co-efficient "ψ"

$$\psi = \frac{gH}{N^2 D^2} \tag{6}$$

Specific Speed "Ns"

$$N_S = \frac{\phi^{\frac{1}{2}}}{\psi^{\frac{1}{4}}} = \frac{NQ^{\frac{1}{2}}}{gH^{\frac{1}{4}}} \tag{7}$$

Specific diameter "Ds"

$$D_S = \frac{\psi^{\frac{1}{4}}}{\phi^{\frac{1}{2}}} = \frac{D(gH)^{\frac{1}{4}}}{Q^{\frac{1}{2}}} \tag{8}$$

Power co-efficient "Cp"

$$C_P = \phi\psi = \frac{P}{\rho N^3 D^5} \text{ where } P = \rho QgH \tag{9}$$

Reynolds number "Re"

$$R_e = \frac{ND^2}{v} \tag{10}$$

These simple relations allow basic scaling predictions and initial design estimates as well as the performance prediction of the pump. Overall size of pump has limitation of available space in the ascending aorta.

As the proposed pump is intended to be placed at aortic root, the overall size of pump needs to be selected according to output mass flow rate taking viscous forces in to account using equation,

$$II_4 = \left(\frac{D}{v}\right)\left(\frac{Q}{D^2}\right) = \frac{Q}{vD} \tag{11}$$

This equation-11 is a form of a Reynolds number, in which the impeller diameter D presents the size of pump, v kinematic viscosity, and Q/D^2 the velocity(Stepanoff, 1957). Placing the Reynolds number of ascending aorta at the left side of equation the outer diameter can be derived. Using this outer diameter for an impeller, specific diameter "Ds" can be derived using equation- 9. That can be rewritten as,

$$D_{tip} = \frac{D_s Q^{\frac{1}{2}}}{(gH)^{\frac{1}{4}}} \tag{12}$$

Based on cordier diagram (Csanády, 1964) for axial flow pump Relationship between specific diameter "Ds" and specific speed "Ns" can be approximated by equation,

$$D_S = \frac{2.95}{N_s^{0.485}} \tag{13}$$

Generally axial flow pump have dimensional hub to tip ratios in the range of 0.3 to 0.7 which is directly connected with the specific speed of pump. That can be determined by the chart presented in Stepanoff AJ (Stepanoff, 1957) . Solidity that is a chord spacing ratio can be determined by the chart available in the same reference. This chord spacing ratio is important in determining the degree to which the flow is guided by the blades. As mention by Earl Logan R. (Logan, 1981) the relation between solidity, hub-tip ratio and specific speed can be approximated by,

$$\frac{C}{S} = \frac{10}{(Dr/Dt)N_S^{1.5}} \tag{14}$$

Where "c" represents the chord length, "s" is the space between the blades, "D_r" is the hub diameter while "D_t" is the tip diameter.

The annular flow area and flow rate can now be used to calculate the axial velocity component "V_a", where

$$V_a = \frac{4Q}{\pi(D_t^2 - D_r^2)} \tag{15}$$

The blade speed "U" can be calculated using

$$U = \frac{ND}{2} \tag{16}$$

Where, "N" is the rotational speed in radians per second and "D" is diameter.

The inlet Velocity diagram shown in figure 3-4 helps in determining the inlet flow angle "β_1".

$$\beta_1 = tan^{-1}\frac{U}{V_a} \tag{17}$$
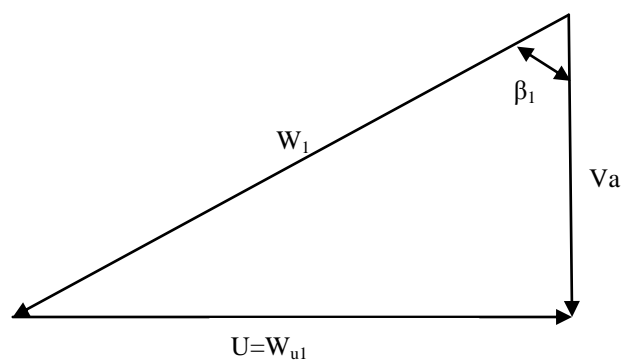
Figure 3-4 Velocity Diagram at Rotor Inlet

Similarly, the flow angle "β_2" can be calculated using velocity diagram at outlet of an impeller shown in figure 3-5. As same annular flow area is available at inlet and

outlet of axial flow pump, the axial velocity "V_a" remains same for outlet which is already derived.
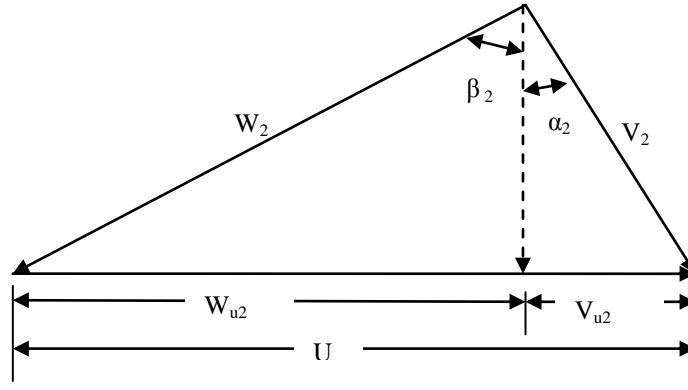
Figure 3-5: Velocity Diagram at

Impeller Outlet

With known pressure rise across pump or head and no inlet whirl *(V_{u1}=0),* we can calculate the whirl velocity at outlet "V_{u2}"using

$$V_{u2} = \frac{gH}{\eta_H U}$$

(18)

The exit flow angle "β_2"can be easily calculated using geometric relation

$$\beta_2 = tan^{-1} \frac{U - V_{u2}}{V_a}$$

(19)

After deriving these flow angles, a calculation for the blade angle is an iterative process. That includes the calculations of incident and deviation angles for subsequent derivation of camber angle.
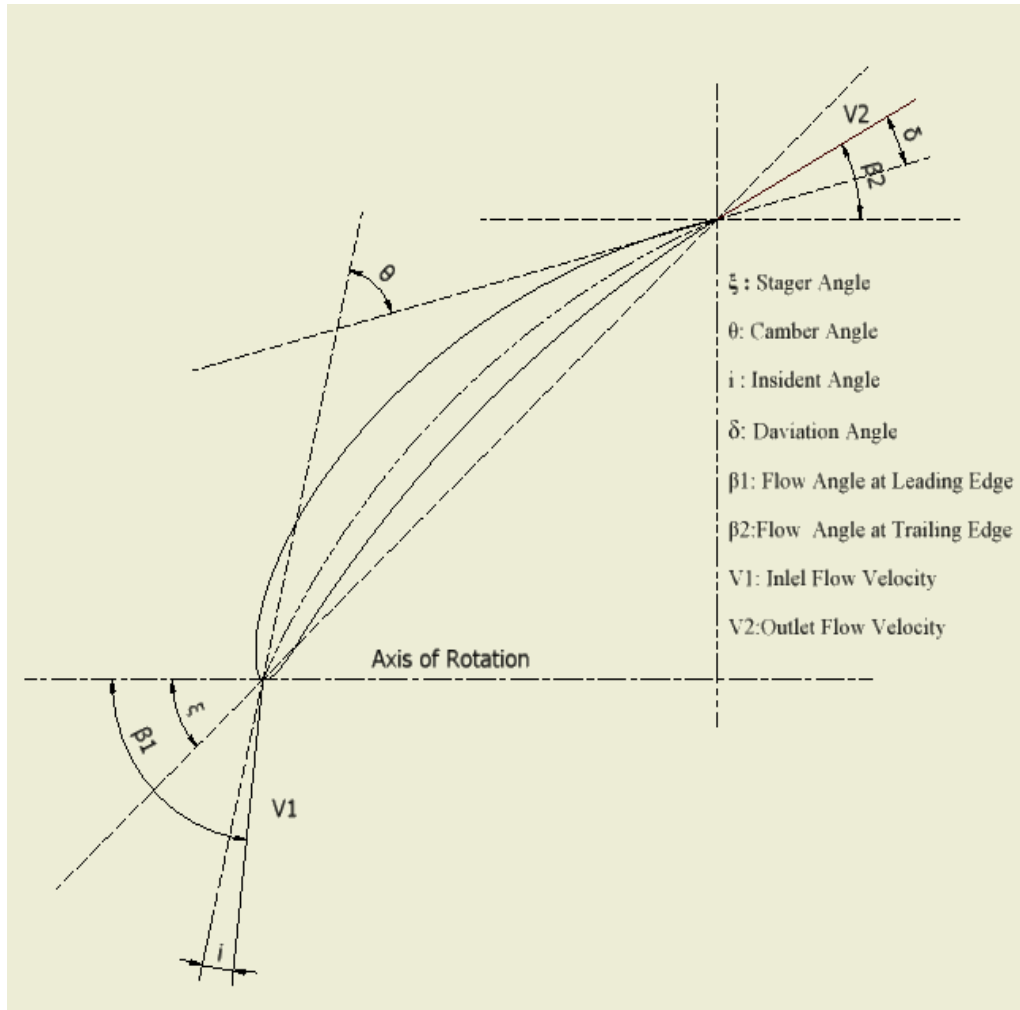
Figure 3-6: Impeller blade angle

The reference (Howard, 2001)contains the related correlations and equations based on Johnsen and Bullock (1965), which commonly is referred to as NASA SP-36 correlations. Considering reference (Howard, 2001) calculation of incident angle, which is the difference between the inlet blade angle and the inlet flow angle, can be derived using

$$i = k_{sh}k_{it}i_o + n\theta \tag{20}$$

Where, i is an incident angle and "k_{sh}" is the correction factor for blade shape and k_{it} is the correction factor for blade thickness. "k_{sh}" differs for the different blades shape as shown in table 3-1.

k_{sh}	Blade shape
0.7	DCA
1	NACA 65-series
1.1	C-series

Table 3-1: Values of ksh for Different Blade Shapes

"k_{it}"can be calculated using percentage of thickness by,

$$k_{it} = -0.0214 + 19.17\left(\frac{t}{c}\right) - 19.17\left(\frac{t}{c}\right)^2 + 312.5\left(\frac{t}{c}\right)^3 \tag{21}$$

And "i_o" can be derived based on percentage of thickness using,

$$i_0 = (0.0325 - 0.0674\sigma) + (-0.002364 + 0.0913\sigma)\beta + (1.64 * 10^{-5} - 2.38 * 10^{-4})\ \beta^2 \tag{22}$$

The variable "n" represents the incident slope factor which can be derived using,

$$n = (-0.063 - 0.02274\sigma) + (-0.0035 + 0.0029\sigma)\beta - (3.79 * 10^{-5} + 1.11 * 10^{-5}\sigma)\ \beta^2 \tag{23}$$

Values of , "σ" & "β" in in the above polynomial equations can be found out in charts and tables available in reference (Howard, 2001).

Deviation angle which is the difference between the blade angle from the trailing edge and the exit flow angle can be derived using equation below which enables designer to use classical Carters rule (Csanády, 1964).

$$\delta = \frac{m_c\theta}{\sqrt{\sigma}} + x \tag{24}$$

Where,"δ" is deviation angle," "m_c" is an empirical function of stager angle, "θ" is camber angle, **"s"** is solidity, and "x" is an experimental factor. This angle is depends on camber angle and stager angle, this makes quite difficult to calculate its

value. One early empirical relation mention in reference (Brennen, 1994) relates the deviation angle to the camber angle "θ", and the solidity, "s/c", through

$$\delta = \frac{0.26\theta}{\sqrt{\frac{s}{c}}} \tag{25}$$

As mentioned in reference (Howard, 2001) deviation angle can be derived using similar equation to incident angle which is,

$$\delta = k_{sh}k_{\delta t}\delta_0 + m\theta \tag{26}$$

"k_{sh}" has the same values mention in table 3-1 while $k_{\delta t}$ can be calculated using

$$k_{\delta t} = 0.0142 + 6.172\left(\frac{t}{c}\right) + 36.63\left(\frac{t}{c}\right)^2 \tag{27}$$

"δ_0" is the deviation angle based on percentage of blade thickness

$$\delta_0 = (-0.0443 + 0.1057\sigma) + (0.0209 - 0.0186\sigma)\beta + (-0.0004 + 0.00076)\beta^2 \tag{28}$$

Variable "m" represents the deviation slope factor by,

$$m = \frac{m'}{\sigma^b} \tag{29}$$

Where
$$b = 0.9655 + 2.538*10^{-3}\beta + 4.221*10^{-5}\beta^2 - 1.3*10^{-6}\beta^3 \tag{30}$$

The "m'" is the modified slop factor that has different values for DCA, NACA & C-series profiles, For NACA-65 series

$$m' = 0.17 - 3.33*10^{-3}\beta(1 - 0.1\beta)\beta \tag{31}$$

For DCA & C- series profile

$$m' = 0.249 + 7.4*10^{-4}\beta - 1.32*10^{-5}\beta^2 + 3.16*10^{-7}\beta^3 \tag{32}$$

Values of "β", "σ", "m'" and "b" in above polynomial equations can be found out in charts and tables available in reference (Howard, 2001).

Once the values of incedent angle and deviation angle is calculated the blade angle "β_{b1}"and "β_{b2}" can be derived using

$$\beta_{b1} = \beta_1 - i \tag{33}$$

$$\beta_{b2} = \beta_2 - \delta \tag{34}$$

Using this "β_{b1}"and "β_{b2}" camber angle"θ" can be calculated using

$$\theta = \beta_{b1} - \beta_{b2} \tag{35}$$

Approximate value for stagger angle "ξ" can be calculated using

$$\xi = (\beta_1 - i) - \frac{\theta}{2} \tag{36}$$

The next important step is to calculate the co-ordinates of blade profile according to the calculated values in previous steps. Through the span of an impeller blade, coordinates of cross sectional profile needs to be calculated from hub to shroud. The mathematical approach is used for determining the aerofoil cross sectional profile. Compare to charts and tabular data to obtain the cross sectional profile, this approach helps to get direct generation of profile coordinates by incorporating equations with a computer program (Wallis, 1983). It also makes it easier to determine the values of area, centroid location, and moment of inertia for aerofoil shape blade profile.

As depicted in figure 3-7, Impeller Blade cross section has three main curves namely camber line, upper surface and lower surface.

Calculation of coordinates for Mean line or camber line can be done by using equation for the x values of chord length as mentioned below

For x < 0.2025

$$Yc = \left[\left(\frac{0.5}{\sin\frac{\theta}{2}} \right)^2 - (x - 0.5)^2 \right]^{\frac{1}{2}} - \frac{0.5}{\tan\frac{\theta}{2}} + [120.5d(x^3 - 0.6075x^2 + 0.1147x)] \tag{37}$$

For x > 0.2025

$$Yc = \left[\left(\frac{0.5}{sin\frac{\theta}{2}}\right)^2 - (x - 0.5)^2\right]^{\frac{1}{2}} - \frac{0.5}{tan\frac{\theta}{2}} + d(1-x)$$ (38)

Figure 3-7: Cross section of an Impeller Blade

Where θ is the camber angle, d is the variable that varies between 0% - 3% for generation of composite camber line, for NACA 65 series. Coordinates of Upper surface of the profile can be derived using,

$$x_u = x - y_t \sin\varphi$$ (39)

$$y_u = y_c + y_t \cos\varphi$$ (40)

In a same manner the coordinates of Lower surface can be derived using,

$$x_l = x + y_t \sin\varphi$$ (41)

$$y_l = y_c - y_t \cos \varphi \tag{42}$$

Where angle $"\varphi"$ is given by,

$$\tan \varphi = \frac{dy_c}{dx} \tag{43}$$

Calculation of thickness function $"y_t"$ depends on the profile selected by designer. For NACA series of blade profile, which is used for the development of VAD, $"y_t"$ is calculated using,

$$\pm y_t = \frac{t}{0.20} \left(0.29690\sqrt{x} - 0.12600x - 0.35160x^2 + 0.28430x^3 - 0.10150x^4\right) \tag{44}$$

Where *"t"* is the percentage of thickness .that can be derived using last two numbers of NACA series and dividing those two numbers by 100. For example, for a unit chord length of NACA 6510 profile has 10% of maximum thickness at position 0.5 of the chord from the leading edge with maximum camber of 6%. The NACA 65 series aerofoils are defined in terms of mean camber line designated by "C_{L0}" This value can be obtained from the reference (Wallis, 1983). The related camber line can be obtained by multiplying the "C_{L0}" value with the values of camber line coordinates.

3.4.1 Limitations of Theory

The thesis objective of pulse generation and VAD design criteria demands the off-design performance from impeller to meet the varying physical demand of oxygen and nutrition for vital organ function. This generates a logical disagreement, with the assumption of constant axial flow through the annulus.

Time varying demand of flow and pressure rise across the impeller represents the need to constant change in the shape of blade that includes the blade angles, length, and the thickness of blade. In theory, we can determine these time varying changes in the shape of the blade, but practical application of these changes in the real world is a technical challenge. Future advances in technology might help in overcoming this technical challenge.

Hence, this thesis focuses on the operating parameters and optimisation of these parameters to pursue its original goal of pulse generation. Despite the differences, assumption of constant axial flow is an essential for calculating the size and shape of VAD components, mainly Impeller.

Generation of pulse according to varying heart rate requires an impeller to be accelerated up to its designed RPM and then decelerated to rest in a cyclic manner as shown in figure 3-8. To operate LVAD in time varying operating condition represent the need to fix the maximum limt (design limits) of RPM for impeller with least traumatic effects on blood components.
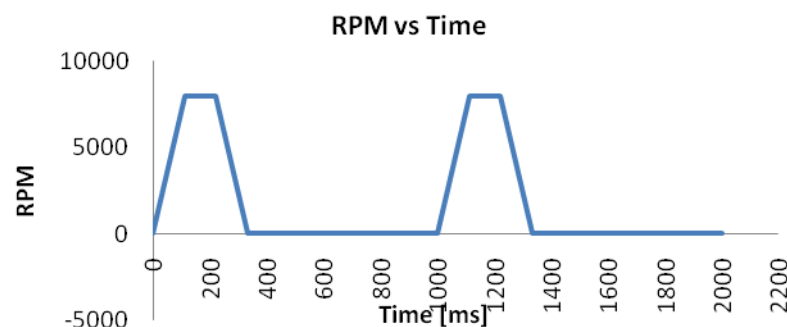
Figure 3-8: RPM Vs Time

The intention behind the optimisation process is to derive optimum speed of rotation by satisfying design criteria and objectives. Shaft's rotational speed is a control

parameter on which all other parameters are dependent, and can be controlled physically by controlling motor speed.

3.5 Computer Aided Design (CAD) of an Axial Flow Pump

Computer aided design (CAD) is helpful in visualising derived geometry using classical theory. For the purpose of this thesis and study, commercially available CAD tool CATIA has been used to develop 3D geometry of various components of VAD. Geometry creation for an impeller requires the skill to generate surfaces for complex impeller geometry, while other components can be modelled with basic parametric geometry functions.

The calculation procedure gives the profile of blade and others geometric parameters on a 2D surface for the each span wise location from hub to shroud. These 2D shapes can be visualised as they are lying on unfold cylindrical surfaces, which has a rectangular shape, with πD as its base length and Hub length as its height. For easy understanding of the concept, only two layers of blade profiles were used to generate figures.

It is very important to decide the axis of rotation at this stage of design. It is advisable to use the default origin of X, Y, Z coordinates and default axis and plane. That smoothes the transfer of geometry data from one design packages to another as well and their use in meshing and simulation software.

The model shown in figure 3-9 uses x-axis as an axis of rotation to place all the calculated coordinates on XY plane. The hub surface can be created by drawing circle with hub diameter on YZ plane and extruding it in the direction of X-axis. As shown in figure 3-9.

For generation of a 3D impeller blade, all the calculated profiles based on its location form hub to shroud needs to be placed on respective 2D planes form hub to tip as shown in figure 3-9.
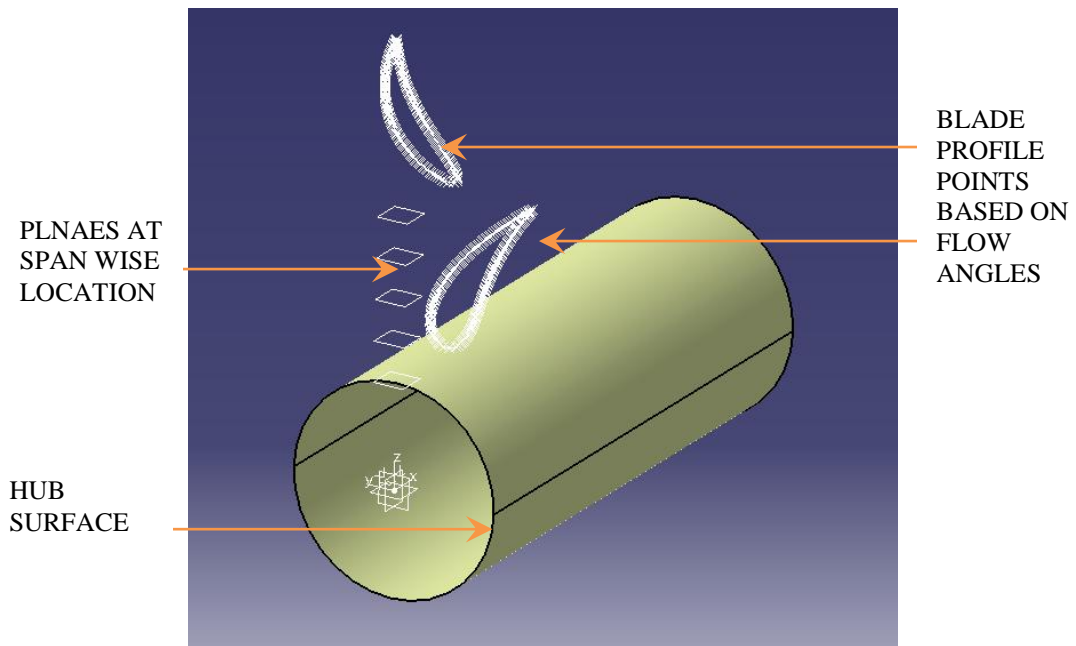
Figure 3-9: Hub and blade profile

Spline curve can be use to generate profile of blade on 2D plane. As shown in figure 3-10 this profile is then projected on the hub surface to get the exact shape of blade on hub surface.
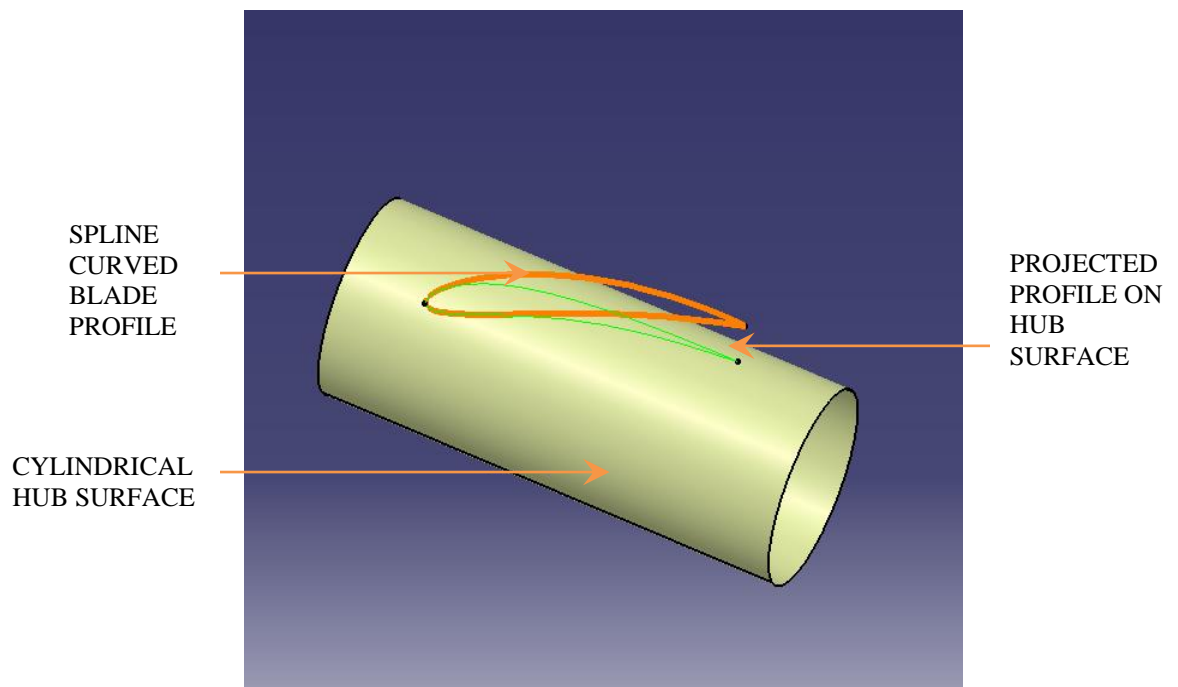
Figure 3-10: Projection of blade profile over hub surfaces.

By following this step for every span wise 2D profile and the derived cylindrical surfaces, the skeleton of blade can be constructed. As shown in figure 3-11.

CONNECTING CURVE FOR TRAILING EDGE

BLADE PROFILE AT SHROUD

CONNECTING CURVE FOR LEADING EDGE

BLADE PROFILE AT HUB
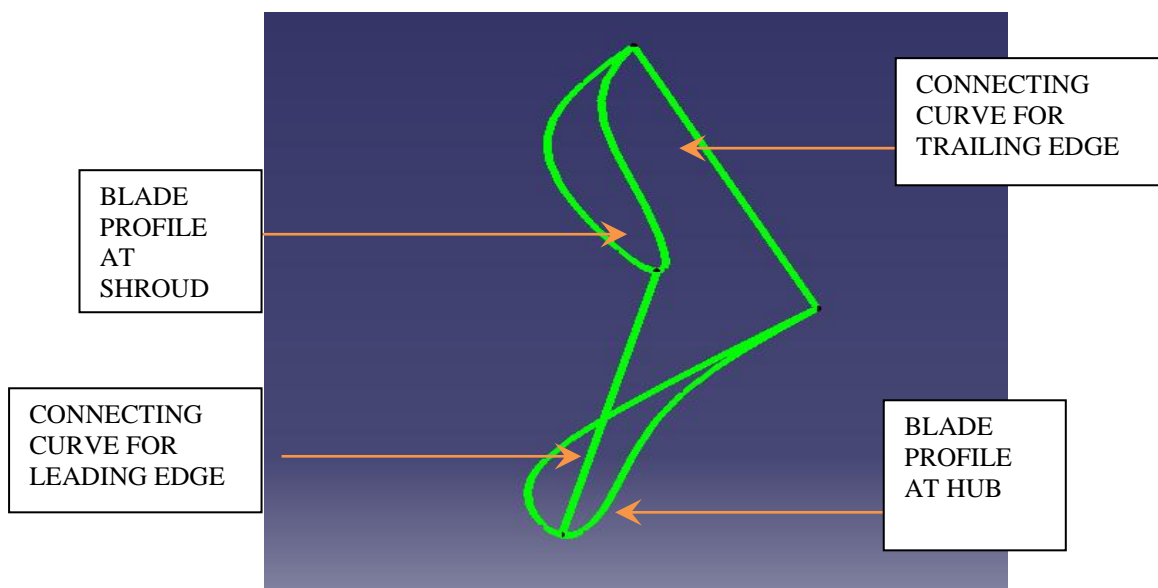
Figure 3-11: Skeleton of Blade Profile in 3D

Using the base curves generated from above step the blade shape can be formed by filling those curves with surfaces. As shown in figure 3-12.
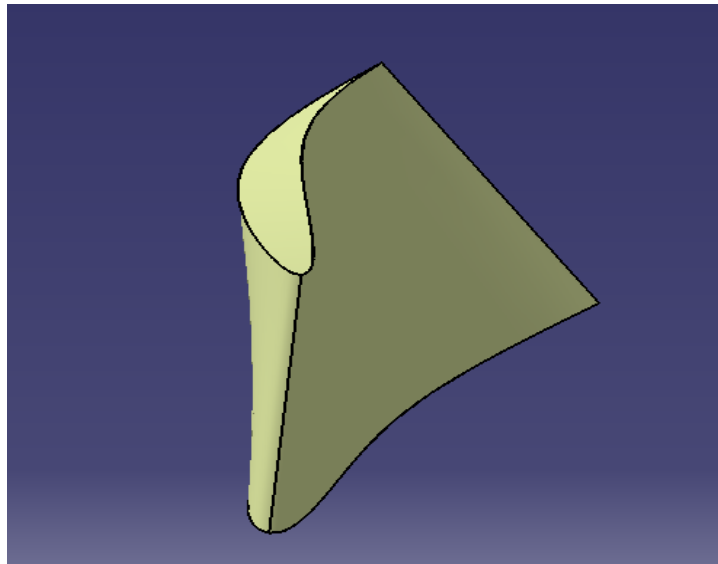
Figure 3-12: 3D Impeller Blade

The advantage of CATIA is its ability to generate hybrid of surface and solid geometries. Using the surfaces of blade and hub, the solid geometry of an impeller can be constructed as shown in figure 3-13.
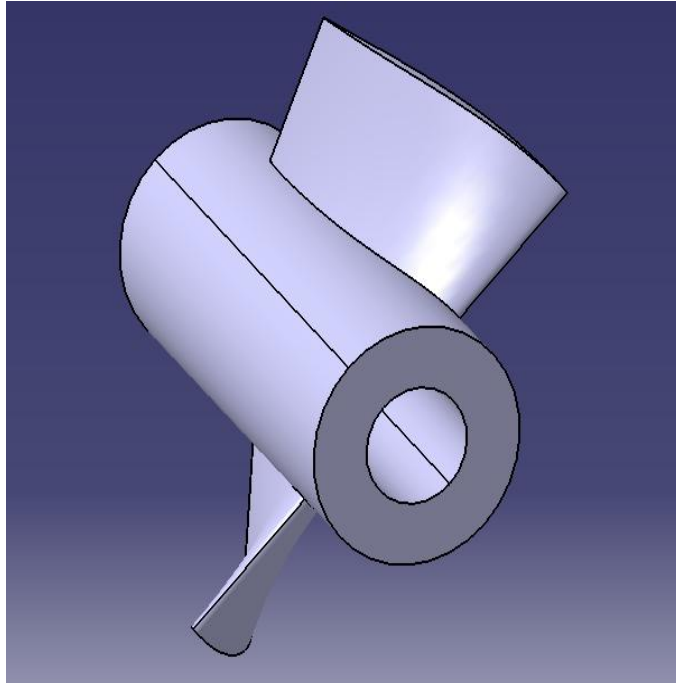
Figure 3-13: Blade Impeller Used for the VAD

3.6 Computational Fluid Dynamics (CFD)

Obtaining a satisfactory design of a pump is an iterative procedure. The derived values of design parameters need an experiment to support the design theory and hypothesis. An experiment at every stage of design procedure can be very expensive and time consuming. Numerical tools like computational fluid dynamics (CFD) can be employed in the early stages of the design process as well as in later stages of optimisation. Along with added benefits of the detail flow visualisation and goal oriented optimisation codes, CFD is a very useful tool for reducing numbers of experiments required for the design of a blood pump.

The pump impeller is a solid object that generates the pressure difference across the pump by rotating within fluid region. In order to study the flow behaviour across the impeller this fluid regions needs to be created using the 3D CAD geometry of an impeller. For the purpose of this thesis and study commercially available "ANSYS CFX" (Ansys Inc., Canonsburg, PA, USA) software has been used. Ansys platform support the smooth flow of data amongst various meshing and numerical tools.

3.6.1 Converting CAD geometry for CFD Analysis

"TurboGrid" is an interactive hexahedral grid generation tool available in ANSYS platform, specifically designed for turbomachinery. Turbo Grid requires the hub curve, shroud curve and the blade curve as an input to create rotating fluid domain. Generation of coordinates of impeller is an essential part of the procedure. That can be done via meshing software available in ANSYS platform. Procedure to incorporate 3D geometry of an impeller within TurboGrid for modelling of fluid region is as follows,

Coordinates for Hub & shroud curves are defined using coordinates of line for the respective geometry. For meshing the solid geometry of an impeller these line needs to be labelled to extract the coordinates of hub, shroud and blade as shown in figure 3-14.
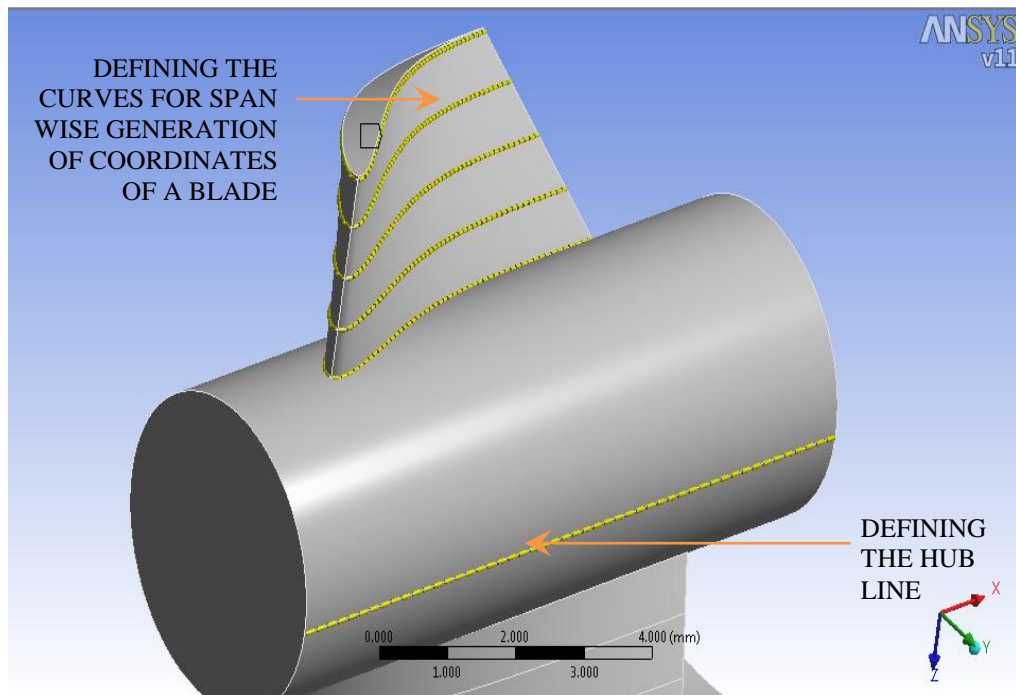
Figure 3-14: Defining the Hub, Shroud & Blade Profile for Generation of Coordinates Required by TurboGrid

All the coordinates should be saved in separate text file with an extension of *.curve or *.crv

Machine data required for the generation of passage of a fluid domain needs to be provided before loading the curve files. That requires the selection of numbers of blade, axis of rotation and units of machine. Select the axis of rotation, which was defined while making 3D solid geometry of an impeller.

Load the hub & shroud curve and blade curve in the details of hub, shroud, and blade set. TurboGrid is pre-programmed with several templates tailored to the complex curvatures of various types of turbomachinery to generate the fluid region and structured mesh of that region. The figure 3-15 shows 3D fluid region generated by TurboGrid based on machine data.
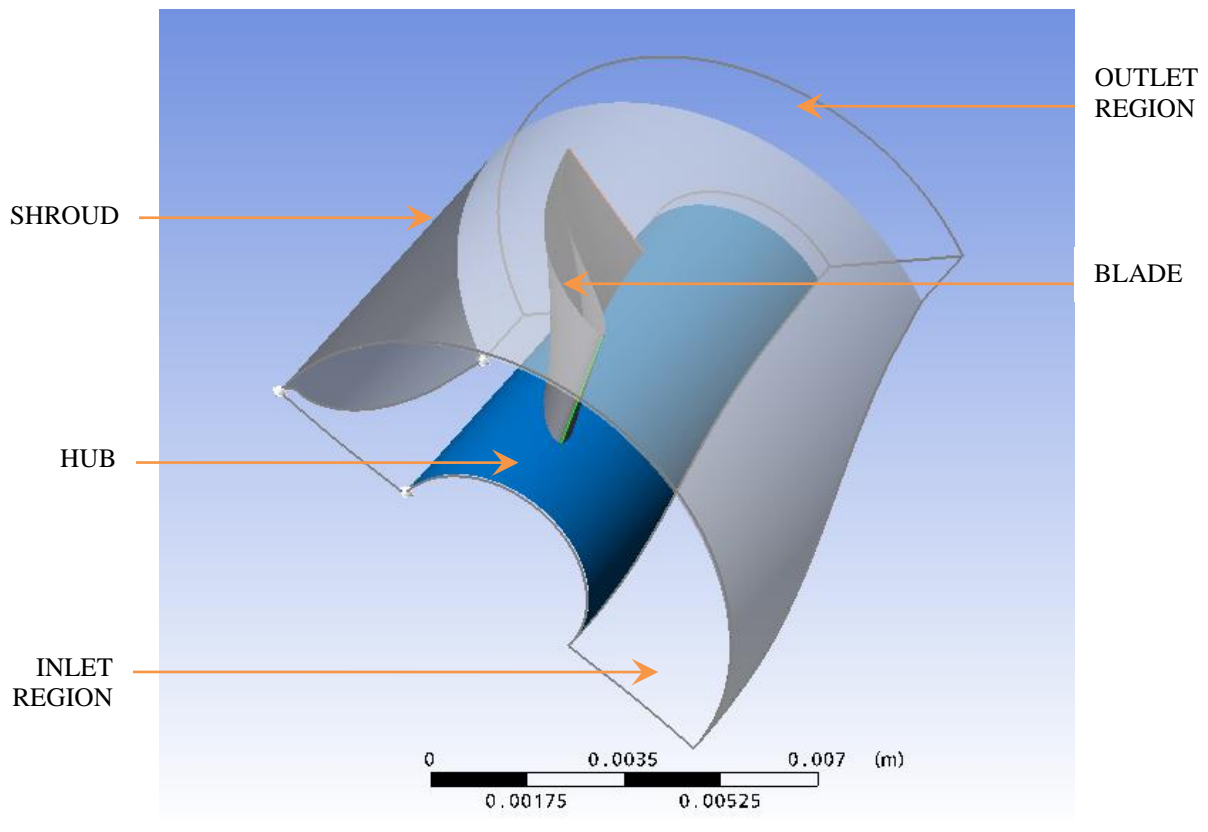
Figure 3-15: Fluid Region Generated By TurboGrid

3.6.2 Mesh Generation

Generation of computational mesh is a vital prerequisite to achieve reliable numerical solution for turbomachinery configurations. Mesh can be a mono domain or multi domain structured, unstructured or hybrid. Based on AGARD-AR-355 (AGARD-AR-355, 1998) listed grid characteristics can have significant affects on accuracy of computational results,

1) Grid type
2) Grid size
3) Near wall characteristic, including normal spacing and cell aspect ratio
4) Grid distortion parameters, including stretching and skewness
5) Tip clearance treatment

Structured mono domain H-grid gives good results for far-field and periodicity conditions while it is not good at near wall region of leading and trailing edge due to

its highly skewed formation (AGARD-AR-355, 1998). A C-grid provides good resolution near leading edge and in wake, but became skewed near inflow and in the wake. While an O-grid gives good resolution, near leading edge and trailing edge but include skewness at inflow, outflow, and periodic boundaries. Use of unstructured tetrahedra gives greater flexibility in mesh generation process but they are less efficient in CPU time compare to structured mesh, however tetrahedral meshes are less tolerant of high aspect ratio, which generally occurs near solid wall boundaries (AGARD-AR-355, 1998). Hybrid meshing approach uses different types of structured and unstructured meshes in a way that makes use of the best of both approaches.

Numbers of investigators have studied the effects of grid size on accuracy of results. Generally this study has shown that an average grid with 200000 points is necessary to capture satisfactory performance characteristic(AGARD-AR-355, 1998). Much finer grid with more than 1000000 points might require isolating the detailed flow features such as secondary flow and tip clearance flow. By using wall function for near wall region the overall number of grid, points can be reduced.
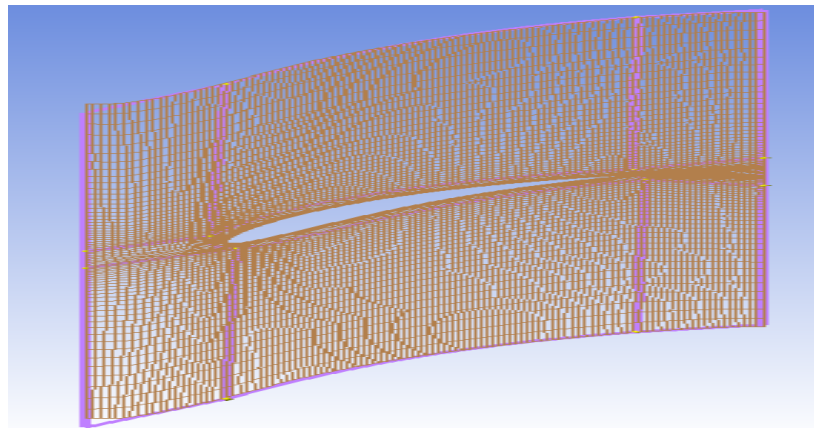
Figure 3-16 Grid distribution over shroud

Grid spacing near to wall and the cell aspect ratio affects the solution accuracy locally in the near wall region of the wall shear layers. A general guideline for calculation suggest the use of Y^+ less then 1,which ensures that the first point of wall lies within the viscous sub-layer of the boundary layer (AGARD-AR-355, 1998) . However, it depends on the turbulence model used for calculation, in contrast

to this guideline, majority of investigators have suggested Y^+ value in between 20 to 60.
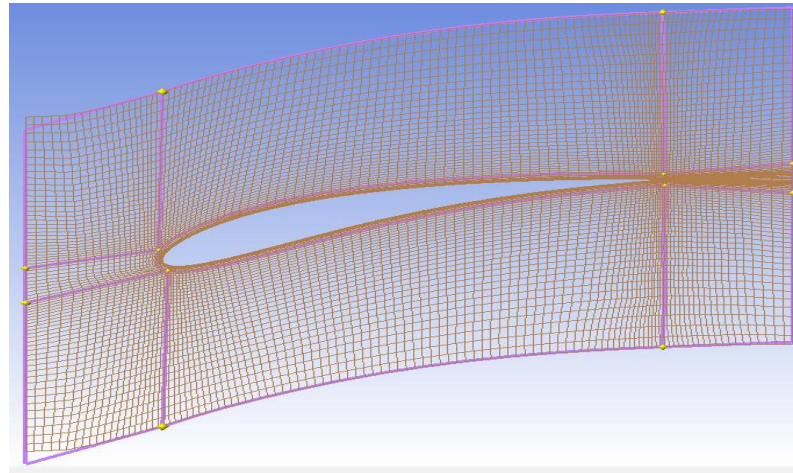
Figure 3-17 Grid distribution over Hub
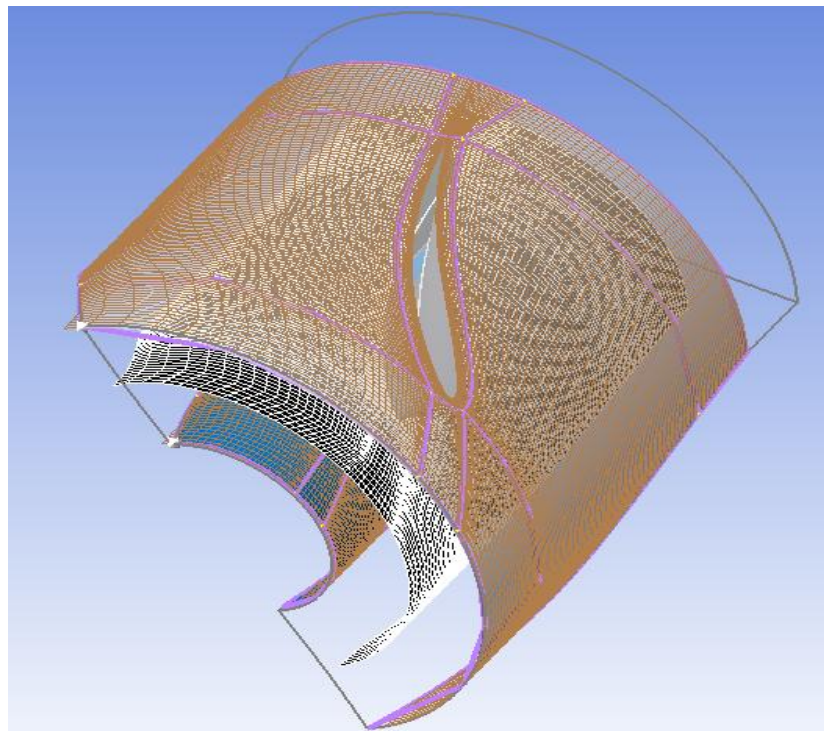
Figure 3-18 Spanwise layers of 3D volume mesh

Cell aspect ratio near the blade and end wall surfaces can become extremely large as points are grouped in those regions (AGARD-AR-355, 1998). Typical recommended values for cell aspect ratio are in the range of 200 to 800.

Grid distortion can be characterised by the degree of grid stretching in any coordinate direction and the degree of grid skewness or shear between any two coordinates(AGARD-AR-355, 1998). The cell-to-cell size ratio should be less than 1.3.

Considering the recommended values for meshing designed impeller: these have been meshed using hybrid structured mesh with C-grid, H-grid and O-grid for better results is as shown in figure 16, 17, 18, 22.

For the purpose of the thesis, the CFD flow domains were generated for the experimental setup that includes the inlet and outlet ducts along with the rotating impeller region [figure 3-19].
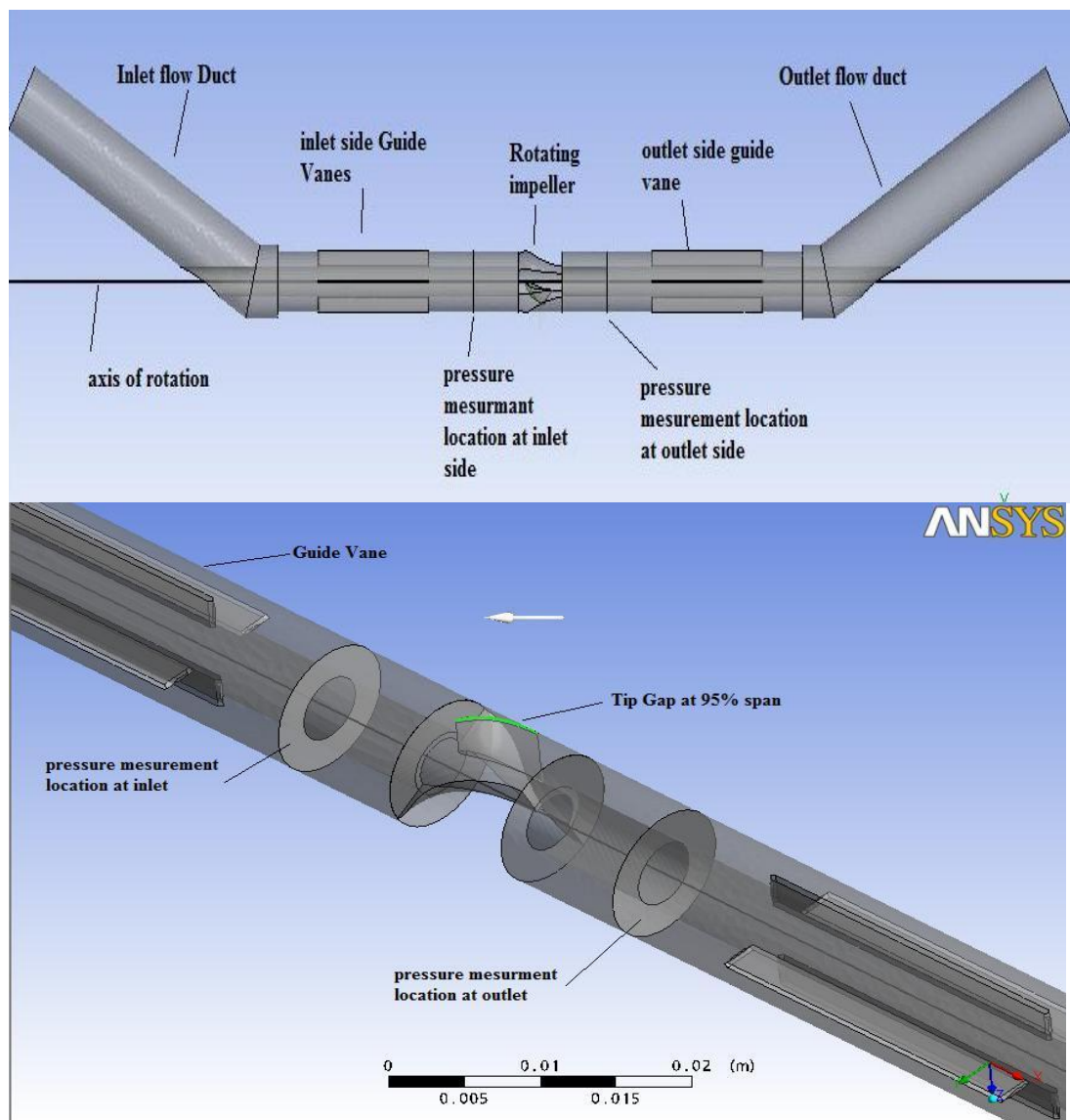
Figure 3-19 Fluid Domain of Experimental Setup

For the entire flow domain, the mesh has been generated using 730604 elements that include prismatic inflation layers at walls of ducts and guide vane along with tetrahedra elements [figure 3-20] that are generated using Ansys CFD meshing tool.
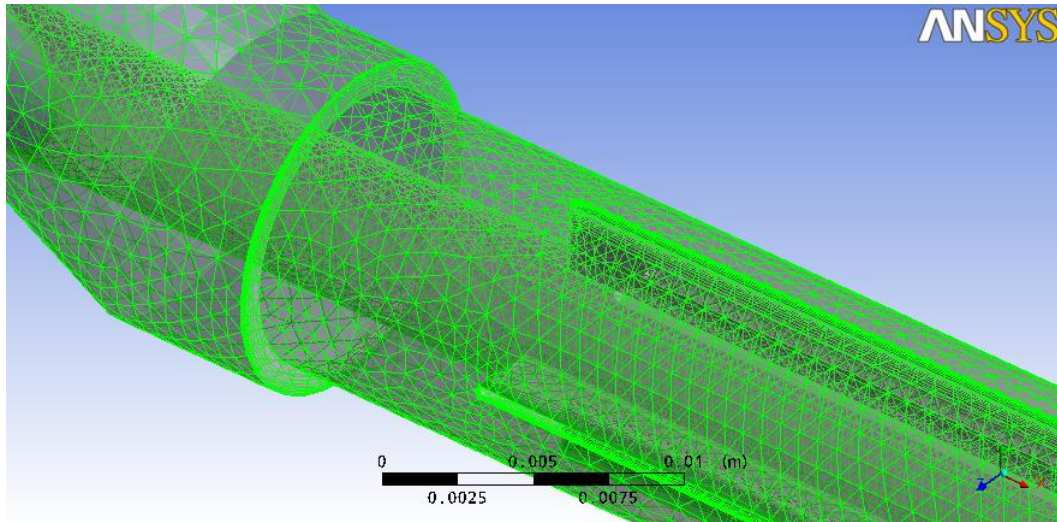
Figure 3-20: Mesh For Static Inlet Duct with Prismatic Layers at Wall surfaces

Rotating fluid region is generated by Ansys TurboGrid using H, J, C, L and O gird with 280708 nodes and 264302 elements per passage of rotating fluid domain. [Figure 3-21]. For rotating mesh generation, the span wise blade distribution parameters are specified using boundary layer method. The Reynolds number 4000 along with y+ 0.1 were used to generate the mesh.
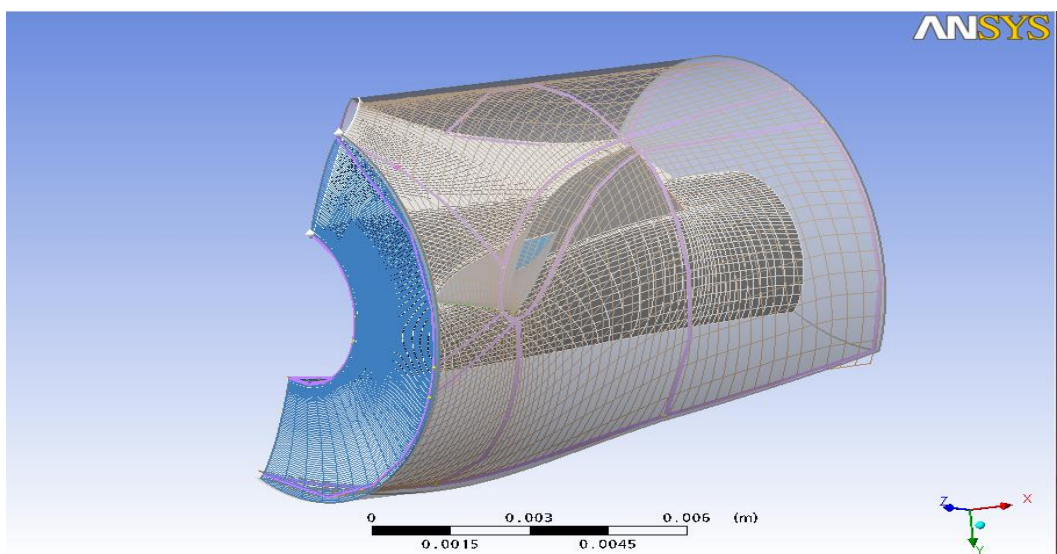
Figure 3-21 Hybrid Structured Hex Mesh for Rotating Fluid Domain
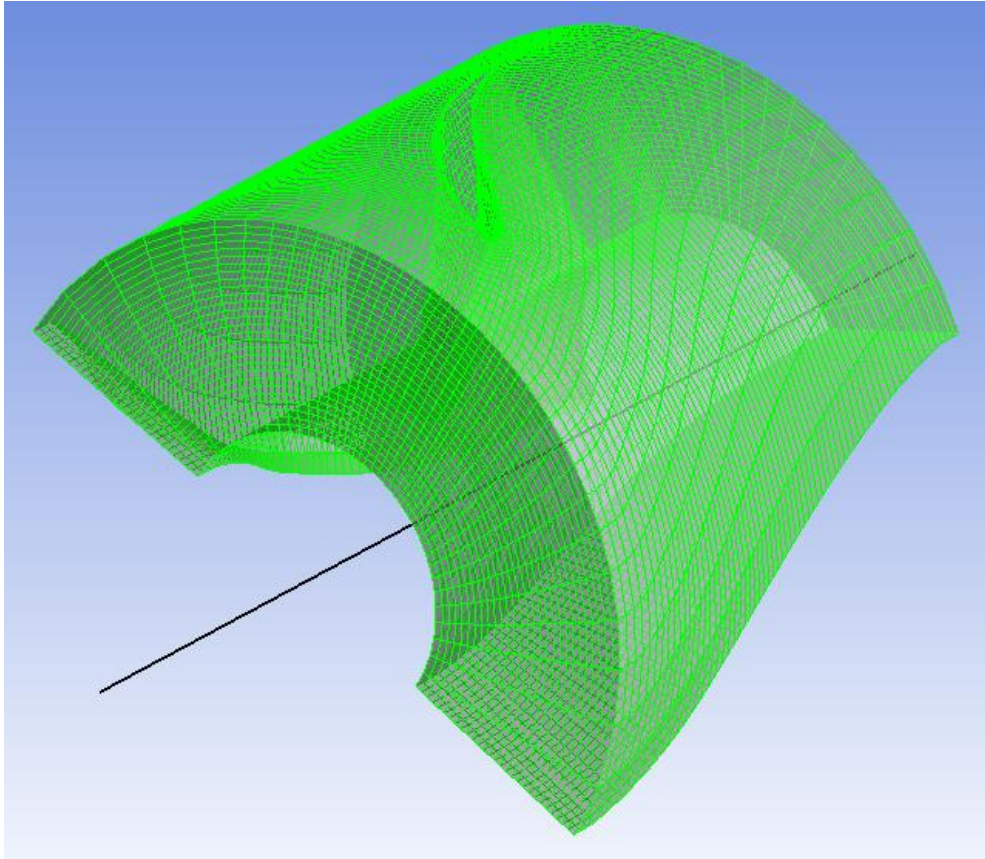
Figure 3-22 Hybrid structured 3D volume mesh
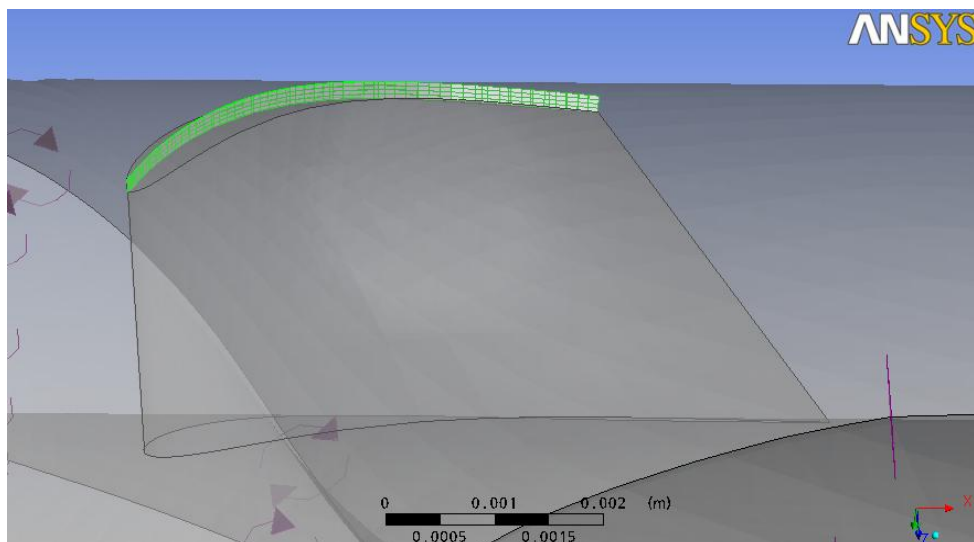
Figure 3-23 Tip Clearance Mesh Using Quad Elements

Tip clearance is also included in model at 95% of span using and 336 quad elements and 430 nodes. [Figure 3-23].

3.6.3 Boundary Condition

Boundary conditions are a set of properties or conditions on surfaces of domains, and are required to fully define the CFD flow simulation(ANSYS, 2011). The boundary parameters should have the meaningful values that represent the physical scenario in virtual CFD environment. However, it also depends on what exactly we want to study by performing a CFD simulation. For an implantable VAD pump the boundary condition needs to be applied according to cardiac events going on during cardiac cycle. Figure 3-24 depicts the cardiac events for the two complete cardiac cycles.
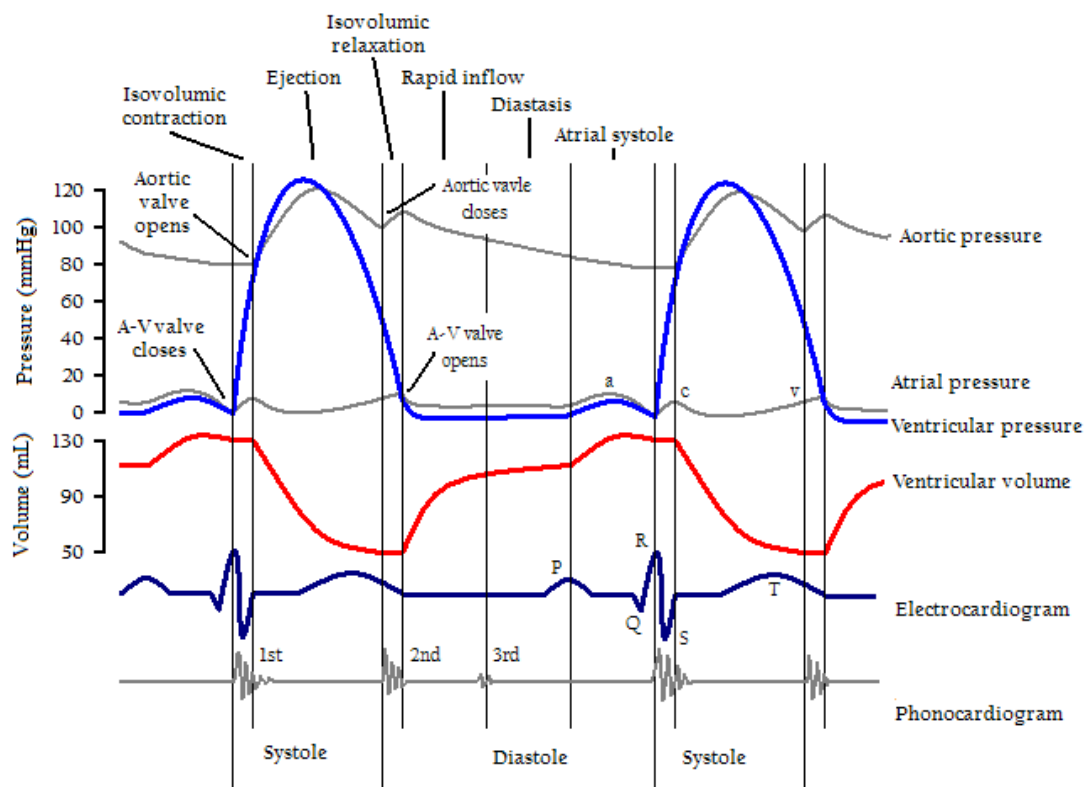
Figure 3-24 Cardiac Events during Two Complete Cardiac Cycles

(Guyton and Hall, 2006)

Mainly two types of boundary are available in ANSYS CFX that is Fluid boundaries, and Solid boundaries. The type of boundary condition that can be set for VAD simulations depends upon the bounding surfaces.

- A fluid boundary is an external surface of the fluid domain excluding surfaces where it meets other domains.
- A solid boundary is an external surface of the solid domain excluding surfaces where it meets other domains.

- A fluid-fluid interface is the interface between two fluid domains.

- A fluid-solid interface is the interface between a solid and fluid domain.

- A solid-solid interface is the interface between two solid domains.
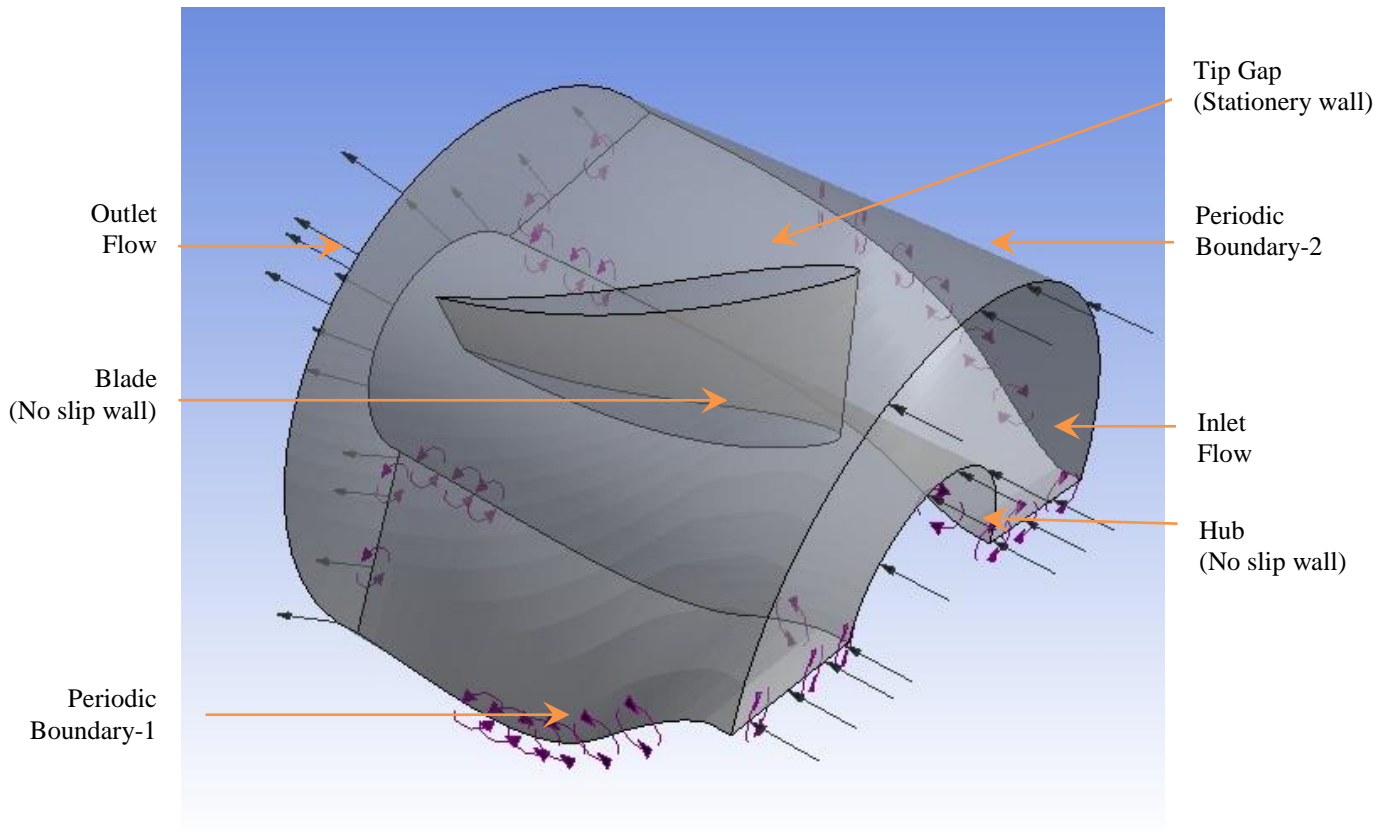
Figure 3-25: Boundary Condition for Rotating Fluid Domain

Figure 3-25 depicts the boundary condition for rotating fluid domain in CFX. A fluid boundary is an external surface of a fluid domain and supports following boundary conditions:

- Inlet Flow- Fluid predominantly flows into the domain.

- Outlet Flow- Fluid predominantly flows out of the domain.

- Wall - Impenetrable boundary to fluid flow.

- Symmetry Plane - A plane of both geometric and flow symmetry.

A solid boundary is an external surface of the solid domain and supports the following boundary conditions:

- Wall - Impenetrable boundary to fluid flow.

- Symmetry Plane - A plane of both geometric and flow symmetry.

3.6.4 Assumptions

For the purpose of this thesis, two main assumptions are made regarding CFD investigation. Those are Turbulence and near-wall modelling and second working fluid blood. **K-ω** turbulence model with no-slip wall boundary (where fluid immediately next to the wall assumes zero velocity of the wall) were assumed for the rigid VAD components, and blood is considered as a Newtonian fluid.

3.6.4.1 Turbulence and near wall modelling

An elastic property of larger arteries clearly plays a significant role in wave reflection, vessel collapse, pressure and velocity profiles (Wiebalck et al., 1993), and may be important to atherosclerosis (one of the causes of myocardial infarction MI). Thus, these properties cannot be ignored when comparing numerical and clinical results.

However, this thesis seeks to compare CFD and experimental models, both of which have rigid walls and thus no accuracy is lost due to no-slip wall (rigid wall) assumption. CFD calculations of the clinical effects of a rigid wall mechanical device in the circulation, are also unaffected by solvers capacity to model the wall elasticity.

The selection of turbulence model is an important factor in CFD simulations. However, determining the best turbulence model for miniature axial flow pump can be challenging task (Behbahani et al., 2009). The default turbulence model available in CFD tools has to be re-evaluated for specific application of small size blood pumps. Wall effects become significant due to the complicated geometry of blood pump and relatively low flow rate.

One of the advantages of the **k-ω** formulation is the near wall treatment for low-Reynolds number computations. The model does not involve the complex non-linear damping functions required for the **k-ε** model and is therefore more accurate and more robust (ANSYS, 2011). A low-Reynolds **k-ε** model would typically require a near wall resolution of $y+ <0.2$, while a low-Reynolds number **k-ω** model would require at least $y+ <2$. In case of VAD flows, even $y+ <2$ cannot be

guaranteed in most of the applications. This is reason for the selection of k-ω turbulence model. That allows for smooth shift from a low-Reynolds number form to a wall function formulation.

3.6.4.2 Blood as Newtonian fluid

Blood plasma is an incompressible fluid with a viscosity of about 1.2 cP (centipoise) slightly higher than water. Elasticity of red blood cell membrane and viscosity of intracellular fluid gives the viscoelastic property to whole blood. These properties depend on the shear rate, temperature and hemotocrit (Hellums, 1994). At constant haematocrit (in large vessels D> 0.5 mm) blood can be considered as uniform fluid of constant viscosity. Physiologically viscosity becomes independent of shear rate more than 1000 1/s (Meyns et al., 1994).

At the macro scale, there exist different models with different degrees of accuracy in capturing the rheological behaviour of blood. In CFD analysis of flow quantities inside VADs blood is usually considered as a Newtonian fluid (Thurston, 1979, Easthope and Brooks, 1980), although it is known to display non-Newtonian properties. Rheological properties mainly viscosity and elasticity are dependent on the rate of flow or shear rate (Sallam and Hwang, 1984). Shear rate that is a product of shear stress and angular velocity is also important parameters for the designing of VAD. Sallam and Hwang et al. measured approximately a threshold stress level of 400Pa for 100 milliseconds during a turbulent jet experiment where Reynolds stresses dominated the flow field (Sallam and Hwang, 1984).

3.6.5 Convergence and Grid Independence

For running a successful CFD simulation for a complex profile like axial flow LVAD, it is essential to monitor the behavior of the numerical process. The concept of residual value is to depict the imbalance error occurring in every node of the grid. Convergence is obtained only when the scaled residual value achieves the specified range of tolerance. There are two types of convergence, namely qualitative and quantitative convergence. A decrease of the residual value by three orders of magnitude during the iteration process indicates the least qualitative convergence

(Anderson, 1995) .For the purpose of this thesis, 10^{-4} is considered as the residual value and at this the results are considered to be converged. There are various reasons for the convergence failing such as poor mesh, improper solver setting, non-physical boundary conditions and selection of inappropriate turbulence models.

Anderson (Anderson, 1995) argues that we cannot confirm the convergence based on getting the residuals obtained from discredited algebraic equations or by getting the time derivative approaching zero with pseudo time stepping will give accurate results. Hence the alternative way of assessing convergence which is quiet common is called grid independence or mesh convergence. By this method, "the successive results obtained by finer and finer grids until the solution variation from one mesh to next mesh are under prescribed tolerance". It means, when the result obtained at "n" number of grid points reflects the result obtained at "(0.5*n)", then it is considered to be grid independent solution.

3.7 Design of Experiment: A Parametric Study

3.7.1 Introduction

To initiate the design procedure for LVAD to achieve clinical objective, the specifications for the design needs to be set for the design of an axial flow pump. The specification parameters can be divided in two groups mainly the independent and the dependent parameters (figure3-26).
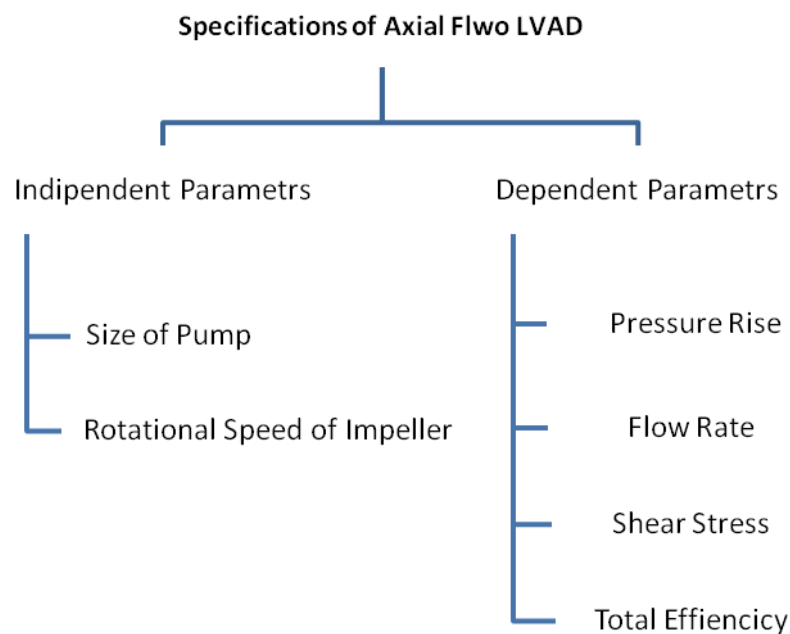
Figure 3-26 Specification and parameters of axial flow VAD

In case of the axial flow, LVAD size can be determined based on hydraulic requirement, surgical procedure, as well as the location of the pump installation. The rotational speed of the pump is the independent parameter that can be controlled physically; in addition, all the dependent parameters vary with the rotating speed. Clinical requirement from LVAD are diverse, that are 6L/min to15 L/min flow rate with 5mmHg to120mmHg of pressure rise depending on the severity of heart failure. This implies the LVAD should be able to operate at different design points rather than the specific design point to satisfy the clinical need. Statistical Design of

Experiment (DOE) technique is used to investigate the responses of the independent and dependent parameters using Design Explorer tool of Ansys.

3.7.2 Design of Experiments (DOE)

The detail explanation provided in this section for DOE is based on the Ansys help (ANSYS, 2011) provided by the Ansys Inc., Canonsburg, PA, USA.

Design of Experiments is a statistical method used to determine the location of sampling points .There are several versions of design of experiments available in engineering literature. These techniques all have one common characteristic: they try to locate the sampling points such that the space of random input parameters is explored in the most efficient way, or obtain the required information with a minimum of sampling points. Sample points in efficient locations will not only reduce the required number of sampling points, but also increase the accuracy of the response surface that is derived from the results of the sampling points. Deterministic method uses a central composite design (CCD), which combines one centre point, points along the axis of the input parameters, and the points determined by a fractional factorial.

3.7.3 Central Composite Design (CCD)

Central Composite Design (CCD) also known as Box-Wilson designs is preferred since the prediction variance is the same for any two locations that are the same distance from the design centre. In addition, there are other criteria to consider for an optimal design setup using the design matrix.

1. The degree of non-orthogonality of regression terms can inflate the variance of model coefficients.
2. The position of sample points in the design can be influential based on its position with respect to others of the input variables in a subset of the entire set of observations.

An optimal CCD design should minimize both the degree of non-orthogonality of term coefficients and the opportunity of sample points having abnormal influence. In

minimizing the degree of non-orthogonality, the Variation Inflation Factor (VIF) of regression terms is used. For an optimal CCD, level is selected such that both the maximum VIF and the maximum advantage are the minimum possible.

It is good practice to always verify some selected points on the response surface with an actual simulation evaluation to determine its validity of use. To capture a drastic change within the design space and to provide a better response surface fit seem to be conflicting in some cases where the response surface might not be as good as that of the Standard DOE due to the limitation of a quadratic response surface in capturing a drastic change within the design space.

The location of the generated design points for the deterministic method is based on a central composite design. If N is the number of input parameters, then a central composite design consists of:

1. One centre point.
2. $2*N$ axis point located at the -α and +α position on each axis of the selected input parameters.
3. $2^{(N-f)}$ factorial points located at the -1 and +1 positions along the diagonals of the input parameter space.

The fraction f of the factorial design and the resulting number of design points are given in the following table:

Number of input parameters	Factorial number f	Number of design points
1	0	5
2	0	9
3	0	15
4	0	25
5	1	27
6	1	45
7	1	79
8	2	81
9	2	147
10	3	149

Table 3-2: Number of Generated Design Points as a Function of the Number of Input Parameters (ANSYS, 2011)

3.7.4 Response Surfaces

There is one response surface or curve for every output parameter. Output parameters are represented in terms of the input parameters, which are treated as independent variables. For the deterministic method, response surfaces for all output parameters are generated in two steps:

- Solving the output parameters for all design points as defined by a design of experiments (DOE).
- Fitting the output parameters as a function of the input parameters using regression analysis techniques.

3.8 Goal Driven Optimisation

The Goal Driven Optimization (GDO) is a multi-objective optimization technique in which the "best" possible designs are obtained from a sample set of parameters. The GDO process is particularly useful in determining the effects of the input parameters with certain objectives on the output parameters.

For the purpose of the thesis, GDO has been performed using Design explorer and CFX available within ANSYS platform by following listed steps:

- Selection & Setup of input & output parameters in CFD simulation using CFX.
- Generation of Pareto optimal set based on input and output parameter using MOGA (NSGA-II).
- Selecting the best candidate using DSP.

To make use of miniature motor for pump with high efficiency and low power consumption with minimum possible traumatic effects on blood components, size of rotary blood pump needs reduction. The pump's operational speed is inversely proportional to the pump's size; thus, a smaller pump corresponds to a higher rotational speed of the impeller. A higher rotor speed implies a higher value of fluid stresses, which could have a traumatic effect on blood components and presents a design trade-off scenario.

In order to generate these trade-off solutions, an old notion of optimality is normally adopted. This notion of optimality was originally introduced by Francis Ysidro Edgeworth in 1881(Edgeworth, 1981) and later generalized by Vilfredo Pareto in 1896 (Pareto, 1896).It is called *Edgeworth-Pareto optimum* or, simply, *Pareto optimum*. In words, this definition says that a solution to a Multi objective problem is Pareto optimal if there exists no other feasible solution, which would decrease some criterion without causing a simultaneous increase in at least one other criterion.

It should not be difficult to realize that the use of this concept almost always gives not a single solution but a set of them, which is called the *Pareto optimal set*. The vectors of the decision variables corresponding to the solutions included in the Pareto optimal set are called *non-dominated*. The plot of the objective functions whose non-dominated vectors are in the Pareto optimal set is called the *Pareto front*.

GDO which uses Multi-objective Genetic Algorithm (MOGA), which can optimize problems with continuous input parameters, have been used for the optimisation of pump operative parameters mainly RPM. The GDO framework allows use of Decision Support Process (DSP) based on satisfying criteria as applied to the parameter attributes using a weighted aggregate method. In effect, the DSP can be viewed as a post processing action on the *Pareto optimal set* as generated by MOGA (NSGA-II).

3.8.1 MOGA (NSGA-II)

The MOGA used for this GDO is a hybrid variant of the popular NSGA-II (Non-dominated Sorted Genetic Algorithm-II) based on controlled elitism concepts.(Weile et al., 1996, Deb et al., 2002, Deb and Goel, 2001).The non-dominated sorting GA (NSGA) proposed by Srinivas and Deb in 1994 has been applied to various problems (Mitra et al., 1998, ANSYS, 2011). The NSGA-II with controlled elitism has much better convergence property than the original NSGA.

The Pareto ranking scheme is done by a fast, non-dominated sorting method that is an order of magnitude faster than traditional Pareto ranking methods (ANSYS, 2011). The constraint handling uses the same non-dominance principle as the objectives, thus penalty functions and Lagrange multipliers are not needed. This also

ensures that the feasible solutions are always ranked higher than the infeasible solutions.

The first Pareto front solutions are archived in a separate sample set internally and are distinct from the evolving sample set (ANSYS, 2011). This ensures minimal disruption of Pareto front patterns already available from earlier iterations.

3.8.2 Decision Support Process (DSP)

GDO framework uses Decision Support Process (DSP) is a goal-based, weighted, aggregation-based design ranking technique(ANSYS, 2011).In these method n- input parameters, m-output parameters, their individual targets, and the collection of objectives is combined into a single, weighted objective function, Φ, which is sampled by means of a direct Monte Carlo method using uniform distribution.

Lower the value of Φ, the better the design with respect to the desired values and importance. Thus, a quasi-random uniform sampling of design points is done by a Hammersley algorithm and the samples are sorted in ascending order of Φ. The desired numbers of designs are then drawn from the top of the sorted list (ANSYS, 2011). A crowding technique is employed to ensure that any two sampled design points are not very close to each other in the space of the input parameters.

Example of candidate generated for design-XX using DSP are shown in table 3-3.

Selected Candidate From The GDO Sample Set using DSP			
	Candidate 1	**Candidate 2**	**Candidate 3**
H In To Out	0.3789	1.2481	1.684
Mass Flow Rate	0.06125	0.16878	0.059452
Shaft Power	6.0089	25.882	26.01
Total Efficiency	45.459	58.653	46.449
RPM	8825	11968	14684

Table 3-3: selected candidates from Pareto fronts using DSP

From the generated candidates set as shown in table 3-3, Candidate 1 is selected as a design point. Further CFX simulations has been carried out to verify the pump performance at the RPM of candidate 1.

3.9 Concluding section

The aim of this chapter was to demonstrate the general methodology used in this study and to describe the main tools involved.

Main points that are discussed in this chapter are as below;

- First section of this chapter helps in identifying the hydraulic and clinical requirement of VAD for the treatment of patients.

- Second section provides the details of the clinical design criteria of VAD along with the details of hemolysis and thrombosis.

- Third section discusses about the conventional design theory and provides equations for initialisation of design procedure. Conventional pump design equations were used to estimate the initial dimensions of the VAD. Depending on the specific desired operating conditions (rotating speed, flow rate, and pressure rise) and clinical requirements, the blade characteristics including diameter, leading/trailing edge angles, thickness and height were estimated using the pump design equations.

- The fourth section discuss about the generation of 3D CAD geometry using the initial design calculation. CAD model helps in visualization of derived geometry and provides the base for the generation of CFD model.

- The fifth section discuss about the CFD in detail that includes converting CAD model into .curve file, mesh generation, boundary condition and assumptions for the turbulence model .In addition it also provides the details for the convergence and gird independency study.

- Sixth section provides the details of parametric design of experiment study.

- Last section discuss about the goal drivel optimization(GDO) including multi objective genetic algorithm(MOGA) and decision support process(DSP) which are helpful in deriving the optimum range of the operating speed of LVAD.

Next chapter discuss about the outcome on the steady state CFD simulations of LVAD operating as a continuous axial flow pump.

Chapter 4 CFD Evaluation of LVAD as a Continuous Axial Flow Pump

4.1 Abstract

The design of an axial flow LVAD is an iterative procedure that requires exploring various impeller geometries and shapes; moreover it involves the verification of those shapes for their suitability to be used as a VAD. CFD simulations results presented for the purpose of this thesis and in this chapter are limited to the particular design that was selected for in vitro experimental evaluation of LVAD.

This chapter provides simulations result of an LVAD operating as a continuous flow pump, that includes the results of CFD based parametric study using statistical design of experimental (DOE) method. This was carried out to analyse the impact of operating speed on the characteristic design parameters. The operating speed of the LVAD is obtained using Goal Driven Optimisation (GDO) considering the hemolysis criteria. The performance of the pump as continuous flow pump is computed using the result of an optimisation. The outcomes of the steady state CFD simulations for pressure, velocity and shear stress are discussed to visualise the internal flow details.

4.2 Design of Experiment (DOE): A Parametric Investigation

The CFD based Design of experiment (DOE) study has been carried out to investigate the response of the dependent parameters mainly Pressure rise, mass flow rate, and the shear stress for the range of the independent parameter that is a rotating speed of LVAD. The design matrix is generated for the range of LVAD rotating speed-varying from 3000 to 30000 RPM, pressure rise of 5mmHg to 120mmHg and flow rate varying from 6L/min - 15L/min. Total efficiency (Incorporate flow leakage and mechanical losses) and shaft power are also taken into consideration while formatting the design matrix using Central Composite Design (CCD) method.

4.2.1 Mass Flow Rate Vs Rotating Speed of LVAD
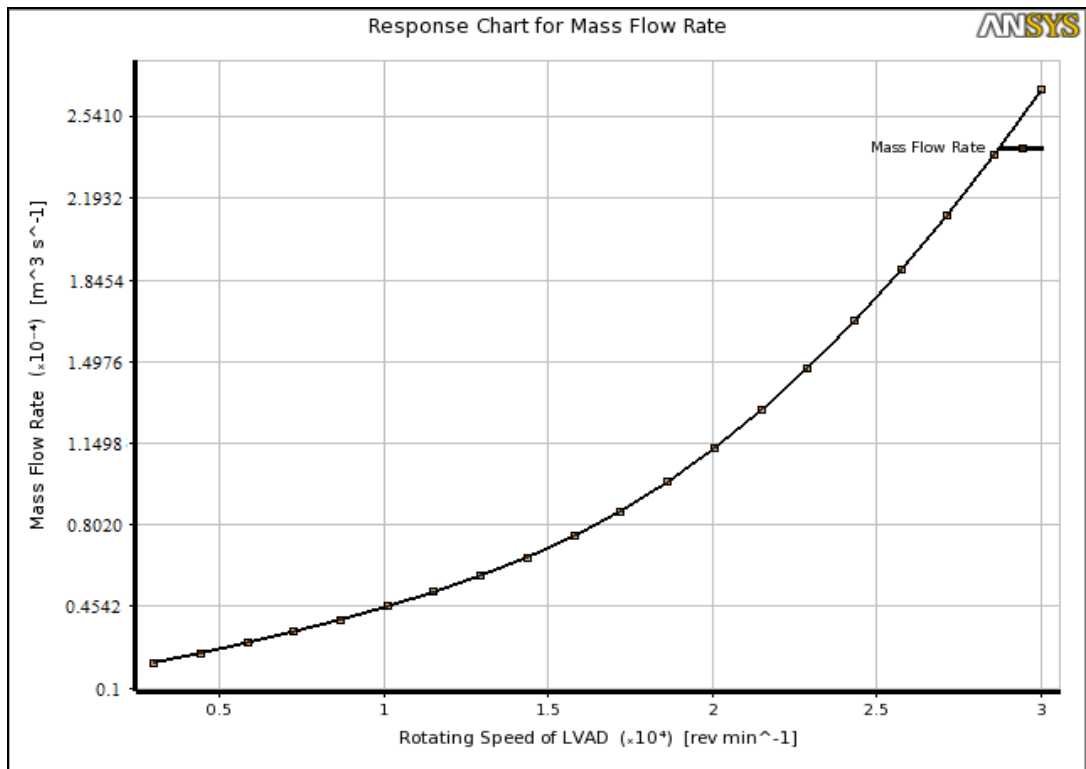
Figure 4-1: Response Chart for Mass Flow Rate

Figure 4-1 depictes the response of mass flow rate of LVAD for the rotating speed,where mass flow rate increases with increasing rotating speed. The maximum flow rate or more than 2.541E-04 M^3/sec is observed at 30000 RPM. The conversion of M^3/sec in cc/sec gives the 254.1 cc/s that gives 15.246 L/min of flow rate. The minimum flow rate of 10.64 cc/sec that is 0.64 L/min ,is observed at 3000 RPM.

4.2.2 Pressure Rise Across Impeller Vs Rotating Speed of LVAD
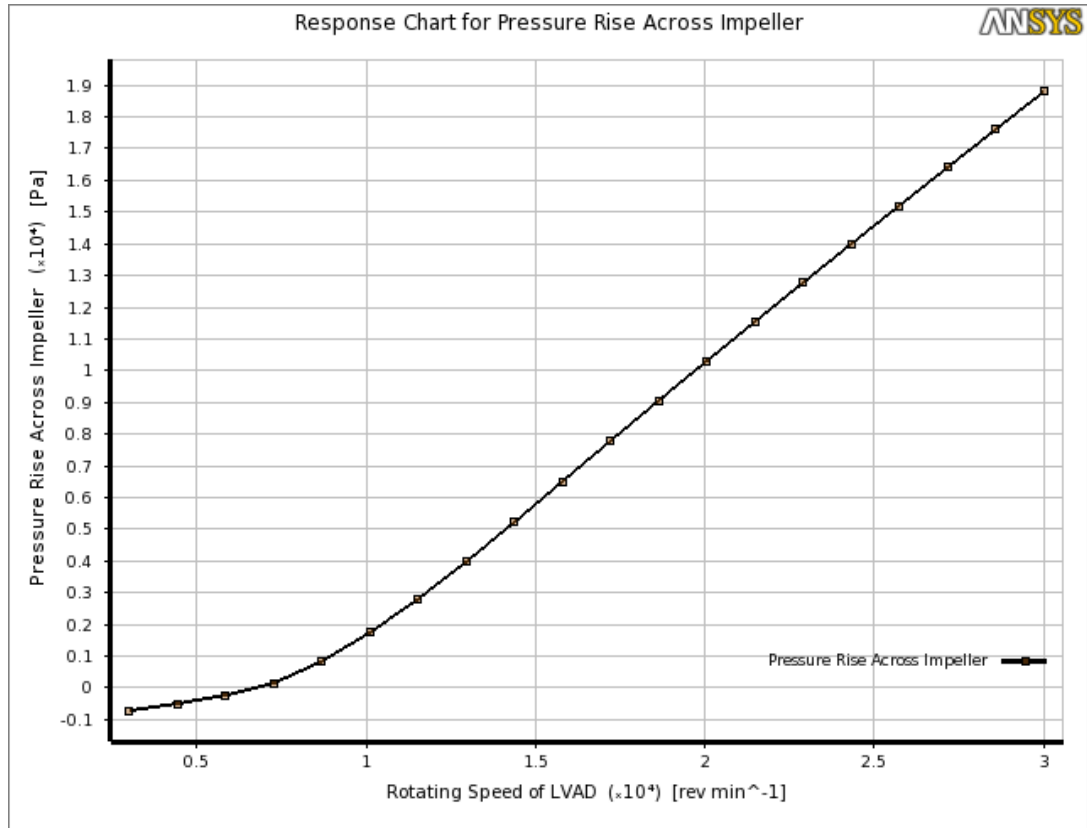
Figure 4-2: Response chart for pressure difference across impeller

Above figure, 4-2 shows the response of pressure difference across impeller against rotating speed of LVAD. The maximum pressure rise of 18.769 KPa that is 140.76 mmHg across the impeller is observed at 30000 RPM. At low speed, the pressure rise is observed to be 0.68 KPa that is 5.1mmHg at 3000 RPM.

4.2.3 Total efficiency Vs Rotating Speed of LVAD
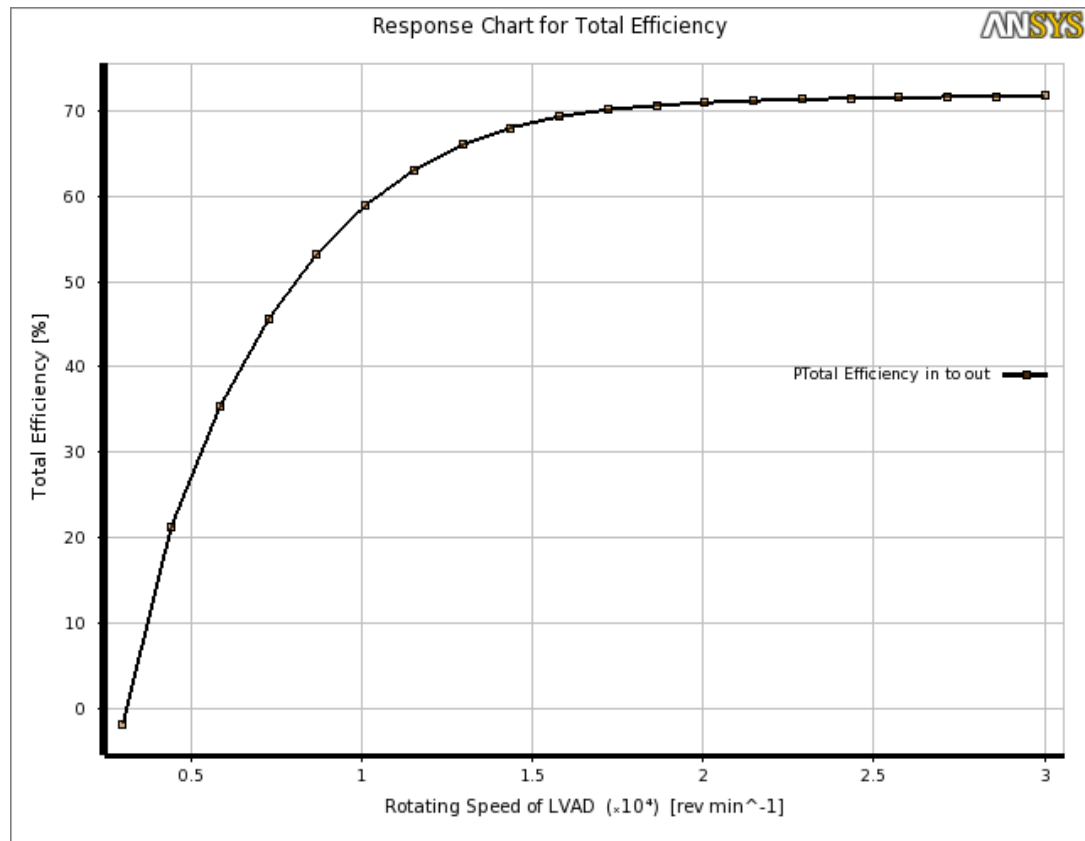
Figure 4-3: Response chart for total efficiency

Figure 4-3 depicts the response of total efficiency for the rotating speed of LVAD. Up to 20000 RPM the efficiency increases with the increasing rotating speed. After that it remains at ~74.5% through the axis. Minimum of 3.6343 % efficiency is observed at 3000 RPM.

4.2.4 Shaft Power Vs Rotating Speed of LVAD
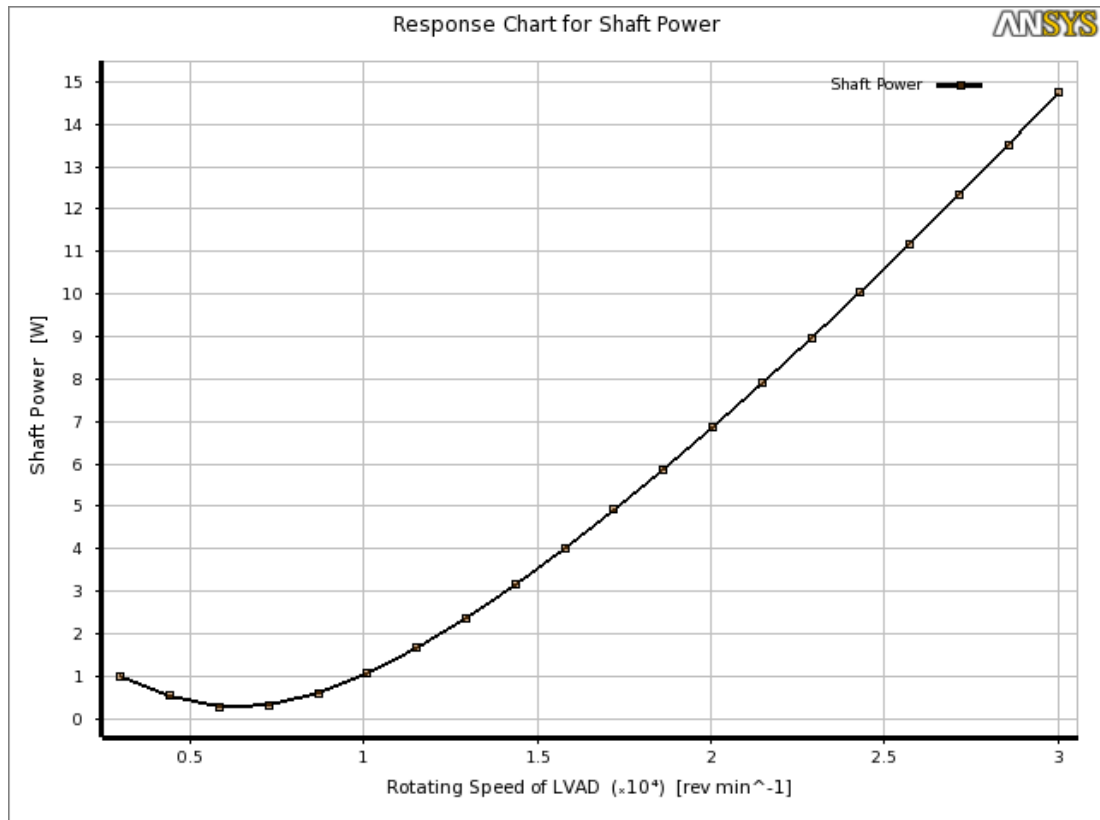
Figure 4-4: Response chart for shaft power

Figure 4-4 shows the shaft power response for the speed of pump. Shaft power decreases with increasing speed up to 5524 RPM, there after it increases with the increasing speed. Maximum ~14.8 watt power is observed at 30000 RPM.

4.2.5 Shear Stress Vs Rotating Speed of LVAD
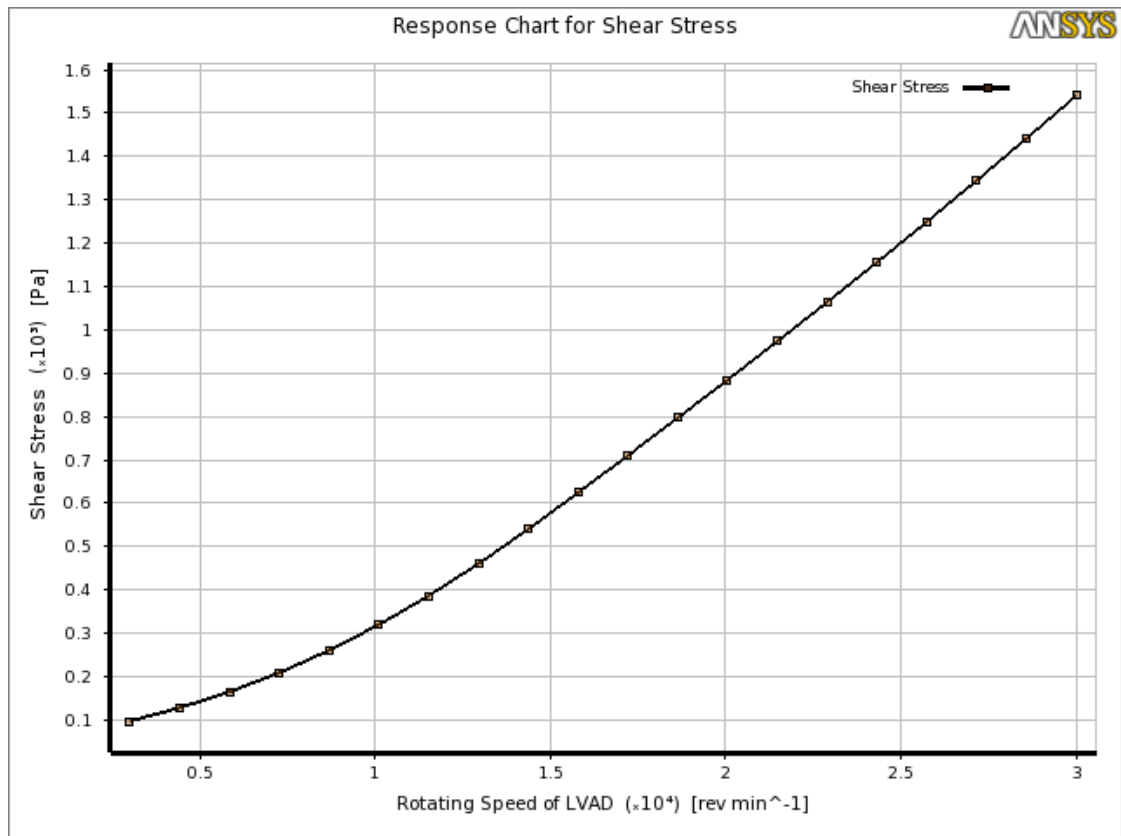
Figure 4-5: Response chart for shear stress

Figure 4-5 depicts the response of shear stress for the rotating speed of LVAD.

The response of shear stress depicted in figure 4-5 was located at the rotating impeller that includes the blades and hub. ~100 Pa shear stress were observed for low rotating speed which increases with the increasing speed. Maximum observed value is around 1550 Pa at 30000 RPM.

4.3 Need of Optimisation

Designs of experiment (DOE) have demonstrated the anticipated performance of design as a continuous flow pump. In addition, it provides the detail view of the pump capacity to provide adequate flow rate and pressure rise for clinical objective. The maxima and minima for various parameters are derived from steady state simulations of LVAD. The best efficiency point 74.226 % is observed at 23083 RPM, where the flow rate was 9.7L/min with the pressure rise of 12.930 KPa that is around 100mmHg pressure rise across the impeller, with the shaft power of 8.33 W. The shear stress is around 1031.3 Pa that is higher than the recommended value of 400 Pa(Sallam and Hwang, 1984). At the best efficiency, the tip speed of the impeller is around 12.08 m/sec which is more than the recommended value of 10 m/s (Reul and Akdis, 2000). Despite having the best efficiency at 23083 RPM, it is unsuitable to operate LVAD at this design point due to complex behaviour of blood as well as the requirement of peripheral circulation. Thus, to operate the pump within the allowable limit of the shear stress for low hemolysis, the pump speed and efficiency are sub-optimal. Below the best efficiency point, the flow rate also reduces along with the require shaft power. In summary, the design parameters exhibit a trade off scenario amongst them for satisfying the design criteria as well as objective of LVAD.

4.4 GDO of Operating Parameters

Purpose of the Goal Driven Optimisation (GDO) is to determine the speed of rotation for LVAD, at which the pump can generate physiological flow rate with the least traumatic effects on blood components. The objectives for GDO were set according to the clinical requirement, primarily shear stress and Mass Flow Rate. The shear stress were set to have less than 300Pa keeping factor of safety of 1.3 based on the limit shear stress 400Pa (Sallam and Hwang, 1984) . Mass flow rate is set for the 6 L/min which is mass flow rate required for an average cardiac patient (Wood et al., 2005). Along with the clinical parameters, the total efficiency and pressure rise across the pump were set to be maximum possible with the shaft power set to have a minimum possible.

The Multi Objective Genetic Algorithm (MOGA) is used to generate the Pareto fronts (sample set of parameters). Total 10000 initial sample set were used to begin the MOGA optimisation process. The total 800 Pareto fronts were generated by MOGA. The trade-off charts for Shear Stress, Mass Flow Rate, Pressure difference across the impeller and Total efficiency are shown in figure 4-6, 4-7, 4-8 and 4-9 respectively. The feasible points are shown in the green color rectangles, where every point is a set of input and output parametrs. The best feasible points(parametrs set) are shown Blue color rectangles while the non feasible points are shown in red color rectangle.
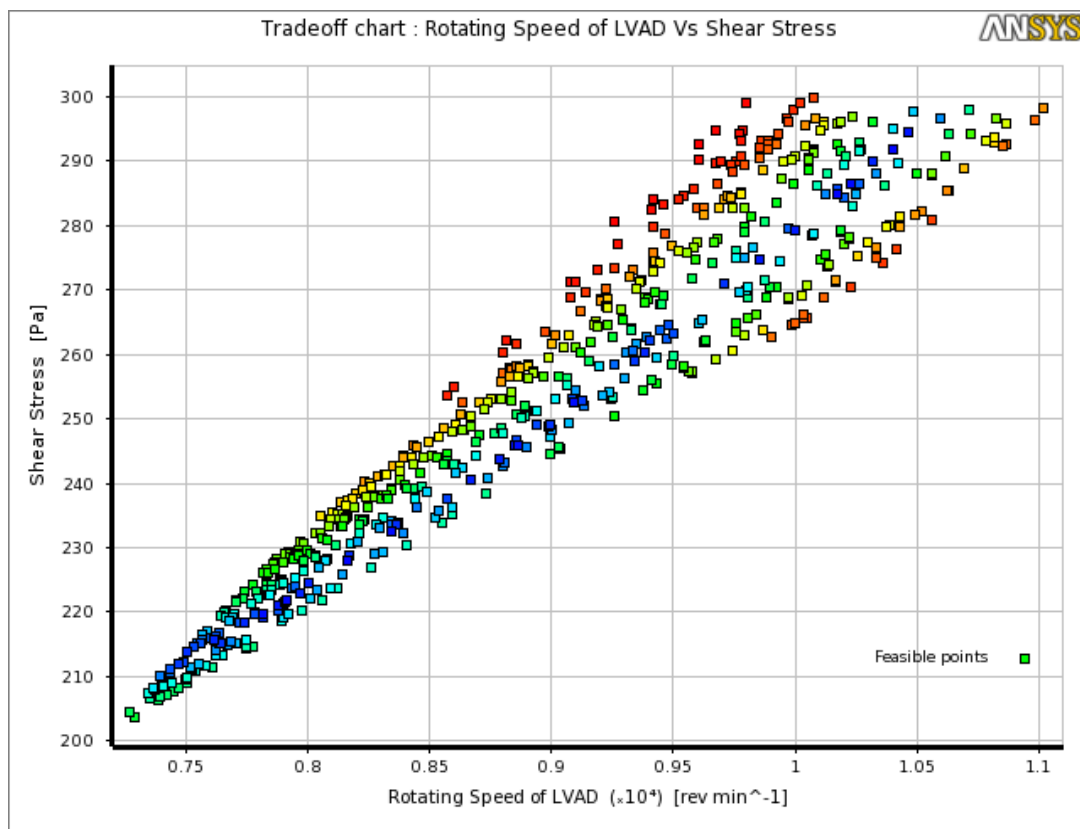
Figure 4-6: Tradeoff chart of rotating speed of LVAD Vs shear stress

The figure 4-6 shows the tradeoff chart for the rotating speed Vs the shear stress. The best feasible points are availabe up to 10500 RPM, where shear stress are well below 300 Pa. For the shear stress below 250 Pa the LVAD speed can go up to 9000 RPM. Up to 8000 RPM the shear stress are observed to be well below 220 Pa.
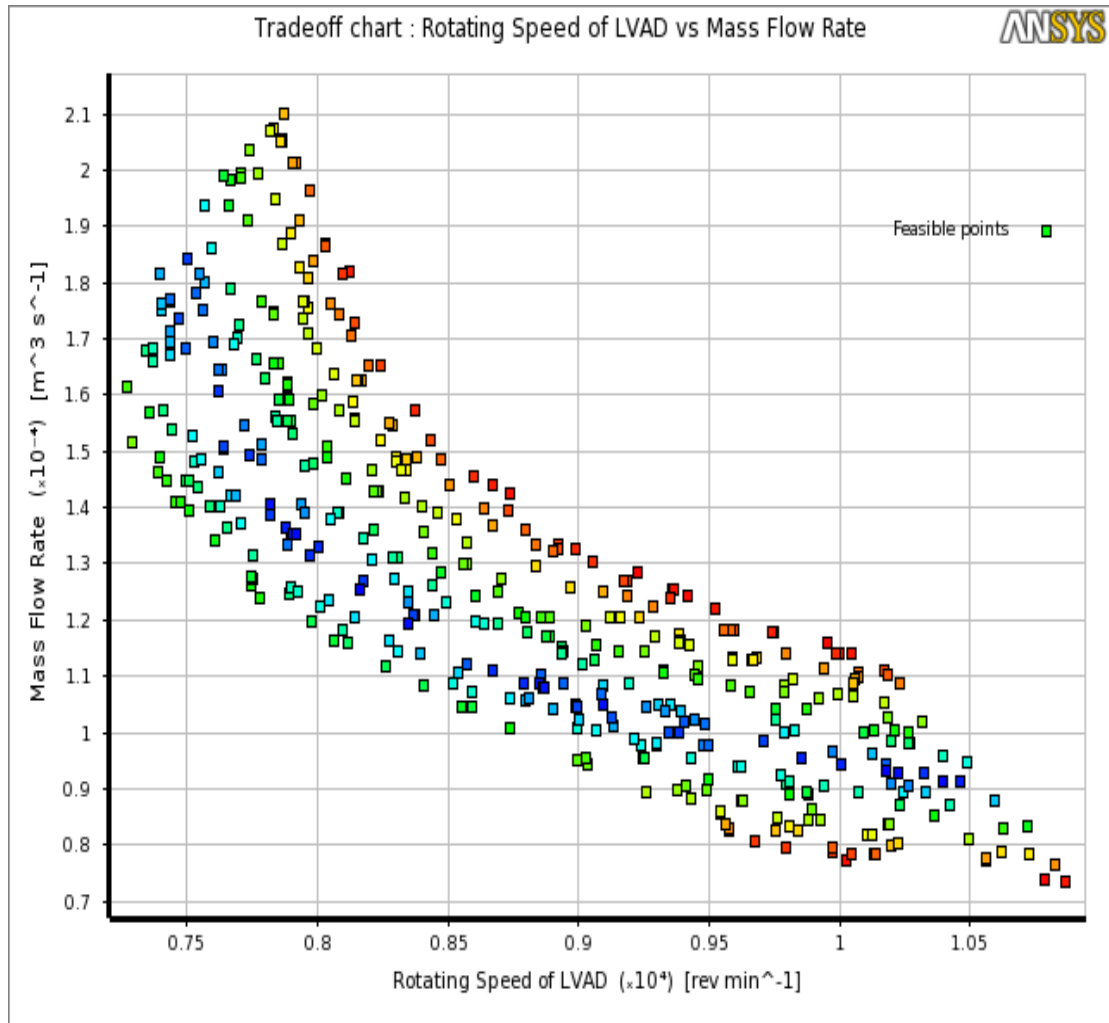
Figure 4-7: Tradeoff chart of rotating speed of LVAD Vs mass flow rate

Figure 4-7 shows the trade-off plot for the mass flow rate against the rotating speed. The best feasible points are available up to 10500 RPM. At the 10000 RPM LVAD can deliver the flow rate up to 6 L/min that is 100 cc/sec.

Figure 4-8: Trade-off chart of rotating speed of LVAD Vs Pressure difference across Impeller

Above figure 4-8 depicts the trade-off amongst the pressure difference across the impeller and the rotating speed of LVAD. The pressure difference increases with the increasing speed of LVAD. Up to 10500 RPM the best feasible points are available that give the pressure rise up to 4.2 kPa that is 31.50 mmHg across the impeller.
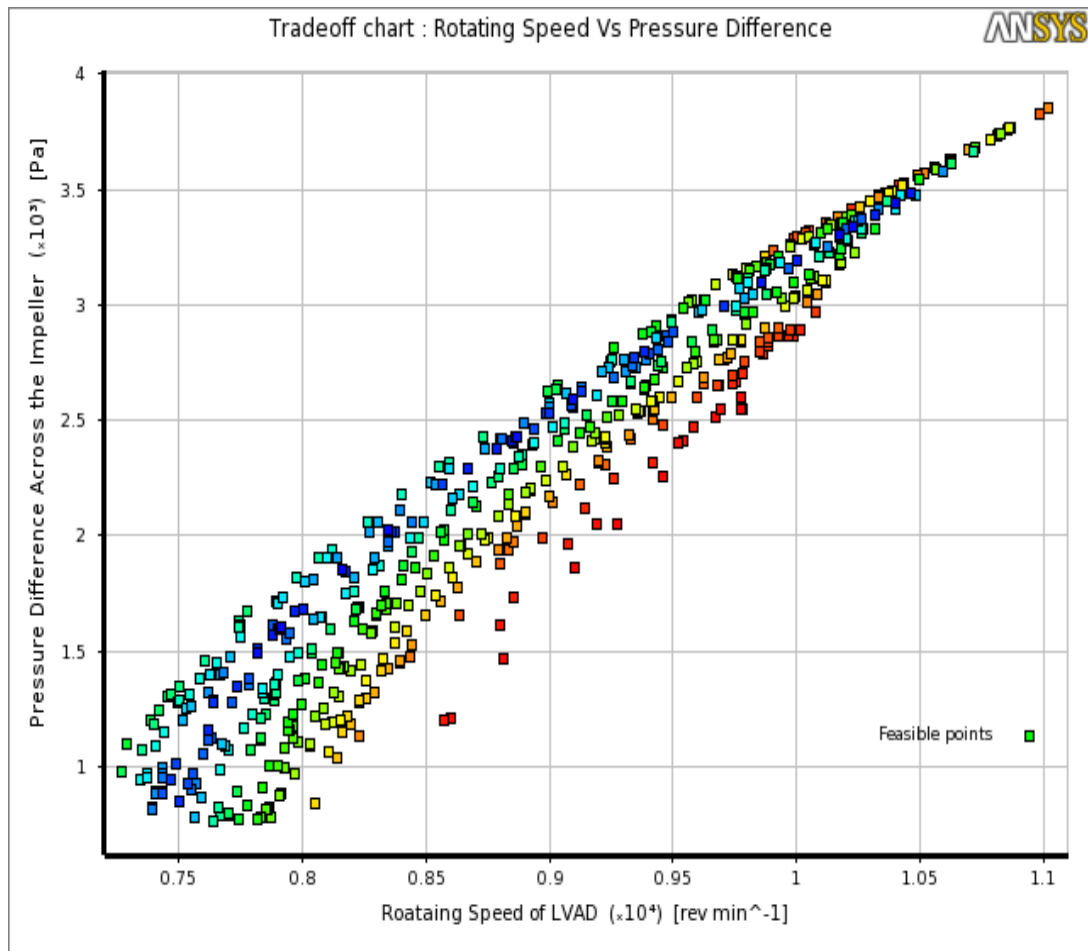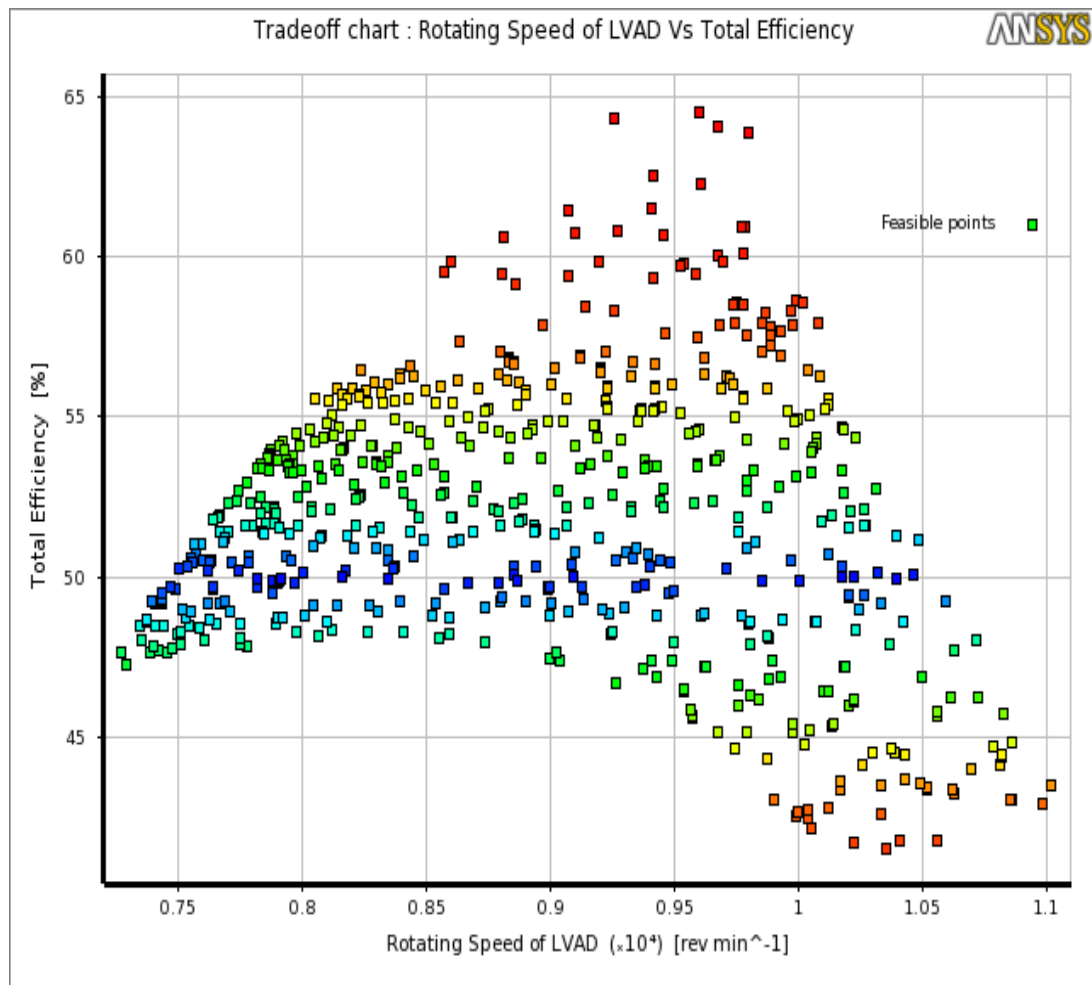
Figure 4-9: Trade-off chart of rotating speed of LVAD Vs total efficiency

Figure 4-9 shows the tradeoff plot for the total efficiency Vs rotating speed of LVAD. The best possiable points are available up to 11000 RPM that are presented around 50% line through the axis.

The tradeoff amongst the parameters shows the numbers of feasible candidate that can satisfy the LVAD requirement. The Decision Support Process (DSP) is employed to find out the best possible solution form the generated feasible solution sets (Pareto fronts). DSP have shortlisted the three best possible candidate that satisfies the clinical objective as well as the hydraulic requirement of the LVAD. The best design point gives the 8167.3, 8853.9, and 10077 RPM. These points show the range of rotating speed of LVAD that is 8000 RPM to 10000 RPM. At this speed, pump can deliver flow rate up to 6 L/min with pressure rise of 31.50mmHg and 50% efficiency with the shear stress well below 300Pa.

4.5 Pressure Vs Flow characteristics of LVAD as a Continuous Flow Pump

The purpose of this CFD study is to find out the performance for the range of rotating speed derived using GDO. Steady state CFD simulations were carried out to investigate the characteristics of LVAD at different RPM. The computational run covers the range of operating condition to obtain the performance curves for an impeller at different RPM. Performance map of the pump is predicted in terms of head and total efficiency of impeller against flow rate. Flow rate is varied keeping RPM constant. Total efficiency has been considered and plotted against flow rate, rather than static efficiency because of the relative importance of velocity head in case of axial flow pump. In case of the low-head pumps, at a given velocity, head loss constitutes a larger percentage of total dynamic head than in a high-head pump. Hence acute and complete evaluation of all head losses must be considered in higher specific speed pumps, since each element of head constitutes an important part of the total head, in case of axial flow pumps. The quality of the prediction deteriorates for the flow rate different from the nominal flow rate. Particularly at very low flow rates, calculations give serious underprediction of the head as well as efficiency.
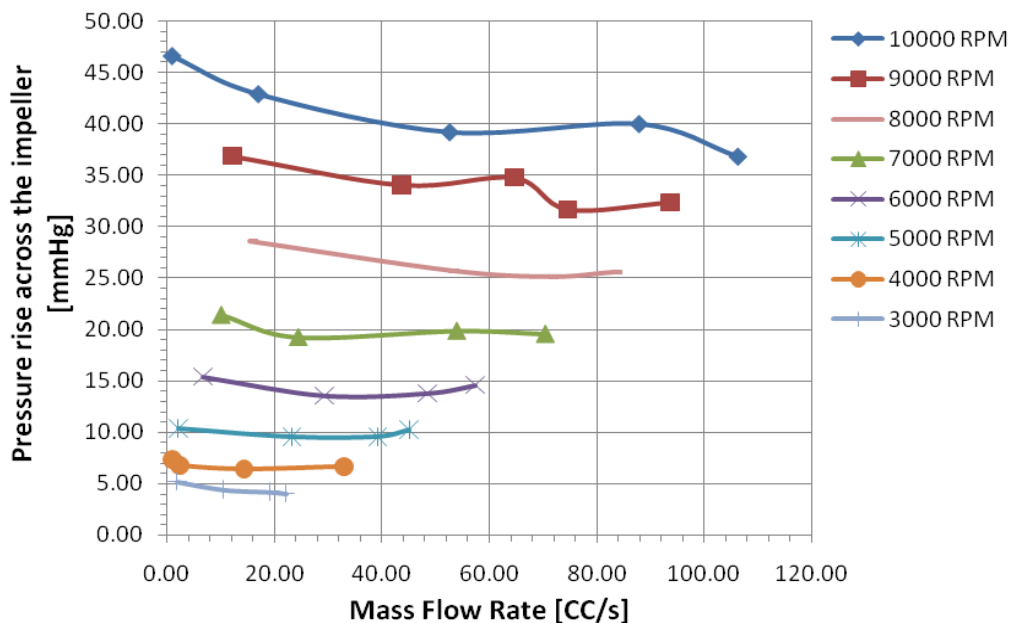

Figure 4-10: Head Vs Flow Rate

Figure-4-10 depicts the predicted performance of LVAD in terms of head against the flow rate for the range of RPM (3000-10000). At 3000 RPM, pump generates 5 mm of Hg pressure rise with 31.411% of total efficiency and 22.48 CC/s of flow rate. The pump generates 36.87 mm of Hg with 106 CC/s of flow rate at 10000 RPM with 49.31% of efficiency. Table 1-1 shows the details for the derived rotating speed range of LVAD.

Rotating speed of LVAD	Total efficiency	Mass Flow Rate	Pressure Rise across the Impeller		Shear Stress
RPM	%	CC/sec	KPa	mmHg	Pa
10000	49.312	106.31	4.92	36.87	314.6
	55.857	87.93	5.34	40.03	333.09
	36.07	52.66	5.23	39.23	317.66
	12.938	17.05	5.72	42.94	261.17
	0.80086	1.01	6.22	46.64	229.15
9000	59.938	93.78	4.31	32.35	276.32
	49.684	74.72	4.22	31.66	286.08
	30.524	64.72	4.64	34.78	264.47
	9.049	43.81	4.54	34.06	217.79
	0.78794	12.24	4.92	36.89	206.17
8000	56.182	82.98	3.41	25.56	231.5
	48.95	71.15	3.35	25.12	237.59
	36.511	52.58	3.43	25.75	239.43
	11.216	15.40	3.81	28.59	295.74

Table 4-1: CFD simulation results for the Optimum range of rotational speed

Shear stress is an important parameter for determing blood trauma. Blood trauma is dependent on stress level and exposure time of blood components with rotating & stationary surfaces of LVAD . Besides pump's performance, it is essential to study the blood damage for the application of LVAD. To investigate the behaviour of wall shear for the range of RPM (3000-10000), predicted values of wall shear is tabulated along with the total efficiency and the flow rate, as shown in table 4-1. Total efficiency increases with increasing flow rate up to its higher efficiency point. Where the pump is generating the pressure head without any restriction at the outlet.

4.6 Detail flow investigation of continuous flow LVAD

Internal flow details are investigated along with the bulk performance parameters. The descriptions of detailed flow are based on results obtained from steady state CFD simulation. The important regions of investigation of detailed flow are mid span, hub wall & tip wall region of LVAD impeller. Concentration of wall shear on the blade surfaces like leading edge, suction side, & pressure side were also deliberated.
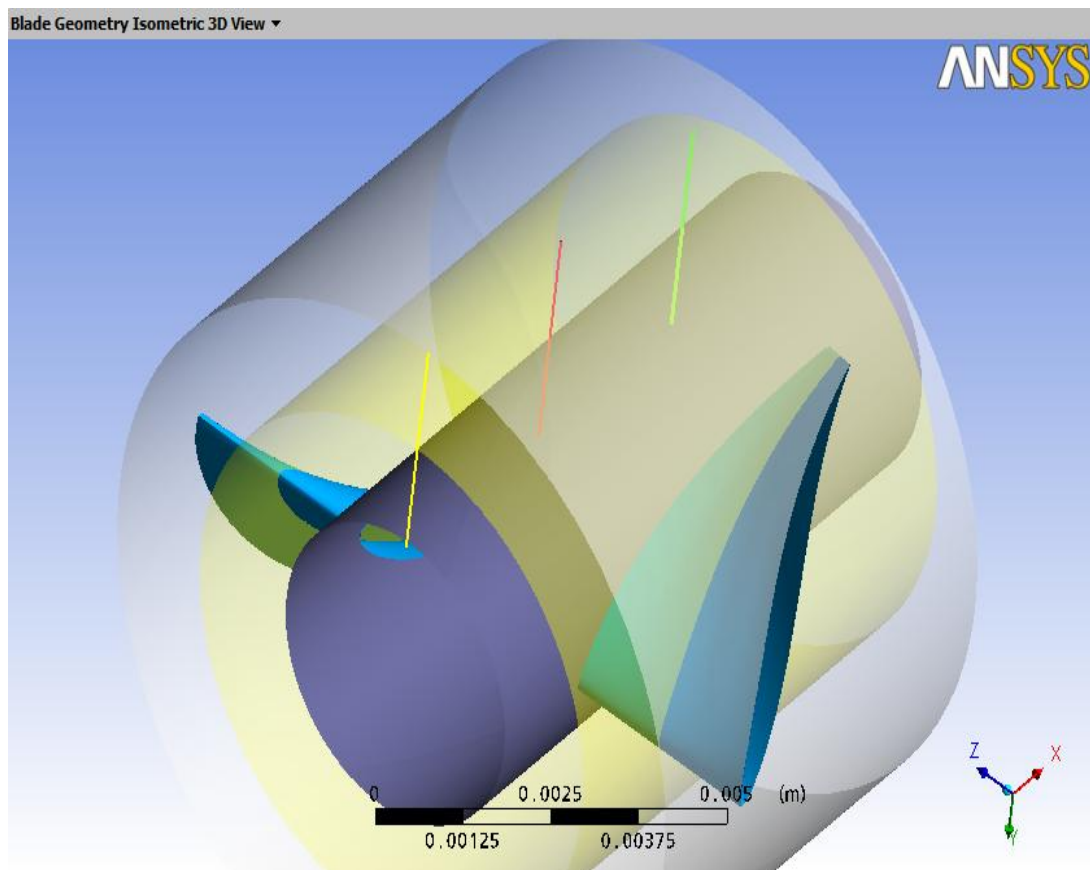
Figure 4-11: Region of Interest

Figure 4-11 depicts the regions of interest where the span wise pressure & velocity data are collected at inlet, mid section and at outlet along the axis of rotation shown in yellow, red and green line. Along the span, hub wall region is presented in dark gray colour, mid span region is presented using transparent yellow cylindrical surface and tip wall region is presented using transparent gray colour. For the purpose of this thesis, results are discussed for the high efficiency point at 8000 RPM.

4.6.1 Pressure

Predicted span wise pressure values are plotted in figure 4-12 for the inlet, mid section & outlet. Predicted values near hub wall region gives the lower pressure below 20% of blade span. After 95% of span, near the tip region, higher pressure is observed. Increment of pressure form, inlet to outlet is also observed.
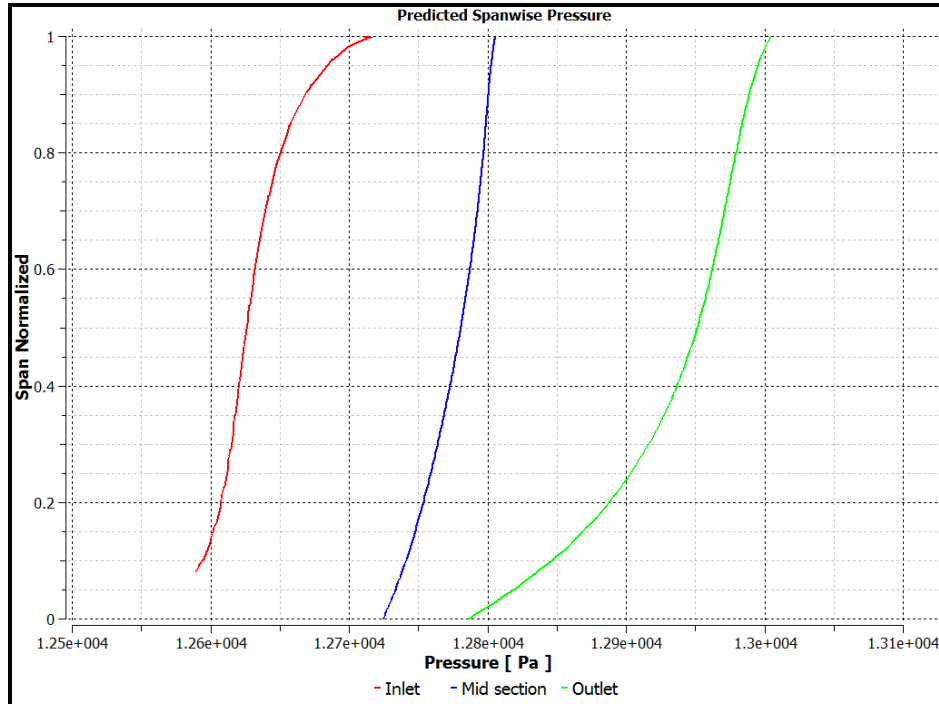
Figure 4-12: Predicted Span Wise Local Pressure

Pressure drop is observed near hub wall region as shown in figure4-13 as well as the drop in mass flow compare to upstream flow shown in figure 4-14. The deficit in mass flow is observed up to 20% of span. Observed pressure drop in the near wall region might be due to difference between the upstream flow with the flow in the cavity of near hub wall region and rotating blade surfaces. From figure 4-13 and 14, it is shown that, pressure side of the blade near leading edge generates higher pressure where mass flow is also higher compared to the surface towards trailing edge of pressure side where deficit in mass flow is observed up to 20% of span.
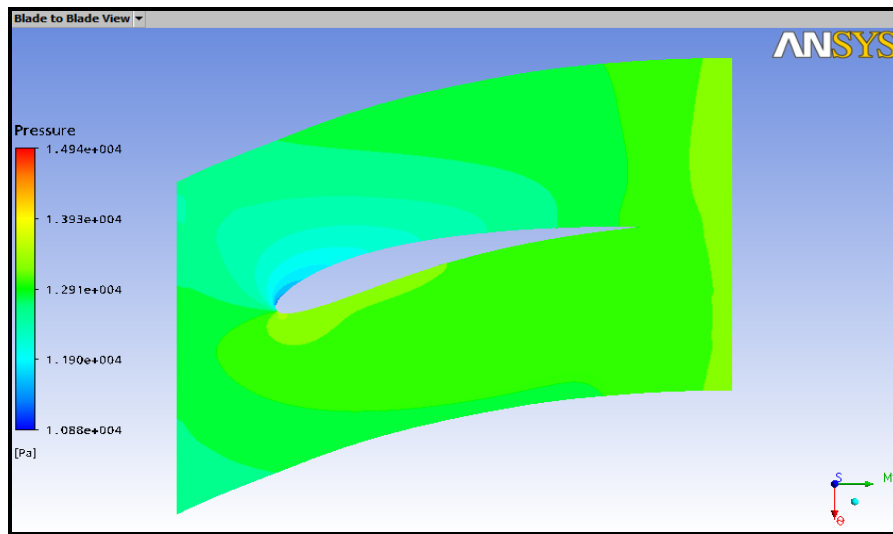
Figure 4-13: Pressure contour at 0.001% of Span
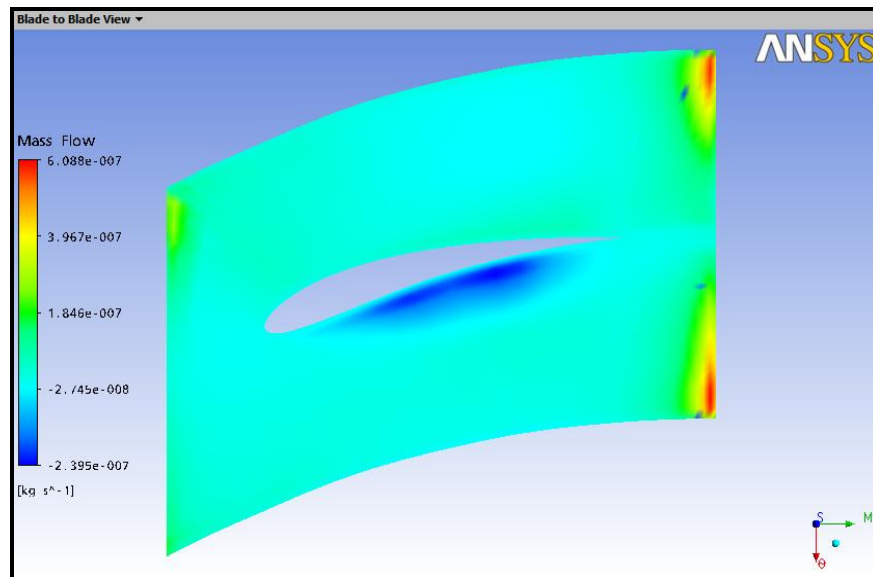
Figure 4-14: Mass flow at 0.001% of Span

Figure 4-15 to 4-17 shows the pressure contour for 20 %, 50%, and 80% of span. At 20% of span, the maximum pressure of 13.49 KPa is observed at leading edge of the aerofoil-sectioned blade, which increases as we move towards tip section with 14.04 KPa at 50% and 14.69 KPa at 80% span.
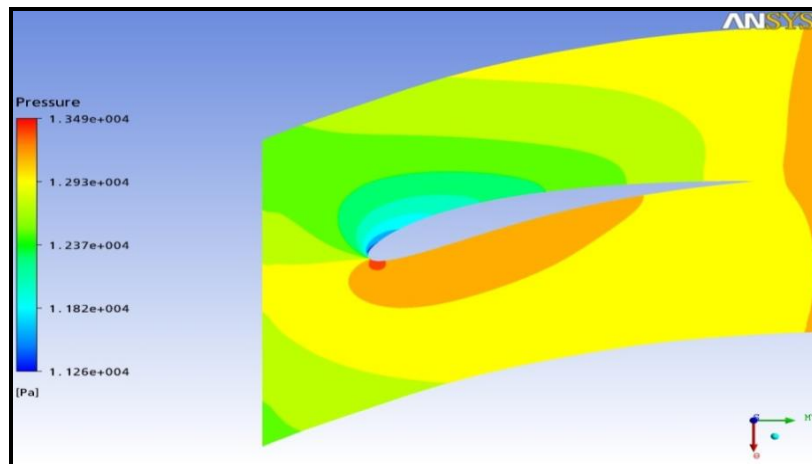
Figure 4-15: Pressure Contour at 20% of Span
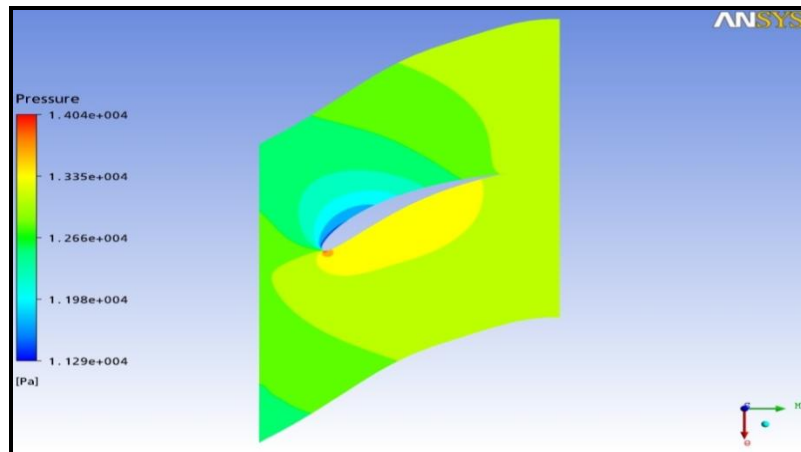
Figure 4-16: Pressure Contour at 50% of Span
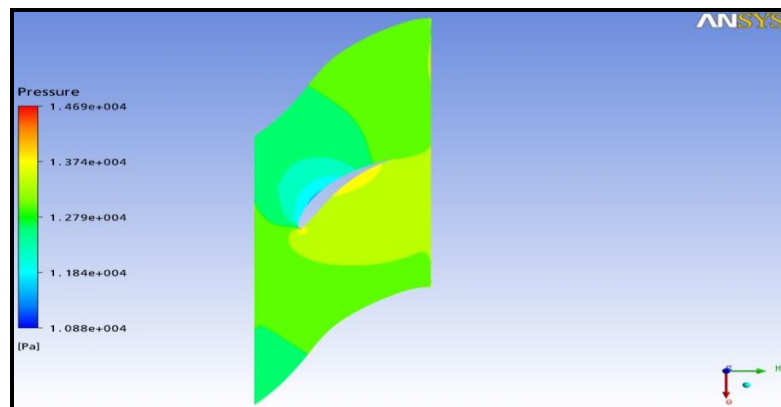
Figure 4-17: Pressure Contour at 80% of Span

4.6.2 Blade loading

Streamwise blade loading chart in figure 4-18, 19 & 20 for respectively 20%, 50% & 80 % of span. Across the length of blade, positive work done is observed over the span. The blade loading chart helps in understanding pressure variation along the surface of the blade; suction surface behaves like a flat plate prior to passage.
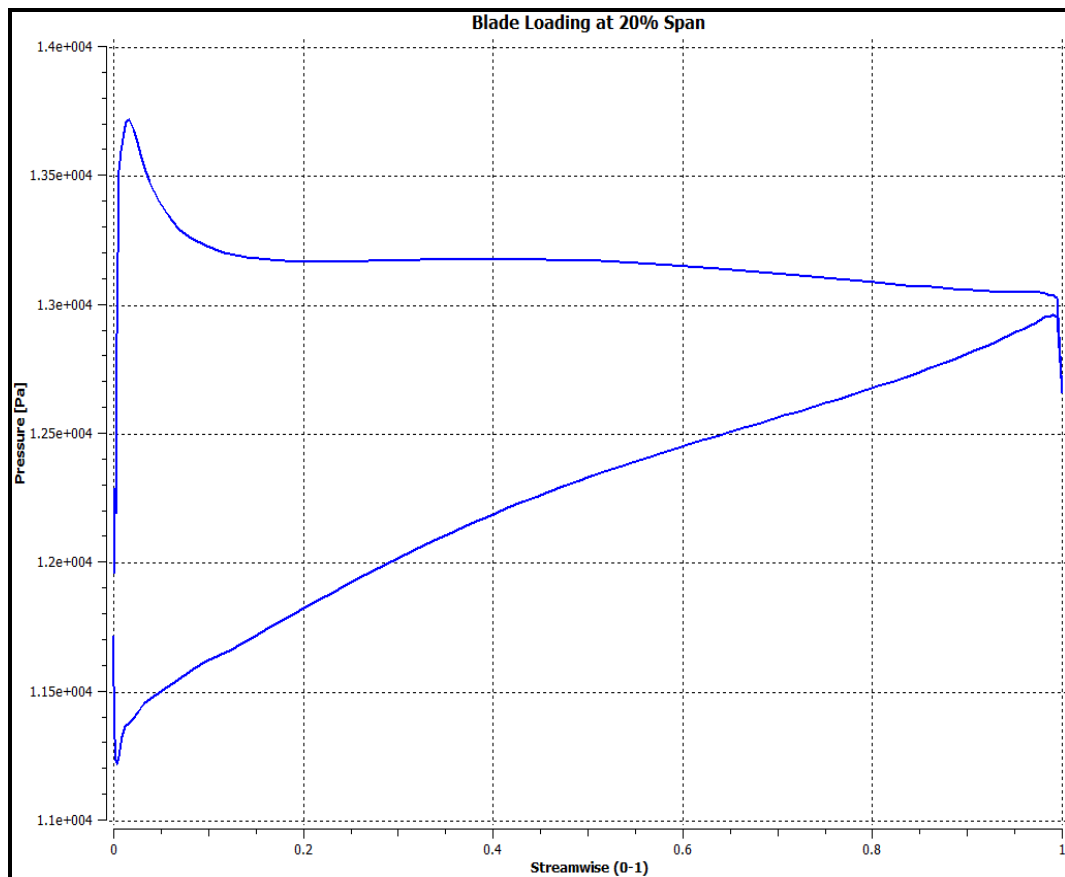
Figure 4-18: Blade Loading at 20% Span
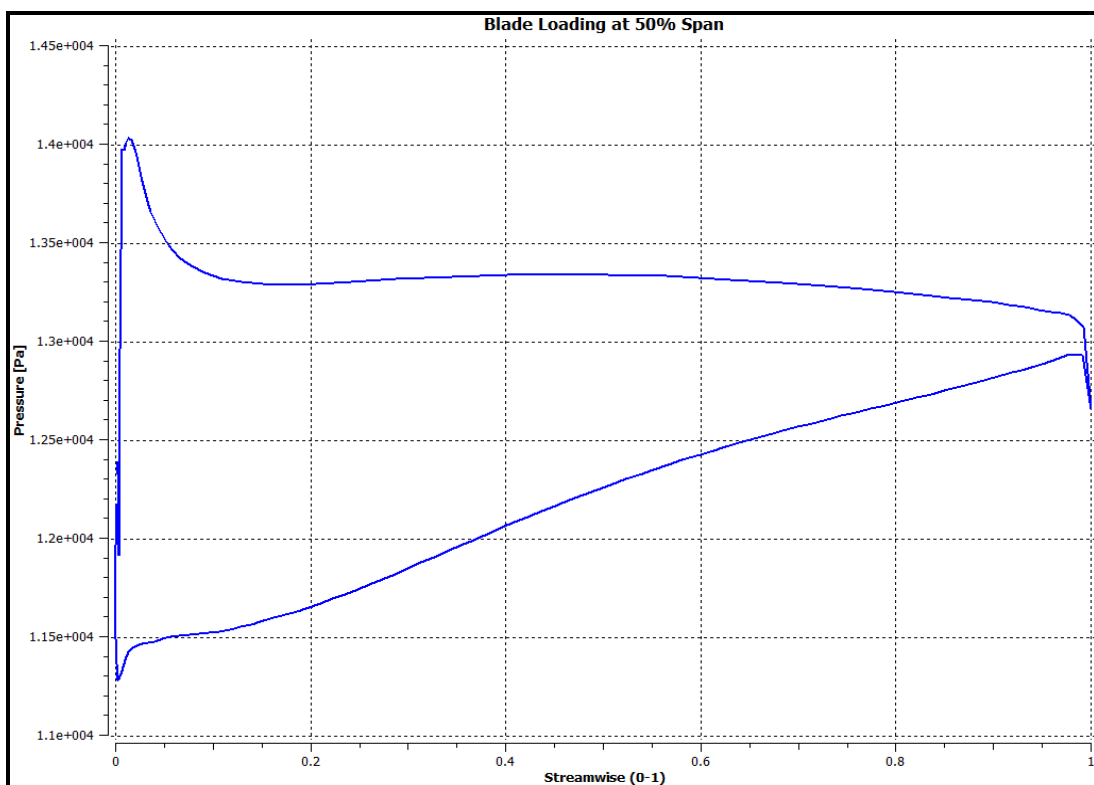
Figure 4-19: Blade Loading at 50% Span
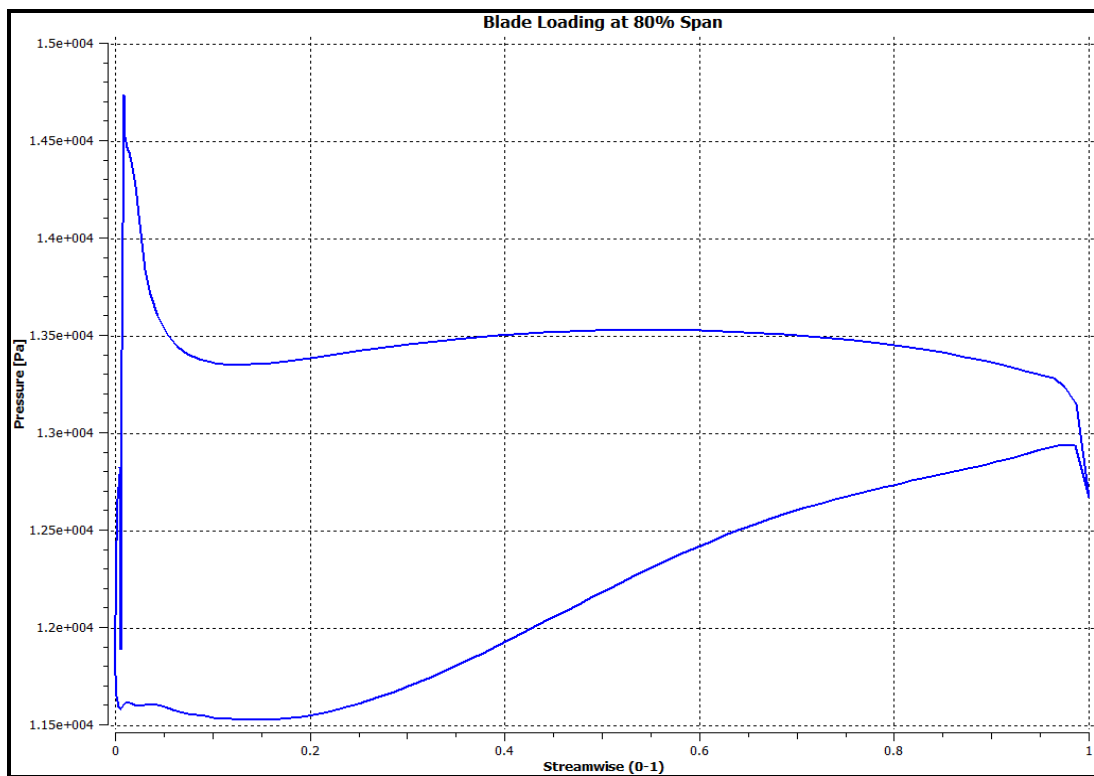
Figure 4-20: Blade Loading at 80% Span

4.6.3 Velocity

Span wise velocities are plotted as shown in figure 4-21. Meridional velocity observed near hub wall region and shroud wall region, are less when compared to mid-span of impeller blade. Maximum meridional velocities are observed between 20% to 80% of span, with maximum at 50% of span.
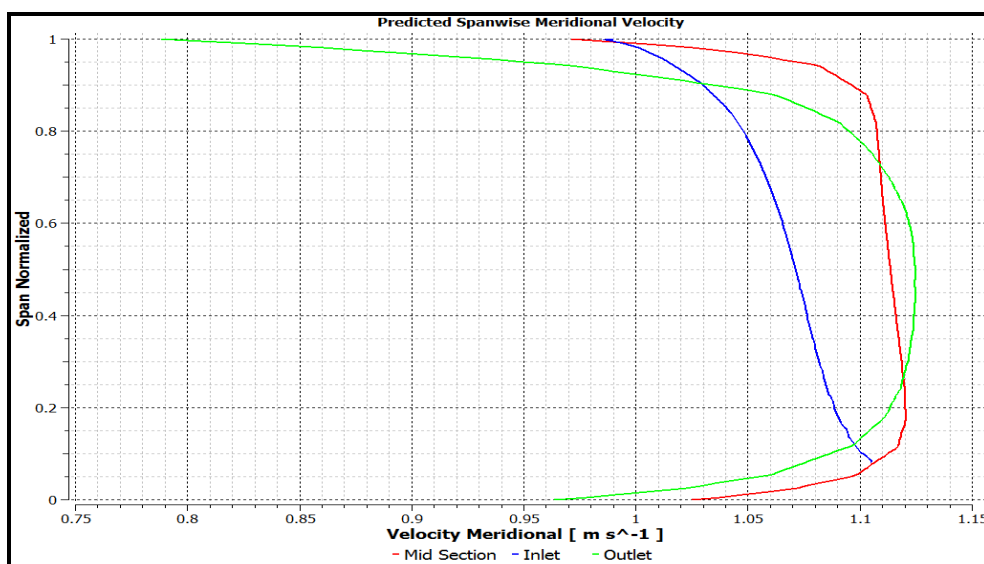
Figure 4-21: Spanwise Meridional Velocity
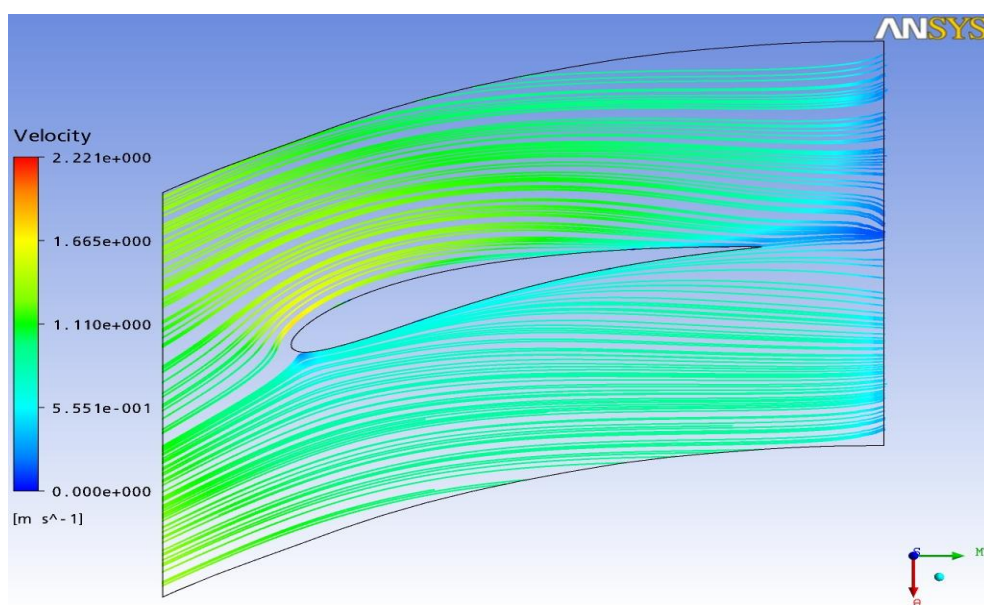
Figure 4-22: Velocity Streamline near hub wall region

Figure 4-22 depicts the velocity streamline across the blade near hub wall region. Streamline are observed parallel to the blade surfaces and have higher velocities at

suction side compare to pressure side of blade. Figure 4-23 shows the velocity streamlines at 50% of span where no recirculation or secondary flow are observed.
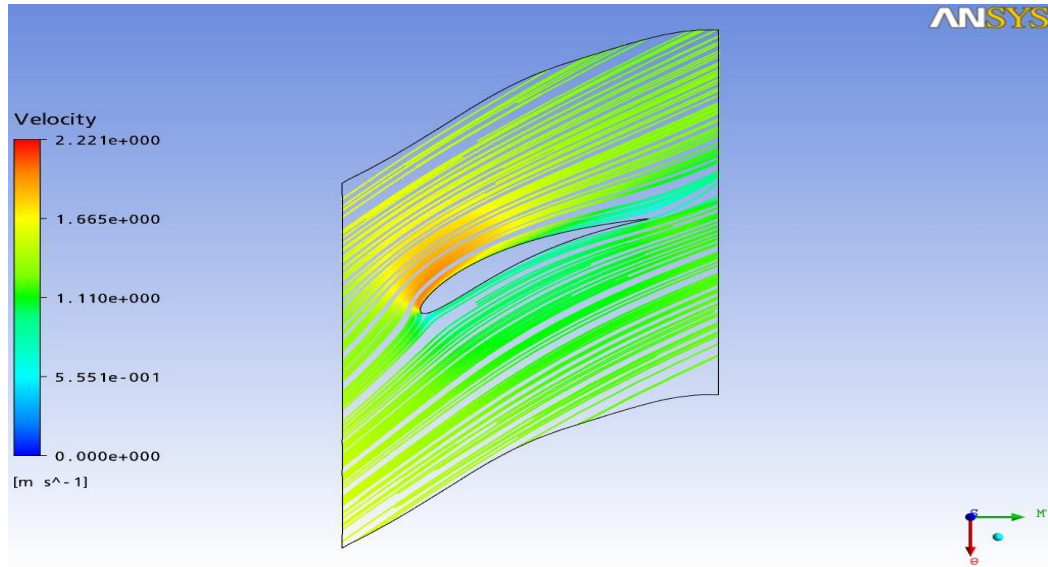
Figure 4-23: Velocity streamline at 50% span
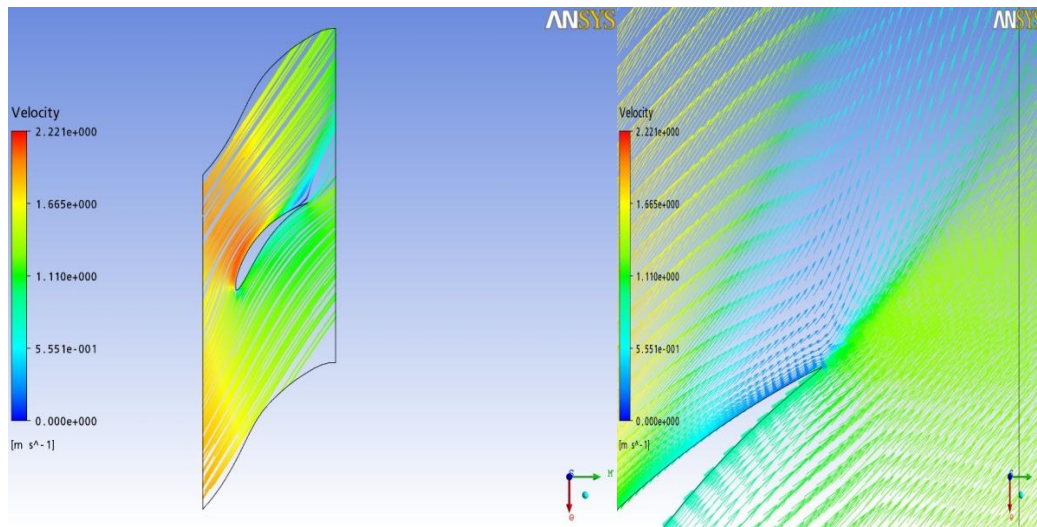
Figure 4-24: Velocity Streamline at Tip with Velocity Vector Plot at Trailing Edge of Blade

At tip section of blade shown in figure 4-24, streamlines at training edge of blade are merging with upstream streamlines and moving away from the tip. This separation show signs of amendments for blade angle β_2 at trailing edge .

4.6.4 Shear Stress

Figure 4-25, 26, 27 and 28 depict the observed shear stress at leading edge of impeller blade and hub wall region. Concentration of wall shear is observed at the leading edge towards suction side of the blade, mostly in the mid span area.
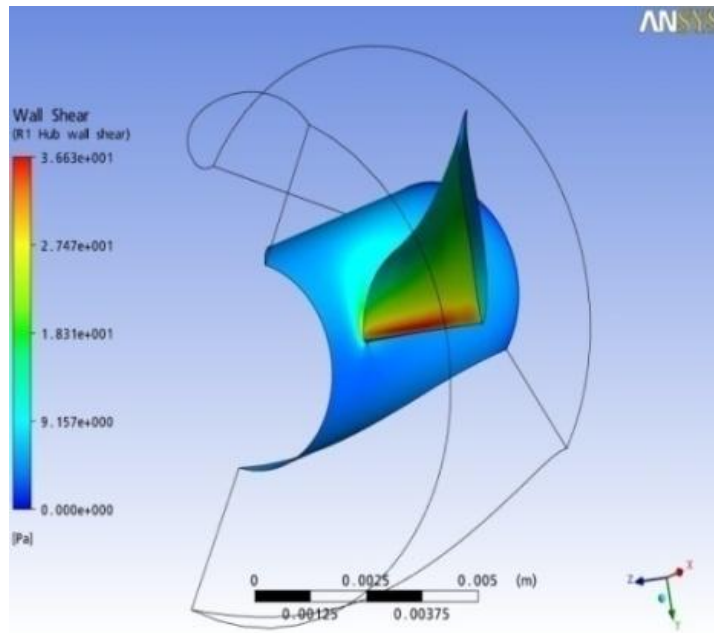
Figure 4-25: Wall Shear at Blade and hub section
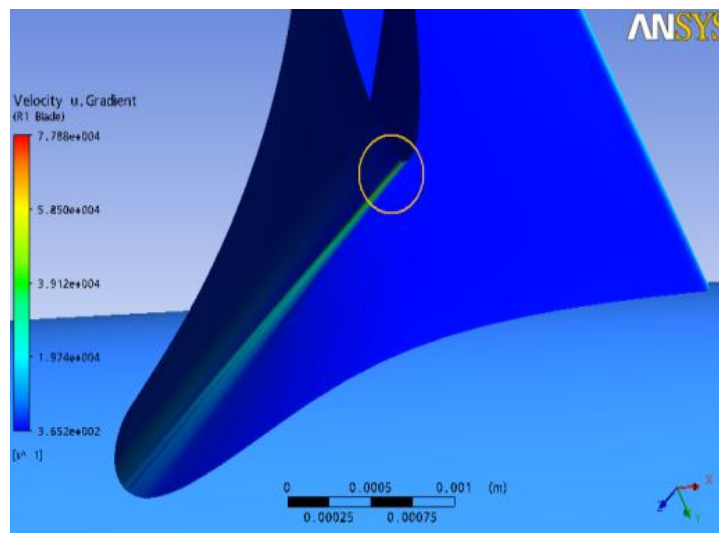
Figure 4-26: Shear Rate
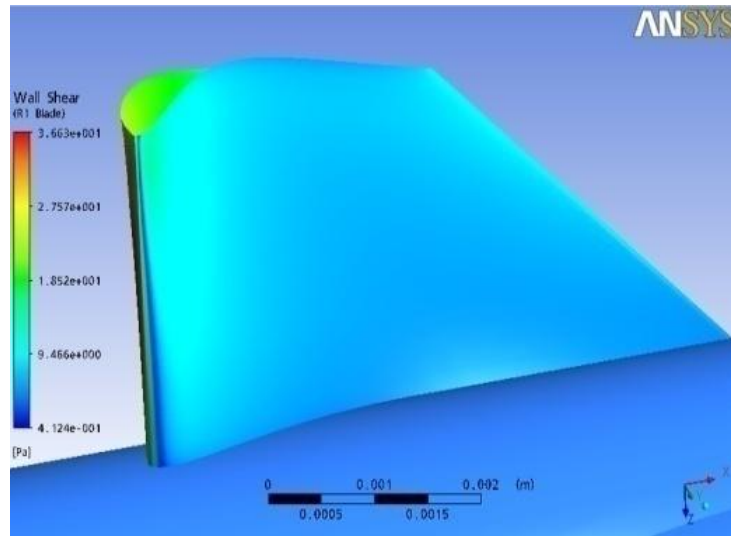
Figure 4-27: Wall shear stress at pressure side
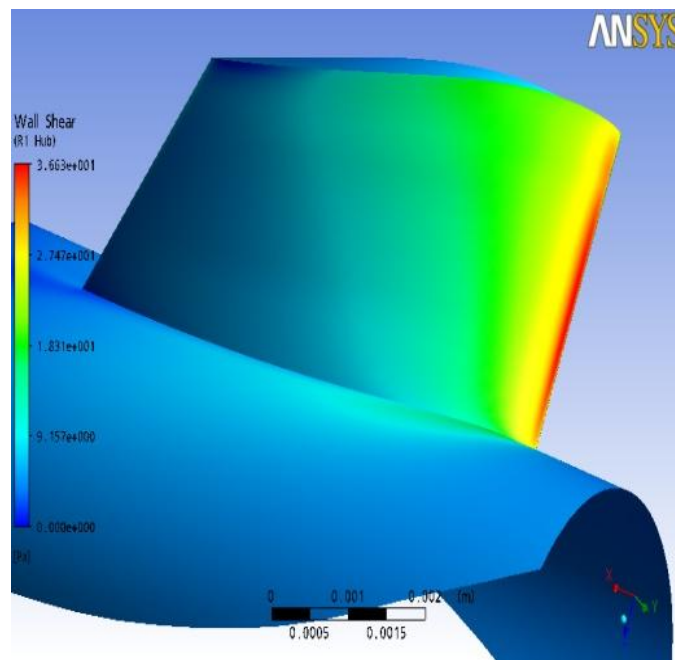
Figure 4-28 : Wall Shear Stress at Suction Side

The high velocity gradient (shear rate) of 49669.539 S^{-1} is observed at tip of the leading edge over 80% of span, shown in figure 4-26. While pressure side shows less wall shear stress below 231.501 Pa, shown in figure 4-27 and 28. Apart from leading

edge of pressure side of the blade, remaining area of blade shows wall shear stress well below 57.876 Pa.

4.7 Concluding Section

This chapter demonstrates use of CFD as an important design tool. The results of the steady state CFD simulation proves the pumps ability to satisfy the hydraulic and clinical requirement of designed axial flow LVAD operating as a continuous flow pump.

The main points, which were observed in this chapter:

- In the first section, CFD based parametric design of experiment (DOE) study helps in verifying the LVAD's ability to generate the physiological flow and pressure rise at different operating speed. This DOE study was mainly carried out to find out the effects of rotating speed on the various hydraulic and clinical design parameters.

- Response charts of the hydraulic and clinical design parameters for the LVAD's operating speed have demonstrated the trade off scenario amongst the parameters that can satisfies both hydraulic and clinical requirements. This trade off amongst the parameters requires the optimisation to get the operating speed of LVAD.

- Third section shows the goal driven optimisation (GDO) which uses Multi-objective Genetic Algorithm (MOGA) and Decision Support Process (DSP) to determine the operating speed of an LVAD. Using DSP, the range of operating speed which is 8000RPM to 10000RPM is derived. At this speed LVAD can deliver blood flow up to 6L/min, with the pressure rise of 31.50 mm of Hg across the impeller with 50% efficiency and shear stresses well below 300Pa.

- Fourth section shows the LVAD's pressure Vs flow characteristics. This characteristic was determined using the approach similar to industrial pump design. Outcome of the study shows the anticipated performance of an axial flow pump. Moreover shear stresses are observed well below the hemolysis

limit for the optimum operating range that makes the axial flow pump suitable to operate as a continuous flow LVAD.

- Last section of this chapter shows internal flow details of continuous flow LVAD. The detailed CFD investigation helps in visualizing the flow behaviour at critical locations of rotating and stationary components of LVAD. The key outcome of the simulations are listed below:

- Velocity streamline for the tip section show the need of amendment to avoid probable recirculation of flow.

- Shear stresses are mainly concentrated towards the leading edge and higher shear rate is observed near the leading edge of the rotating impeller blade. The maximum shear stresses are observed below the hemolysis limits.

Next chapter will demonstrate the use of CFD for the evaluation of LVAD as pulsatile axial flow pump.

Chapter 5 CFD Evaluation of LVAD as Pulsatile Axial Flow Pump

5.1 Abstract

Generation of a pulsatile flow using an axial flow pump is a novel feature of this thesis. This chapter demonstrates the results of transient CFD simulations that are used to investigate axial flow pump performance for the pulsatile mode of operation. Transient CFD simulations allow more realistic calculations of the velocity and pressure fluctuations within LVAD during dynamic flow conditions. The outcome of the transient CFD analysis of an axial flow pump including pressure flow characteristics and shear stress estimation are discussed in detail. Furthermore internal flow details for the time varying changes for pressure, velocity and the shear stress is illustrated.

5.2 Boundary condition for CFD simulation of pulsatile flow.

After successful mesh generation for transient simulation, boundary condition for computational flow model, were set to initiate the simulations. Flow through the pump was defined to be transient for the investigation of flow behaviour of single pulse based on the heart rate. The reservoir pressure (hydrostatic tank) was applied at the inlet and outlet for initiation of simulation. The time varying motor speed was applied to rotating domain for generation of pulse using parabolic function based on heart rate [figure 5-1]. The optimised speed range that is 8000RPM to 10000 RPM was selected as a limit speed for the transient CFD simulations.
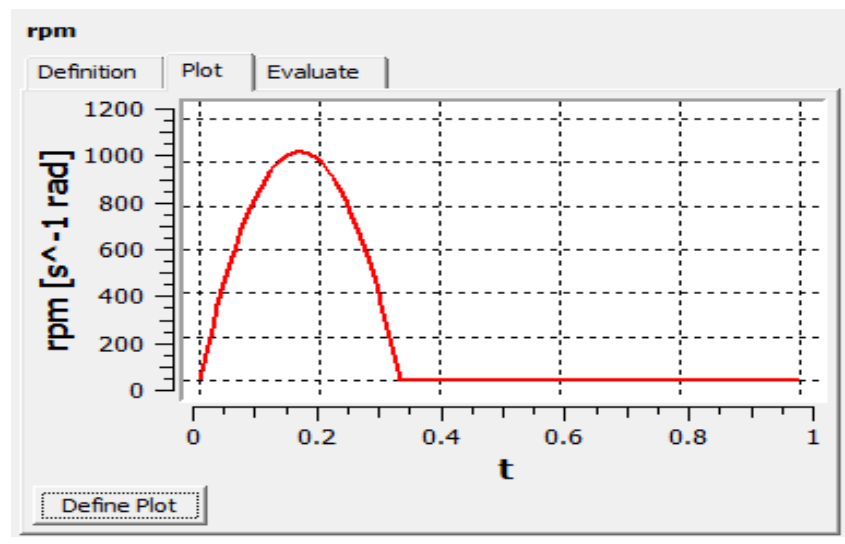
Figure 5-1: Time Varying Speed for Rotating Domain

Following the standard CFD practice, prior to each transient run the steady state CFD simulation were carried out to define the initial condition to fluid domain. The pressure rise across the impeller, flow rate and shear stress data were collected at each 0.01 s of the time step.

5.3 Pressure Vs Flow characteristic of LVAD as Pulsatile Axial flow Pump

Pressure Vs flow characteristics helps in understanding the performance of pump during systole and diastole. Traditionally, this characteristic is obtained by keeping the shaft rotating at a constant speed and by restricting the flow at the outlet. In case of pulsatile flow LVAD, the shaft speed varies with time for the respective heart rate. Hence, the characteristics are obtained by varying the rotating speed and observing the outlet flow for the single pulse based on the heart rate. Figure 5-2 depicts pressure rise across the impeller against mass flow rate that is generated for 40, 60, 80, and 100 BPM heart rate for the 10000 RPM limit speed. Despite the different heart rate, the pressure rise across the impeller Vs flow rate curve remains the same as shown in figure 5-2. In addition, Figure 5-3 shows the time varying flow rate and pressure rise for the same pulse. And figure 5-4 and 5-5 shows the time varying pressure and flow characteristics for the different heart rate.

The chart shows Pressure Rise Across Impeller [KPa] on the y-axis versus Mass flow Rate [cc/s] on the x-axis, with a SYSTOLE curve and DIASTOLE curve.

$y = 0.010x^2 - 0.095x - 0.171$

$y = -0.143x + 1.627$
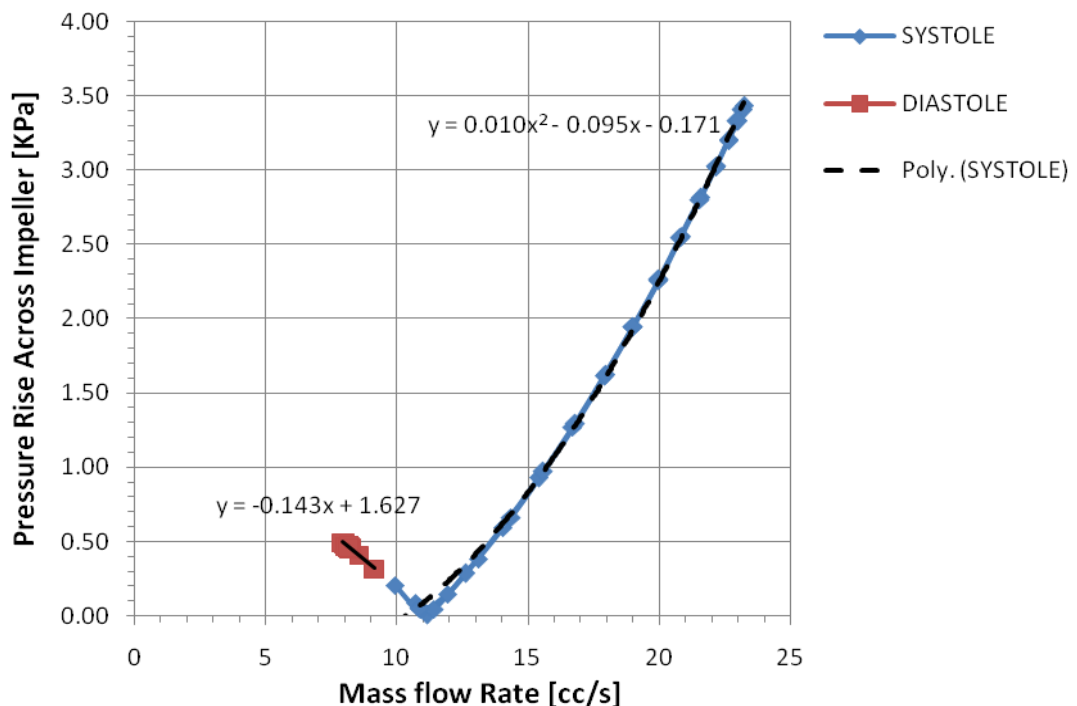
Figure 5-2: Pressure Vs Mass Flow Rate for 10000 RPM
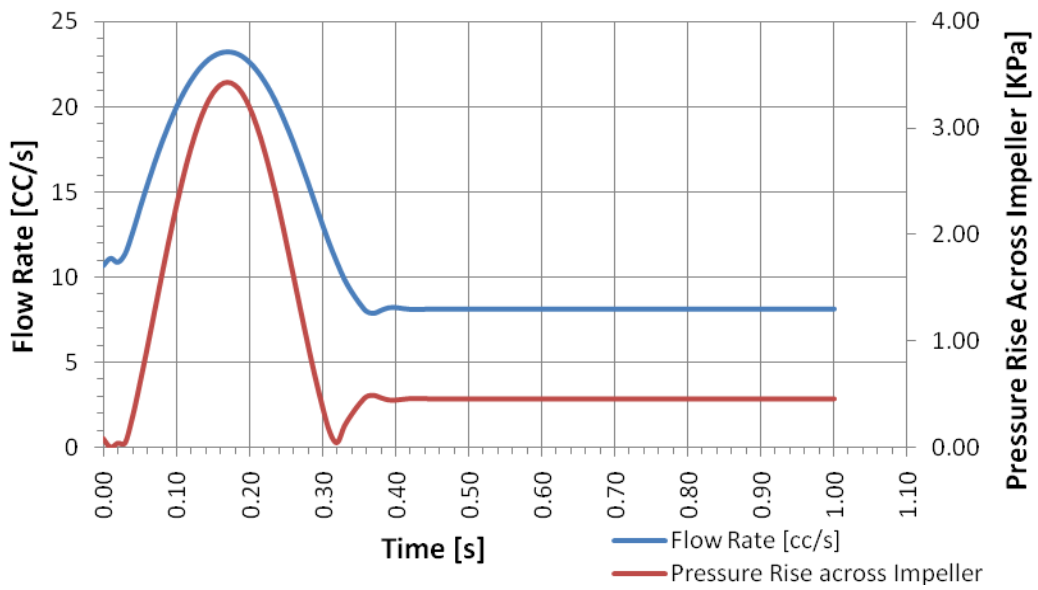
Figure 5-3: Flow Rate and Pressure Rise Across Impeller Vs Time

Pressure rise across the impeller varies according to the varying rotational speed during acceleration and deceleration phases of systole. Respective pressure and flow values forms a curve as shown in figure 5-3. During diastole, the pressure rise and flow remain constant. Despite this, the pressure rise is stopped at the end of systole, the flow remain continue during diastole. A constant pressure difference is also observed across the impeller during diastole.
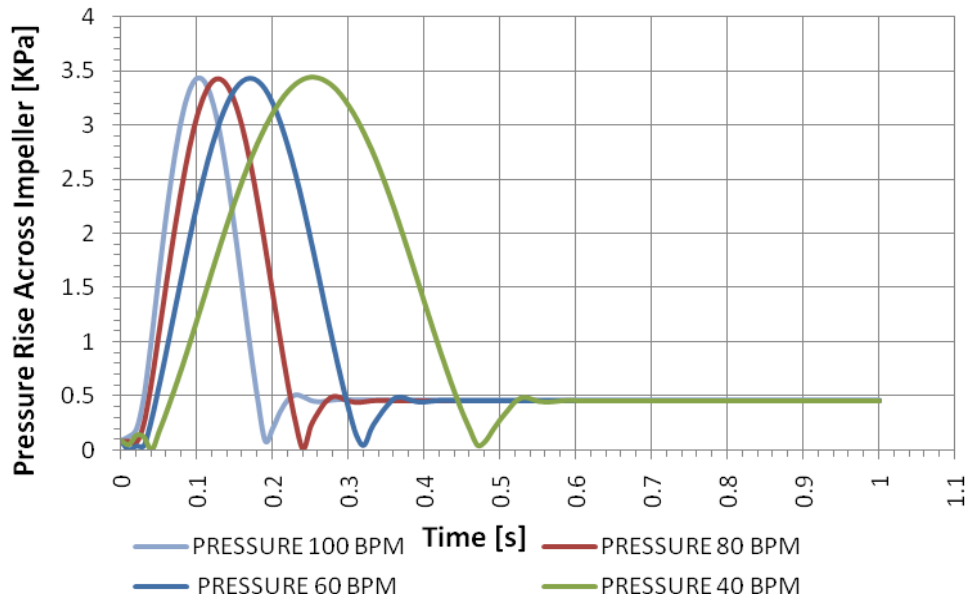
Figure 5-4: Pressure Vs Time based on Heart Rate
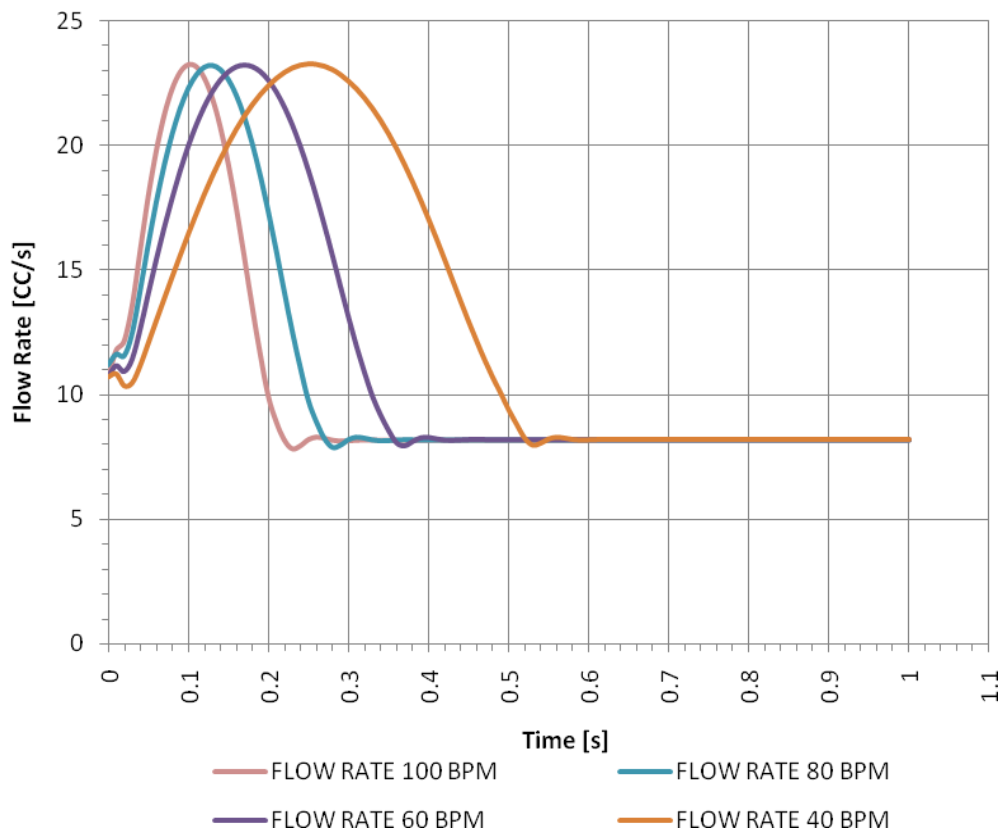
Figure 5-5: Flow Rate Vs Time based on Heart Rate

For10000 RPM limit speed, Figure 5-4 shows the pressure rise across the impeller Vs time for different heart rate and figure 5-5 shows the flow rate Vs time for the different heart rate.

5.4 Detail flow investigation of pulsatile axial flow LVAD

The detail CFD investigation of pulse generation using transient analysis has been carried out, for 40, 60, 80, and 100 BPM heart rate and the limit speed of impeller varying from 5000 to 10,000 RPM. For the purpose of this thesis, outcomes of 60BPM heart rate with 10,000RPM limit speed are discussed in detail.

5.4.1 Pressure
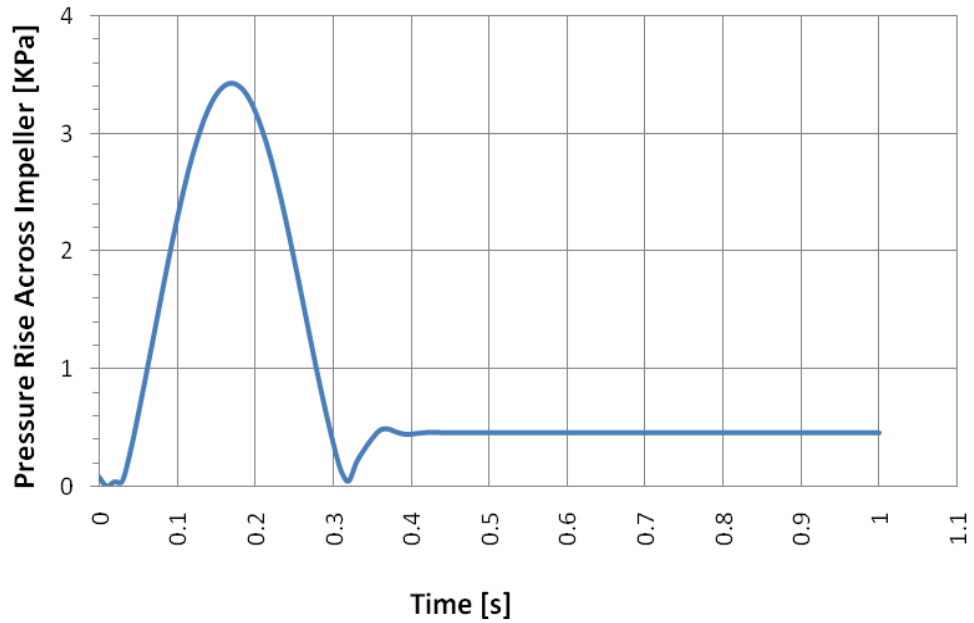
Figure 5-6: Pressure rise across rotating domain (Pout -Pin)

Computed time varying pressure rise across the impeller is depicted in figure 5-6. The maximum pressure rise of 3.43 KPa across the impeller is observed at 0.17 sec which is almost at the same time of the maximum RPM that is shown in figure 5-7.
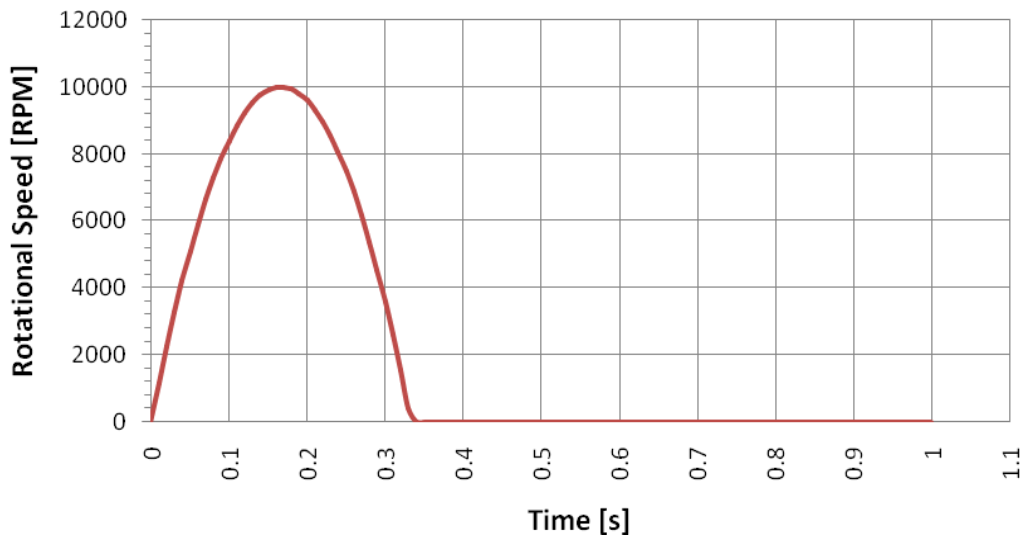
Figure 5-7: Rotational Speed Vs Time

These figures are generated for 60 BPM heart rate considering 0.333-systole duration. Rotating domain accelerates up to limit speed and decelerates back to zero within

333ms. Pressure rise across the pump is negligible for initial 30ms. From 40ms to 170ms, the pressure rise across the impeller rises with the increasing rotational speed, then decreases in correspondence to rotational speed up to 333 ms. Further increments in pressure rise across the impeller is observed even after the rotational speed reaches zero. This remains until the end of pulse with 0.5KPa magnitude. Even though there is no energy transferred to the fluid domain, this evident pressure difference drives the flow across fluid domain.

5.4.1.1 Span wise pressure distribution at 15% span

Time varying span wise pressure distribution near hub at 15% span are depicted in figures below. These figures are generated for the 0,70,150,220,270,300,333,360, 700 and 999 ms that covers the pulse generated during systole (0-333msec) as well as diastole (333-1000msec).
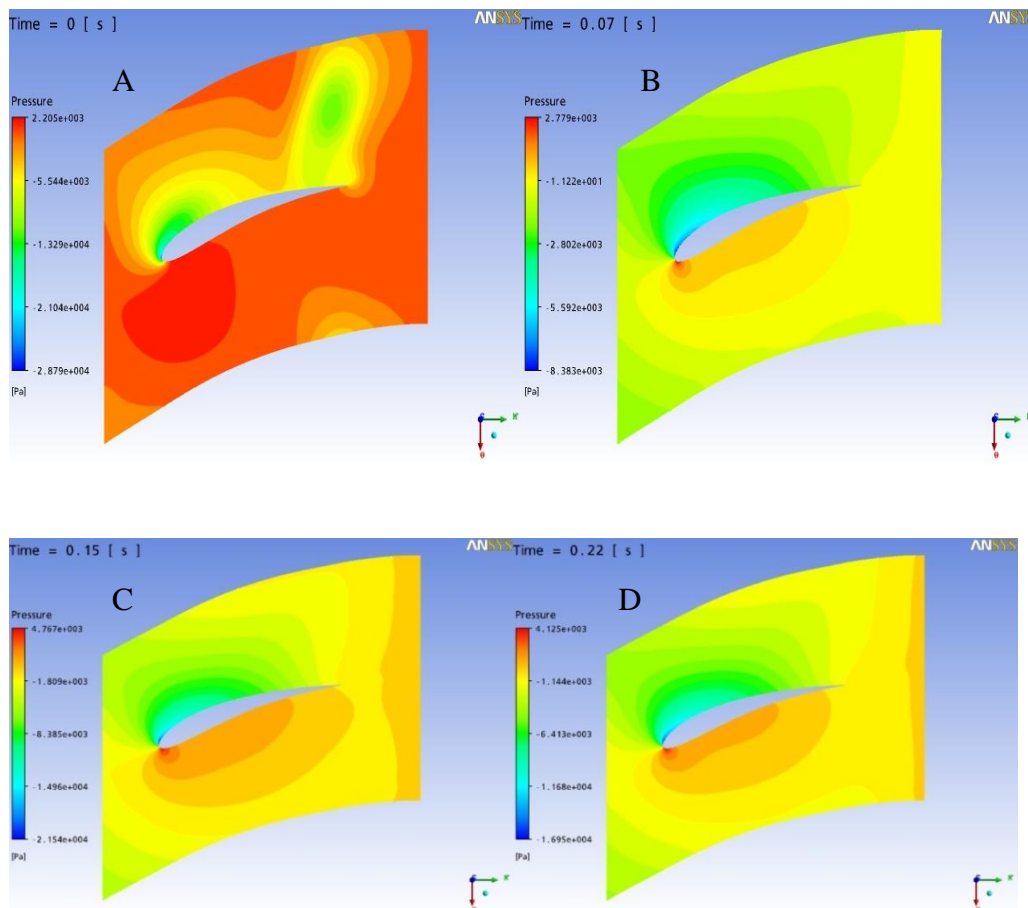
Figure 5-8: Pressure Distribution At 15% Span. A) Pressure Distribution at 0ms B) At 70ms C) At 150ms D) At 220ms E) At 270ms F) At 300ms G) At 333ms H) At 360ms I) At 700ms J) At 999m

At the beginning of acceleration (initial 30ms), the pressure difference between inlet and outlet of the rotating domain is negligible and corresponding span wise pressure contour plots at hub, shows the pressure difference across the blade, where the high pressure is evident at lower surface. Upper surface shows the formation of low-

pressure region near the leading edge and the trailing edge. During this initial period of 30 ms, high pressure is observed at both inlet and outlet. With progressing time during systolic phase, high pressure is observed at lower surface of blade and the upper surface shows evenly distributed low pressure through out the length of blade, which is evident in the figures for systolic time duration of 0 to 300 ms. During the systolic time period, the pressure difference between the inlet and outlet increase with increasing rotational speed and decreases with the reducing speed. At 333ms, the systolic phase of VAD finished and the impeller is at rest. During this period, the pressure rise across the blade is observed to be negligible. Further increase in pressure difference across the fluid domain is observed in diastolic period where inlet pressure is more than outlet pressure: this in contrast to the systolic phase where outlet pressure in observed to be more than inlet pressure. In addition, the high pressure in observed at the upper surface, near leading edge and low pressure is observed at lower surface of blade.

5.4.1.2 Span wise pressure distribution at 50% span.

Span wise pressure distribution near mid span at 50% span are depicted in figures below. These figures are generated for the same periods of the previous section. Time varying Pressure distribution is similar to the near hub region with the noticeable difference in the magnitude of pressure, where at the beginning of systole lower pressure is observed through the length of blade along with the separate low-pressure region in fluid domain above the upper surface near trailing edge side.

Figure 5-9: Pressure Distribution at 50% Span. A) Pressure Distribution at 0ms B) at 70ms C) at 150ms D) at 220ms E) at 270ms F) at 300ms G) at 333ms H) at 360ms I) at 700ms J) at 999ms.

5.4.1.3 Span wise pressure distribution at 85% span.

Span wise pressure distribution near mid span at 85% span are depicted in figures. These figures are generated for the same periods of 15% and 50% span.
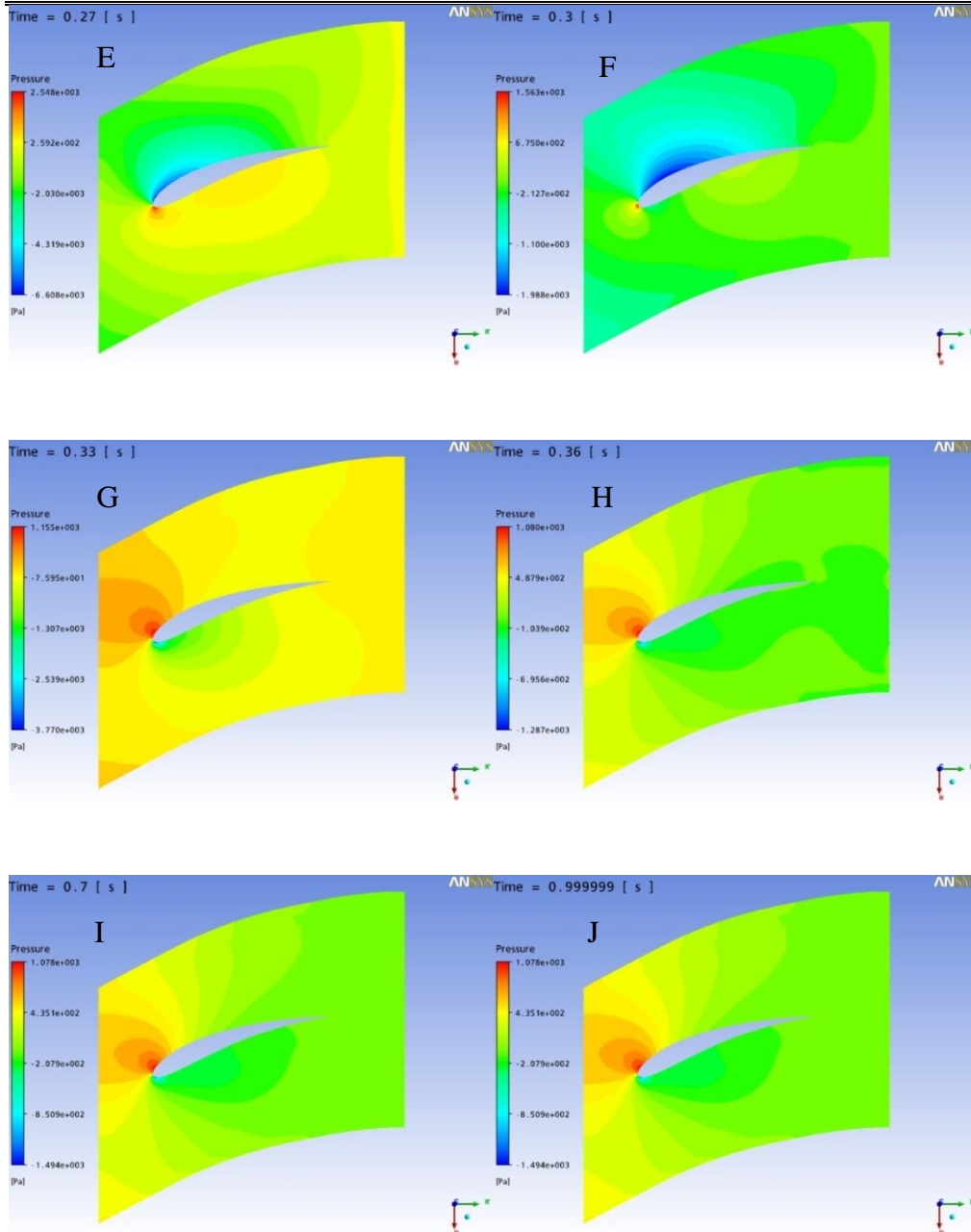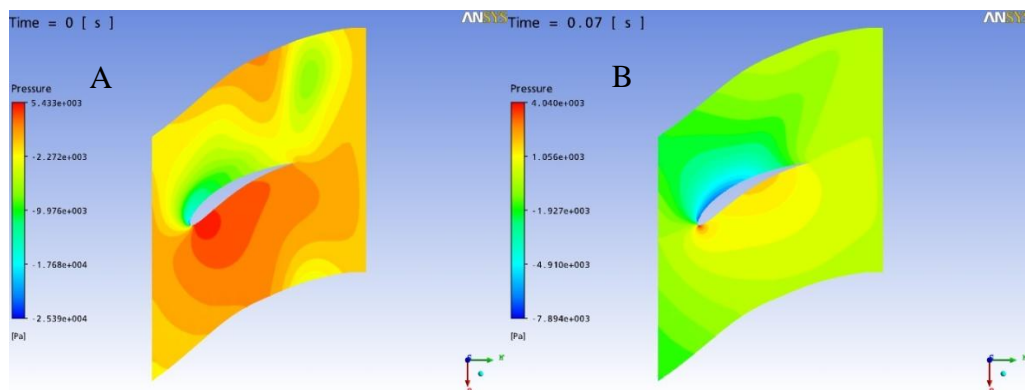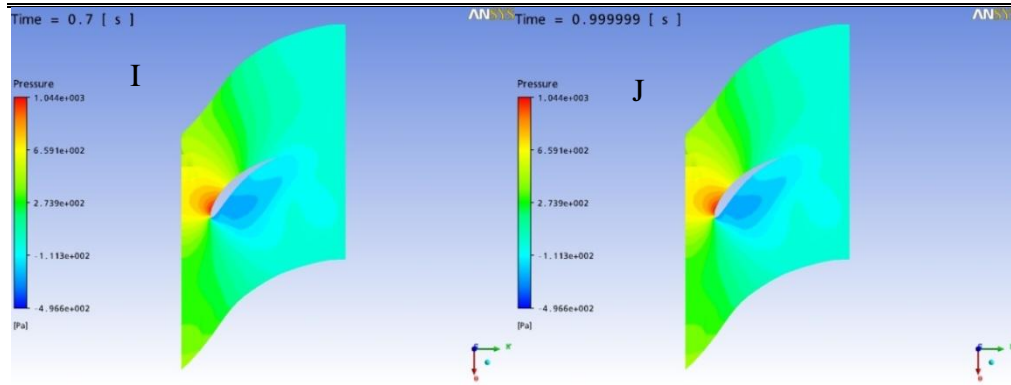
Figure 5-10: Pressure Distribution at 85% Span. A) Pressure Distribution at 0ms B) at 70ms C) at 150ms D) at 220ms E) at 270ms F) at 300ms G) at 333ms H) at 360ms I) at 700ms J) at 999ms.

At the beginning of systole, similar to mid span and near hub region at 85% span, high pressure is observed at lower surface however, no separate high or low-pressure region in fluid domain is observed. During acceleration period of systole near trailing edge of lower surface, a high-pressure region is observed. At the same time, low-pressure region at upper surface seem to be dragging the blade against rotation. Similar to mid span and near hub region during diastole, the low-pressure region is observed at lower surface mainly at the leading edge side. Further in time frame, at the end of diastole this low-pressure region expands across the length of lower surface along with the concentration of low-pressure moves away from lower surface within the fluid domain.

5.4.1.4 Meridional Pressure Distribution

In this section, time varying meridional pressure distribution are depicted in the figures. Meridional plots helps in observing the pressure distribution along the axis of rotating fluid domain. Periods of these plots are in line with the previous section. During the systolic phase, low-pressure at inlet and high pressure at outlet is observed.

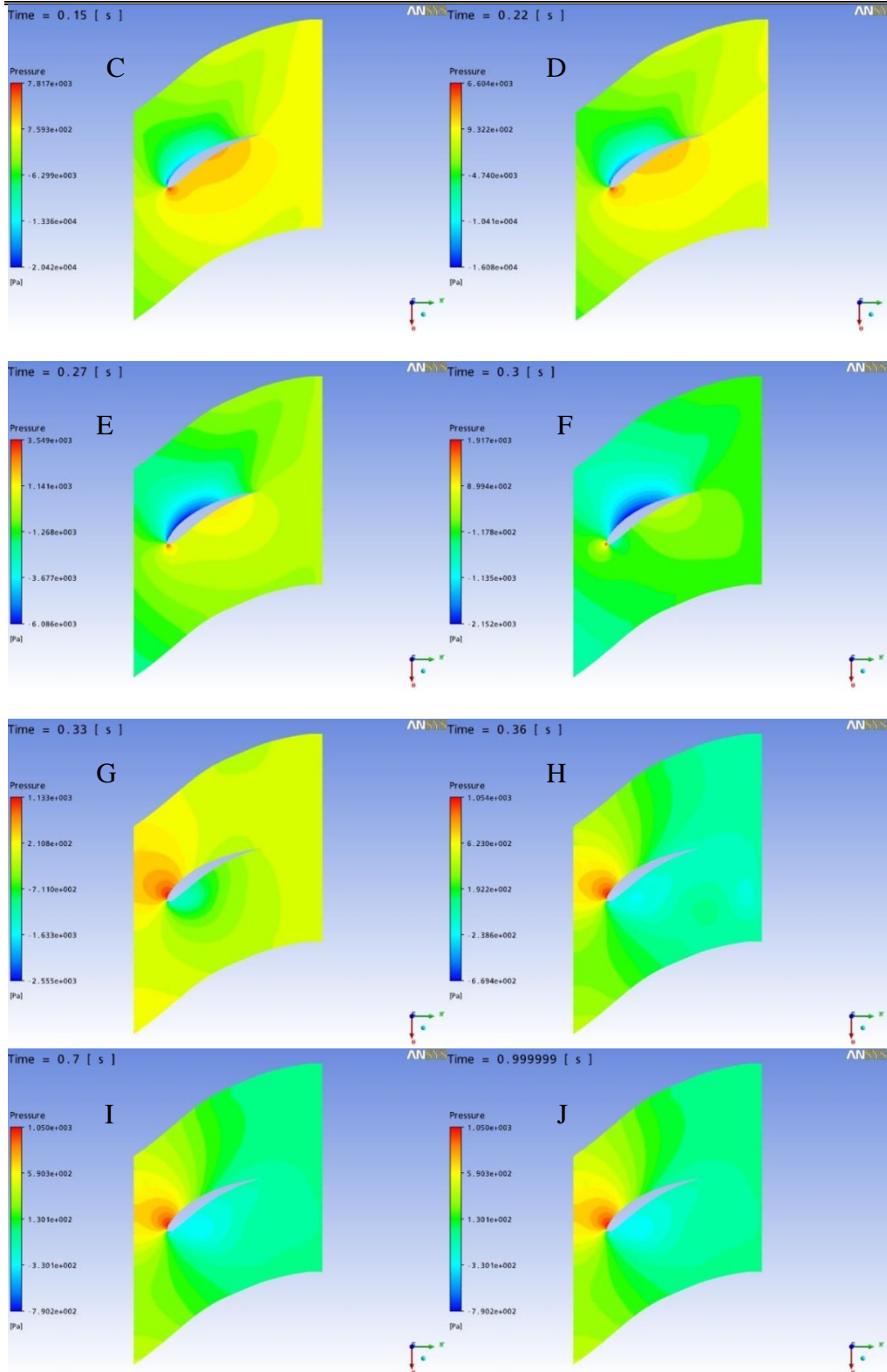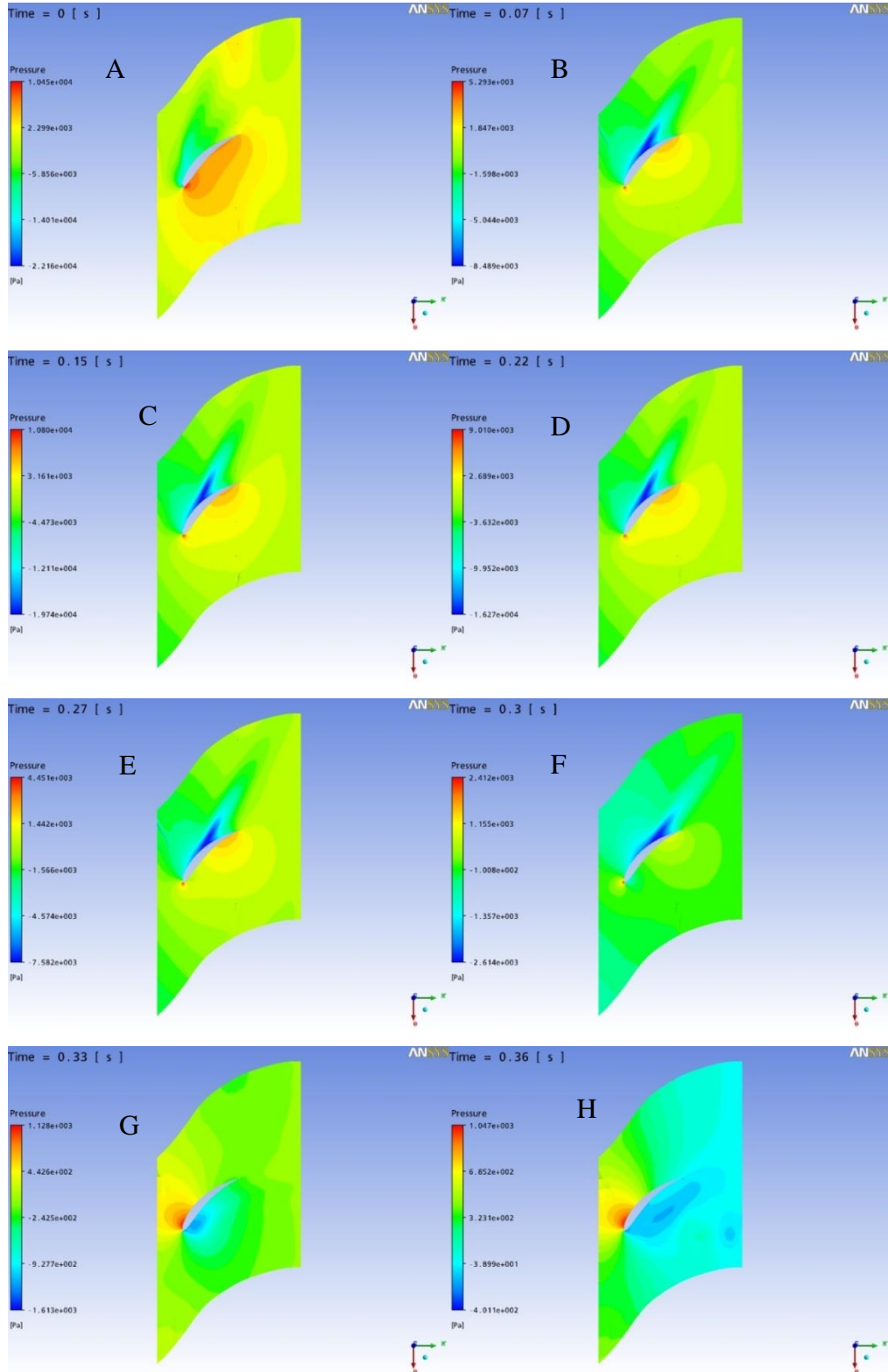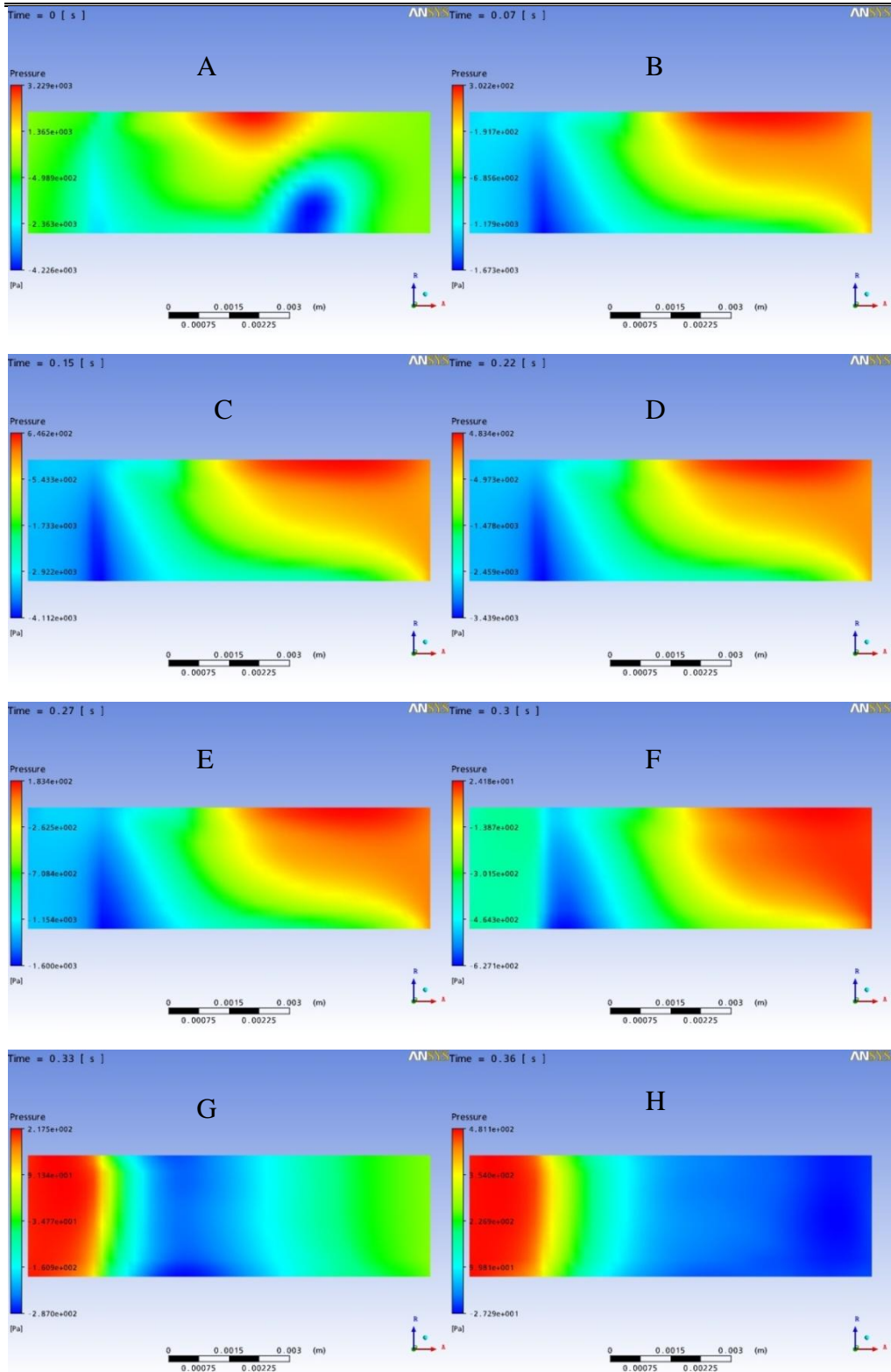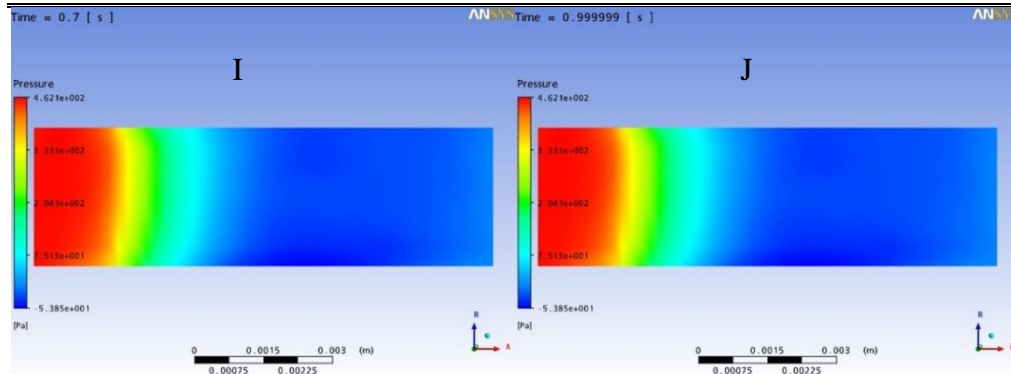**Figure 5-11: Meridional Pressure Distribution. A) Meridional Pressure Distribution at 0ms B) at 70ms C) at 150ms D) at 220ms E) at 270ms F) at 300ms G) at 333ms H) at 360ms I) at 700ms J) at 999ms.**

At the end of systole the pressure at inlet is observed to be higher than the outlet and the difference between the two sides remain almost same for rest of the diastolic period [figure 5-11].

5.4.2 Velocity
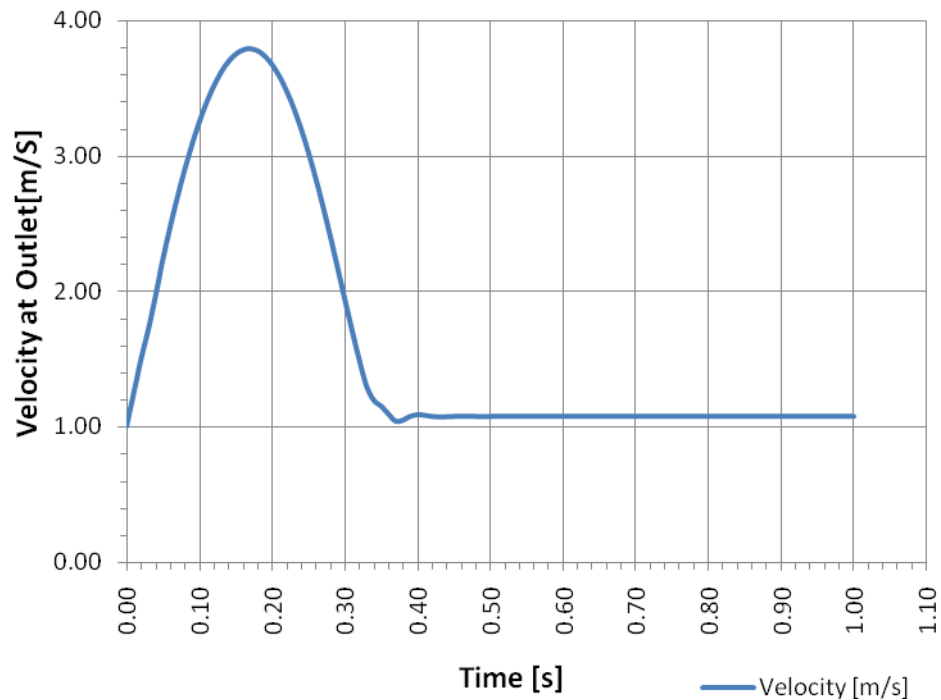
Figure 5-12: Velocity Vs Time

Computed time varying velocity at outlet is depicted in figure 5-12. Maximum of 3.79 m/s is observed at 170 ms during systole. During diastole, velocity remains almost 1.07m/s. The velocity streamline provides information concerning areas of irregular flow patterns. These velocity profiles can be examined along any plane of interest in computational flow field to identify regions of irregular flow patterns and large gradients resulting in fluid stresses. The velocity streamline plotted at 15% span that is near to hub region, at 50% span near the mid section and at 85% span near to the tip of impeller.

5.4.2.1 Velocity streamline plot at 15% span

The velocity streamline depicted in figures below are generated for the near-hub region at 15% span. At the beginning of systole, streamline shows the disturbance in flow. During acceleration and deceleration, the streamline from inlet and outlet are observed to be in parallel to the blade surfaces and have higher velocity at upper

surfaces of the blade compared to lower surfaces of blade. In addition, no recirculation or secondary flows are observed.
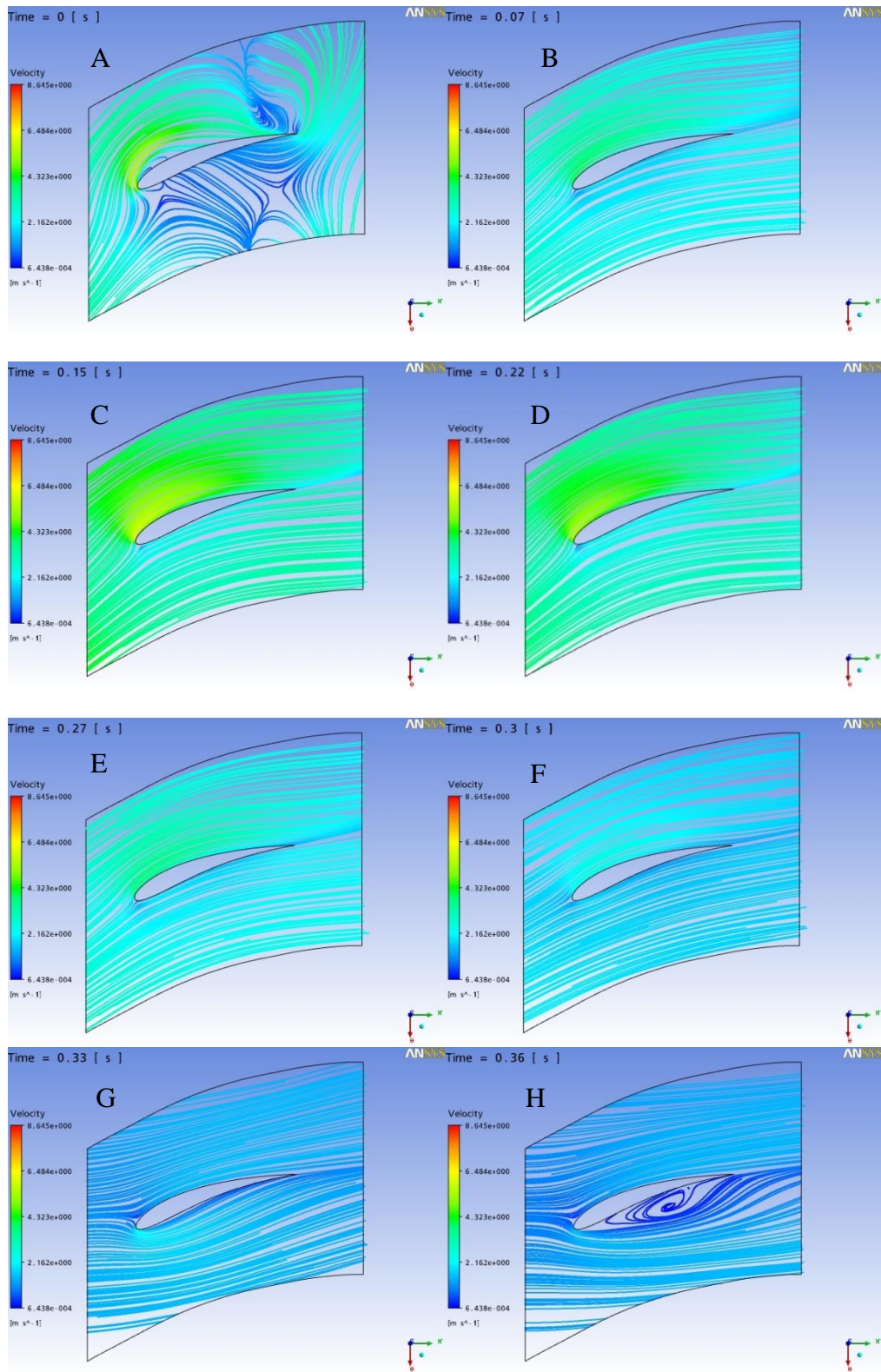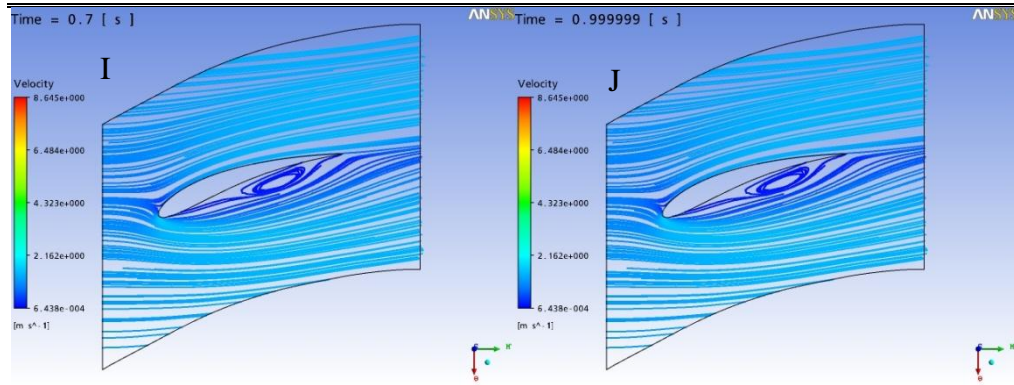
Figure 5-13: Velocity Streamline Plot at 15% Span. A) Velocity streamline plot at 0ms B) at 70ms C) at 150ms D) at 220ms E) at 270ms F) at 300ms G) at 333ms H) at 360ms I) at 700ms J) at 999ms.

During diastole phase where impeller is at rest the streamline shows the formation of recirculation regions at the lower surface of the blade. Because flow continues during this phase, the impeller blade behaves as an obstacle for the flowing fluid.

5.4.2.2 Velocity streamline plot at 50% span

Velocity streamline plot at 50% span shows similar behaviour of the near hub region during systole and diastole. Noticeable difference in the magnitude of velocity at the mid span, where the flow velocities are higher than the near hub region. Despite that recirculation and secondary flows are absent during systole.
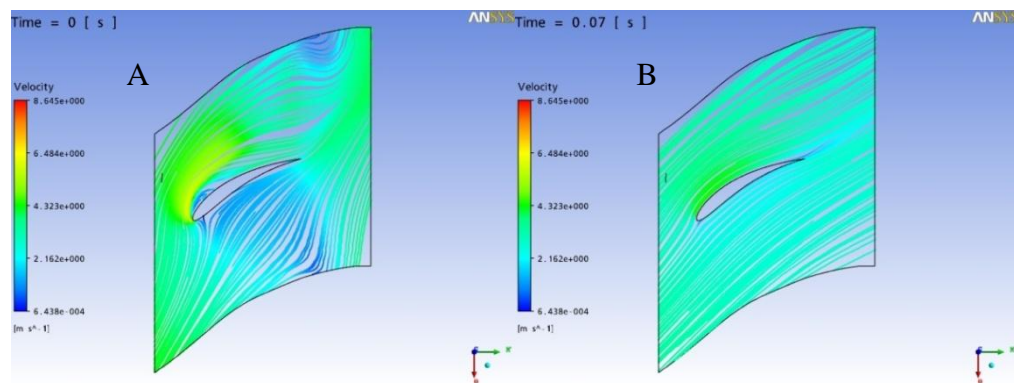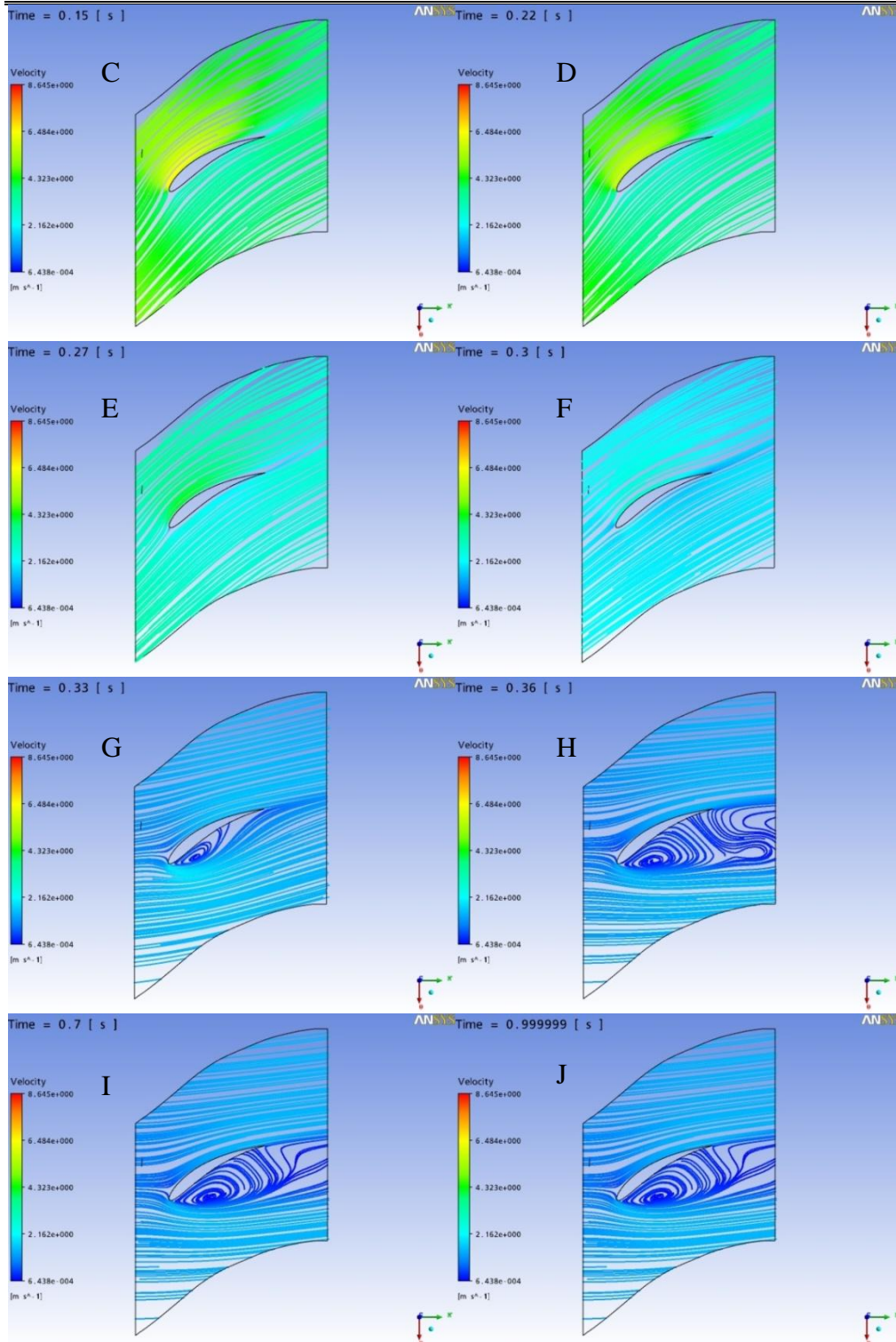
Figure 5-14: Velocity Streamlines Plot at 50% Span. A) Velocity streamline plot at 0ms B) at 70ms C) at 150ms D) at 220ms E) at 270ms F) at 300ms G) at 333ms H)at 360ms I) at 700ms J) at 999ms.

During diastole, the recirculation region is observed near leading edge of lower surface of the blade.

5.4.2.3 Velocity streamline plot at 85% span

In this section figures shows the Velocity streamline at 50% span for the systole and diastole phase. Velocity streamline shows the similar behaviour that is observed at 15% and 50% spans.
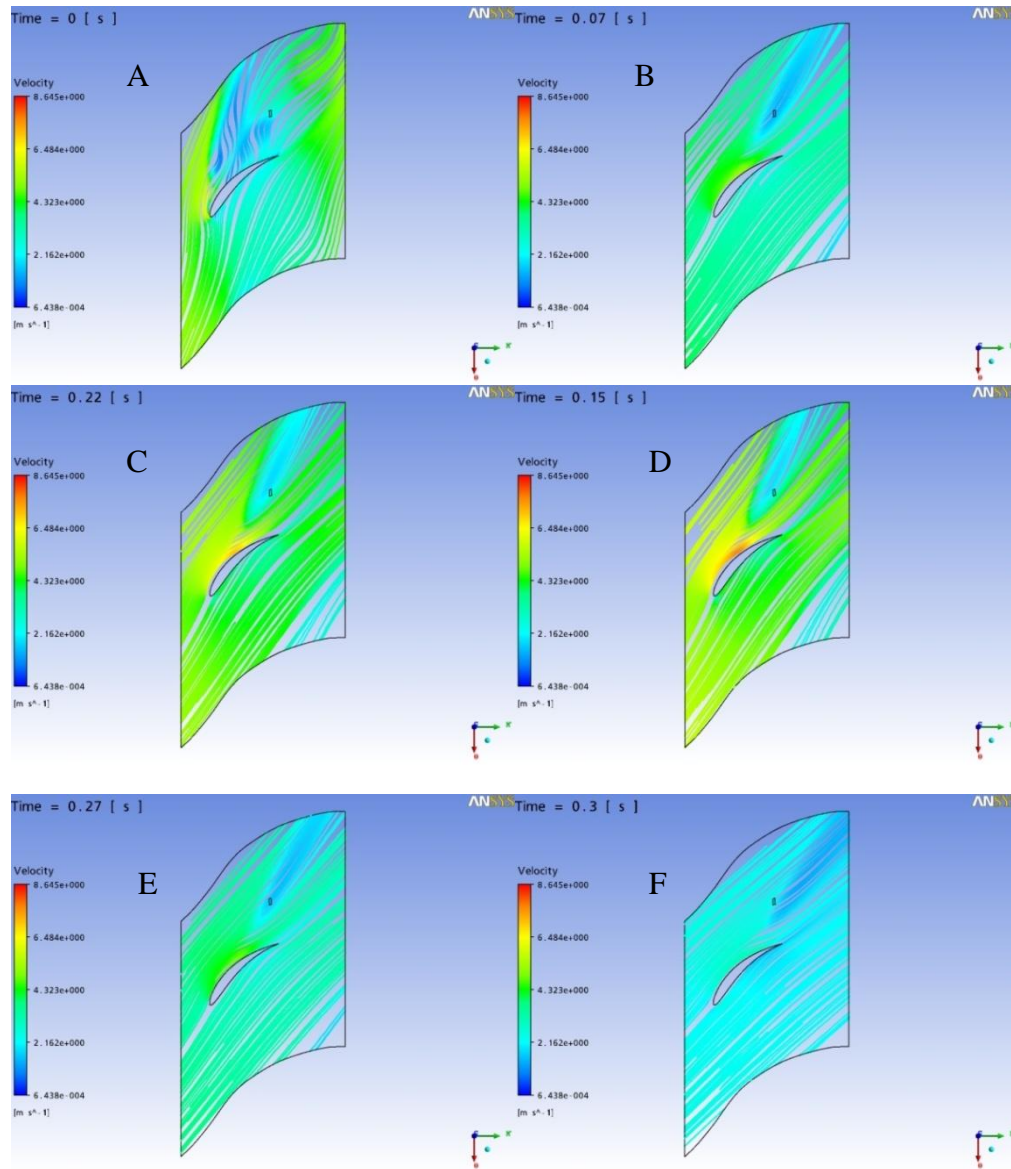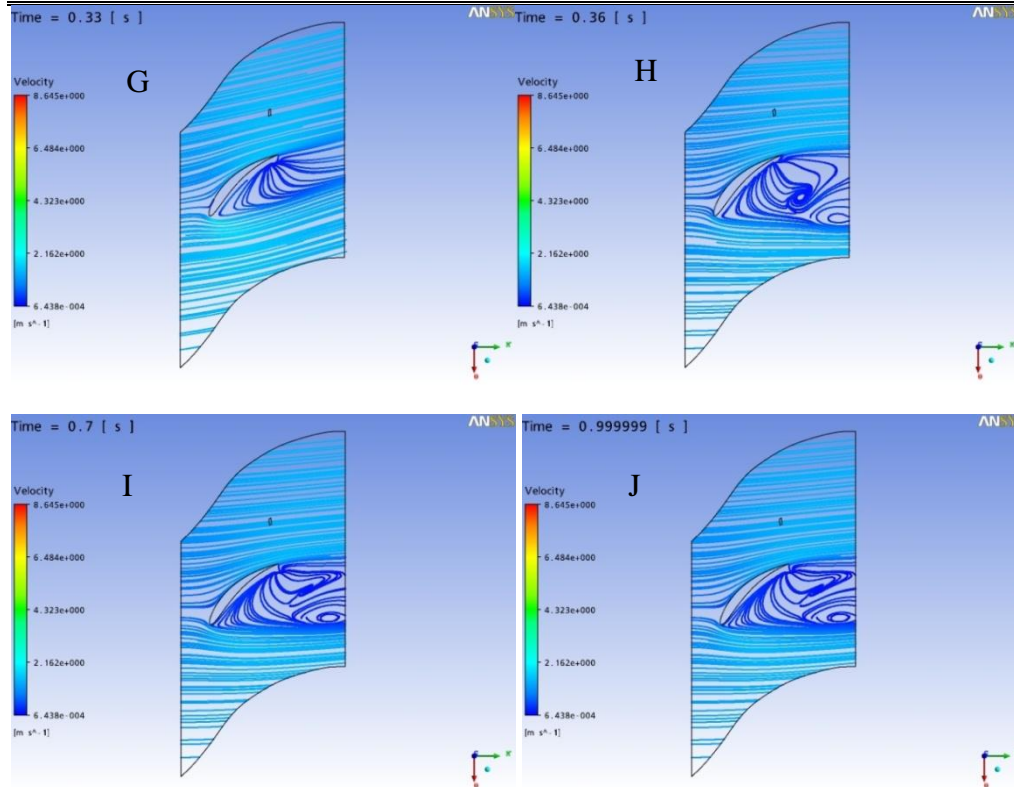
Figure 5-15: Velocity streamline plot at 85% span. A) Velocity streamline plot at 0ms B) at 70ms C) at 150ms D) at 220ms E) at 270ms F) at 300ms G) at 333ms H)at 360ms I) at 700ms J) at 999ms.

Noticeable low velocity streamlines were observed in fluid domain above the upper surface of blade in fluid region during systole.

5.4.2.4 Meridional velocity plot

Times varying meridional velocity are depicted in figures for the period of systole and diastole. During systole, the higher velocity is observed at the inlet of pump and near shroud region. At the beginning of systole, the velocity vectors show the flow in both direction that is in the direction towards inlet and outlet. For the same period, the pressure rise across the pump is also negligible. With the increase in acceleration, the velocity vectors show the flow from inlet to outlet, with higher velocity near shroud region.
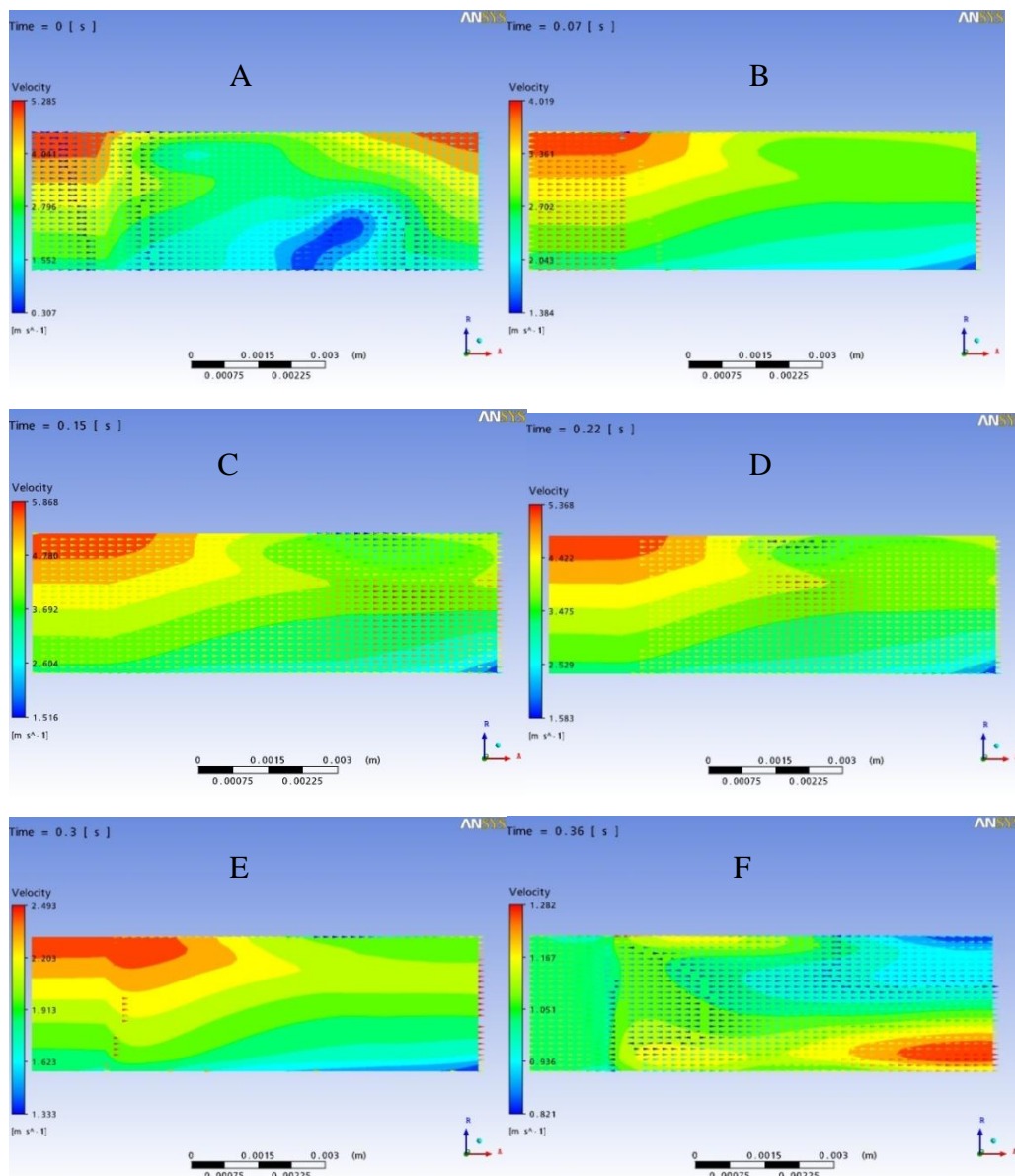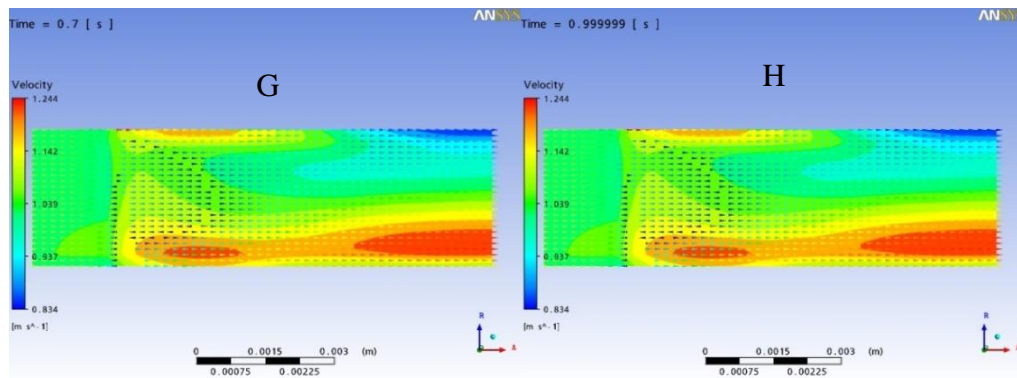
Figure 5-16: Meridional Velocity Plot. A) Meridional Velocity Plot at 0 msec. B) at 70msec C) at 150msec D) at 220msec E) at 333msec F) at 360msc G) at 700msc H) at 999msec.

Through the acceleration and deceleration during systolic phase, recirculation or secondary flow were absent within the fluid domain. During diastole the higher flow velocity were observed near the hub region compared to the shroud region. The magnitude of the velocity during systole is 1.07 m/s that is very low compared to the peak velocity of 3.79 m/s. Similar to the streamline observations the recirculation is observed near hub region during diastole, that remains till the end of diastole.

5.4.3 Shear stress

To avoid hemolysis, shear stress on the impeller is one of the crucial design concerns. Figure 5-17 shows the graphical representation of time varying maximum shear stress levels in VAD. This graphical representation provides predictions regarding regions of low and high stresses in VAD. At 170 ms highest shear stress is observed at the tip of blade as well as the leading edge [figure 5-18] that is around 320 Pa which is far below the value of 400 Pa quantified by Sallam and Hwang (Sallam and Hwang, 1984) threshold at which hemolysis occurs. The lower stresses ware found near the hub.
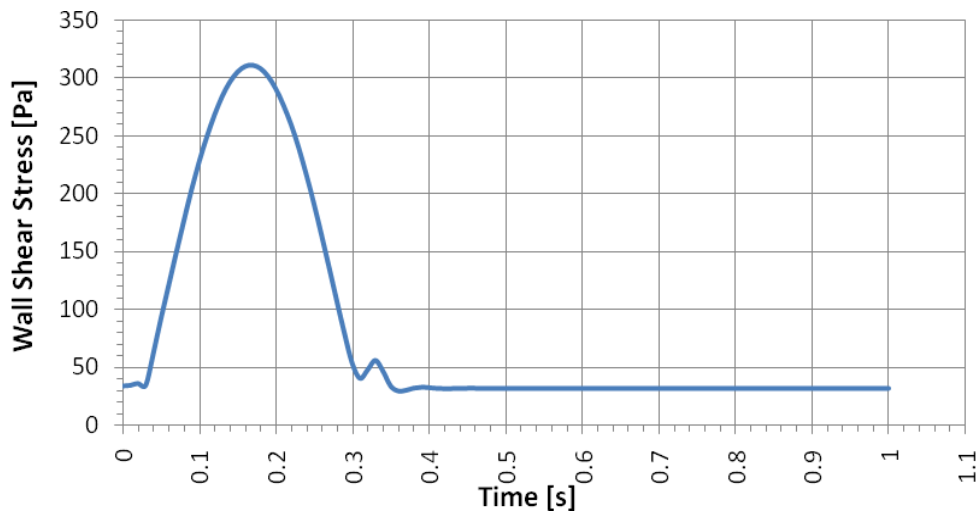
Figure 5-17: Wall Shear Stress Vs Time
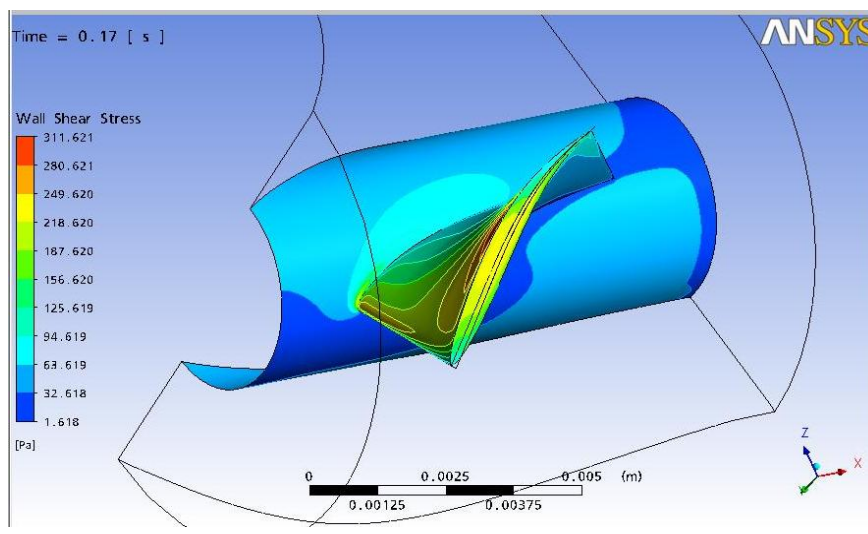
Figure 5-18: Wall Shear Stress At 170ms

The fluid is exposed to higher shear stress during systole compare to diastole. At higher values (above 300 Pa) fluid is exposed for 50ms time duration. The average shear stress in rotating component during systole is 175.55 Pa for 333ms. During diastole, fluid is exposed to 32Pa shear stress for 667ms time duration.

5.4.3.1 Shear rate

Shear rate that is a product of shear stress and angular velocity is also important parameters for the design of VAD. It is also critical due to the fact that the blood is a viscoelastic fluid and its rheological properties mainly viscosity and elasticity are depends on the rate of flow or a shear rate(Hellums, 1994). Figure 5-19 depicts the time varying shear rate in X, Y and Z direction during systolic and diastolic phase of pulse.
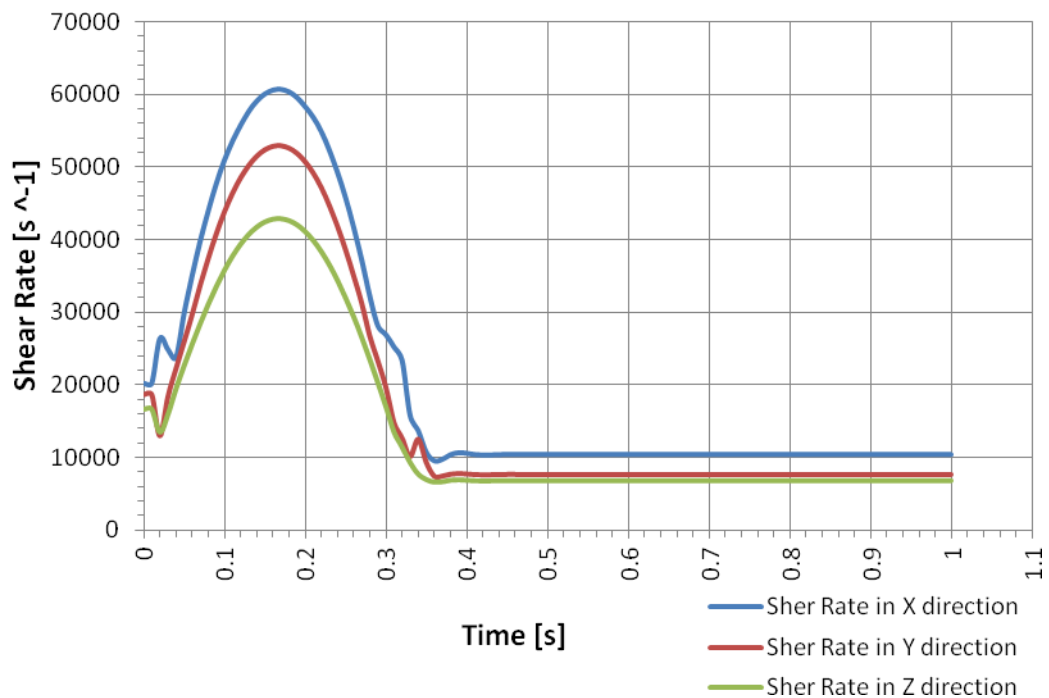
Figure 5-19 : shear rate Vs Time

The shear rate varies with the time varying speed of rotating fluid domains and remains predominant in the direction of flow. Similar to shear stress observation, fluid is exposed to high shear rate for shorter duration of systole and low shear rate is observed for longer duration than diastole. The fluid is exposed to shear rate above

50000 s^{-1} for 150 ms and average shear rate of 42319.8 s^{-1} is observed for total systole of 333 ms.

5.5 Concluding Section

This chapter demonstrates the use of CFD for characterisation of LVAD's pulsatile flow .The results of the transient CFD simulations proves the unique feature of the thesis that is a generation of pulse using an axial flow LVAD. The characteristic curves were generated for 40, 60, 80 and 100 BPM heart rates and limit operating speed in between 8000 to 10000 RPM. The results presented in this section are mainly for the 10000RPM.

The key findings of this chapter are listed below.

- The first section discusses about the boundary conditions needed to simulate the real world scenario of a pulsatile flow LVAD where the rotating domain speed varies with time to generate a pulsatile flow. Prior to each transient run the steady state CFD simulation are helpful in defining the initial condition of fluid domain.

- Second section discusses about the characterisation of a pulsatile axial flow LVAD. This novel feature of thesis was presented using the tabulated data collected at each 0.01 s of the time step for systolic and diastolic pressure rise across the impeller and a time varying mass flow rate. Outcome of these data clearly shows the LVAD's ability to generate pulse by controlling the operating speed of an axial flow pump impeller.

- Last section of this chapter shows flow details of pulsatile axial flow LVAD for systole and diastole at different time frame. The time varying flow details helps in understating the flow behaviour during the single pulse. The key features are as below;
  - Pressure distribution shows the high pressure at lower surface of blade during systole, while during diastole the pressure concentration is observed at the upper surface of the blade. For the same time frame the high pressure is generated by impeller at outlet section during systole while it reverses during diastole.

o Velocity distribution has shown the disturbance in flow at the beginning of systole, while during systole the smooth steamlines were observed. Higher velocity streamline observed at upper section of the blade. During diastole blade is seems to behave as an obstacle to flowing fluid. Recirculation regions were observed near the lower surface of blade.

o During systole, higher shear stresses and shear rate were observed at tip and leading edge. As anticipated the shear stresses and shear rate were increasing during acceleration phase of systole. While during diastole low shear stresses and shear rate are observed throughout the rotating domain.

Next chapter will discuss the experimental setup which was design and manufactured for the purpose of the study and thesis.

.

Chapter 6 Experimental Setup

6.1 Abstract

Experiments are essential to validate the mathematical (CFD) model as well as the geometrical design of a pulsatile axial flow LVAD. It also helps to assess LVAD functions under dynamic flow conditions and analyzes the LVAD's ability to perform in animal and support life. The special purpose experimental setup, control and data accusation system were developed for the purpose of the thesis. This chapter provides the step-by-step details for the experimental setup and its various electro-mechanical components. Moreover the limitations of experimental setups are discussed in detail.

6.2 Introduction

This section introduces the general features of the experimental setup with the description of the components, calibration, and limitations. The experimental setup is mainly built for in vitro evaluation of pulsatile pumping function. The motor control system is specifically designed and developed for generation of pulsatile flow at different heart rates. It can also be used for the validation of CFD simulations of impeller.

Figure 6-1 shows the schematic overview of the experimental setup. In the setup, water comes from the reservoir which was placed at a certain height that provides pressures of 10.66KPa, 13.2KPa and 16KPa. These pressures are equivalent to ventricular pre-load of 80mmHg, 100mmHg, and 120mmHg respectively. Two silicon tubes of 12mm diameter were placed between the reservoir and setup.

The two pressure transducers were inserted at the inlet (P1) and outlet (P2) respectively through a Y-Junction and advanced inside the tubes until the desired position was reached. An ultrasonic flow probe was attached to the tube, which is near to outlet. Rotating shaft with impeller was placed in the middle of housing with two flow straightners on both sides. Distal end of shaft was connected to motor, which is connected to the PC based motor controller. Data was acquired from: pressure transducer-1, pressure transducer-2 and ultrasound flow probe.

An angle of 30° was maintained between the axis of rotation and inlet as well as outlet tubes, which allows the motor to remain outside the flowing fluid. That helps in selection of a normal DC motor without any waterproofing functionality. Flow straightners blades were placed at the either side of the rotating impeller; to eliminate flow disturbance that might occurs due to 30° inclination of tubes angle.
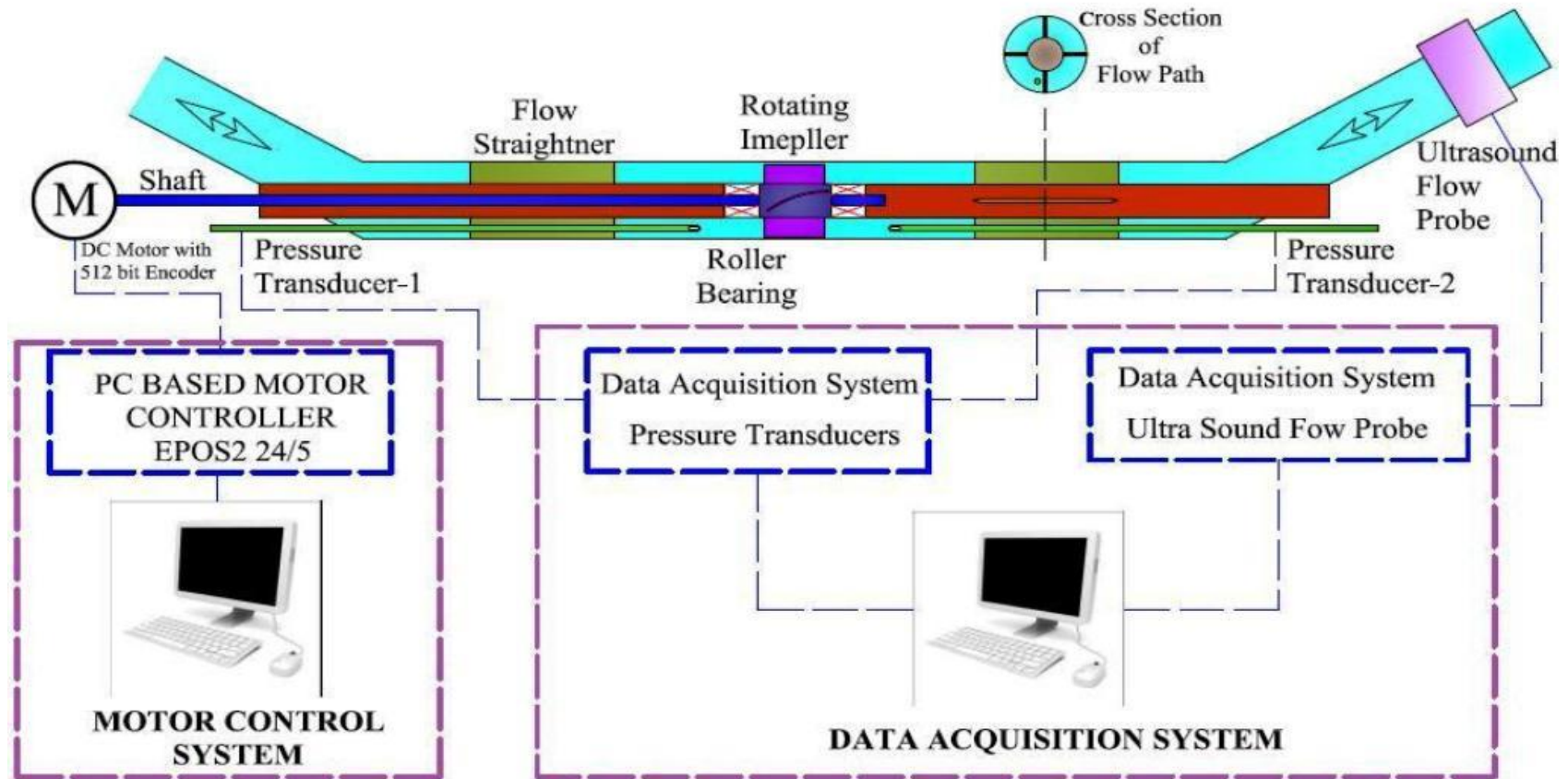
Figure 6-1: Schematic view of the experimental setup used for pulsatile flow experiments as well as CFD validation

6.3 Experimental Setup
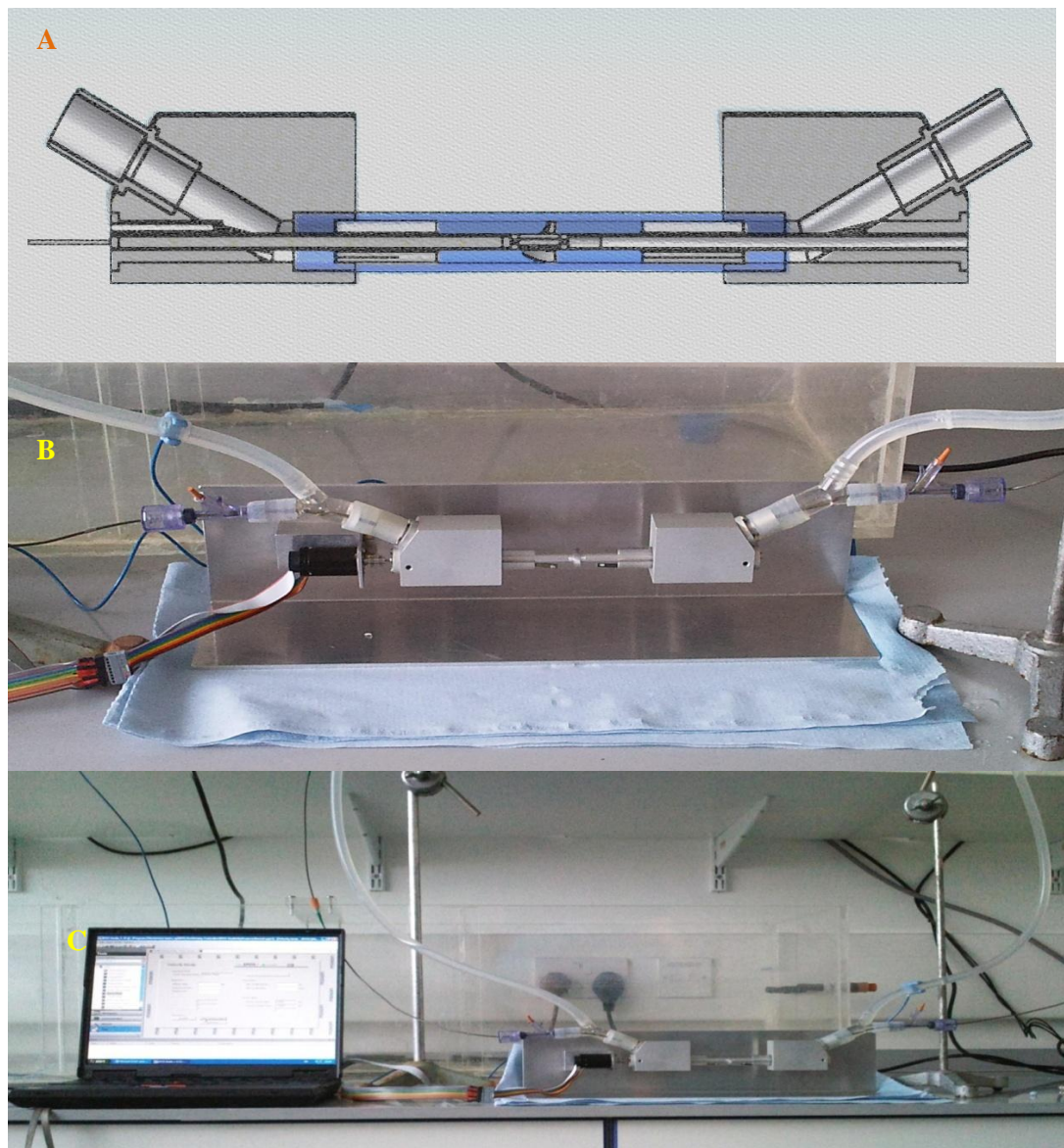
Figure 6-2 A) CAD model of experimental setup. B) Experimental setup.
C) Experimental setup with control computer.

6.3.1 Components of Setup

6.3.1.1 End block

End blocks are designed to provide the structural support to various components of setup. It is made of aluminum alloy and coated with corrosion resistant material. The Y shape internal ducting helps to accommodate flow straighteners and end covers,

Single opening of the end block provide the structural support for the impeller casing that is a made up of a transparent Perspex material.
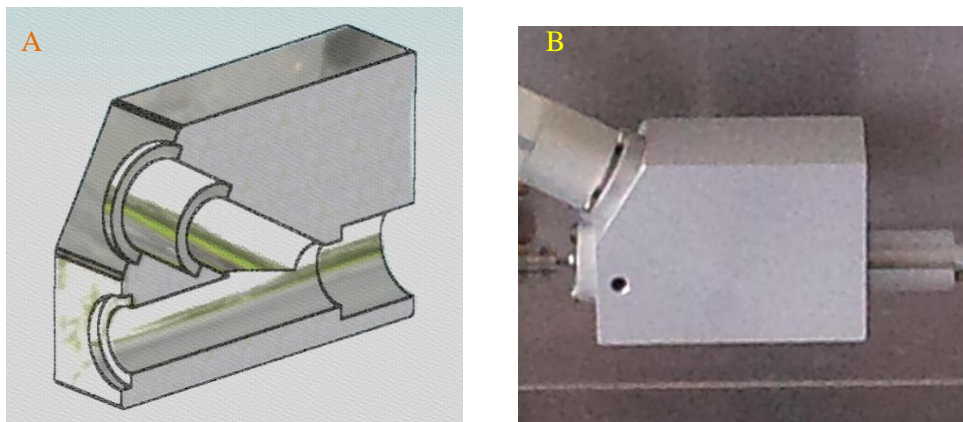
Figure 6-3: A) CAD cross-sectional model of end block. B) Experimental setup of end block.

6.3.1.2 Flow straighteners with End cover
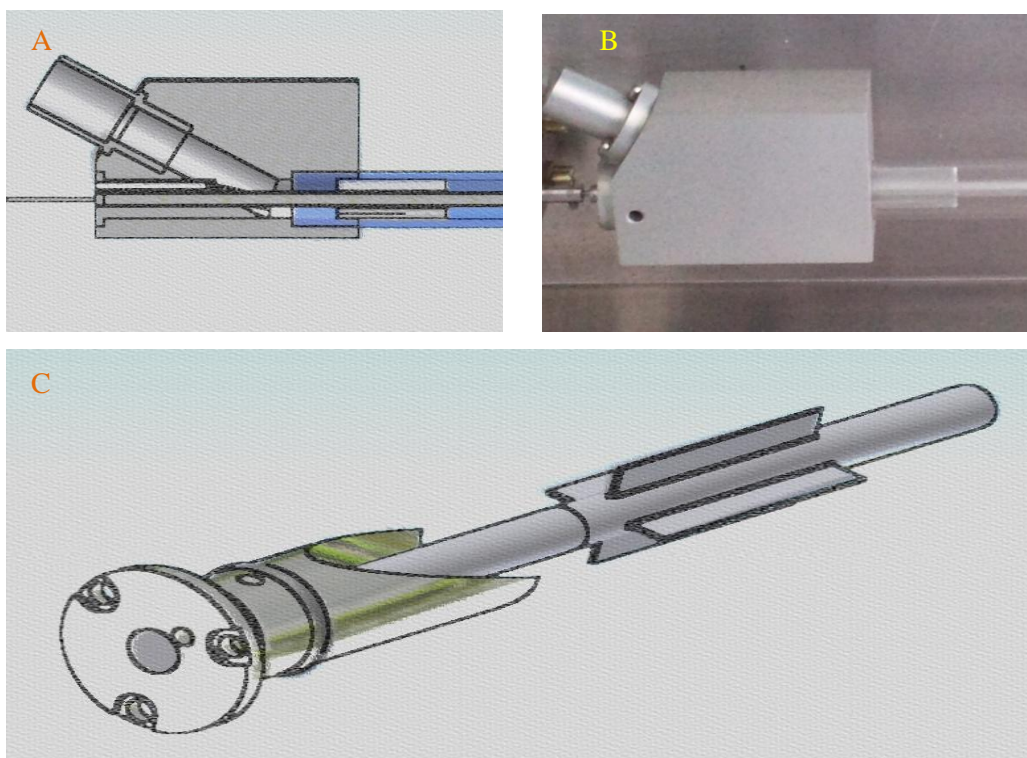
Figure 6:6-4: A) Straighteners assembly with end block. B) Experimental setup with end block. C) CAD assembly of straighteners with end block.

The flow straighteners lies inside the end block housing nearby inlet and outlet. Flow straighteners with End cover are made of aluminum alloy and coated with corrosion

resistant material. It helps to maintain the flow in straight line thereby eliminate the flow disturbance as well as pre-whirl in front of impeller.

6.3.1.3 Impeller

The VAD impeller is made of titanium- Ti6Al4v that helps in its biocompatibility as well as making the impeller lightweight. It is made using 5-axis CNC machine with two blades positioned 180 degrees apart.
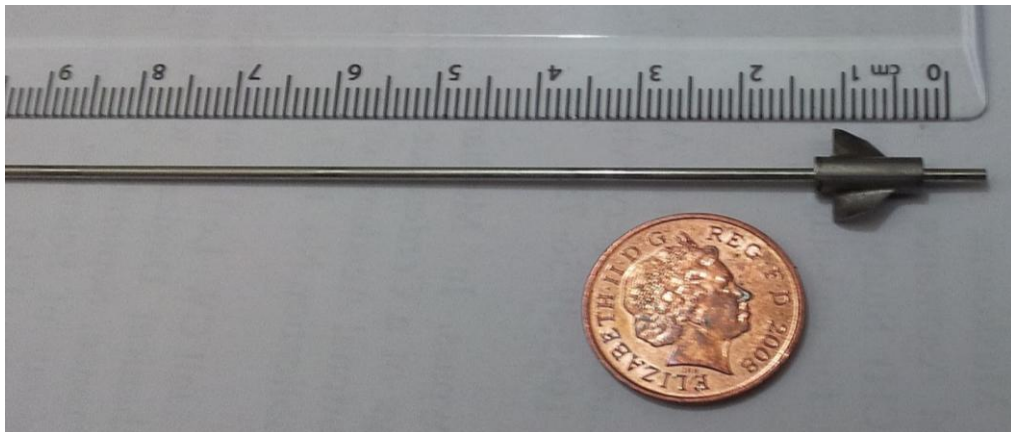
Figure 6-5 Impeller with rotating shaft

6.3.1.4 Ducts and Reservoir

12 mm silicone tubes are used to carry the water between reservoir and pump: two cocks and one-way valve, controls the flow of water inside these ducts.

Figure 6-6 Reservoir

6.3.1.5 Rotating shaft

A 120mm long rotating shaft made of stainless steel, rotates within the straightener and end cover assembly without coming in contact with working fluid. The dynamic FEA simulation has been carried out for the shaft impeller assembly using 10609 triangular elements to find out the total deformation during pulsating mode of operation. Maximum deformation 0.003049 mm is observed at 12000 RPM.
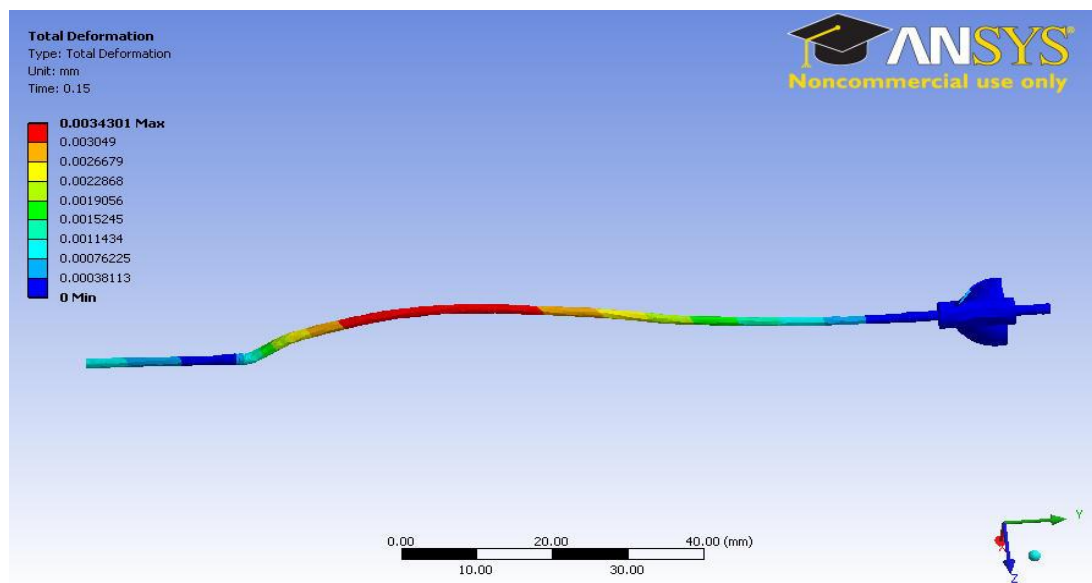
Figure 6-7 FEA stimulation of rotating shaft depicting total deformation at 15msec.

6.3.1.6 DC motor

The pump is driven by an EC-MAX 22 brushless 12 W DC motor (Maxon Motor ag, Sachseln, Switzerland). The motor has embedded Hall-effect sensors and 512 CPT encoder at the end of the axes.

Figure 6-8 DC motor assembly with experimental setup.

6.3.1.7 Y-connectors

Two Y shaped connectors are used to connect the ducts and inlet of setup. They are mainly used to insert the pressure transducers within fluid region of setup.

Y-connecters are also useful in maintaining water levels in reservoirs as well as the pre-load for VAD impellers.
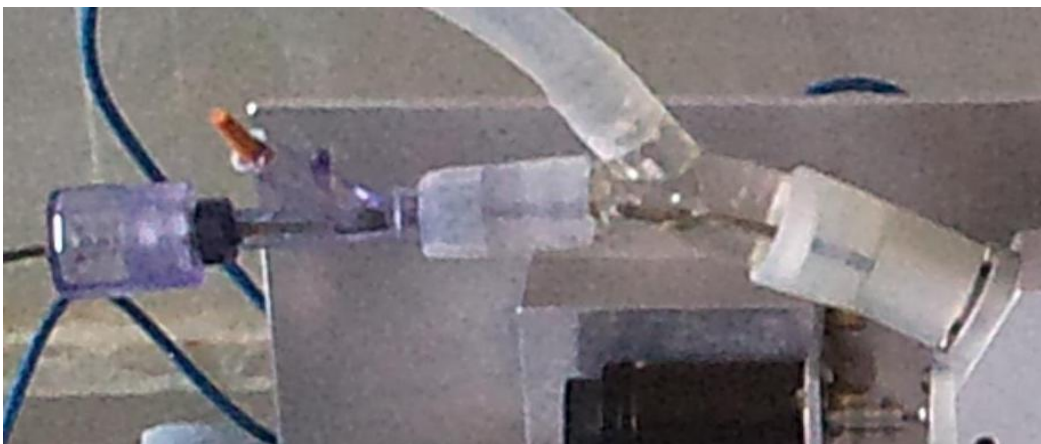
Figure 6-9 Y connectors attached to experimental setup.

6.4 Control and Data Acquisition Systems

For the purpose of this thesis, two separate systems are used for motor control and data acquisition purpose. The motor control system is specifically designed and developed for generation of pulsatile flow for different heart rate. For pressure and flow rate measurement, commercially available Sonometrics data acquisition system is used.

6.4.1 Motor Control System Using EPOS 2 24/5 Positioning   Controller and Lab View
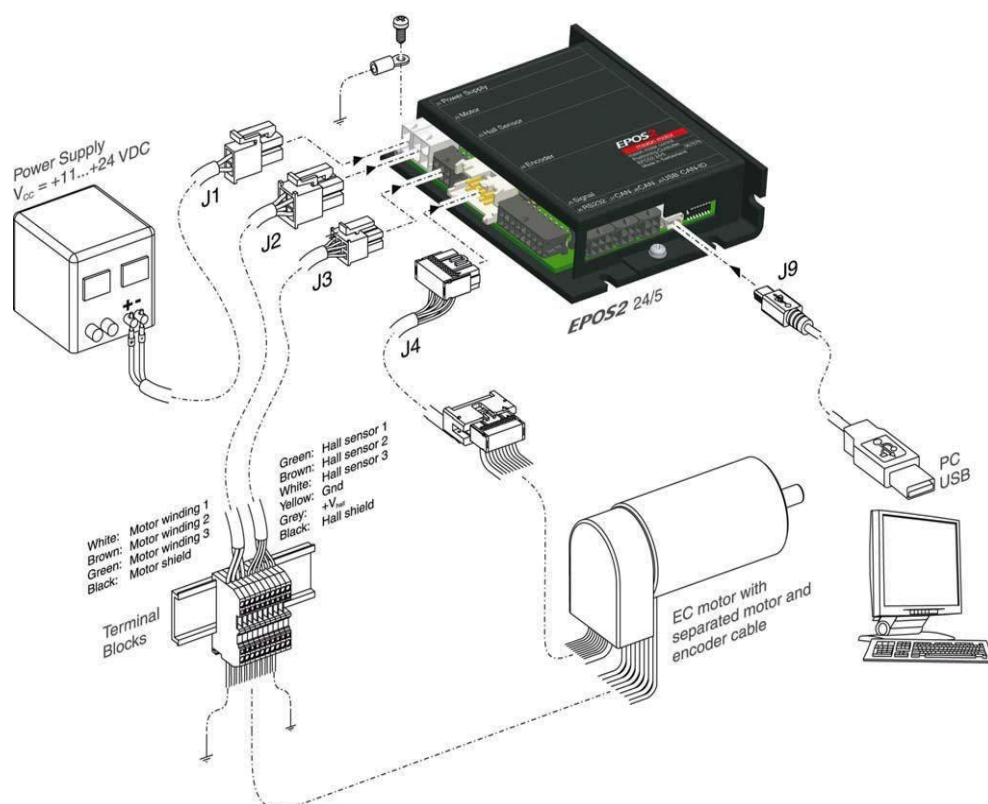
Figure 6-10 Wire diagram of EPOS 2 24/5 controller system

EPOS2 24/5 features 32-bit Digital Signal Processor Technology permitting outstanding motion control functionalities. EPOS2 24/5 executes complex mathematic algorithms with high efficiency. The encoder input offers a resolution of up to 2 500 000 increments and an input frequency of up to 5 MHz. Due to Interpolated Position Mode, the positioning unit is able to synchronously run a path specified by interpolating points; this with great dynamics and high accuracy.

Coordinated multiple-axes movements within a master system or any profile within a single-axis system can also be executed using EPOS2 24/5.

6.4.1.1 Calibration of Velocity, Speed and Current

Prior to experiment, regulation tuning permits an extremely efficient adjustment of current, velocity, speed (RPM) or position regulation. The Graphic User Interface (GUI) EPOS Studio allows fast-automated calibration. This GUI tool helps in tuning the motor control parameter after assembly in setup, which helps to assure accurate and precise control over impeller speed.

6.4.1.2 LabView interface using EPOS2 24/5

An integrated data acquisition and control system is designed using LabView for a DC motor in an experimental setup. The EPOS2 can be controlled by means of a CAN Master (for example PLC, Soft PLC) or with PC via USB or RS232. The standardized CAN open interface permits integration and coordination of several drives. Additionally integrated gateway functions (USB-to-CAN, RS232-to-CAN) facilitate access to CAN frame-works once more. IBM ThinkPad, P3 1.1 GHz and 512 MB RAM, laptop computer have been used to control EPOS2 24/5 unit.
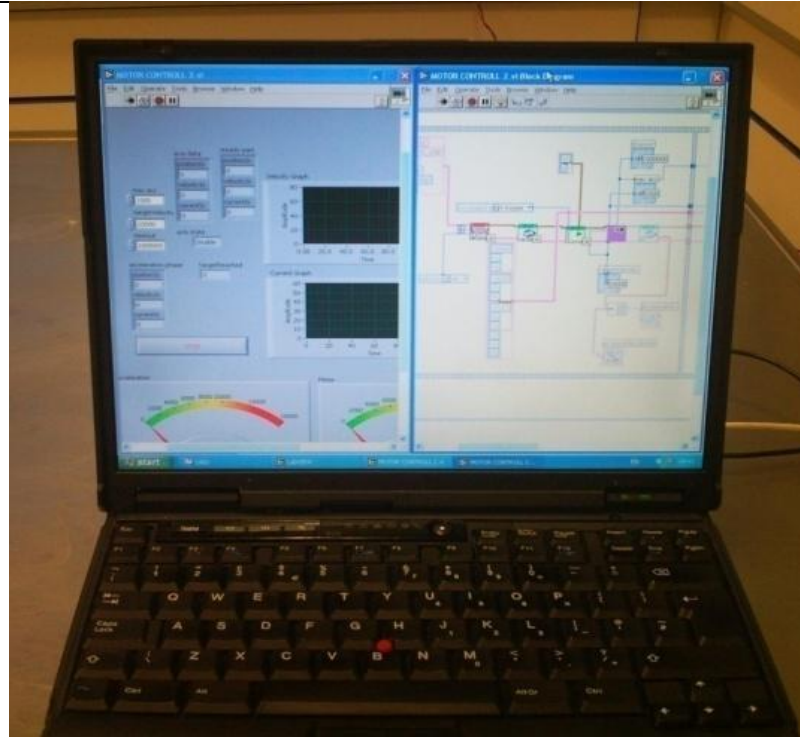
Figure 6-11 Labview control box for experimental setup.

LabView software (National Instruments Corporation) provides seamless hardware integration for control and data acquisition. EPOS.dll file provides useful tools for integration of EPOS2 unit with PC using LabView for motor control and data recording purpose. Using embedded motor encoder and hall sensors, the control and data acquisition code has been developed for generating pulse at heart rate varying from 0 to 120 beats per minute. This code also record the time based current, speed, and position of axis in ".txt" format. This is very helpful in future post processing of the data.

6.4.2 Data Acquisition System for Pressure and Flow Measurement

Two Ø2.0 mm pressure catheters, Millar Instruments Inc, Houston, TX, USA with sensors and an Ø12 mm ultrasonic flow probe, Transonic, Ithaca, NY, USA were used to detect real time pulsating flow. For collection of signals from the pressure and flow transducers, they were connected to a PC. Signals from that were fed into custom-made programs for data processing and logging, based on the PC running SonoLAB on Sonometrics data acquisition software (Sonometrics Corporation, London, Ontario, Canada). SonoLAB helps in collecting real time data for flow rate in CC/s and pressure in KPa. Sonolab also helps in converting data into ".txt" format.

6.4.2.1 Calibration of Pressure and Flow Probes

At the beginning of each experiment, the calibration of two pressure probes and one flow probe is necessary. The calibration of the two pressure probes were done by inserting both the probes together in column of water at different levels to ensure consistent calibration between the probes. Depending on measured value, the slope is derived, which gives the calibration value for pressure probes.
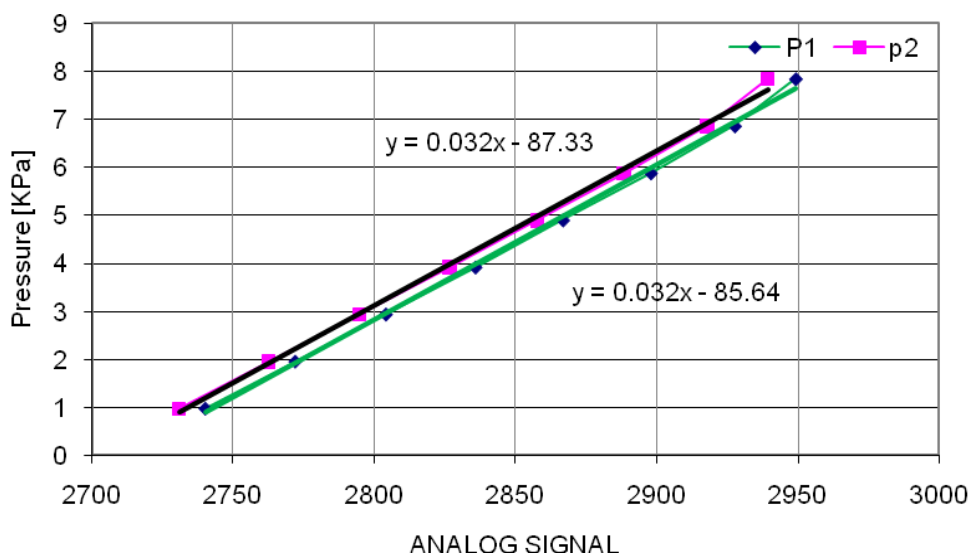
Figure 6-12 Calibration chart for pressure

Flow probe calibration was done by use of a continuous flow pump with valve to control the flow. Values obtained by timed collection of water in measuring jar at different flow rate. The slope for flow calibration was then obtained by plotting these values on the graph.
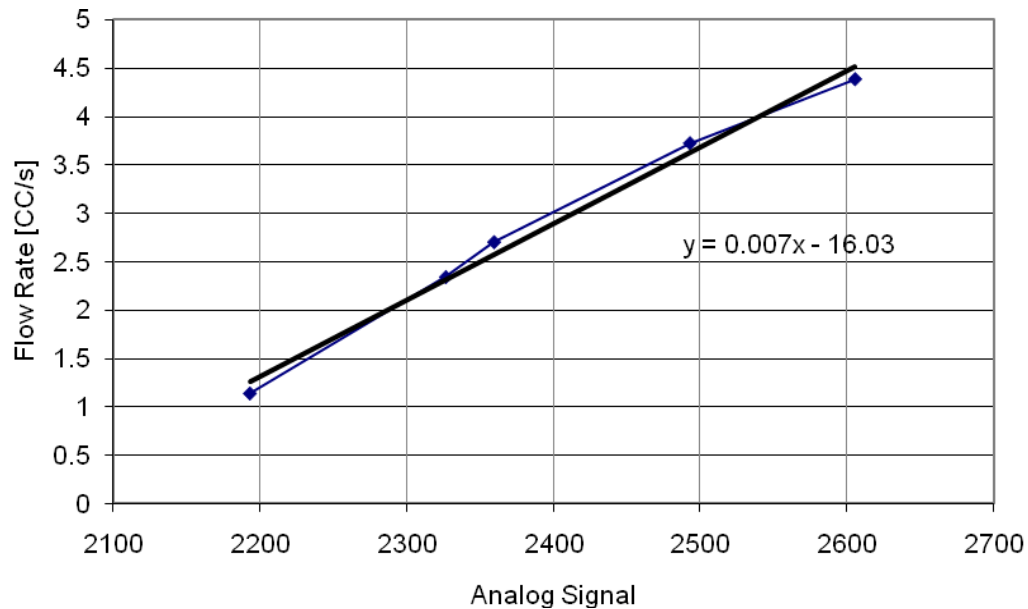
Figure 6-13 Calibration chart for flow rate.

6.5 Technical Limitation of Experimental Setup

Experimental setup consists of various mechanical and electronic components. Despite the best efforts made during manufacturing and assembling the components, certain physical limitation might affect the outcome of the experiments.

6.5.1 Time delay

Electronics components like EPOS-2, Pressure transducers and ultrasound flow probes have inherent time delay. Control and data acquisition systems have 10-millisecond time delay. In addition these devices are connected to computers. The CPU time delay might also affect the outcome of the control and data actuation systems.

6.5.2 Sampling Rate

The cardiac events are in the range of millisecond that is 333ms for systole based on heart rate. While the sampling rate for the data acquisition system used for the experimental setup, has 1000Hz sampling rate that gives one sample per millisecond. Therefore, for systole the 333 samples and for diastole the 667 samples can be acquired using the existing system. That is considered acceptable as the experiments are carried out in vitro without using blood as working fluid.

For the further detailed experimental investigation the sampling rate should be more than 1000 Hz with real time control and data acquisitions systems, are recommended.

6.5.3 Vibration of rotary components

While designing and manufacturing the rotating shaft, the total deformation was minimised to 3 micron at 12000 RPM and roller bearings were used to minimise the friction. Despite that, vibration might occur due to mis- alignment or loose fittings of the components, while rotating at high speed. A vibrating shaft can reduces the tip gap between the blade and casing. In the worst scenario shaft could be suddenly blocked during operation. A vibrating shaft can also adversely affect the encoder of the motor.

6.5.4 Silicon tubes

Silicon tubes were used to connect the reservoir and the control valves were also connected using these elastic tubes during continuous and pulsatile mode of experimental evaluation. The silicon tubes can inflate under the pressure that can create extra space for the fluid to accommodate. This inflation acts as a capacitor that can affect pressure and flow rate observation.

6.6 Concluding Section

This chapter introduces the various features of the experimental setup. The setups was mainly designed and built for the in vitro evaluation of LVAD's impeller. Using the dedicated control system setup is capable to investigate the LVAD's performance in both continuous and pulsatile mode. It was also used for the validation of mathematical model (CFD).

The main points, which were reviewed in this chapter:

- The first section of this chapter provides the schematic overview of the experimental setup.
- Second section describes various components of setup in detail.
- Third section discusses the dedicated control and data accusation systems. This section also provides the details for the calibration of pressure probes and ultrasound flow probes.
- Last section shows the limitation of setup that might affect the outcome of an experiment.

Next chapter will provide the results of in vitro experiments of LVAD as a continuous flow pump.

Chapter 7 In Vitro Evaluation of LVAD as a Continuous Axial Flow Pump

7.1 Abstract

This chapter details the experimental results of an LVAD operating as a continuous flow pump. In Vitro, experiments were carried out to evaluate the performance of an axial flow LVAD as a continuous flow pump. The pressure rise across the impeller and flow rate were measured for the impeller rotating at a constant speed. Experiments were carried out for the range of rotating speeds without exceeding the limit speed derived using GDO.

7.2 Setup Preparation

Prior to each experiment, calibration of pressure and ultrasound flow probes were performed and motor tuning was done to ensure the quality of measurement and control. The prototype impeller was mounted in the experimental setup and inlet and outlet port of setup were connected to reservoir. The motor was connected with the experimental setup and tuning was done to verify smooth impeller rotation in the assembly. Calibrated pressure transducers were placed 10mm away from the suction and pressure side of the rotating impeller, thought Y-connectors. Water was filled within circuit though the reservoir. A manual control valve was placed at the outlet and the ultrasonic flow probe at the inlet for flow measurement. The motor was then started to initiate the experiment.

7.3 Protocol

The control valve was kept open during the start-up of motor. The flow was freely allowed to come at constant rate before controlling the valve to initiate the experiment. The speed of motor was kept constant and valve was kept open for the first observation. Subsequence measurements were done by keeping the motor speed constant and the restricting the flow by closing the control valve. Flow rate and motor speed were maintained in line with the flow rate and the rotating speed of VAD used for the steady state CFD simulation.

The pressure and flow signals were acquired for the 10 sec duration at a sampling rate of 1000 Hz. At least two minutes gap is maintained between the acquisitions of each measurement for the system to settle. The pressure and flow data were acquired for the range of motor speed varying from 1000 RPM to 10000 RPM. Valve was operated to maintain the flow rate according to the steady state CFD simulations.

7.4 Pressure Vs flow characteristics of LVAD

Results presented in this section are in line with the objective of the in vitro experiment of the LVAD as a continuous flow pump. Experimentally obtained pressure and flow signals were post processed and tabulated to derive the pressure

against flow characterises of the LVAD. The experimental data are presented in the form of figure 7-1 for the different range of motor speed.
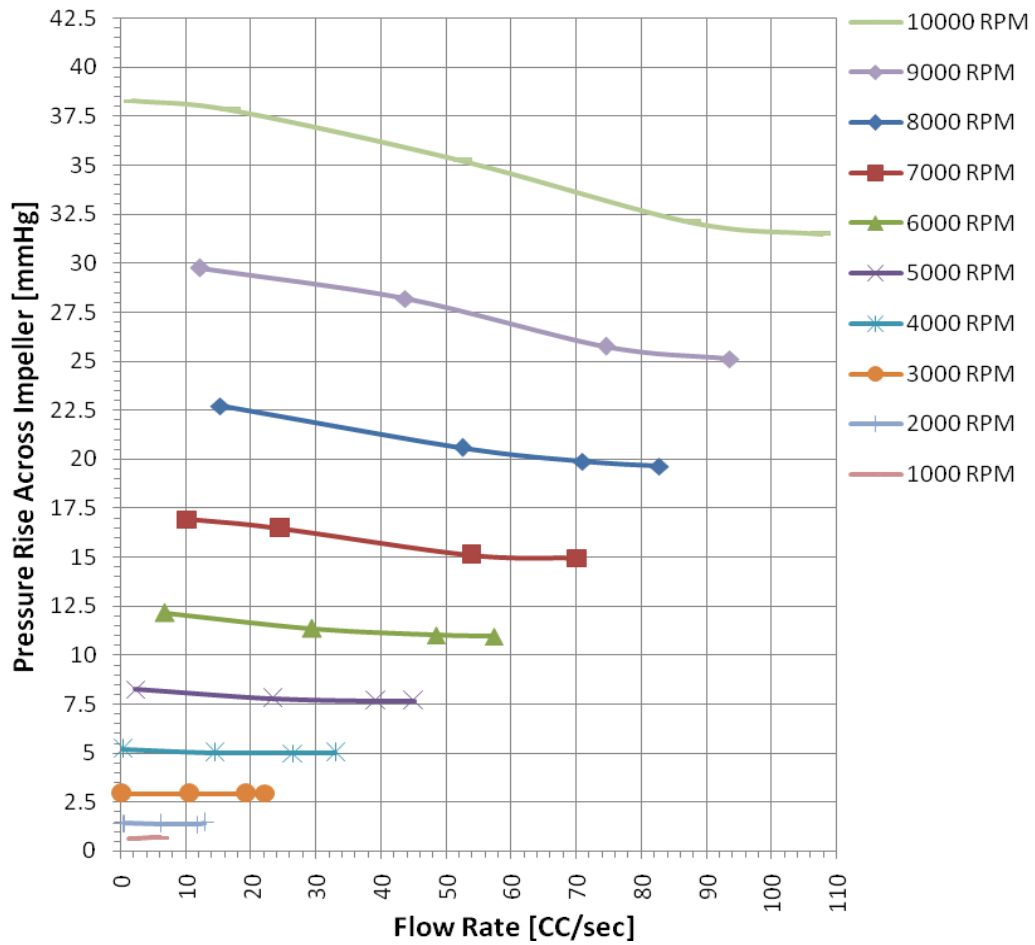
Figure 7-1: Pressure Vs Flow Characteristics of LVAD

As shown in figure 7-1, it is evident that the pressure rise across the impeller increase with the increasing speed. At any constant speed, the variation in mass flow rate also affects the pressure rise across the impeller. For the full valve open condition the maximum mass flow rate is observed and for the same operating point, the minimum pressure rise across the impeller is observed. Maximum pressure rise of 38.29mmHg is observed at full valve closed position at 10000 RPM. For the same motor speed, at the full valve open condition 31.49mmHg pressure rise is observed with the 107.67 CC/sec flow rate. Experimental data for the optimum range of motor speed are tabulated in table 7-1.

Rotating speed of LVAD	Mass Flow Rate	Pressure Rise across the Impeller	
RPM	CC/sec	KPa	mmHg
10000	107.67	4.20	31.50
	87.67	4.28	32.10
	52.50	4.69	35.18
	17.00	5.04	37.80
	1.83	5.10	38.25
9000	93.50	3.35	25.13
	74.50	3.43	25.73
	43.67	3.76	28.20
	12.17	3.97	29.78
	-0.03	4.06	30.45
8000	82.74	2.62	19.65
	70.94	2.65	19.89
	52.43	2.74	20.58
	15.30	3.03	22.71
	-0.01	3.09	23.16

Table 7-1: Experimental data for the optimum rage of motor speed

At the lower motor speeds the difference between the values of pressure rise across the impeller at full valve open and completely closed, reduces when comparing difference at higher motor speed. When the motor speed is below 6000 RPM, the pressure Vs flow rate curve is almost linear with negligible differences for the maximum flow and the no-flow condition.

7.5 Concluding Section

This chapter demonstrate the LVAD's ability to support failing hearts as a continuous flow pump. Pressure flow characteristic curves are generated for the operating speeds from 1000 to 10000 RPM. The outcomes of optimum range of operating speeds were separately tabulated.

Next chapter deals with the experimental results of LVAD operating as pulsatile axial flow pump.

Chapter 8 In Vitro Evaluation of LVAD as a Pulsatile Axial Flow Pump

8.1 Abstract

This chapter discusses the results of an in vitro experimental work carried out to validate the novel feature of this thesis. It also demonstrates the way to characterise the pulsatile flow for an axial flow pump. Characterisation of LVAD's inlet-outlet pressure and flow for the different heart rate are discussed in detail.

8.2 Introduction

In Vitro, experiments were performed to evaluate the pumping function of a pulsatile axial flow LVAD. Prior to each experiment, calibration of pressure and ultrasound flow probes were performed and motor tuning was done to ensure the quality of measurement and control. The prototype impeller was mounted in the experimental setup and inlet and outlet port were connected to a reservoir. Motor was connected to setup and tuning was done to verify smooth impeller rotation within setup. Calibrated pressure transducers were placed at 10mm away from the suction and pressure side of rotating impeller, thought Y-connectors. Water was filled within circuit though the reservoir. Water level in open reservoir was maintained at room temperature and atmospheric pressure.

8.3 Experiment 1: Characterisation of LVAD's Inlet and Outlet Pressure

The objective of this experiment is characterisation of pump inlet and outlet pressure and to further document the behaviour of inlet and outlet pressures generated at different heart rate.

The LVAD impeller was accelerated up to a limit speed and decelerated back to zero within systolic time frame for the generation of pulsatile flow at 40, 60, 80, and 100 beats per minutes (BPM) of heart rate (HR). Time of systole is considered as $1/3^{rd}$ of the total length of heartbeat, which is kept constant for the generation of pulse. Irrespective of motor speed, that gives systolic period of 333 ms for 60 BPM of heart rate.

As shown in figure 8-1 the motor accelerates up to 5000 RPM and decelerate back to zero within the systolic period, that is 0.3 of a second (333 ms) and it remains stationary during diastolic phase. The pressure signals were acquired at a sampling rate of 1000 Hz and at least two minutes gap was maintained between the acquisitions of each measurement for the system to settle. The further data has been recorded for speeds of 5000, 6000, 8000 and 10000 RPM to document the effects of motor speed for 40, 60, 80, and 100 beats per minutes of heart rate.
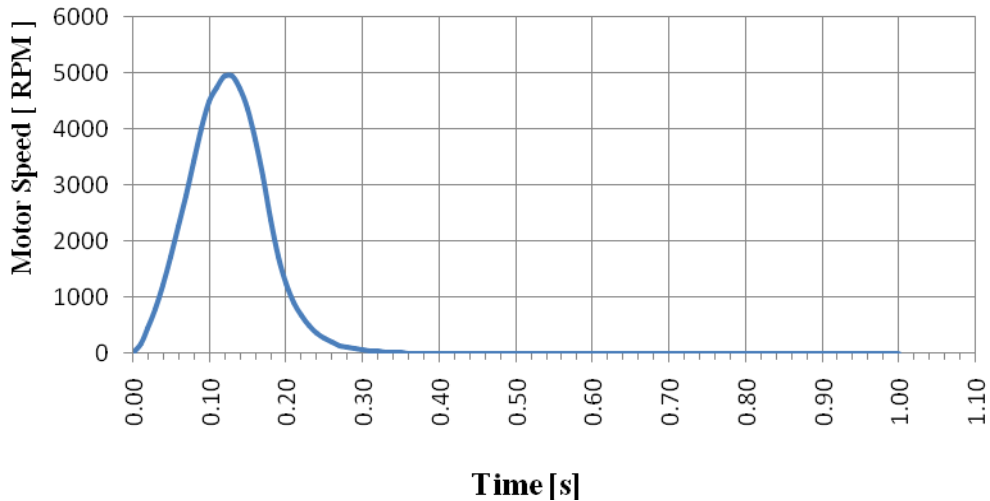
Figure 8-1: Motor Speed [RPM] Vs Time [s]

8.3.1 Result-1

Results that are presented in this section are inline with the objective of the experiment -1. Inlet pressure and outlet pressure data were collected for 40, 60, 80 and 100 BPM heart rate at different limit speed of 5000, 6000, 8000, and 10000 RPM. The characterisation of inlet and out pressure is shown in figure-8-9 that has been produced by taking pressure rise across the impeller against heart rate for different limit speed of motor.

8.3.1.1 Inlet pressure
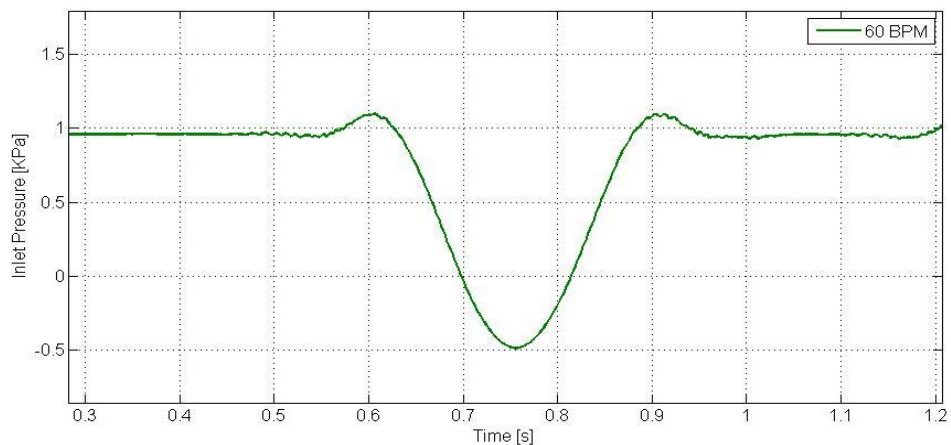
Figure 8-2: Single pressure pulse at inlet for 60 BPM

Figure 8-2 depicts the single pressure pulse generated at the inlet for 60 BPM heart rate for limit speed of 10000 RPM. Pulse duration of 0.3s is observed with

172

negative pressure of -0.5KPa at suction side of impeller. 0.3s is matched with motor speed, that is accelerated and decelerated to generate pulse within systolic time frame of $1/3^{rd}$ of a second at 60BPM. A small positive pressure rise is observed at the beginning as well as at the end of suction pressure curve.
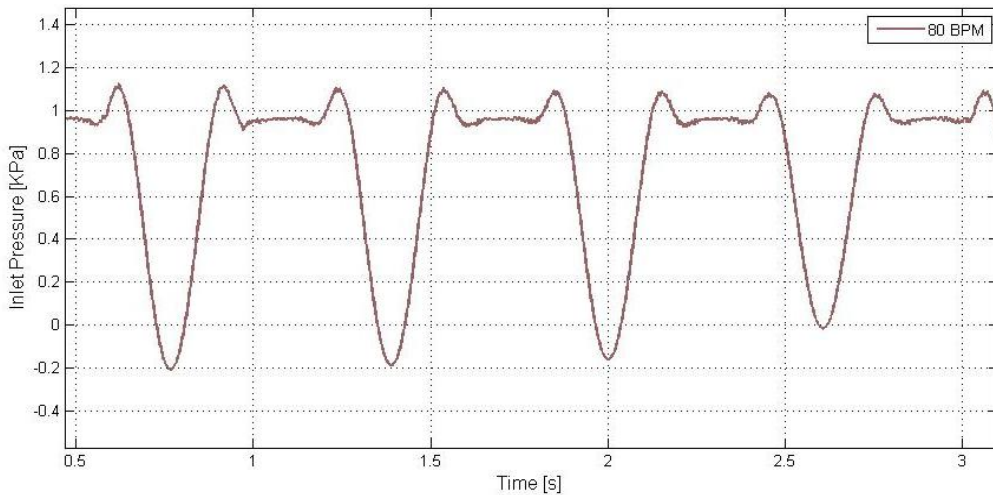
Figure 8-3: Inlet pressure Vs time for 80 BPM for 10000 RPM

Above figure 8-3 depicts the inlet pressure based on time. A total of four pulses are observed in 3 second, equivalent to 80 BPM at the limit speed of 10000 RPM. The peak value of individual pulse varies and the average suction pressure of -0.2 KPa is observed for the 80 BPM heart rate for the limit speed of 10000 RPM.
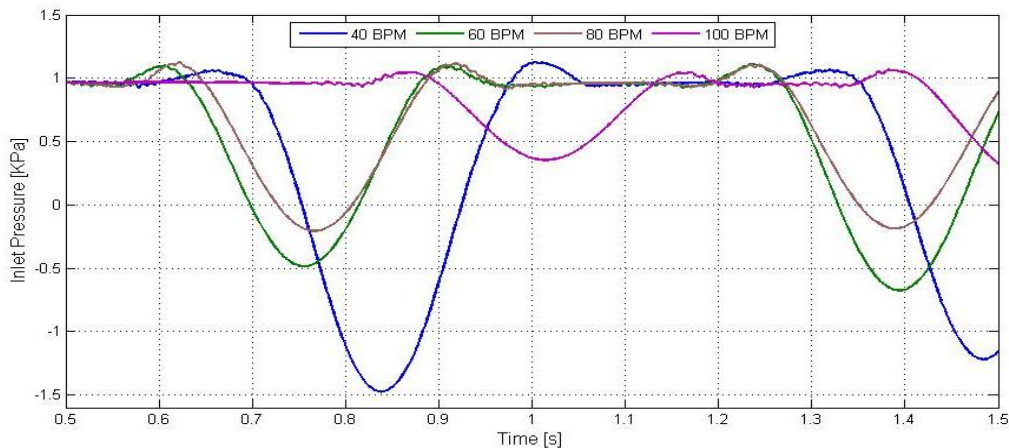
Figure 8-4: Inlet pressure Vs time for 40, 60, 80, and 100 BPM for 10000 RPM

Figure 8-4, demonstrates the suction pressure generated for 40, 60, 80, and100 BPM at the limit speed of 10000 RPM. It clearly shows the decrement of inlet suction

pressure with increment of heart rate. Maximum suction pressure is observed at 40 BPM that is an average peak pressure of -1.2 KPa. While for 100 BPM, the average peak suction pressure is 0.6 KPa.

8.3.1.2 Outlet pressure
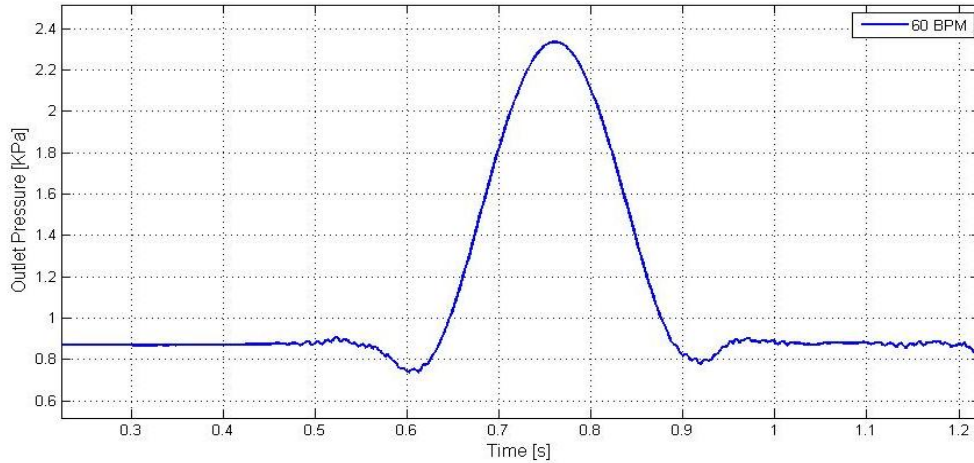
Figure 8-5: Single outlet pressure pulse at 60 BPM

Figure 8-5 depicts the single pressure pulse at 60 BPM for limit speed of 10000RPM. The duration of the outlet pressure pulse is 0.3s that matches with inlet pulse duration. In contrast to inlet pressure curve, a small decrement is observed at the beginning and end of the pressure pulse. The peak pressure rise of 2.3KPa is observed for 60BPM.
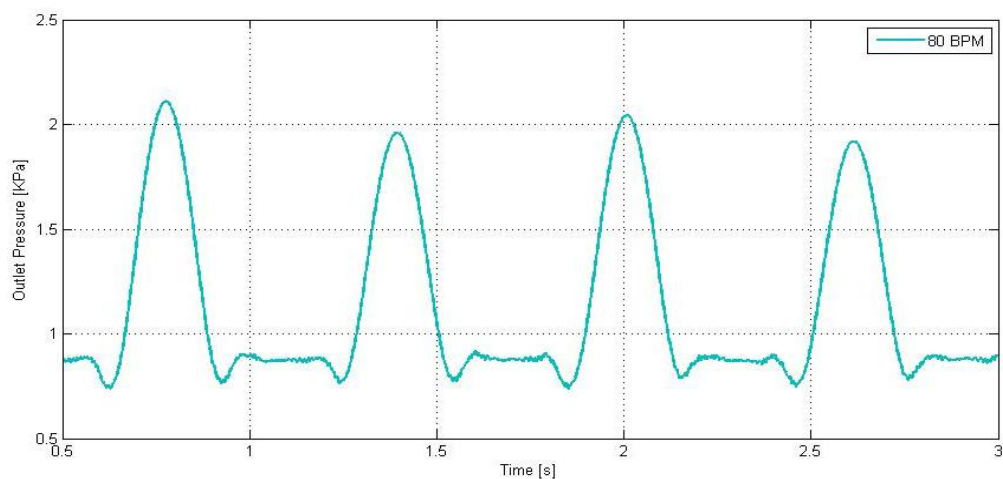
Figure 8-6: outlet pressure Vs Time for 80BPM heart rate at 10000 RPM

Figure 8-6 shows the outlet pressure variation based on time. A total four beats are observed in 3 sec that matches 80 BPM heart rate. The peak value of individual pulse varies, 1.8KPa pressure rise is observed in outlet pressure.
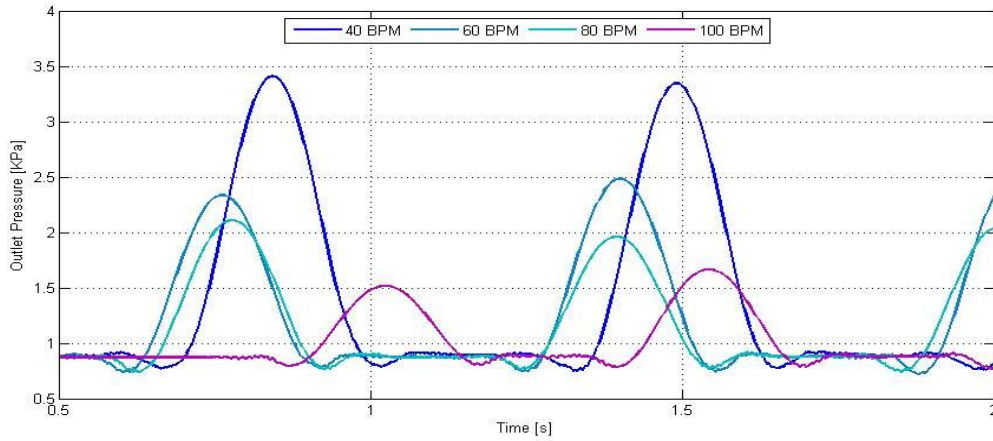
Figure 8-7: Outlet pressure Vs time for 40, 60, 80, and 100 BPM for 10000 RPM

Figure 8-7, depicts the pressure rise at outlet for 40, 60, 80, and100 BPM at the limit speed of 10000 RPM. The peak value of pressure reduces with the increasing heart rate. The maximum pressure rise is observed at 40BPM while minimum is observed at 100 BPM. The difference between the inlet and outlet pressure rise during pulse generation means pressure rise across the impeller is shown in figure 8-8. The peak of outlet pressure is observed after ~20ms of the peak of suction pressure. Total difference between the two peaks is 3.464 KPa that is 25 mmHg for limit speed of 10000 RPM.
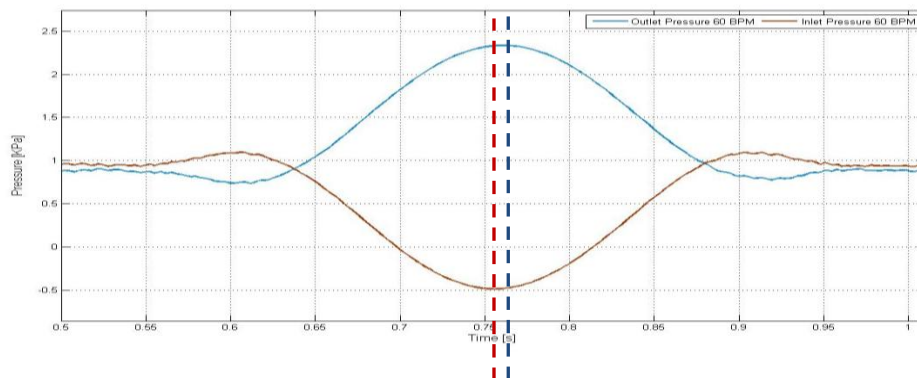
Figure 8-8: Pressure pulse at inlet and outlet for 60BPM
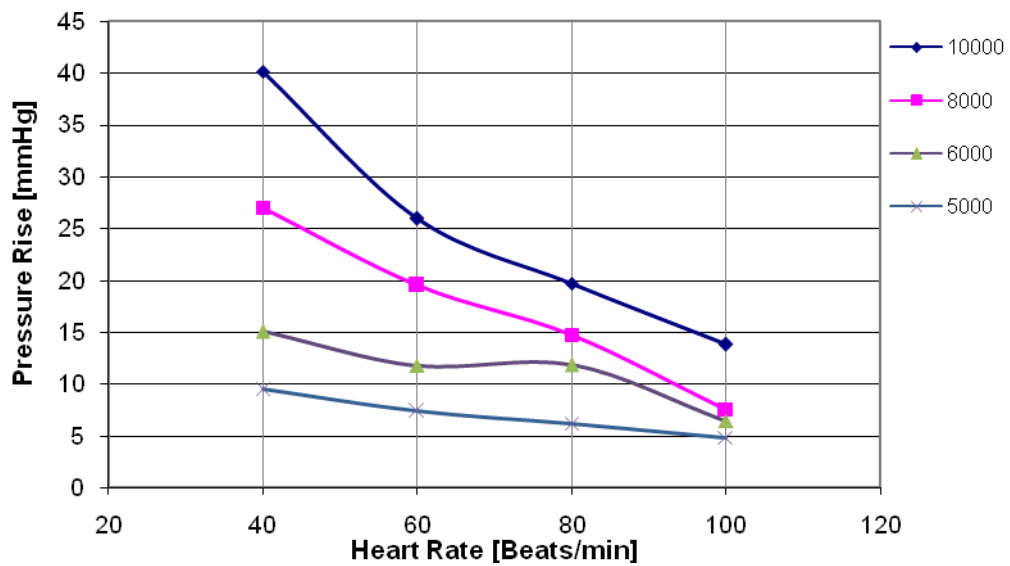
Figure 8-9: Characteristic curve of Pressure rise Vs Heart Rate

Above figure 8-9, demonstrates the characteristic of pressure rise across the impeller of LVAD with respect to heart rate. The experimental data are generated for the limit speed of 5000, 6000, 8000 and 10000 RPM. The linear relationship is observed between pressure rise across the impeller and heart rate. With increment in limit speed of LVAD's impeller, the pressure rise across impeller is also increasing. At the limit speed of 5000 RPM, the maximum pressure rise of 9.553mmHg is observed for 40 BPM heart rate. The slope of the linear relationship between the Pressure rise and HR also increases with the increment in limit speed. It is evident from the observation where slope of 5000RPM is less than the slope of 10000RPM. At 10,000 RPM, the maximum pressure rise of 40.119 mmHg is observed for 40 BPM heart rate.

8.4 Experiment 2: Characterisation of LVAD Output Flow

The objective of this experiment is to determine the nature and timing of Outflow, verifying the pulsating outflow similar to a pure displacement pump. This experiment verifies the unique feature of this thesis where axial the flow pump generates the pulsatile flow.

Setup preparation was similar to the experiment-1 and the experiment was carried for 40, 60, 80, and 100 BPM of heart rate. Ultrasound flow probe was placed at setup outlet for the flow measurement. Pressure data were also recorded for the detail investigation purpose.

Flow signals and pressure signals were acquired at a sampling rate of 1000 Hz and at least two minutes gap is maintained between two measurements. Further data had been recorded for 5000, 6000, 8000, and 10000 RPM to document the effects of motor speed for different heart rate (frequency).

8.4.1 Result-2

Results that are presented in this section are inline with the objective of the experiment -2. Flow rate along with Inlet pressure and outlet pressure data are collected for 40, 60, 80 and 100 BPM heart rate at different limit speed of 5000, 6000, 8000, and 10000 RPM.
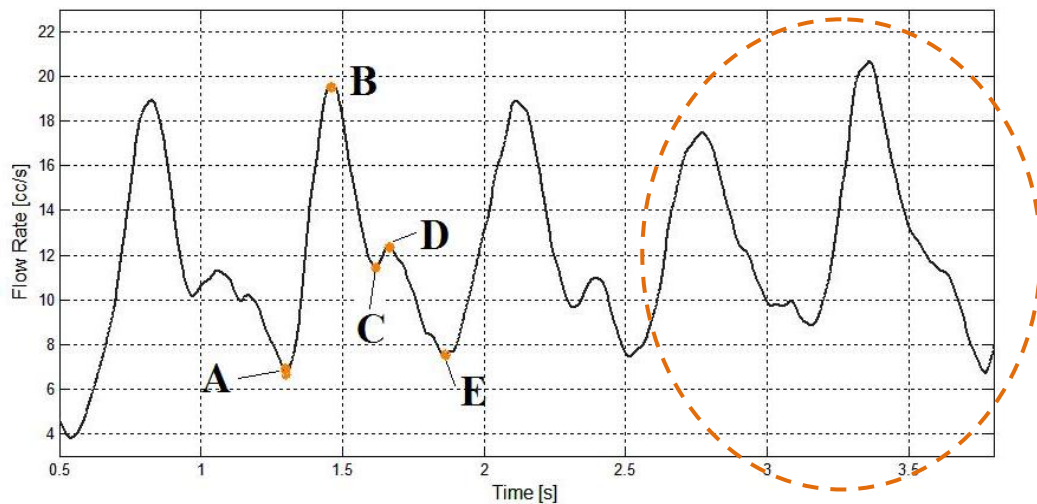
Figure 8-10: Flow rate Vs Time

The figure 8-10 depicts the flow rate with time. A pattern is evident almost in every pulse of flow recorded for purpose of this investigation. As shown in figure the flow

rate increases sharply during AB. Followed by BC where rate decreases almost at the same rate of an increment flow during AB. The CD shows the increment in flow rate followed by DE where rate decreases gradually. The decrement rate of the DE is less than the increment rate of AB. In some of the pulses as shown in figure 8-10 that are marked in brown ellipse, CD phase is showing gradual decrement in flow rate. For the same flow pulse, the pressure rise is also observed low between the two peaks in flow curve that is shown in figure 8-11. Apart from such low-pressure peaks, the flow rate curve has shown the ABCDE pattern.
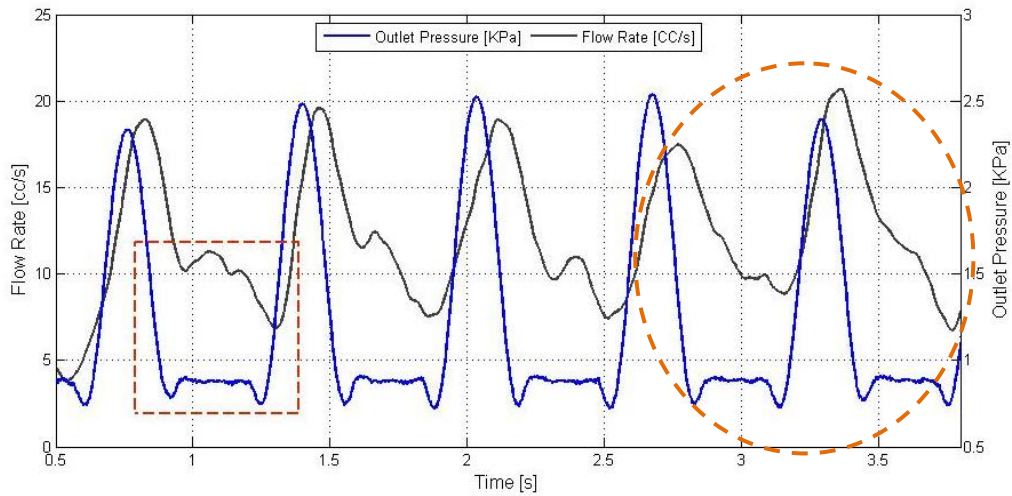
Figure 8-11: Flow rate, Outlet Pressure Vs Time

Above figure 8-11, is generated to demonstrate the pulse with respect to time and the pressure rise. The figure shows the flow rate in CC/s at the left side Y-axis and at the right side Y-axis, shows the outlet pressure in KPa. It has been observed that the pressure pulse occurs during the systole. From figure 8-11, it is also evident that the flow rate curve is also following the pressure curve. In other words the pressure difference across the impeller is driving the flow within the systolic and diastolic period. The flow rate curve AB starts with the beginning of the pressure pulse. Rise of AB curve is observed during the rise of pressure pulse. In addition, the flow curve BC follows the decreasing pressure. The flow rate curve CD is observed almost at the same time, when the pressure reaches back to its normal static reservoir pressure. This is shown as a red rectangle. The figure also shows the flow rate curve DE decreases gradually till the next decrement in pressure pulse start prior to

reaching its peak. The area under the flow curve ABC is considered as flow generated by VAD's impeller during systole.

.
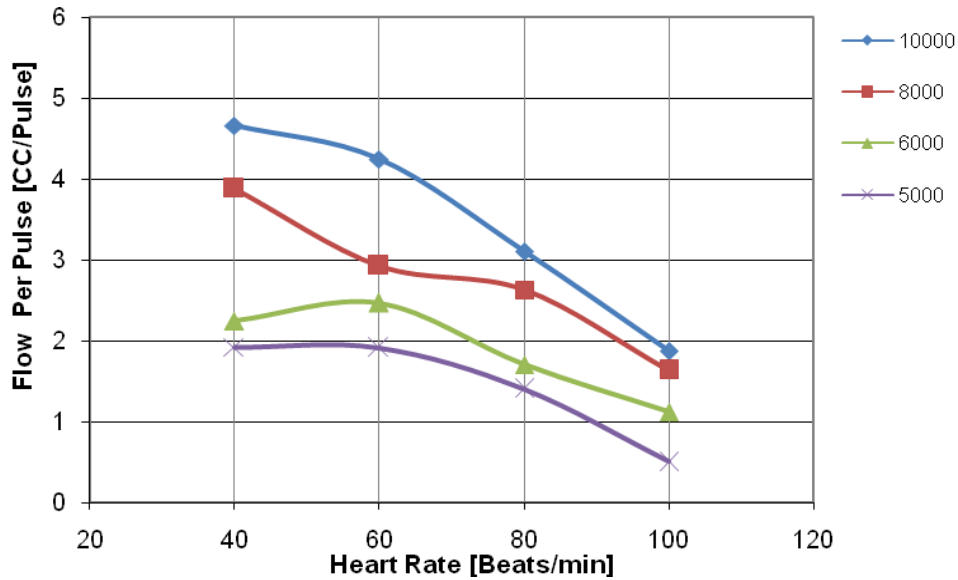
Figure 8-12: Characteristic curve of flow per pulse Vs Heart rate

Above figure 8-12, depicts the characteristic of flow per pulse at 40, 60, 80, and 100 BPM heart rate, and peak motor speed of 5000, 6000, 8000, and 10000 RPM. Flow per pulse has shown the linear relationship with heart rate. With increasing heart rate, the flow per pulse reduces linearly. The flow per pulse also linearly increases with the increasing limit speed of motor. The slope remains almost the same for all RPM rates despite increment in motor limit speed. The maximum flow per pulse is generated at 10000 RPM limit speed at 40 BPM which is 4.66 CC while minimum flow per pulse of 0.50 CC is observed at 100 BPM with the limit speed of 5000 RPM.

8.5 Experiment 3: Characterisation of Flow Rate vs. Frequency (HR)

The objective of this experiment is to determine the relationship between LVAD's flow output and frequency (heart rate). This will provide a better understanding of the effects of heart rate on the flow rate, delivered by pump.

Setup preparation was similar to experiment 1 and 2. Data for the flow rate and pressure were acquired for 40, 60, 80, and 100 BPM heart rate. Further data were documented by varying motor speed for 5000, 6000, 8000, and 10000RPM.

8.5.1 Result-3

Flow rate data were collected for 40, 60, 80 and 100 BPM heart rate at different limit speed of 5000, 6000, 8000, and 10000 RPM. Results of these data is presented in figure 8-13.
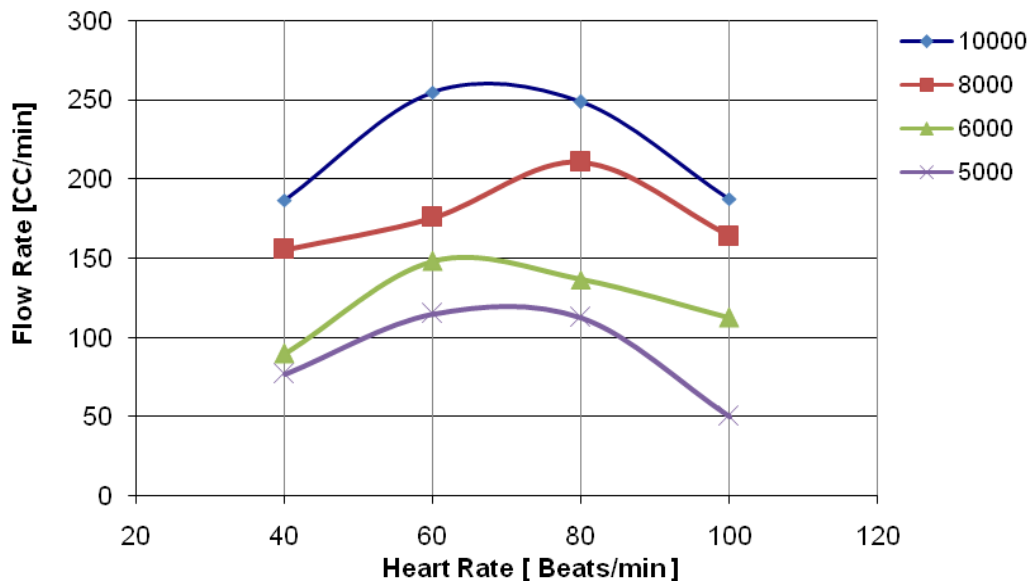
Figure 8-13: Flow rate Vs Heart rate

Above figure 8-13, represent the characteristic of flow rate with respect to heart rate. Non-linear relation is observed between the flow rate and heart rate. From 40 BPM to 60 BPM flow rate increases with the increasing heart rate. In addition, in the range of 80 BPM to 100 BPM the flow rate decreases with the increasing heart rate. The nature of relationships between heart frequency and flow, remains the same with increment in the motor limit speed.

8.6 Concluding Section

This chapter demonstrates the LVAD's ability to generate a controlled pulse using an axial flow pump that fulfils the aim of the thesis. In addition this chapter shows the techniques for experimental characterisation of a pulsatile axial flow LVAD. Experiments were carried out for 40, 60, 80 and 100 BPM heart rate at different limit speed of 5000, 6000, 8000, and 10000 RPM.

The key findings of this chapter are as below;

- A small positive pressure rise is observed at the beginning as well as at the end of suction pressure curve at inlet. Moreover decrement of peak inlet suction pressure with increasing heart rate is also observed.

- In contrast to inlet pressure, outlet pressure curves shows small decrement in the beginning as well as at the end of pressure pulse. While in accordance to inlet pressure, peak value of outlet pressure has shown decrement with increasing heart rate.

- Characteristics curves of pressure rise Vs heart rate shows a liner relationship where with increasing heart rate results in low pressure rise across the impeller. With increasing operating limit speed, pressure rise across the impeller increases.

- Pressure difference across the impeller is driving the flow during the systolic and diastolic period. Flow per pulse shows linear relation with the heart rate, where the flow per pulse reduces with the increment in heart rate. With increasing operating limit speed flow per pulse increases.

- Characteristics curves of flow rate Vs heart rate shows the nonlinear relationship where the flow rate increases with increasing heart rate from 40BPM to 60 BPM and further reduces from 80BPM to 100 BPM heart rate. Shape of curve remains same for all the operating limit speed.

Chapter 9 Discussion

Generation of pulsatile flow using an axial flow pump is a novel feature of the thesis. Pulsatile flow is a natural phenomena occurring in the human body. Moreover, researchers have demonstrated the benefits of pulsatile flow for vital organ function and end organ recovery during acute and chronic mechanical circulatory support (Undar, 2004)[67]. Due to the small size and tubular configuration, axial flow pumps are easy to implant using minimal invasive surgical procedures that reduces surgical stress on the patient's body. In addition, the small size axial flow pump reduces the risk of infection related complications. The initial design of axial flow pump geometry is done using the classical design theory to generate continuous flow at a fixed hydrostatic head. This initial assumption has helped in the evaluation of pulsatile flow as well as providing the base to initiate the study.

To satisfy hydraulic and clinical requirement of the LVAD, a detailed parametric investigation has been carried out using the statistical Design of Experiment (DOE) method to see the effects of rotational speed of the impeller on the design parameters, mainly the flow rate, pressure rise and wall shear stress. The parametric study shows the overall behaviour of the pump for the whole range of speed. It has demonstrated the LVAD's ability to generate mass flow rate and pressure rise that can satisfy the hydraulic requirement. At very high motor speed (30,000 RPM), the axial flow pump can generate 15.246 L/min with 140mmHg pressure rise and shear stress reaching 1550 Pa.

The clinical requirement of low hemolysis constrains the rotating tip speed below 10m/s (Reul and Akdis, 2000). The hemolysis depends on shear stress and the exposure time. Sallam and Hwang (Sallam and Hwang, 1984) have measured the threshold level for the shear stress 400Pa for 100 ms. The Leverett (Leverett et al., 1972) found that above 150Pa shear stress, hemolysis occur primarily in bulk rather than near wall region. With the corresponding value of 50000 S^{-1} shear rate for whole blood where the RBC membrane reaches its 6% strain limits.

Operating the LVAD within safe hemolysis levels, a tradeoff is required amongst design parameters. Thus, Goal Driven Optimisation has been performed to find out safe operating range of LVAD that can generate the flow rate up to 6.0 L/min and hemolysis levels below 300 Pa and maintains the left ventricular and the aortic pressure difference across the impeller. The optimised rotating speed ranges from 8000RPM to 10000 RPM that can match the hydraulic and clinical requirements. The steady state CFD simulations were carried out to find out the performance of the LVAD as a continuous flow pump.

The computed estimation of pressure and flow characteristics using steady state CFD simulations are shown in figure 4-10 for the rotational speeds of 3000 to 10000 RPM. At 3000 RPM, pump generates 5 mm of Hg pressure rise with 31.411% of total efficiency and 22.48 CC/s of flow rate. Pump generates 36.87 mm of Hg of pressure rise with 106 CC/s of flow rate at 10000 RPM with 49.31% of efficiency. The internal flow details shows the flow velocity near hub region around 0.90 m/s and the maximum axial flow is observed near 50% span that is around 1.12 m/s. Blade loading chart have shown the positive work done by blade through the span. The shear stress are observed reaching up to the maximum 333.09 Pa at 10000 RPM at the tip and the leading edge of the blade. The remaining area of blade and hub have shown the shear stress below 58Pa. At the lower rotating speed, the low shear shear stress were observed compared to 10000 RPM. For the optimised range, the shear stress ranges between the 206Pa – 333 Pa. Based on the axial velociy of 1.12 m/s the transition time is 8.93 ms for the 10mm length of the rotating fluid domain. Considering the maximum value of the shear stress, the hemolysis was approximately 3.229 % , based on the equation-3.1 developed by Giersiepen (Giersiepen et al., 1990).

The steady state CFD simulations were mainly carried out for the experimental validation of the CFD model. The parametric DOE study as well as the optimisation were performed using the same CFD model that was used in steady state CFD simulation. Moreover, the difference between the pulsatile and continuous CFD simulation is the time varying rotating speed of a rotating fluid domain. Thus, it is

important to experimentally validate the CFD model before using it for the pulsatile flow simulations.

9.1 Comparison of CFD and Experimental Results of LVAD as a Continuous Flow Pump.

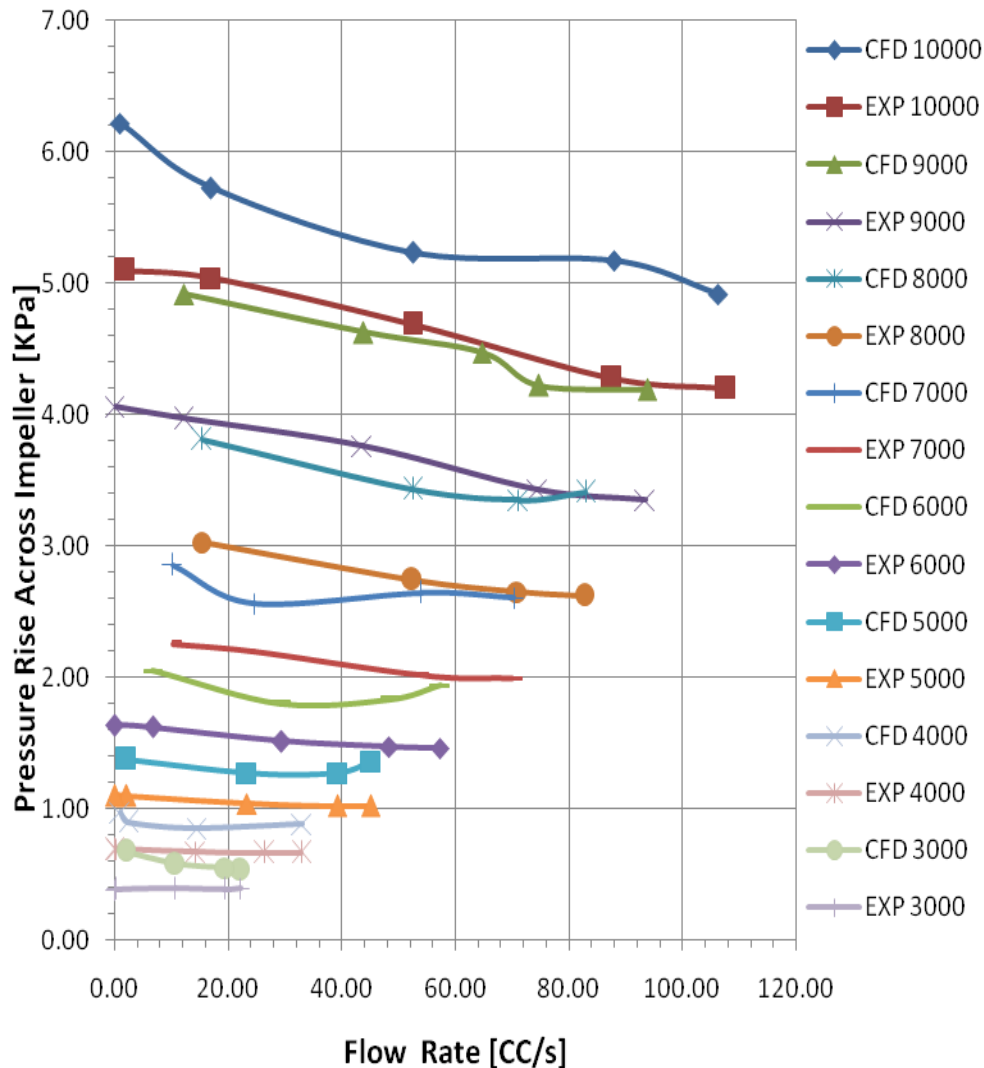**Figure 9-1: CFD and experimental results of LVAD as a continuous axial flow pump.**

Experimental evaluation of LVAD was carried out mainly for rotating speeds of 3000 to 10000 RPM. The main objective of the experimental evaluation was to validate the CFD based work that was done using commercially available tools. The experimental performance consisting of tests of the LVAD prototype, have shown

results comparable to the steady state CFD performance. The CFD results were having higher values compared to experimental outcome. The difference between the experimental and CFD is observed to be less than 20% for the majority of the flow rate condition. For the very low flow rate, the difference is observed to be less the 30%. The allowable deviation between the commercially available CFD tools and the experimental results are in the range of 10% to 20% (Throckmorton et al., 2007). Turbulent flow above Reynolds's number (Re) 3000 is also expected for the experimental work. The reason behind the difference might be due to the turbulence model. The standard K-ω model is used for the CFD simulation that has shown comparable results, according to the available literature. By applying the experimental pressure rise and flow rate for the CFD simulation, the difference reduces to 5%, which increases the confidence in the use of generated CFD model to predict the LVAD's behaviour with pulsatile flow. It also increases the confidence in the DOE parametric study as well as the optimisation.

9.2 Comparison of CFD and Experimental results LVAD as pulsatile flow pump

The VADs impeller accelerates and decelerates during systole to generate the pulse. Normally duration of the systolic phase is 1/3rd of a pulse. In vitro experiments were carried out to derive the pressure flow characteristics of the pulsatile flow. The Outcome of Experiment-1 shows the decrement in pressure at inlet and increment in pressure at outlet during the acceleration phase of the systole. This trend reverses during the deceleration phase of the systole. A peak inlet suction pressure and outlet pressure occurs with the 20ms time delay between them. At the initial phase of every beat, the pressure at inlet and outlet shows the small rise and fall at inlet and outlet respectively. The CFD simulations have also revealed the similar trend at the beginning and at the end of the systolic phase. During diastole, the pump pressure remains at the reservoir pressure. Outcomes of Experiment-1 shows, the pressure rise across the pump " ΔP " is inversely proportional to heart rate and directly proportional to the limit speed of motor. The relation amongst these parameters can be defined using the following equation.

$$\Delta P = Pc * \frac{N}{HR}$$

Where "ΔP" is the pressure rise is across the impeller, "N" is the limit speed of impeller, "HR" is heart rate, and the Pc is a constant that relates the peak pressure rise during the pulse with the operating parameters that are limited by the speed of pump, which varies according to heart rate. Figure 9-2 shows CFD and experimental results of the pressure rise across the impeller for single pulse of 60 BPM heart rate at the limit speed of 10000 RPM.
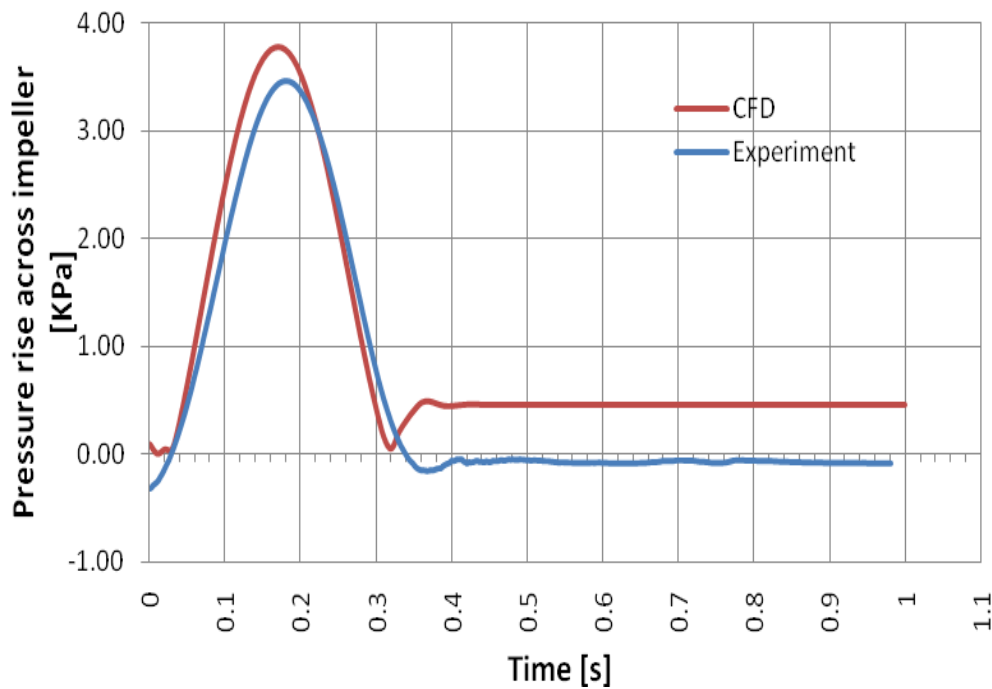
Figure 9-2: CFD and Experimental Pressure Rise Vs Time

The experimental performance of the axial flow pulsatile VAD shows the pressure rise across the impeller is comparable to the CFD prediction. The experimental duration of systole is delayed by 17 ms that is around 6 % higher compare to CFD. Around 10% difference amongst the peak value for pressure rise is observed at 150ms where the CFD predicts higher values than the experimental results. During the diastole, the difference remains less than 20%.
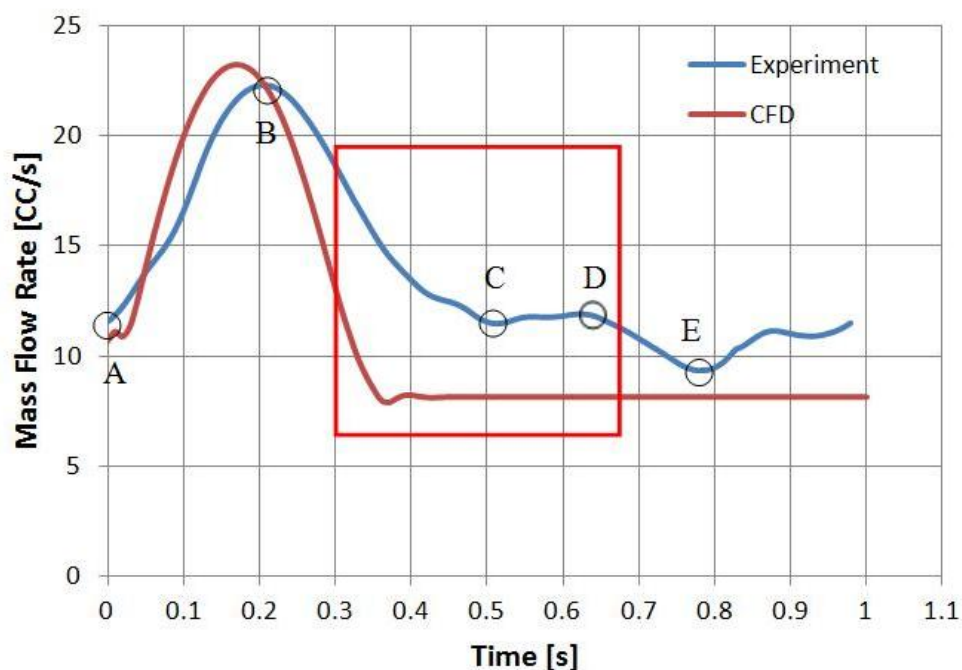
Figure 9-3: CFD and Experimental Mass Flow Rate Vs Time

Figure 9-3 shows the CFD and experimental results of mass flow rate. A CFD result shows the higher mass flow rate during the systolic acceleration phase compare to the experimental values. The peak values have around the 25ms delay with the less than 10% difference between the CFD and experimental results. At the end of acceleration phase of systole, the flow rate reduces with the time in case of CFD predictions while for the same period flow rate shows the higher values in experiments. The difference of CFD and experiment results during this deceleration phase is around 30%. As shown in the red rectangle, the experimental flow rate reduces gradually compared to the CFD and continues thus even during diastole. Further decrease in mass flow rate is also observed during diastole that is shown in curve DE. At the point E, the difference between the CFD and experiment is around 10%. After point E flow rate continues with the values remaining below point D. In the case of CFD prediction, the flow rate remains constant during diastole. Through the diastole, the higher values are observed in experiments compared to the CFD model.

In summary, the pressure and mass flow rate results have shown agreement amongst the CFD and experimental values. More than 20% difference is observed for the mass flow rate during diastole. At that time, the impeller is not rotating during experiments. Moreover, the difference of CFD and experiment for the pressure rise during the diastole is less than 20%.

9.3 Hemolysis in Pulsatile Axial Flow LVAD

Giersiepen (Giersiepen et al., 1990) has developed correlation for the hemolysis (equation 3-1) that is based on the shear stress and the exposure time using the Couette experimental system. Using the similar Couette model, S.Klaus (Klaus et al., 2001) have demonstrated that , hemolysis starts at the shear stress of 400 Pa with the exposure time more than 400ms. In this thesis, higher shear stresses are observed in CFD simulation during systolic phase where the total time duration of systole is 333 ms for the 60 BPM heart rate. For the same heart rate, above 300 Pa, shear stresses were observed for the total 20ms time duration with the peak value of 320Pa for 10000RPM rotating speed. Exposure time of the high shear stress in pulsatile LVAD is less than the continuous flow pump. In addition, the peak value is observed for the 1ms time duration. Less exposure time of high shear stress in pulsatile LVAD have demonstrated the LVAD's ability to satisfy the hydraulic and clinical requirement for the varying heart rate with low hemolysis levels.

Chapter 10 Conclusions

This thesis demonstrates the design and development of a pulsatile axial flow Left ventricular assist device (LVAD). The performance evaluation using CFD and experimental testing of a LVAD prototype specifies an acceptable design to build upon and optimised pulsatile LVAD. The experimental and CFD results of LVAD as a pulsatile axial flow pump have shown the way to develop a controlled pulsatile flow that can satisfy the hydraulic requirement with low hemolysis levels for treating patient.

The range of operating condition chosen for this study is intended to cover the range of condition that the pulsatile LVAD will experience during clinical use when operating with the native heart. Pulsatile LVAD can support the range of pressure and flow rate requirement with low hemolysis levels by operating it at a different limit speeds. The main difference among the continuous and pulsatile axial flow pump is a method of operating the rotating impeller. Hence, the classical design theory of an axial flow pump can be employed to design the axial flow pump that can generate a controlled pulsatile flow. As an initial design step, the operating parameters were optimised for the continuous flow and pressure rise with low hemolysis, the pulsatile LVAD can assist patients as a continuous flow pump.

The proposed pulsatile axial flow LVAD will improve the clinical treatment of the patients with early stage of heart failure, myocardial infarction, myocardial infection, and cardiogenic shock as a Bridge To Recovery (BTR) or Bridge To Decision (BTD) device.

Future work

In Vitro, evaluation of the first prototype of the pulsatile axial flow LVAD pump has provided data to support technical proof-of-concept for pulsatile flow generation using an axial flow pump. The in and outflow characteristics have been mapped, providing a better understanding of the pulsatile pumping mechanism. However, the first generation prototype was deliberately designed to pump saline or water, with a viscosity much lower than blood.

The future development work is needed to design and develop the second-generation experimental setup that will allow in vitro evaluation by LVAD using of blood or a suitable blood mimic as fluid.

Moreover, a second generation setup needs to include the artificial heart that can simulate certain diseased heart conditions in the fluid circulation loop that will allow a more realistic in vitro evaluation of the pulsatile axial pump.

The second generation pulsatile LVAD needs to include the real time control and data acquisition systems along with small size motors that will be used for in-vivo experiments.

The first generation prototype impeller is designed using the standard equation to generate coordinates of the blade profile. The second-generation prototype needs to be developed using the optimised blade shape for the low hemolysis levels.

In the long-term, the third-generation prototype of the pulsatile axial flow LVAD system needs to be developed for in vivo evaluation in a suitable animal model such as pig. The third-generation prototype will be a full system prototype, including a power supply and control system that is clinically relevant. This will involve issues that have been outside the scope the current thesis.

Reference

1991. Effect of enalapril on survival in patients with reduced left ventricular ejection fractions and congestive heart failure. The SOLVD Investigators. *N Engl J Med,* 325**,** 293-302.

1992. Effect of enalapril on mortality and the development of heart failure in asymptomatic patients with reduced left ventricular ejection fractions. The SOLVD Investigattors. *N Engl J Med,* 327**,** 685-91.

1997. The effect of digoxin on mortality and morbidity in patients with heart failure. The Digitalis Investigation Group. *N Engl J Med,* 336**,** 525-33.

2009a. BHF coronary heart disease statistics. *British Heart Foundation.*

2009b. Congestive Heart Failure in the United States: A New Epidemic. *National Heart, Lung, and Blood Institute.*

AGARD-AR-355 1998. CFD Validation for Propulsion System Components. NATO Research and Technology Organisation.

ALLEN, G. S., MURRAY, K. D. & OLSEN, D. B. 1997. The importance of pulsatile and nonpulsatile flow in the design of blood pumps. *Artif Organs,* 21**,** 922-8.

ALLENDER, S., SCARBOROUGH, P. & PETO, V. 2008. European Cardiovascular Disease Statistics.

ANDERSON, J. D. 1995. *Computational fluid dynamics: the basics with applications*, McGraw-Hill.

ANSYS, I. 2011. ANSYS Help. www.ansys.com/support.

ARORA, D., BEHR, M. & PASQUALI, M. 2004. A tensor-based measure for estimating blood damage. *Artif Organs,* 28**,** 1002-15.

AYRES, S. M., SCHLICHTIG, R. & STERLING, M. J. 1988. *Care of the critically ill,* Chicago Year Book Medical Publishers.

BALJE, O. E. 1981. *Turbomachines: A Guide to Design Selection and Theory*, Wiley.

BARNARD, C. N. 1967. The operation. A human cardiac transplant: an interim report of a successful operation performed at Groote Schuur Hospital, Cape Town. *S Afr Med J,* 41**,** 1271-4.

BEHBAHANI, M., BEHR, M., HORMES, M., STEINSEIFER, U., ARORA, D., CORONADO, O. & PASQUALI, M. 2009. A review of computational fluid dynamics analysis of blood pumps. *European Journal of Applied Mathematics,* 20**,** 363-397.

BIRKS, E. J. 2010. Left ventricular assist devices. *Heart,* 96**,** 63-71.

BLUDSZUWEIT, C. 1995a. Model for a general mechanical blood damage prediction. *Artif Organs,* 19**,** 583-9.

BLUDSZUWEIT, C. 1995b. Three-dimensional numerical prediction of stress loading of blood particles in a centrifugal pump. *Artif Organs,* 19**,** 590-6.

BRENNEN, C. E. 1994. *Hydrodynamics of pumps*, Concepts ETI.

BRENNEN, C. E. 2011. *Hydrodynamics of Pumps*, Cambridge University Press.

COHN, J. N., JOHNSON, G., ZIESCHE, S., COBB, F., FRANCIS, G., TRISTANI, F., SMITH, R., DUNKMAN, W. B., LOEB, H., WONG, M. & ET AL. 1991. A comparison of enalapril with hydralazine-isosorbide dinitrate in the treatment of chronic congestive heart failure. *N Engl J Med,* 325**,** 303-10.

COOLEY, D. A. 1988. Staged cardiac transplantation: use of mechanical circulatory support devices including the total artificial heart as 'bridges' to cardiac transplantation. *Adv Cardiol,* 36**,** 261-6.

CRESWELL, L. L., ROSENBLOOM, M., COX, J. L., FERGUSON, T. B., SR., KOUCHOUKOS, N. T., SPRAY, T. L., PASQUE, M. K., FERGUSON, T. B., JR., WAREING, T. H. & HUDDLESTON, C. B. 1992. Intraaortic balloon counterpulsation: patterns of usage and outcome in cardiac surgery patients. *Ann Thorac Surg,* 54**,** 11-8; discussion 18-20.

CSANÁDY, G. T. 1964. *Theory of turbomachines*, McGraw-Hill.

DEB, K. & GOEL, T. Controlled elitist non-dominated sorting genetic algorithms for better convergence. 2001. Springer, 67-81.

DEB, K., PRATAP, A., AGARWAL, S. & MEYARIVAN, T. 2002. A fast and elitist multiobjective genetic algorithm: NSGA-II. *Evolutionary Computation, IEEE Transactions on,* 6**,** 182-197.

DEBAKEY, M., LIOTTA, D. & HALL, C. 1964. Left heart bypass using an implantable blood pump. *Mechanical Devices to Assist the Failing Heart,* 223.

DEBAKEY, M. E. 1971. Left ventricular bypass pump for cardiac assistance. Clinical experience. *Am J Cardiol, 27,* 3-11.

DREWS, T. N., LOEBE, M., JURMANN, M. J., WENG, Y., WENDELMUTH, C. & HETZER, R. 2003. Outpatients on mechanical circulatory support. *Ann Thorac Surg, 75,* 780-5; discussion 785.

EASTHOPE, P. L. & BROOKS, D. E. 1980. A comparison of rheological constitutive functions for whole human blood. *Biorheology, 17,* 235-47.

EDGEWORTH, F. Y. 1981. *Mathematical Physics,* 1 PATERNOSTER SQUARE,LONDON, C. KEGAN PAUL & CO.

FARRAR, D. J., LITWAK, P., LAWSON, J. H., WARD, R. S., WHITE, K. A., ROBINSON, A. J., RODVIEN, R. & HILL, J. D. 1988. In vivo evaluations of a new thromboresistant polyurethane for artificial heart blood pumps. *J Thorac Cardiovasc Surg, 95,* 191-200.

FIGUEROA, M. S. & PETERS, J. I. 2006. Congestive heart failure: Diagnosis, pathophysiology, therapy, and implications for respiratory care. *Respir Care, 51,* 403-12.

FRAZIER, O. H. 1994. First use of an untethered, vented electric left ventricular assist device for long-term support. *Circulation, 89,* 2908-14.

FRAZIER, O. H. & DELGADO, R. M. 2003. Mechanical circulatory support for advanced heart failure: where does it stand in 2003? *Circulation, 108,* 3064-8.

GARTNER, M. J., WILHELM, C. R., GAGE, K. L., FABRIZIO, M. C. & WAGNER, W. R. 2000. Modeling flow effects on thrombotic deposition in a membrane oxygenator. *Artif Organs, 24,* 29-36.

GIERSIEPEN, M., WURZINGER, L. J., OPITZ, R. & REUL, H. 1990. Estimation of shear stress-related blood damage in heart valve prostheses--in vitro comparison of 25 aortic valves. *Int J Artif Organs, 13,* 300-6.

GOLDSTEIN, D. J. & OZ, M. 2000. *Cardiac Assist Devices*, Futura Publishing Company.

GUYTON, A. C. & HALL, J. E. 2006. *Textbook Of Medical Physiology*, Elsevier Saunders.

HALL, C. W., LIOTTA, D., HENLY, W. S., CRAWFORD, E. S. & DEBAKERY, M. E. 1964. Development of Artificial Intrathoracic Circulatory Pumps. *Am J Surg,* 108**,** 685-92.

HEDENMARK, J., AHN, H., HENZE, A., NYSTROM, S. O., SVEDJEHOLM, R. & TYDEN, H. 1989. Intra-aortic balloon counterpulsation with special reference to determinants of survival. *Scand J Thorac Cardiovasc Surg,* 23**,** 57-62.

HELLUMS, J. D. 1994. 1993 Whitaker Lecture: biorheology in thrombosis research. *Ann Biomed Eng,* 22**,** 445-55.

HETZER, R., MULLER, J. H., WENG, Y., MEYER, R. & DANDEL, M. 2001. Bridging-to-recovery. *Ann Thorac Surg,* 71**,** S109-13; discussion S114-5.

HEUSER, G. & OPITZ, R. 1980. A Couette viscometer for short time shearing of blood. *Biorheology,* 17**,** 17-24.

HJALMARSON, A., GOLDSTEIN, S., FAGERBERG, B., WEDEL, H., WAAGSTEIN, F., KJEKSHUS, J., WIKSTRAND, J., EL ALLAF, D., VITOVEC, J., ALDERSHVILE, J., HALINEN, M., DIETZ, R., NEUHAUS, K. L., JANOSI, A., THORGEIRSSON, G., DUNSELMAN, P. H., GULLESTAD, L., KUCH, J., HERLITZ, J., RICKENBACHER, P., BALL, S., GOTTLIEB, S. & DEEDWANIA, P. 2000. Effects of controlled-release metoprolol on total mortality, hospitalizations, and well-being in patients with heart failure: the Metoprolol CR/XL Randomized Intervention Trial in congestive heart failure (MERIT-HF). MERIT-HF Study Group. *JAMA,* 283**,** 1295-302.

HOWARD, J. H. G. 2001. *Axial fan and compressor modelling.*

HUNT, S. A. & FRAZIER, O. H. 1998. Mechanical circulatory support and cardiac transplantation. *Circulation,* 97**,** 2079-90.

KHAN, T., DELGADO, R. M., RADOVANCEVIC, B., TORRE-AMIONE, G., ABRAMS, J., MILLER, K., MYERS, T., OKERBERG, K., STETSON, S. J., GREGORIC, I., HERNANDEZ, A. & FRAZIER, O. H. 2003. Dobutamine stress echocardiography predicts myocardial improvement in patients supported by left ventricular assist devices (LVADs): hemodynamic and histologic evidence of improvement before LVAD explantation. *J Heart Lung Transplant,* 22**,** 137-46.

KLAUS, S., PAUL, R., REUL, H., MOTTAGHY, K. & GLASMACHER, B. 2001. Investigation of flow and material induced hemolysis with a Couette type high shear system. *Materialwissenschaft und Werkstofftechnik,* 32**,** 922-925.

LAZAR, H. L., BUCKBERG, G. D., FOGLIA, R. P., MANGANARO, A. J. & MALONEY, J. V., JR. 1981. Detrimental effects of premature use of inotropic drugs to discontinue cardiopulmonary bypass. *J Thorac Cardiovasc Surg,* 82**,** 18-25.

LAZAR, H. L., BUCKBERG, G. D., MANGANARO, A. J., BECKER, H. & MALONEY, J. V., JR. 1980. Reversal of ischemic damage with amino acid substrate enhancement during reperfusion. *Surgery,* 88**,** 702-9.

LEVERETT, L. B., HELLUMS, J. D., ALFREY, C. P. & LYNCH, E. C. 1972. Red blood cell damage by shear stress. *Biophys J,* 12**,** 257-73.

LOGAN, E. 1981. *Turbomachinery: basic theory and applications*, M. Dekker.

MACCIOLI, G. A. 1997. *Intra-aortic balloon pump therapy,* Baltimore, Williams & Wilkins.

MAGOVERN, J. A. & PIERCE, W. S. 1990. *Mechanical Circulatory Assistance before Heart Transplantation,* Philadelphia, Saunders.

MASTERS, R. G. 1999. *Surgical Options for the Treatment of Heart Failure,* 101 Philip Drive,Norwell,MA 02061,U.S.A., Kluwer Academic Publishers

MATHERS, C. D. & LONCAR, D. 2006. Projections of global mortality and burden of disease from 2002 to 2030. *PLoS Med,* 3**,** e442.

MCCARTHY, P. M., SMEDIRA, N. O., VARGO, R. L., GOORMASTIC, M., HOBBS, R. E., STARLING, R. C. & YOUNG, J. B. 1998. One hundred patients with the HeartMate left ventricular assist device: evolving concepts and technology. *J Thorac Cardiovasc Surg,* 115**,** 904-12.

MEHTA, S. M., AUFIERO, T. X., PAE, W. E., JR., MILLER, C. A. & PIERCE, W. S. 1996. Results of mechanical ventricular assistance for the treatment of post cardiotomy cardiogenic shock. *ASAIO J,* 42**,** 211-8.

MEYNS, B., VANERMEN, H., VANHAECKE, J., SERGEANT, P., DAENEN, W. & FLAMENG, W. 1994. Hemopump fails as bridge to transplantation in postinfarction ventricular septal defect. *J Heart Lung Transplant,* 13**,** 1133-7.

MITRA, K., DEB, K. & GUPTA, S. K. 1998. Multiobjective dynamic optimization of an industrial nylon 6 semibatch reactor using genetic algorithm. *Journal of Applied Polymer Science,* 69**,** 69-87.

MOULOPOULOS, S. D., TOPAZ, S. R. & KOLFF, W. J. 1962. Extracorporeal assistance to the circulation and intraaortic balloon pumping. *Trans Am Soc Artif Intern Organs,* 8**,** 85-9.

MURAKAMI, T., KINO, K., IRIE, H., KIOKA, Y., INDO, S., KAWAKAMI, S., YAMADA, M. & SHIMIZU, N. 1994. Results of circulatory support for postoperative cardiogenic shock. *Artif Organs,* 18**,** 691-7.

NATIONAL HEART LUNG AND BLOOD INSTITUTE. 2011. *What Is a Heart Attack?* [Online]. http://www.nhlbi.nih.gov/health/health-topics/topics/heartattack/.

PACKER, M., GHEORGHIADE, M., YOUNG, J. B., COSTANTINI, P. J., ADAMS, K. F., CODY, R. J., SMITH, L. K., VAN VOORHEES, L., GOURLEY, L. A. & JOLLY, M. K. 1993. Withdrawal of digoxin from patients with chronic heart failure treated with angiotensin-converting-enzyme inhibitors. RADIANCE Study. *N Engl J Med,* 329**,** 1-7.

PARETO, V. 1896. *Cours D'Economie Politique, volume I and II,* F. Rouge, Lausanne.

PARKER, J. D., PARKER, A. B., FARRELL, B. & PARKER, J. O. 1996. Effects of diuretic therapy on the development of tolerance to nitroglycerin and exercise capacity in patients with chronic stable angina. *Circulation,* 93**,** 691-6.

PENNINGTON, D. G., MCBRIDE, L. R., MILLER, L. W. & SWARTZ, M. T. 1994. Eleven years' experience with the Pierce-Donachy ventricular assist device. *J Heart Lung Transplant,* 13**,** 803-10.

PFEFFER, M. A., BRAUNWALD, E., MOYE, L. A., BASTA, L., BROWN, E. J., JR., CUDDY, T. E., DAVIS, B. R., GELTMAN, E. M., GOLDMAN, S., FLAKER, G. C. & ET AL. 1992. Effect of captopril on mortality and morbidity in patients with left ventricular dysfunction after myocardial infarction. Results of the survival and ventricular enlargement trial. The SAVE Investigators. *N Engl J Med,* 327**,** 669-77.

PITT, B., ZANNAD, F., REMME, W. J., CODY, R., CASTAIGNE, A., PEREZ, A., PALENSKY, J. & WITTES, J. 1999. The effect of spironolactone on morbidity and mortality in patients with severe heart failure. Randomized Aldactone Evaluation Study Investigators. *N Engl J Med,* 341**,** 709-17.

REUL, H. M. & AKDIS, M. 2000. Blood pumps for circulatory support. *Perfusion,* 15**,** 295-311.

RICHARDSON, A., BAYLISS, J., SCRIVEN, A. J., PARAMESHWAR, J., POOLE-WILSON, P. A. & SUTTON, G. C. 1987. Double-blind comparison of captopril alone against frusemide plus amiloride in mild heart failure. *Lancet,* 2**,** 709-11.

ROOKE, T. W., HIRSCH, A. T., MISRA, S., SIDAWY, A. N., BECKMAN, J. A., FINDEISS, L. K., GOLZARIAN, J., GORNIK, H. L., HALPERIN, J. L., JAFF, M. R., MONETA, G. L., OLIN, J. W., STANLEY, J. C., WHITE, C. J., WHITE, J. V., ZIERLER, R. E., AMERICAN COLLEGE OF CARDIOLOGY, F., AMERICAN HEART, A., SOCIETY FOR CARDIOVASCULAR, A., INTERVENTIONS, SOCIETY OF INTERVENTIONAL, R., SOCIETY FOR VASCULAR, M. & SOCIETY FOR VASCULAR, S. 2012. 2011 ACCF/AHA focused update of the

guideline for the management of patients with peripheral artery disease (updating the 2005 guideline): a report of the American College of Cardiology Foundation/American Heart Association Task Force on Practice Guidelines: developed in collaboration with the Society for Cardiovascular Angiography and Interventions, Society of Interventional Radiology, Society for Vascular Medicine, and Society for Vascular Surgery. *Catheter Cardiovasc Interv,* 79**,** 501-31.

ROSE, E. A., GELIJNS, A. C., MOSKOWITZ, A. J., HEITJAN, D. F., STEVENSON, L. W., DEMBITSKY, W., LONG, J. W., ASCHEIM, D. D., TIERNEY, A. R., LEVITAN, R. G., WATSON, J. T., MEIER, P., RONAN, N. S., SHAPIRO, P. A., LAZAR, R. M., MILLER, L. W., GUPTA, L., FRAZIER, O. H., DESVIGNE-NICKENS, P., OZ, M. C., POIRIER, V. L. & RANDOMIZED EVALUATION OF MECHANICAL ASSISTANCE FOR THE TREATMENT OF CONGESTIVE HEART FAILURE STUDY, G. 2001. Long-term use of a left ventricular assist device for end-stage heart failure. *N Engl J Med,* 345**,** 1435-43.

SALLAM, A. M. & HWANG, N. H. 1984. Human red blood cell hemolysis in a turbulent shear flow: contribution of Reynolds shear stresses. *Biorheology,* 21**,** 783-97.

SKALAK, R. & CHIEN, S. 1987. *Handbook of bioengineering*, McGraw-Hill.

SONG, X., THROCKMORTON, A. L., UNTAROIU, A., PATEL, S., ALLAIRE, P. E., WOOD, H. G. & OLSEN, D. B. 2003a. Axial flow blood pumps. *ASAIO J,* 49**,** 355-64.

SONG, X., THROCKMORTON, A. L., WOOD, H. G., ANTAKI, J. F. & OLSEN, D. B. 2003b. Computational fluid dynamics prediction of blood damage in a centrifugal pump. *Artif Organs,* 27**,** 938-41.

SONG, X., WOOD, H. G., DAY, S. W. & OLSEN, D. B. 2003c. Studies of turbulence models in a computational fluid dynamics model of a blood pump. *Artif Organs,* 27**,** 935-7.

SPENCER, F. C., EISEMAN, B., TRINKLE, J. K. & ROSSI, N. P. 1965. Assisted Circulation for Cardiac Failure Following Intracardiac Surgery with Cardiopulmonary Bypass. *J Thorac Cardiovasc Surg,* 49**,** 56-73.

STEPANOFF, A. J. 1957. *Centrifugal and axial flow pumps: theory, design, and application*, Krieger Pub. Co.

STEVENSON, L. W., KORMOS, R. L., BOURGE, R. C., GELIJNS, A., GRIFFITH, B. P., HERSHBERGER, R. E., HUNT, S., KIRKLIN, J., MILLER, L. W., PAE, W. E., JR., PANTALOS, G., PENNINGTON, D. G., ROSE, E. A., WATSON, J. T., WILLERSON, J. T., YOUNG, J. B., BARR, M. L., COSTANZO, M. R., DESVIGNE-NICKENS, P., FELDMAN, A. M., FRAZIER, O. H.,

FRIEDMAN, L., HILL, J. D., KONSTAM, M. A., MCCARTHY, P. M., MICHLER, R. E., OZ, M. C., ROSENGARD, B. R., SAPIRSTEIN, W., SHANKER, R., SMITH, C. R., STARLING, R. C., TAYLOR, D. O. & WICHMAN, A. 2001. Mechanical cardiac support 2000: current applications and future trial design. June 15-16, 2000 Bethesda, Maryland. *J Am Coll Cardiol,* 37**,** 340-70.

SUN, B. C., CATANESE, K. A., SPANIER, T. B., FLANNERY, M. R., GARDOCKI, M. T., MARCUS, L. S., LEVIN, H. R., ROSE, E. A. & OZ, M. C. 1999. 100 long-term implantable left ventricular assist devices: the Columbia Presbyterian interim experience. *Ann Thorac Surg,* 68**,** 688-94.

SVEDJEHOLM, R., HAKANSON, E. & VANHANEN, I. 1995a. Rationale for metabolic support with amino acids and glucose-insulin-potassium (GIK) in cardiac surgery. *Ann Thorac Surg,* 59**,** S15-22.

SVEDJEHOLM, R., HULJEBRANT, I., HAKANSON, E. & VANHANEN, I. 1995b. Glutamate and high-dose glucose-insulin-potassium (GIK) in the treatment of severe cardiac failure after cardiac operations. *Ann Thorac Surg,* 59**,** S23-30.

SVENSSON, S., EKROTH, R., NILSSON, F., PONTEN, J. & WILLIAM-OLSSON, G. 1989. Insulin as a vasodilating agent in the first hour after cardiopulmonary bypass. *Scand J Thorac Cardiovasc Surg,* 23**,** 139-43.

SVENSSON, S., SVEDJEHOLM, R., EKROTH, R., MILOCCO, I., NILSSON, F., SABEL, K. G. & WILLIAM-OLSSON, G. 1990. Trauma metabolism and the heart. Uptake of substrates and effects of insulin early after cardiac operations. *J Thorac Cardiovasc Surg,* 99**,** 1063-73.

SWEDBERG, K. & KJEKSHUS, J. 1988. Effects of enalapril on mortality in severe congestive heart failure: results of the Cooperative North Scandinavian Enalapril Survival Study (CONSENSUS). *Am J Cardiol,* 62**,** 60A-66A.

TAHY, A. 1998. Management of chronic heart failure. *Orv Hetil,* 139**,** 2555-65.

THE CRITERIA COMMITTEE OF THE NEW YORK HEART ASSOCIATION 1994. Nomenclature and Criteria for Diagnosis of Diseases of the Heart and Great Vessels. 9th ed**,** 253-256.

THOM, T., HAASE, N., ROSAMOND, W., HOWARD, V. J., RUMSFELD, J., MANOLIO, T., ZHENG, Z. J., FLEGAL, K., O'DONNELL, C., KITTNER, S., LLOYD-JONES, D., GOFF, D. C., JR., HONG, Y., ADAMS, R., FRIDAY, G., FURIE, K., GORELICK, P., KISSELA, B., MARLER, J., MEIGS, J., ROGER, V., SIDNEY, S., SORLIE, P., STEINBERGER, J., WASSERTHIEL-SMOLLER, S., WILSON, M., WOLF, P., AMERICAN HEART ASSOCIATION STATISTICS, C. & STROKE STATISTICS, S. 2006. Heart disease and stroke statistics--2006 update:

a report from the American Heart Association Statistics Committee and Stroke Statistics Subcommittee. *Circulation,* 113**,** e85-151.

THROCKMORTON, A. L., UNTAROIU, A., ALLAIRE, P. E., WOOD, H. G., LIM, D. S., MCCULLOCH, M. A. & OLSEN, D. B. 2007. Numerical design and experimental hydraulic testing of an axial flow ventricular assist device for infants and children. *ASAIO J,* 53**,** 754-61.

THURSTON, G. B. 1979. Rheological parameters for the viscosity viscoelasticity and thixotropy of blood. *Biorheology,* 16**,** 149-62.

TRANSPLANTATION, U. S. B. O. H. R. D. D. O. O., TRANSPLANTATION, U. S. H. R. S. A. D. & UNOS 1993. *Annual report of the U.S. scientific registry of transplant recipients and the organ procurement and transplantation network*, U. S. Dept. of Health and Human Services, Public Health Service, Bureau of Health Resources Development, Division of Organ Transplantation.

TRAUMA, N. R. C. C. O. 1966. *Mechanical devices to assist the failing heart: proceedings*, National Academy of Sciences-National Research Council.

UNDAR, A. 2004. Myths and truths of pulsatile and nonpulsatile perfusion during acute and chronic cardiac support. *Artif Organs,* 28**,** 439-43.

URETSKY, B. F., YOUNG, J. B., SHAHIDI, F. E., YELLEN, L. G., HARRISON, M. C. & JOLLY, M. K. 1993. Randomized study assessing the effect of digoxin withdrawal in patients with mild to moderate chronic congestive heart failure: results of the PROVED trial. PROVED Investigative Group. *J Am Coll Cardiol,* 22**,** 955-62.

VANHANEN, I., SVEDJEHOLM, R., HAKANSON, E., JOACHIMSSON, P. O., JORFELDT, L., NILSSON, L. & VANKY, F. 1998. Assessment of myocardial glutamate requirements early after coronary artery bypass surgery. *Scand Cardiovasc J,* 32**,** 145-52.

VINTEN-JOHANSEN, J. & NAKANISHI, K. 1993. Postcardioplegia acute cardiac dysfunction and reperfusion injury. *J Cardiothorac Vasc Anesth,* 7**,** 6-18.

WAAGSTEIN, F., BRISTOW, M. R., SWEDBERG, K., CAMERINI, F., FOWLER, M. B., SILVER, M. A., GILBERT, E. M., JOHNSON, M. R., GOSS, F. G. & HJALMARSON, A. 1993. Beneficial effects of metoprolol in idiopathic dilated cardiomyopathy. Metoprolol in Dilated Cardiomyopathy (MDC) Trial Study Group. *Lancet,* 342**,** 1441-6.

WALLIS, R. A. 1983. *Axial flow fans and ducts*, Wiley.

WEILE, D. S., MICHIELSSEN, E. & GOLDBERG, D. E. 1996. Genetic algorithm design of Pareto optimal broadband microwave absorbers. *Electromagnetic Compatibility, IEEE Transactions on,* 38**,** 518-525.

WHEELDON, D. R. 2003. Mechanical circulatory support: state of the art and future perspectives. *Perfusion,* 18**,** 233-43.

WHEELDON, D. R., LAFORGE, D. H., LEE, J., JANSEN, P. G., JASSAWALLA, J. S. & PORTNER, P. M. 2002. Novacor left ventricular assist system long-term performance: comparison of clinical experience with demonstrated in vitro reliability. *ASAIO J,* 48**,** 546-51.

WIEBALCK, A. C., WOUTERS, P. F., WALDENBERGER, F. R., AKPINAR, B., LAUWERS, P. M., DEMEYERE, R. H., SERGEANT, P. T., DAENEN, W. J. & FLAMENG, W. J. 1993. Left ventricular assist with an axial flow pump (Hemopump): clinical application. *Ann Thorac Surg,* 55**,** 1141-6.

WOOD, H. G., THROCKMORTON, A. L., UNTAROIU, A. & SONG, X. 2005. The medical physics of ventricular assist devices. *Reports on Progress in Physics* Volume 68 31.

WU, J., PADEN, B. E., BOROVETZ, H. S. & ANTAKI, J. F. 2010. Computational fluid dynamics analysis of blade tip clearances on hemodynamic performance and blood damage in a centrifugal ventricular assist device. *Artif Organs,* 34**,** 402-11.

WU, Y., ALLAIRE, P., TAO, G. & LIU, Y. In vitro test of an adaptive flow controller for a continuous flow LVAD. 2004a. IEEE, 1647-1648 vol. 2.

WU, Y., ALLAIRE, P., TAO, G., WOOD, H., OLSEN, D. & TRIBBLE, C. 2003. An advanced physiological controller design for a left ventricular assist device to prevent left ventricular collapse. *Artif Organs,* 27**,** 926-30.

WU, Y., ALLAIRE, P. E., TAO, G., ADAMS, M., LIU, Y., WOOD, H. & OLSEN, D. B. 2004b. A bridge from short-term to long-term left ventricular assist device-- experimental verification of a physiological controller. *Artif Organs,* 28**,** 927-32.

YACOUB, M. H. 2001. A novel strategy to maximize the efficacy of left ventricular assist devices as a bridge to recovery. *Eur Heart J,* 22**,** 534-40.

Appendix

Appendix-1: Figures of existing VADS.

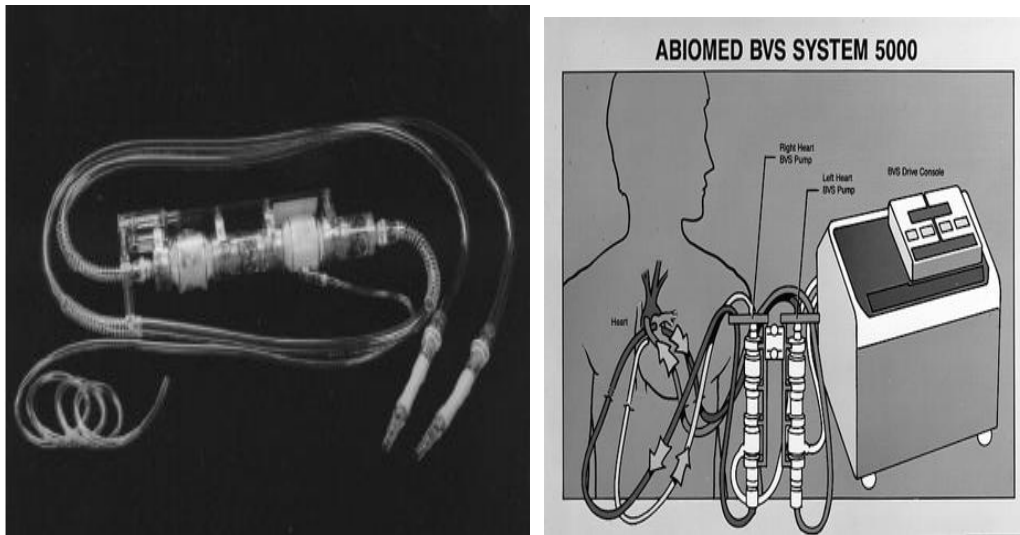## 1. AbioMed BVS 5000 system

Figure 1: AbioMed BVS 5000 system
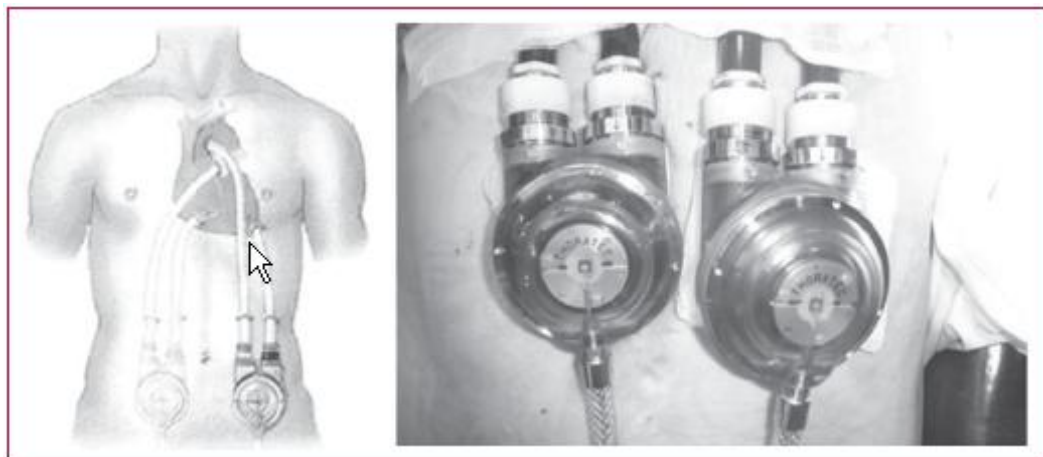
2. AbioMed AB 5000 system

Figure 2 :AbioMed AB 5000 system

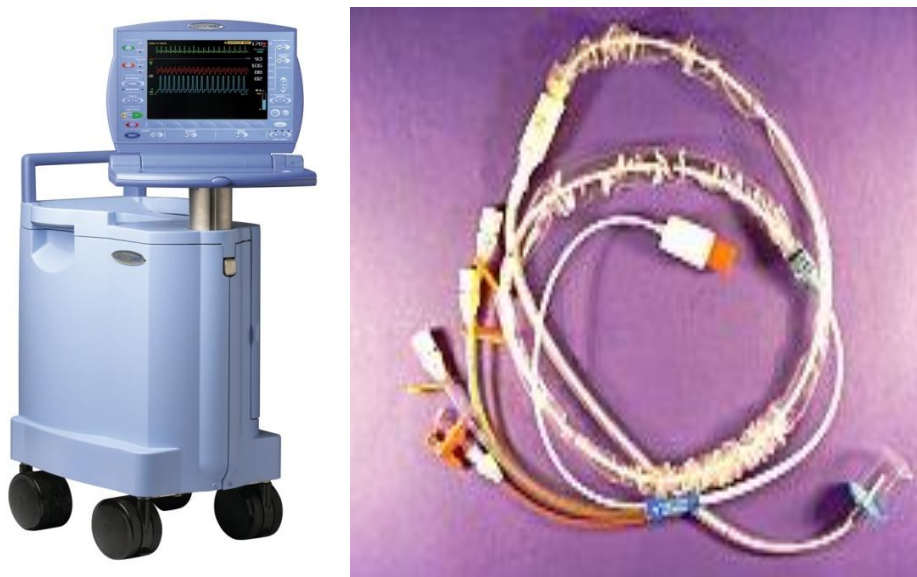## 3. Arrow Int. Intra-Aortic Balloon Pump

Figure 3: Arrow Int. Intra-Aortic Balloon Pump

4. DataScope CS100 / System 98XT

Figure 4 : DataScope CS100 / System 98XT

5 : Medtronic Biopump (80ml & 48ml)

Figure 5 : Medtronic Biopump (80ml & 48ml)

6. Thoratec VAD

Figure 6 : Thoratec VAD

7. Thoratec HeartMate XVE LVAS
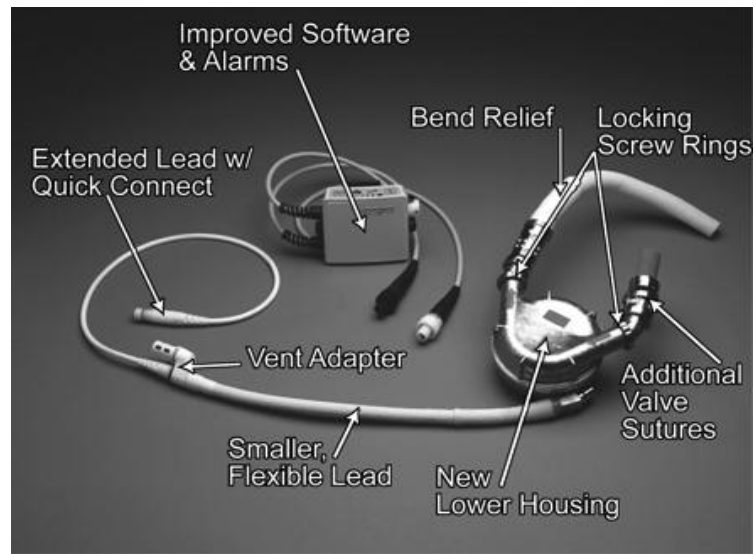
Figure 7 :Thoratec HeartMate XVE LVAS

8. World Heart Novacor
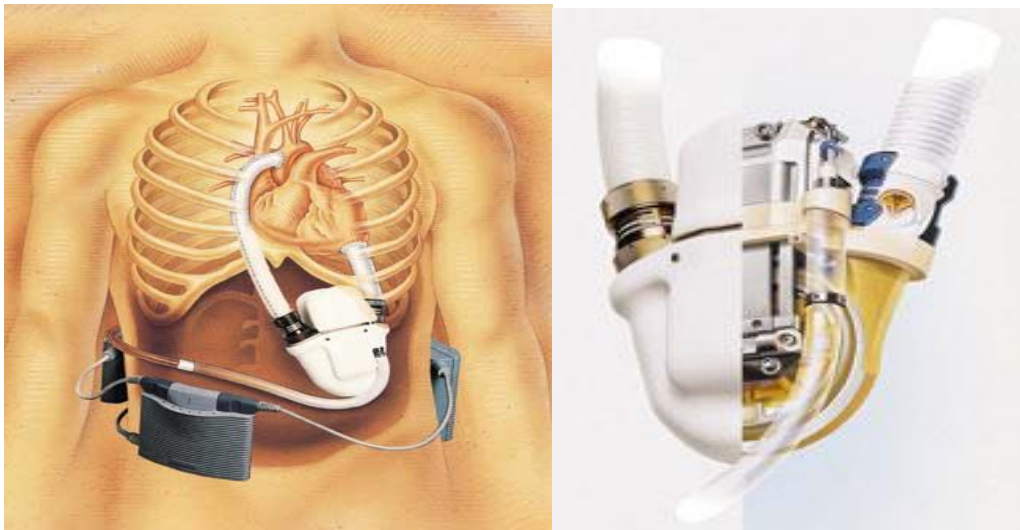
Figure 8 : World Heart Novacor

9. Abiomed Abiocor

Figure 9 : Abiomed Abiocor

10. Arrow Int. CorAide

Figure 10: Arrow Int. CorAide

11. Berlin Heart Excor (10 to 80ml versions)

Figure 11: Berlin Heart Excor (10 to 80ml versions)

12.Berlin Heart Incor
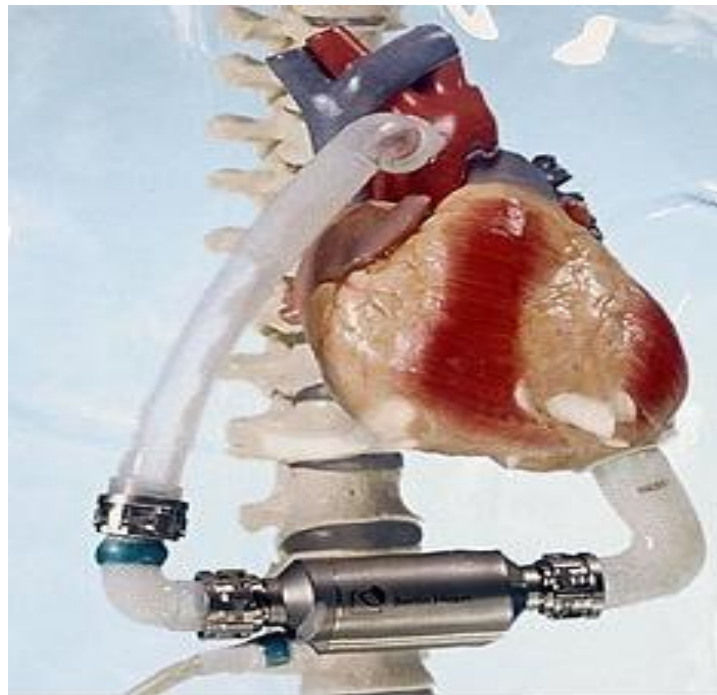
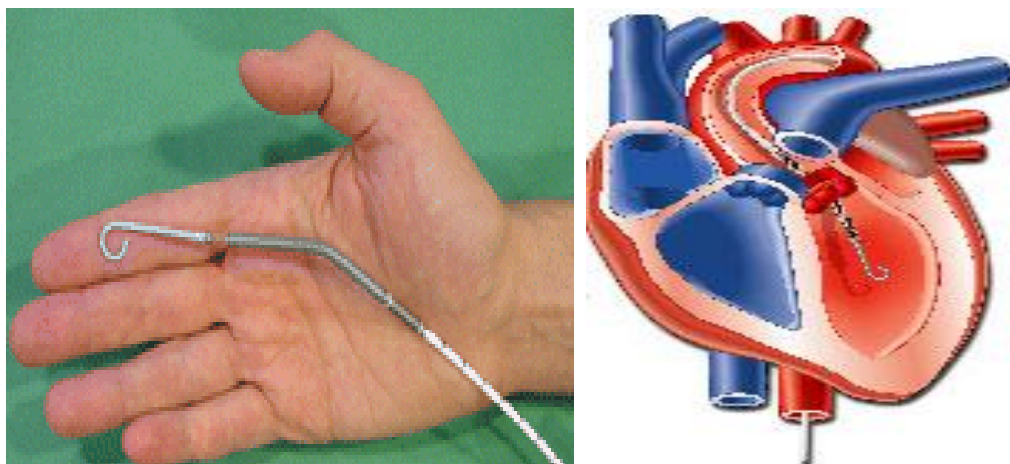**Figure 12: Berlin Heart Incor**

13. Impella Recover LP 2,5 & LP 5,0

Figure 13 : Impella Recover LP 2,5 & LP 5,0

14. Jarvik Heart Jarvik 2000 FlowMaker

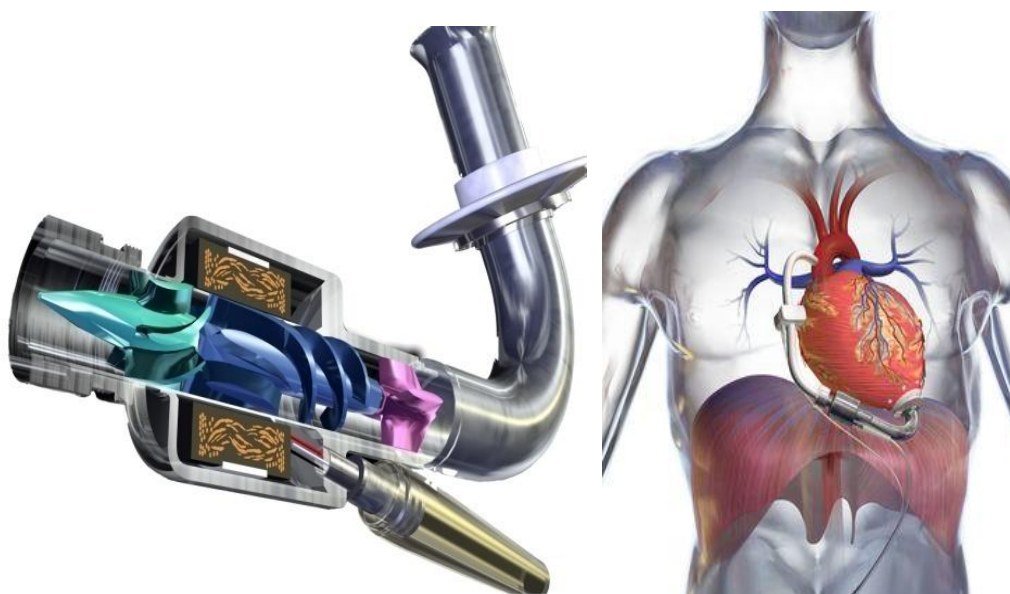**Figure 14 : Jarvik Heart Jarvik 2000 FlowMaker**

15.Micromed DeBakey

Figure 15 : Micromed DeBakey

16.Terumo DuraHeart

Figure 16 : Terumo DuraHeart

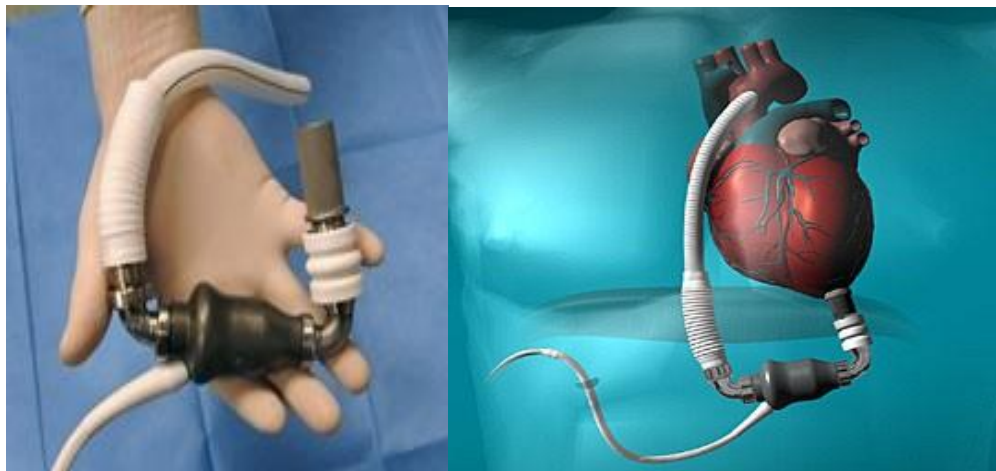## 17. Thoratec HeartMate III

Figure 17 : Thoratec HeartMate III

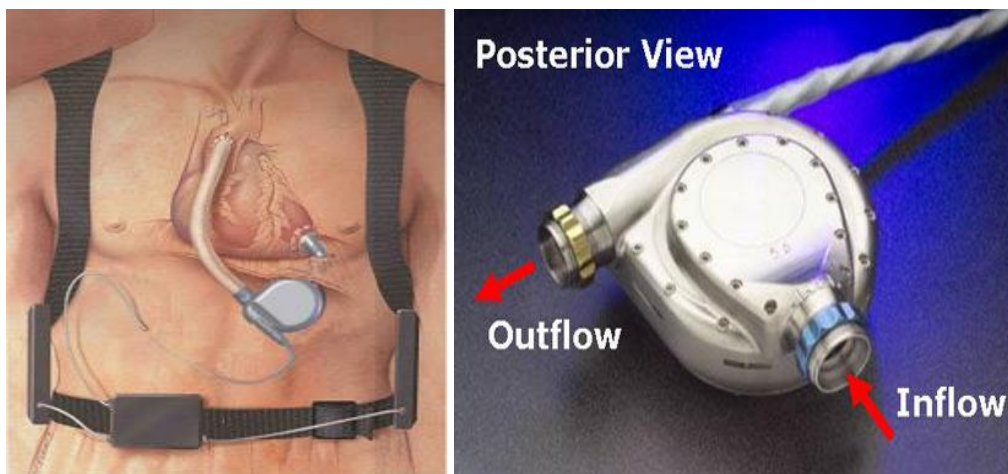## 18. Ventracor VentrAssist

Figure 18:Ventracor VentrAssist

19. World Heart HeartQuest VAD

Figure 19:World Heart HeartQuest VAD